Development of a novel 96-well bioreactor platform for the combined assessment of drug efficacy and toxicity in human liver and kidney

Rebecca Scott

Doctor of Philosophy

Biosciences Institute

Faculty of Medical Science

Newcastle University

September 2023

Abstract

Background and Aims

Bringing a new drug to market can cost as much as $2.8 billion, with significant attrition rates in later phase trials. As many as 20-40% of these exclusions are due to unforeseen toxicity. Current predictive 2D cell culture and *in vivo* animal models have limitations, therefore human tissue pre-clinical modelling platforms for efficacy and toxicity testing of novel compounds, may provide a solution. This project aimed to develop a novel 96-well bioreactor to culture precision cut tissue slices (PCTS) to assess the efficacy and potential toxicities of novel therapeutics. As major sites of xenobiotic metabolism and excretion, PCTS generated from human liver and kidney tissue were selected for this.

Methods

3mm PCTS generated from 250µm thick tissue sheets were cultured for up to 96h with daily media changes. Viability, health and disease biomarkers were assessed using resazurin assays, ELISAs, histology/immunohistochemistry and MSD panels.

Results

In 96-well plate cultured human liver and kidney slices, fibrogenesis was induced upon challenge with fibrotic stimuli TGFβ1/PDGFββ, and acute inflammation was promoted using LPS, IL-1α and IL-1β. Challenge with TGFβ1/PDGFββ increased collagen deposition, measured by PSR and soluble collagen 1a1 ELISA, and increased myofibroblast activation, measured by αSMA staining. Challenge with inflammatory stimuli upregulated production of pro-inflammatory cytokines such as IL-6, IL-8 and TNFα. Modelling of fibrogenesis and inflammation was reproducible across multiple donors and could be dose dependently supressed using Alk5 or IKK2 inhibitors respectively. Next, the predictive value of the bioreactor in toxicity modelling was assessed using clinically approved drugs known to be hepatotoxic or nephrotoxic. Different treatment regimens were used to identify the best way to predict adverse outcomes in bioreactor cultured PCTS.

Conclusion

The novel 96-well bioreactor platform can be used for target validation of anti-fibrotic and anti-inflammatory compounds and to assess toxicity. *Ex vivo* bioreactor cultured PCTS are a helpful tool to test novel therapeutics and can reduce reliance on less physiologically relevant 2D models.

Acknowledgements

I would like to say thank you to Professor Fiona Oakley for all the support you have given me over the past 3 years, you have been a fantastic supervisor and I will always be grateful for the opportunity you have given me. Also, thank you to Professors Derek Mann and Jelena Mann and Dr Lee Borthwick for their advice and support over the course of my project.

I want to thank all of the members of the fibrosis group and colleagues at FibroFind both present and those who have left, for their help with both experimental work and keeping me from going mad. Particular thanks to Rachel Burgoyne, Ben Barksby and Hannah Paish for their help with the MSD panel experiments and data analysis.

Special acknowledgement must be given to the theatre staff at the Freeman Hospital, Lucy Bates and the patients who consented to be part of this research. Without any of them, this work would not be possible.

Lastly I would like to thank my family for supporting me throughout my career, to my husband David for looking after me through the whole process, I definitely could not have done this without you, and also our cats Millie and Bramble who kept me sane with their fluffy madness.

Table of Contents

List of Figures

List of Tables

List of Abbreviations

Absorption, Distribution, Metabolism and Excretion (ADME)

Acute Kidney Disease (AKD)

Alanine Aminotransferase (ALT)

Alkaline Phosphatase (ALP)

Alpha Smooth Muscle Actin (αSMA)

Aspartate Aminotransferase (AST)

Apoptosis Signal-Regulating Kinase (ASK)

Bile Duct Ligation (BDL)

Carbon Tetrachloride (CCl_4)

Chronic Kidney Disease (CKD)

Chronic Liver Disease (CLD)

Chronic Myeloid Leukaemia (CML)

c-Jun N-terminal Kinase (JNK)

Cutaneous T Cell-Attracting Chemokine (CTACK)

Cytochrome P450 (CYP)

Damage Associated Molecular Patterns (DAMPS)

Diabetic Nephropathy (DN)

Drug Induced Liver Injury (DILI)

Epithelial Neutrophil Activating Protein 78 (ENA78)

Extracellular Matrix (ECM)

Extracellular Signal Regulated Kinas (ERK)

Food and Drug Administration (FDA)

Formalin Fixed Paraffin Embedded (FFPE)

Gamma Glutamyl Transpeptidase (γGT)

Glycoprotein 130 (gp130)

Granulocyte-Macrophage Colony Stimulating Factor (GM-CSF)

Haematoxylin and Eosin (H&E)

Heat Shock Protein 70 (HSP70)

Hepatic Stellate Cells (HSC)

Hepatocellular Carcinoma (HCC)

Induced Pluripotent Stem Cells (iPSCs)

Inhibitor Kappa B Kinase II (IKK2)

Inhibitor Kappa B Kinase II Inhibitor VI (IKK2VI)

Inhibitor of Kappa B Alpha (IκBα)

Interferon (IFN)

Interferon Gamma-Inducing Protein 10 (IP-10)

Interleukin (IL)

International consortium for innovation and quality in pharmaceutical development (IQ)

Janus Kinase (JAK)

Lipopolysaccharide (LPS)

Macrophage Derived Chemokine (MDC)

Macrophage Inflammatory Protein 1 Alpha (MIP-1α)

Macrophage Inflammatory Protein 1 Beta (MIP-1β)

Matrix Metalloproteinases (MMPS)

Meso-Scale Discovery (MSD)

Messenger RNA (mRNA)

Microphysiological systems affiliate (MPS)

Mitogen Activated Protein Kinase (MAPK)

Mitogen Activated Protein Kinase Kinase (MEK)

Monocyte Chemoattractant Protein (MCP)

N-Acetyl-P-Benzoquinone Imine (NAPQI)

Non-Alcoholic Fatty Liver Disease (NAFLD)

Non-Alcoholic Steatohepatitis (NASH)

Non- Obese Diabetic (NOD)

Nuclear Factor Kappa B (NF-κB)

Nuclear Factor Kappa B Inducing Kinase (NIK)

Pathogen Associated Molecular Patterns (PAMPS)

Pattern Recognition Receptors (PRRs)

Placental Growth Factor (PIGF)

Platelet-Derived Growth Factor beta (PDGFβ)

Precision Cut Kidney Slices (PCKS)

Precision Cut Liver Slices (PCLS)

Precision Cut Tissue Slices (PCTS)

Programmed Death Ligand 1 (PD-L1)

Rapidly Accelerated Fibrosarcoma (RAF)

Signal Transducer and Activator of Transcription (STAT)

Solute Carrier Family 22 Member 1 (SLC22A1)

Solute Carrier Family 22 Member 2 (SLC22A2)

Solute Carrier Family 47 Member 1 (SLC47A1)

Solute Carrier Family 47 Member 2 (SLC47A2)

Suppressors of Cytokine Signalling (SOCS)

Tissue Inhibitor of Matrix Metalloproteinases (TIMPS)

Toll-Like Receptors (TLRs)

Transforming Growth Factor Beta (TGFβ)

Transforming Growth Factor Beta- Activated Kinase (TAK)

Tumour Necrosis Factor (TNF)

Unilateral Ureteral Obstruction (UUO)

Vascular Endothelial Growth Factor A (VEGF-A)

Chapter 1. Introduction

1.1 Liver Biology

1.1.1 Basic Anatomy and Cell Types

Macroanatomy

The liver is the largest internal organ in humans, weighing about 1.5kg (1). It is supplied by the hepatic artery with oxygenated blood and the portal vein with nutrient rich deoxygenated blood. The hepatic vein and bile duct are responsible for draining waste products and bile respectively, from the liver. The functional unit of the liver is the lobule. It is roughly hexagonal in shape, marked by a portal triad at each corner with a central vein in the middle (Figure 1). The portal triad consists of a branch of the hepatic artery, a branch of the portal vein and an intrahepatic bile duct. Highly fenestrated vessels known as sinusoids, run through the lobule, supplied by both the hepatic artery and the portal vein. They bring the mixture of oxygenated blood and nutrients to multiple rows of hepatocytes, enabling a bidirectional flow of components for filtering and absorption. The waste products from the liver are either carried away to the inferior vena cava through the hepatic veins in one direction, or bile products such as salts, bilirubin and phospholipids are removed in the opposite direction via bile canaliculi draining eventually into duodenum (1–3).

Organs such as the lungs and kidneys have limited regenerative capacity, however the liver is able to, under normal conditions, fully regenerate and replace lost cells. The regenerative capabilities of the liver will diminish in response to prolonged and/or repeated insult, culminating in end stage liver disease (1,4).

Hepatocytes

Hepatocytes make up around 80% of the total cell population in the liver. They are arranged into cords which run from the peri-poral zone, at the portal triad, to the peri-central zone, at the centre of the lobule (Figure 1). They are polarised cells with an apical membrane forming bile canaliculi and a basolateral membrane adjacent to the sinusoids and are unique in that they may have several apical and basolateral domains across the cell membrane (2).

Hepatocytes have a wide range of functions in the healthy liver. The maintenance of glucose and iron homeostasis, and metabolism of lipids are all crucial roles of hepatocytes.

These functions make the hepatocyte a protein and biliary secretion factory. They produce large quantities of albumin, clotting factors for blood maintenance, as well as bile acids for emulsification of dietary fats (2). They also act as a biological filter, removing potentially toxic substances from the blood that arrive via the gastrointestinal tract to protect other organs. By producing drug metabolising enzymes such as cytochrome P450's, hepatocytes are able to chemically alter xenobiotics leading to their activation, detoxification and solubilisation ready for excretion, usually via the renal system, from the body (2,5).

Stellate Cells

Hepatic stellate cells (HSCs) or Ito cells, were discovered in 1876 by von Kupffer and make up around 10% of the liver cell population. They reside in the Space of Disse which lies between the sinusoidal endothelial cells and the hepatocytes (6,7). Normally in a quiescent state, the most distinctive feature of HSCs is the storage of vitamin A held within lipid droplets in the cytoplasm. In response to paracrine damage signals, HSCs transdifferentiate into proliferative, contractile myofibroblasts which are capable of enhanced production of extracellular matrix (ECM), cytokines , matrix metalloproteinases (MMPs), and tissue inhibitor of matrix metalloproteinases (TIMPs), creating a pro-fibrotic and pro-inflammatory environment (6,8). This activation occurs in response to liver damage with the goal of tissue repair. During transdifferentiation, HSCs lose their vitamin A storing capacity and produce alpha-smooth muscle actin (αSMA), pro-fibrotic cytokines, such as transforming growth factor beta (TGFβ) and platelet-derived growth factor beta (PDGFβ), and pro-inflammatory cytokines which can recruit immune cells, as well as significant upregulation in ECM genes such as collagen 1A1 (6,7,9). Once the insult has ceased and the fibrotic stimuli resolved, a large proportion of HSC are able to deactivate and return to a quiescent phenotype and relocate back to the Space of Disse with a lower threshold for reactivation than naive quiescent HSCs. Cells may be cleared via apoptosis. The chronic activation of HSC by prolonged liver injury can result in the development of fibrosis and subsequently cirrhosis, increasing the risk of liver cancer (9–11).

Kupffer Cells

The liver microanatomy leads to the exposure of hepatocytes to toxins and pathogens such as alcohol, drugs or viruses (2). Liver resident macrophages, known as Kupffer cells,

are responsible for identifying and eliminating pathogens that enter the liver from the gastrointestinal tract via the portal vein, before they cause damage to the liver parenchyma. These phagocytes reside within the sinusoids, adhering to the endothelial cells that comprise these vessels (12).

In response to liver injury, Kupffer cells produce pro-inflammatory cytokines and chemokines to recruit other immune cells and activate HSC. Their numbers are increased in chronic liver diseases caused by excessive alcohol, hepatitis viruses and metabolic disorders (13). More generally, macrophages can be polarised to M1 type or M2 type which are pro or anti-inflammatory/fibrotic respectively in response to various stimuli. During the early response to tissue injury, M1 type macrophages promote fibrosis and inflammation to promote wound healing and removal of cell debris, in the later stages there are more M2 type cells which promote scar remodelling (14).

1.1.2 Zonation of liver

The concept of zonation of the liver lobule was first described by Rappaport in the mid 1900's (15). These zones are the peri-portal zone (zone 1), the midzone (zone 2) and the peri-central zone (zone 3). As well as the zones being defined by what architecture is distinct to a local area, oxygen concentrations, nutrient availability and susceptibility to damage are different in each zone (15,16). Hepatocytes in the oxygen rich peri-portal zone carry out the majority of metabolic functions such as protein synthesis and lipid metabolism, whereas cells near the peri-central region are relatively oxygen poor are responsible for the biotransformation of most xenobiotics (Figure 1) (16–18).

Loss of liver zonation can occur as part of the development of liver disease but this is not always well characterised. The impact of fibrosis has been shown to have a catastrophic impact on lobule homeostasis. Using multiple etiologies, fibrosis disrupts the natural gene expression patterns across the lobule and pushes the peri-central regions to adopt a peri-portal pattern instead. This results in loss of cytochrome P450 enzymes within the central region and an increase in blood ammonia concentration (18,19).

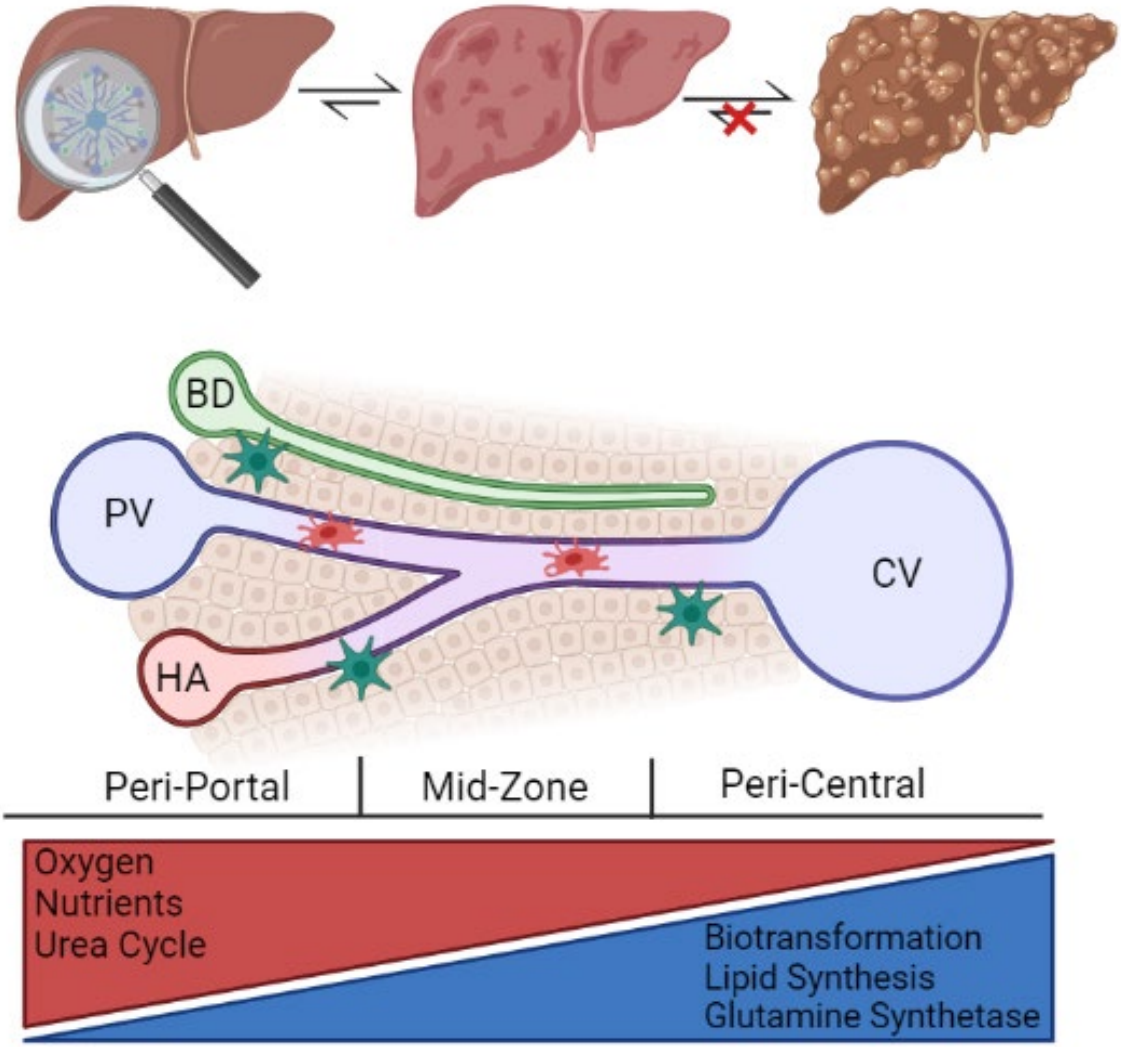

Figure 1. Anatomy of the Liver

The basic functional unit of the liver is the hexagonal shaped lobule, with a central vein (CV) in the middle and a portal triad consisting of a portal vein (PV), a hepatic artery (HA) and bile duct (BD). Hepatic stellate cells (green) reside in the space between the hepatocytes and sinusoids and Kupffer cells (red) patrol the vessels, alert to pathogens and toxicants that may enter the liver from the gut. Progressive damage to hepatocytes can develop into chronic liver disease. This damage is considered reversible to a point, but prolonged insult from drugs/alcohol, high fat diet or viral infection can cause such severe damage the regenerative capability of the liver is lost and cirrhosis of the liver develops. The lobule can be split in to 3 zones across which a gradient of numerous metabolic processes has been established. Image created in Biorender.

1.2 Kidney Biology

1.2.1 Basic Anatomy and Cell Types

Macroanatomy

The kidneys compose part of the renal system. Bean shaped and small in size, these organs are very complex in their microanatomy (20). They receive around 25% of cardiac output via the renal artery and are subsequently drained by the renal vein and ureter. There is an oxygen gradient across the kidney where 85% of renal blood is within the cortex and 15% across the medulla (21). Their unique vasculature leaves the kidney vulnerable to injury from drugs and, unlike the liver, they are not able to regenerate fully so any damage caused is permanent (20,21).

The functional unit of the kidney is the nephron (Figure 2), there are an estimated 1 million nephrons within each kidney. Nephrons span both the cortex and medulla in a loop with a capillary network surrounding each one (peritubular network) (20). The glomerulus is at the head of the nephron and is the site of initial plasma filtration. The capillary bed in the glomeruli is fed by the afferent arteriole from the renal artery, these fenestrated vessels allow small molecules to leave the blood plasma into the proximal convoluted tubule. Blood exits the glomerulus via the efferent arteriole which goes on to form the peritubular network. From the proximal convoluted tubule, the loop of Henle descends down to the medulla then ascends back into the cortex. The tubules are lined by epithelial cells that are able to reabsorb large amounts of the glomerular filtrate, whilst excreting metabolic waste products and toxins from the blood that were too large to pass through the initial filtration system. The distal convoluted tubule is the last part of the renal tubular system and it clears the newly formed urine away into the collecting ducts, leading to the bladder (20,21).

The Glomerulus

The glomerulus is situated at the head of a nephron, also called the renal corpuscle. Contained within the Bowman's capsule sits a capillary network which enters and exits the glomerulus at the vascular end (20). Opposite to this is the opening to the remainder of the nephron via the proximal tubule. There are a number of specialised cell types that reside within the glomerulus which filter the blood and keep the blood and urinary products separate. Starting at the outermost layer of the glomerulus, there is a basement

membrane with a layer of parietal epithelial cells facing into the Bowman's space (20,22). This space is a cavity between the parietal epithelium and the visceral epithelial layer. Also known as podocytes, the visceral epithelial cell layer covers the outer side of the glomerular capillaries (22,23). The podocytes and the capillary epithelial cells share an ECM known as the glomerular basement membrane. This three-layered barrier is responsible for the filtration of molecules based on size and charge. Small positively charged molecules are able to pass through the barrier to form pre-urine whereas larger proteins and molecules with a negative charge remain in the blood and are carried through the capillaries to the peritubular network (20,22). Located in between the gaps in the capillary bed are mesangial cells, these make up 30-40% of the cells within the glomerulus. They provide structural support to the glomerulus and direct the fate of precursor cells in the local area. Mesangial cells display phagocytic properties and are able to attract immune cells in response to injury alongside repairing the damage themselves (20,23,24).

The Proximal Tubule

The proximal tubule is the first section of the nephron post glomerulus. It receives the filtered pre-urine from the Bowman's space and its primary function is to reabsorb most of what has been lost to this filtrate (20). In humans, there are three distinct sections of the proximal tubule named S1, S2 and S3 (20,23). The S1 segment begins at the glomerulus and includes roughly two thirds of the convoluted section, the S2 segment includes the last third of the convoluted tubule and the beginning of the straight portion of the proximal tubule (pars recta). The S3 segment is the remainder of the pars recta. Differences in cellular structure and gene expression in the epithelial cells that line the proximal tubule mean that the S1, S2 and S3 segments are distinguishable from each other. These differences have been shown to make some segments more vulnerable to damage from renal toxic substances such as the inorganic chemical potassium dichromate (S1 and S2) and the cancer therapeutic cisplatin (S3) (20,23,25,26).

The Loop of Henle

The Loop of Henle is the section of the nephron that connects the proximal and distal tubules. It extends down into the medullary region of the kidney from the S3 segment of the proximal tubule and forms a hairpin bend where the ascending limb joins the distal

tubule back within the cortex (20). The ascending limb is split into two sections, the thin ascending limb and the thick ascending limb. The key function of the Loop of Henle is to maintain an osmotic gradient and is responsible for producing either concentrated or dilute urine (20,23). The cells that line this section of the nephron can be grouped into four morphologically distinct epithelial types with each specialised to maintain the osmotic gradient. The descending limb is permeable to water but relatively low amounts of sodium are able to be transported across the cell membranes whereas the thin and thick ascending limb sections are impermeable to water but are able to reabsorb ions such as sodium either passively (thin limb) or actively (thick limb) (20,27).

The Distal Tubule

The distal convoluted tubule is the portion of the nephron after the thick ascending limb of the Loop of Henle and leads into the collecting duct where newly formed urine is passed towards the bladder (20). The distal tubule regulates the concentrations of potassium, sodium and calcium in the blood plasma as well as pH (23). Cells in this region are taller than those in the thick ascending limb and have a greater basolateral membrane than apical membrane. It reabsorbs the last 5-10% of filtered sodium and chloride ions and is important in maintaining calcium and magnesium homeostasis (20,28).

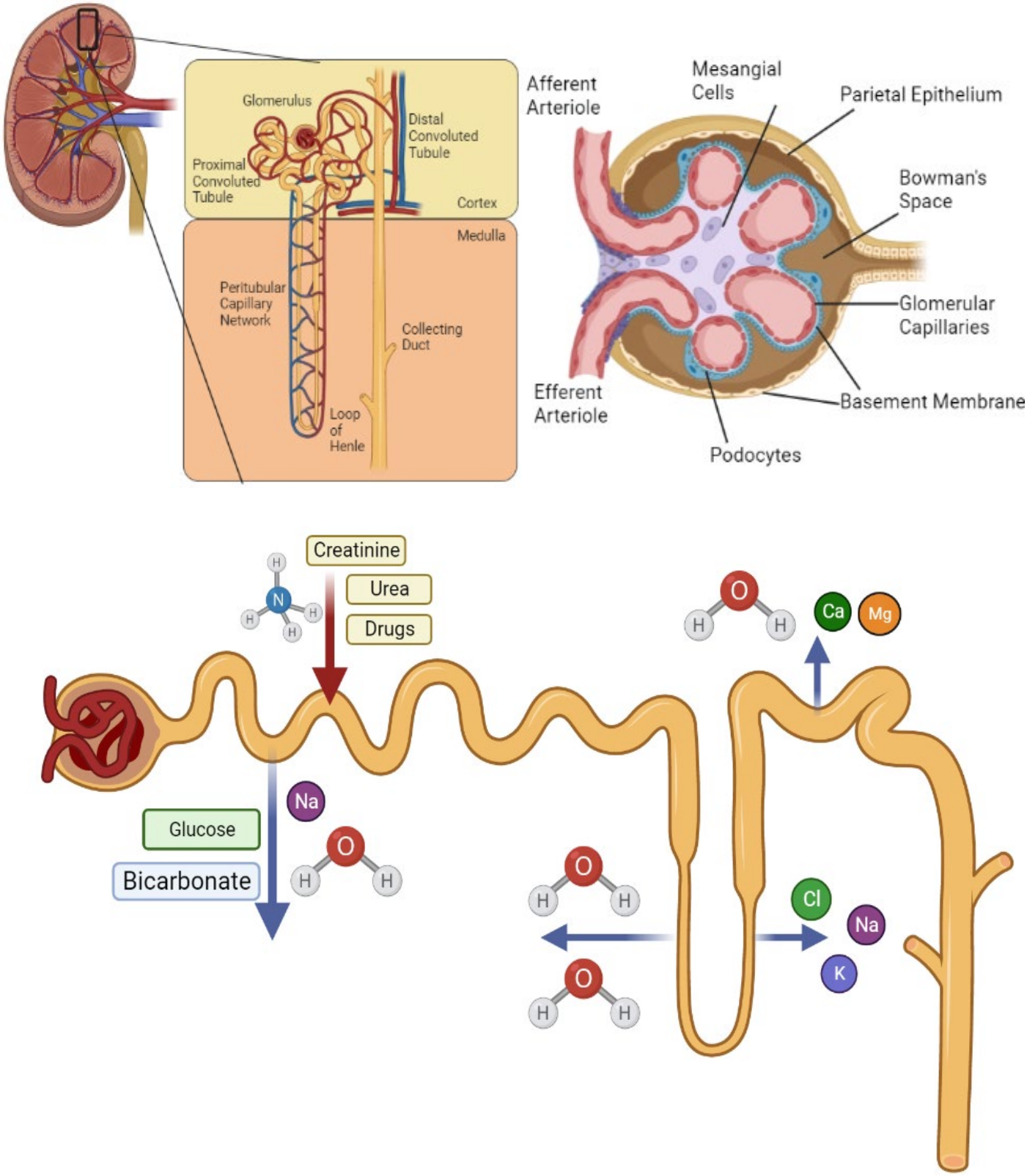

Figure 2. Anatomy of the Kidney.

The nephron spans the cortex and medulla in the kidney. The glomerulus sits at the head of the nephron within the cortex, this is the site of filtration from the blood. Across the proximal convoluted tubule, loop of Henle and distal convoluted tubule, water, ions and other small molecules are reabsorbed and larger waste products are moved from the peritubular network across into the nephron lumen. Newly formed urine is passed down through the collecting duct for passage to the bladder. Image created in Biorender.

1.3 The Development of Chronic Disease

1.3.1 Chronic Liver Disease

Chronic liver disease (CLD) is characterised by the loss of liver function over time and can be caused by numerous underlying pathologies. Described as 'a significant public health concern', CLD was implicated in 1.32 million deaths worldwide in 2017 (29). Hepatitis viruses B and C have historically been the major cause of CLD development, however in more recent years, global increases in obesity and alcohol consumption have seen an uptick in metabolic disorder associated CLD. It is projected that over the next 10 years, the burden of obesity and alcohol related CLD could increase by 168% in the USA alone (29,30).

Metabolic dysfunction-associated steatotic liver disease (MASLD) (previously known as non-alcoholic fatty liver disease (NAFLD)) is now recognised as the most common underlying cause of CLD (31,32). It is diagnosed when an individual presents with hepatic steatosis (lipid accumulation in the liver) where there are no other secondary causes such as excessive alcohol consumption, viral infection or hereditary disorders (31). These patients tend to present with other comorbidities such as type 2 diabetes. The current gold standard for diagnosis and prognosis is a liver biopsy which is invasive and comes with risk of complications. Less invasive methods of diagnosis such as imaging or biomarker panels have been suggested, however there are currently no widely accepted methods for establishing disease state (31). Steatotic liver disease encompasses a range of disorders beginning with simple steatosis to, MASLD, MASLD with increased alcohol intake and non-alcoholic steatohepatitis (NASH) (32). NASH is associated with chronic inflammation of the liver and often leads to the development of fibrosis (33). Steatotic liver disease is considered to be reversible with significant lifestyle changes to diet and exercise as there are currently no approved therapeutic interventions available to these patients (34). In cases where CLD develops past the reversible stages, patients develop cirrhosis of the liver, which is considered end stage disease (33). Patients at this point may have a significantly reduced liver functionality resulting in portal hypertension, ascites and internal bleeding along with a higher risk of developing hepatocellular carcinoma (HCC). The focus at this point for patients is more management than cure, with liver transplant currently the only life-extending option (33,35).

1.3.2 Chronic Kidney Disease

Chronic kidney disease (CKD), like CLD, is a progressive disorder that disrupts the structure and function of the organ over time and can develop as a result of a range of pathologies (36). Diagnosis is defined as a reduction in glomerular filtration rate to less than 60ml/min per 1.73m^2 with blood and protein in the urine present for more than 3 months (36). CKD is a significant health threat that effects 10-15% of the global population, equating to approximately 840 million people. CKD is projected to become the 5th leading cause of death globally by 2040 (36,37).

Diabetes is considered the most common cause of CKD, with 40% of diabetic patients developing diabetic nephropathy (38). There are also conditions that arise as a result of co-morbidities such as hypertension and glomerulonephritis that contribute to the development of CKD (38,39). Glomerulonephritis is an inflammation of the glomerulus and can result from a range of other pathologies including viral and bacterial infection. The exact mechanism behind the development of glomerulonephritis is not fully understood. Whilst this may begin as an acute injury, repeated flare ups can cause scarring and the development of CKD (38,39).

1.3.3 Inflammation

Pathogenesis

Inflammation is a common feature of almost all human disease and can be thought of as both protective and pathological (40). Acute inflammation is a response to a disruption to the norm as a result of injury or infection, bringing immune cells to the site via chemotaxis to defend against invading pathogens and promote wound healing. Acute inflammation aids in wound healing, but persistent inflammation is a driver of chronic disease. In the liver, chronic inflammation can be induced by a variety of conditions including NASH, ALD, viral infection and physical injury which can ultimately lead to CLD and cirrhosis. (40–43). Also a feature of CKD, inflammation can be hugely disruptive when not properly resolved, leads to glomerulonephritis and tubular cell injury culminating in renal fibrosis (41).

Development of Inflammation

The initiation of the inflammatory response can be split into stages, recognition of detrimental stimuli, activation of inflammatory pathways, the release of pro-inflammatory cytokines and the recruitment of inflammatory cells (41). Pathogen associated molecular patterns (PAMPs) and damage associated molecular patterns (DAMPs) can be recognised by pattern recognition receptors (PRRs) on the surface of immune and non-immune cells. DAMPs are released from injured somatic cells with or without pathogens and PAMPs such as lipopolysaccharide (LPS), are present as a result of an invading microorganism (41). There are several families of PRRs with Toll-like receptors (TLRs) being the most well studied. Activation of the inflammatory system via pattern receptors is the best understood, but there are other methods including loss of homeostasis due to stressors such as extreme cold or starvation (40). From this initial recognition of danger signals, nuclear factor kappa b (NF-κB), mitogen activated protein kinase (MAPK) and Janus kinase (JAK)-signal transducer and activator of transcription (STAT) signalling pathways (Figure 3) can be activated which go on to produce cytokines for wound healing and immune cell recruitment (40,41,44).

NF-κB Signalling

The NF-κB family is made up of 5 proteins, Rel-A/p65, Rel-B, c-Rel, p105/p50 and p100/p52. This signalling pathway takes two forms, the canonical and the non-canonical signalling pathways (45). The canonical pathway is activated by a diverse range of external stimuli and involves Rel-A and p50 heterodimers which reside in the cytoplasm in an inactive state under the control inhibitors of NF-κB proteins such as inhibitor of κB alpha (IκBα). After ligand binding, a cascade of intermediary proteins results in the phosphorylation of IκBα by Inhibitor Kappa B Kinase II (IKK2), causing the proteasomal degradation of IκBα, leaving uninhibited NF-κB dimers free to translocate to the nucleus, NF-κB dependant genes, which include pro-inflammatory cytokines (44–46).

The non-canonical pathway involves Rel-B and p100/p52 (45). Under normal conditions, p100 acts as an NF-κB inhibitor preventing the translocation of Rel-B to the nucleus. After ligand binding, p100 undergoes a proteolytic processing step converting it to p52. This Rel-B/p52 dimer is then able to translocate to the nucleus and induce transcription. This pathway is much more specific, only being activated by a small number of tumour necrosis

factor (TNF) superfamily receptors, and conversion of p100 to p52 is under the control of IKK1 (as opposed to IKK2 in the canonical pathway) and NF-κB inducing kinase (NIK) (45).

JAK-STAT Signalling

The JAK-STAT pathway, activated by for example IL-6, is the simplest pathway post ligand binding, of the three major inflammatory pathways. Under the control of type 1 and 2 cytokine receptors and type 1 and 2 interferon (IF) receptors. A JAK family member (JAK 1, JAK2, JAK3 or TYK2) phosphorylates the ligand bound receptor allowing the binding of a STAT family member (STAT1, STAT2, STAT3, STAT4, STAT5a, STAT5b or STAT6) (44). The STAT protein is then phosphorylated by the JAK protein which then translocates to the nucleus. There are several receptors in the type1/type 2 cytokine and IF groups each of which can be activated by a few different ligands (more than 50 in total) but each ligand will only bind to its specific receptor. Each different receptor then interacts with a specific pairing of one JAK family member and one STAT family member which can be in turn suppressed by one member of the suppressors of cytokine signalling (SOCS) family in a negative feedback loop (47,48).

MAPK Signalling

The last, and probably most complex, of the three main regulators of inflammation is the MAPK pathway, activated by binding to tyrosine kinase receptors. Ligands include growth factors, PAMPS and TNF family members (41). The initial stimulus activates rapidly accelerated fibrosarcoma (RAF) A, B and C, apoptosis signal-regulating kinase (ASK)-1 and TGFβ-activated kinase (TAK)-1 among others. Activated RAF proteins go on to phosphorylate MAPK kinase (MEK) 1/2, ASK1 phosphorylates both MEK4/7 and MEK3/6 and TAK1 can phosphorylate MEK4/7 and also IKK (inducing NF-κB). These subsequently activate extracellular signal-regulated kinase (ERK)1/2 (by MEK1/2), c-Jun N-terminal kinase (JNK) (by MEK4/7) and p38 (by MEK 3/6) which allow transcription factors TCF/ELK1, ATF2 and AP1 to induce pro inflammatory cytokine production (44,49).

The subsequent recruitment of leukocytes, macrophages and dendritic cells in response to these cytokines, remove the source of the injury, clearing pathogens and damaged cells ready for healing and repair (40,50).

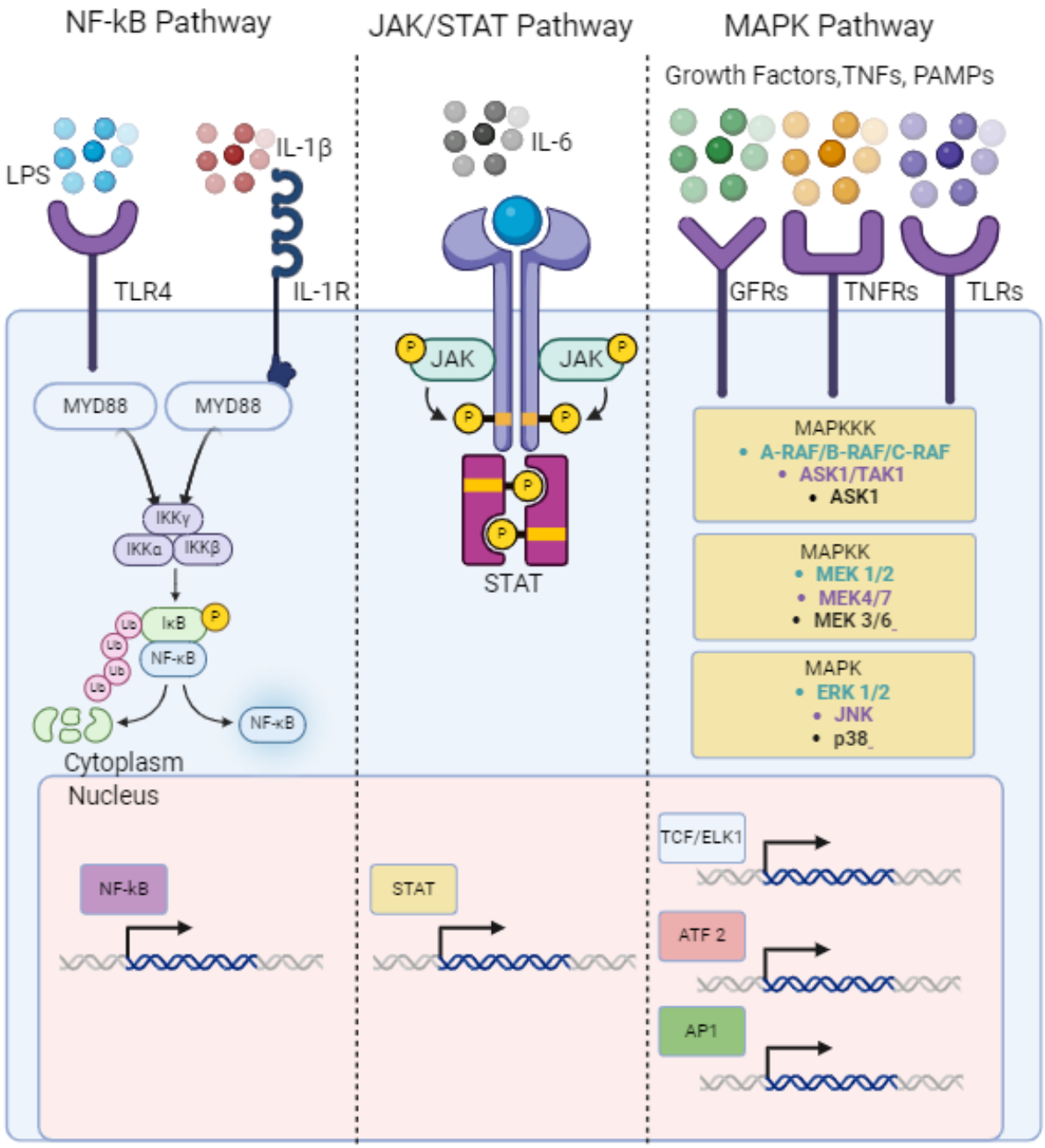

Figure 3. Inflammatory Regulatory Pathways

NF-κB Pathway: Activated by binding of ligands such as IL-1ɓ to TLRs and IL-1R. Binding recruits MyD88 and downstream signalling by IRAK-TRAF6, activating the IKK complex which in turn goes on to phosphorylate Iκβα. This inhibitory complex detaches from NF-kB proteins which can then translocate to the nucleus to promote pro inflammatory cytokine production. JAK/STAT Pathway: Controlled by Type 1 and 2 cytokine receptors and Type 1 and Type 2 interferon receptors. Ligand binding activated a JAK family member which phosphorylates the receptor to act as a dock for a STAT family member. The STAT family member is the activated by the JAK family member and translocates to the nucleus to promote pro inflammatory cytokines. MAPK Pathway: Can be activated by GFs, TNFs and PAMPS. Ligand binding activates a MAPKKK protein, which phosphorylates a MAPKK protein which further activates a MAPK protein. MAPK proteins then go on to activate transcription factors which translocate to the nucleus to promote pro inflammatory cytokine production. Image drawn in Biorender.

Key Drivers of Inflammation

Cytokines that drive inflammation can be grouped into, TNFα and related proteins, the interleukin (IL)-1 family, TGFβs, factors that signal via tyrosine kinase receptors and factors that signal via JAK/STAT signalling (41). Many work as part of a positive feedback loop, generated by one immune cell and upon release can stimulate other immune cells. As well as drivers from somatic origin, inflammation can be induced via pathogen invasion. Produced by gram negative bacteria, LPS is recognised by TLR4 on antigen presenting cells, like Kupffer cells resident in the liver, inducing the NF-κB pathway (41,46,47).

A list of mediators involved in inflammation are shown in Table 1, with a description of some that are crucial to the development of chronic inflammation below.

Table 1. Inflammatory Mediators in Chronic Inflammation

Inflammatory Mediator	Main Sources	Function	Reference
IL-1β	Macrophages	Pro Inflammatory, Induces NF-kB pathway	(41,50)
TNFα	Macrophages and Natural Killer Cells	Pro Inflammatory, induces M1 type macrophages	(41,50)
IL-6	Macrophages and T Cells	Pro Inflammatory,	(41,50)
IL-8	Macrophages and epithelial cells	Pro Inflammatory,	(41)
IL-10	T cells and B cells	Anti-inflammatory, induces M2 type macrophages	(41,50)
IL-12	Macrophages and Dendritic cells	Pro Inflammatory,	(41)
IL-17	Natural Killer cells	Pro Inflammatory,	(41)
GM-CSF	Macrophages and T cells	Pro Inflammatory,	(41)
TGFβ	Macrophages and T cells	Anti-inflammatory, pro fibrogenic	(41,50)

MCP1-4	Epithelial and endothelial cells, macrophages and fibroblasts	Pro Inflammatory, attracts monocyte infiltration to liver	(50–52)

IL-1β

IL-β is a pro-inflammatory cytokine that, whilst not present in healthy liver, is involved in all inflammatory processes in the organ (53). It is part of the IL-1 family and has pleiotropic functions including stellate cell activation, inducing hepatocyte steatosis and amplification of inflammatory signalling. Active IL-1β binds to IL-1 receptors and is able to activate both the MAPK and NF-κB pathways and high levels have been shown to be self-sustaining (53,54).

IL-1β has a crucial role in the development of NASH, fibrosis and some cancers with some genetic variants able to accelerate disease progression (54). Its importance to the development of chronic inflammation has been shown using a range of different mouse models. Using antibodies to block IL-1β, or the creation of knock out mice targeting individual components of the IL-1 signalling pathway, has shown to significantly reduce inflammation in response to challenge compared to controls and reduce the progression of NAFLD and NASH in diet induced mouse models (54).

IL-6

IL-6 is a pro-inflammatory cytokine that can be induced by NF-κB or JAK/STAT signalling in response to TLR binding from other inflammatory mediators such as IL-1 or TNFα family members. For successful signalling, both the IL-6 receptor and signal transducer glycoprotein 130 (gp130) must be present on the surface of the cell. The gp130 signal transducer is found in many tissues but the IL-6 receptor is present almost exclusively on the surface of hepatocytes and myeloid cells. In order for IL-6 signalling to occur elsewhere in the body, soluble IL-6 receptor is produced ready to be transported to other tissues to make them receptive (55,56).

IL-6 is a key cytokine in driving the inflammatory response and so when expression and signalling becomes dysregulated numerous diseases can develop. It has been found to be an important driver in NAFLD and NASH progression, with a positive correlation between plasma levels and degree of hepatic inflammation (56,57). IL-6 knockout mice were shown to have an impaired immune response and a separate study found that the inhibition of

the IL-6 receptor reduced steatosis in mice, suggesting IL-6 as a therapeutic target for NASH patients (55,58). A similar finding was observed in CKD, where patients have higher IL-6 levels in the plasma compared to healthy controls and inhibition in mice lead to a reduction in kidney fibrosis (59). A clinical study involving over 600 patients also found an association with NASH severity and polymorphisms of IL-6 (54).

1.3.4 Fibrosis

Pathogenesis

Fibrosis is a common feature in the development of CLD. A result of aberrant wound healing and chronic inflammation, this dynamic process leads to the development of a fibrotic scar distorting local tissue architecture, compromising the functionality of the liver (60,61). If the source of injury is not removed, the development of more serious and advanced diseases such as cirrhosis or HCC can occur (61). Hepatotoxic and cholestatic injury are the 2 main categories into which a range of causative agents can be grouped in the development of CLD and fibrosis. Cholestatic injury occurs as a restriction or blockage to the flow of bile from the liver. Hepatotoxic injury is much more wide ranging and includes anything that causes injury to hepatocytes which can include drugs and alcohol, infection and metabolic syndromes such as NAFLD (60–63).

The development of kidney fibrosis shares many hallmarks with that of liver fibrosis. Excess ECM production, myofibroblast recruitment and structural damage to the organ are all observed. Fibrotic scar generation can begin in different regions of the nephron depending on the type of insult (64–66). Glomerulosclerosis describes the destruction of the capillary bed within the glomerulus. Fibrosis that develops in the glomerulus can be focal (some but not all glomeruli) and segmental (portions of but not a whole glomerulus) (67). Tubulointerstitial fibrosis develops in the space between nephrons, causing rarefaction of the peritubular capillary network, chronic hypoxia and loss of tubule cells (68). Fibrosis of the kidney can occur as a result of repeated insult from infection or drugs or as part of a more complex co-morbidity, the most common being diabetes (67).

Myofibroblast Recruitment

Resident HSC are the main source of myofibroblasts in hepatotoxic-driven liver fibrosis. These normally quiescent cells are activated and differentiate to myofibroblasts which are proliferative, inflammatory and have enhanced secretion of ECM components. In response to cholestatic injury, portal fibroblasts are the major contributors to the myofibroblast population (7). The population of activated myofibroblasts in kidney fibrosis are more heterogeneous, as they arise from a number of sources. There is disagreement as to the extent to which different cell types contribute to the overall myofibroblast population but the evidence so far suggests contributions from resident mesenchymal cells, epithelial and endothelial cells that have undergone epithelial/endothelial-mesenchymal transition and bone marrow derived cells (66,69–72).

TGFβ is considered the most potent cytokine in driving fibrosis. TGFβ binds to its transmembrane receptor, where the intracellular tyrosine kinase domain phosphorylates SMAD 2 and SMAD 3, which subsequently binds to SMAD4. This complex then translocates to the nucleus, where it induces expression of αSMA, Collagen 1A1 and Collagen 3A1 (7,10,73,74). Studies have shown that the inhibition of TGFβ can reduce the migration and activation of HSC in response to chemically induced liver damage and as a consequence, lower grade fibrosis development within the organ. These highlight the importance of TGFβ in the development of fibrosis and the therapeutic potential of this cytokine (75,76).

PDGFβ is another key mitogen in fibrosis development. Produced by myofibroblasts, it drives proliferation and migration in a positive feedback loop. Both PDGFβ and its receptor are rapidly upregulated at the onset of liver injury (7,10,73). The importance of PDGFβ as a driver of fibrosis has been demonstrated using different techniques. Inhibition with drugs suppressed the migratory ability of HSC in culture and also prevented their activation to myofibroblasts. The subsequent anti-fibrotic effect of this was observed in carbon tetrachloride (CCl_4) treated rodents, where inhibitor treated animals developed significantly less fibrosis in their livers than the vehicle control group (76,77).

Fibrotic Scar Formation

Acute injury to the liver normally is resolved by a wound healing response, during which myofibroblasts secrete large quantities of pro-fibrogenic ECM components. These include

mostly collagens (type I and III) for structural support, but also enzymes that modulate the ECM such as TIMPs which block the breakdown of the newly developed scar. Post regeneration of hepatocytes, the newly made fibrotic scar is remodelled and removed by the action of MMPs (61,71,78,79). Persistent injury from alcohol/drug intake, high fat diet or viral infection causes a continual cycle of hepatocyte death and fibrotic scar development (80). Cellular injury releases DAMPs, recruiting immune cells and myofibroblasts to the site of injury (81). The resulting pro-fibrotic ECM production replaces the non-fibrogenic collagens and inhibits the production of MMPs forming a dense scar that is not remodelled. It has also been found that deactivated HSC have a lower threshold for repeat activation compared to their naïve counterparts making repeat insult more likely to contribute to an already developing scar. The scar that develops overtime distorts the local architecture, compromising nutrient and metabolite exchange in the organ (10,80,81).

1.4 Development of Novel Therapeutics and Preclinical Screening

The research and development of new therapeutics is suggested to cost as much as $2.8 billion per new medicine (82,83). This great expense is accompanied by a complicated development pipeline starting at target identification and basic scientific research, moving to preclinical work with lead candidate identification, culminating in approval from medical authorities such as the Food and Drug Administration (FDA) for sale post human clinical trials (84). With drug attrition rates across all clinical trial phases at around 95%, the probability of a novel medication moving from clinical trial to market stands at 8% (85). Toxicology accounts for 20-40% of these eliminations, with the liver and kidney being common sites of drug induced damage (84,85).

1.4.1 Current Pitfalls in Identifying Toxic Candidates

Drug induced hepatotoxicity or drug induced liver injury (DILI) remains a concern for the development of new drugs and the current use of approved medications. The liver is particularly susceptible to toxicity from drugs due to its central role in xenobiotic metabolism and drugs that cause DILI can be hepatotoxic, cholestatic or a mixture of both (86). Clinical signs of hepatocellular injury include an elevation in alanine amino transferase (ALT) and aspartate aminotransferase (AST) with fatigue and weakness in the patient. Cholestatic injury presents differently with increases in alkaline phosphatase (ALP) and gamma glutamyl transpeptidase (γGT) and jaundice and itching experienced by the patient. Drugs that cause a mixture of both injuries to the liver show all of these features clinically (86,87).

Direct hepatotoxicity is caused by ingestion of drugs that have an intrinsic toxicity to hepatocytes (86). Acute hepatic necrosis can be observed in patients affected by direct hepatotoxicity, alongside increased serum levels of ALT and AST. The liver response is reproducible in preclinical models and is dose dependent, so predicting response and suitable doses for patients can be done with a degree of confidence. Indirect and idiosyncratic hepatotoxicity are much more difficult to predict when developing new therapeutics (86). These types of liver damage are much more difficult to model and are not dose dependent. Symptoms may not appear until several months after the course of treatment making it difficult to determine a link (86).

The difficulty in predicting adverse responses of new drugs in whole organ systems becomes very apparent when we consider that 20% acute kidney disease (AKD) cases are

caused by nephrotoxic medicines in critically ill patients (88). The solubilised drug metabolites are removed as waste via the renal system, exposing the cells of the nephron to high concentrations of biotransformed xenobiotics. These can affect the cells in different ways, for example tenofovir is transported into cells where it is able to inhibit the transport of other waste products from the blood to the nephron lumen. Cisplatin is another example where it is transported into proximal tubule cells and induced DNA damage. Other therapeutics like nitrofurantonin (an antibiotic), can crystallise out in the nephron lumen causing obstructions which can lead to cell death and AKD (88,89).

Currently we use mostly 2D and animal models for initial screening to test biological response and toxicity but, as discussed in more detail later, these models are not representative of human disease and it has been suggested that 90% of *in vivo* results do not match up with human clinical trial data with toxicity related predictions correct in only 43% of cases (90,91). Differences in absorption, distribution, metabolism and excretion (ADME) are the major reason behind the discrepancies resulting in a failure to identify potential adverse effects at this developmental stage (90,91).

An interesting example of differences in ADME rates between species, and the dangers of over reliance on animal modelling for toxicity identification, is paracetamol. Paracetamol is ranked in the FDA's DILI list as 'most concern' (92). This drug is widely available over the counter and when taken correctly is considered safe, however paracetamol overdose is the most common cause of DILI induced liver failure in the US. It is readily absorbed with most being broken down to non-toxic metabolites which are excreted in the renal system, during overdose the metabolic pathway becomes saturated and the toxic metabolite N-acetyl-p-benzoquinone imine (NAPQI) is able to cause cell death via mitochondrial interference (93,94). Rats however, are more resistant to paracetamol induced hepatotoxicity due to high anti-oxidant capacity and liver injury associated biomarkers decrease much faster than in humans (94).

1.4.2 Considerations for Clinical Modelling of Lead Candidates

Drug metabolism occurs in two phases (I and II). Phase I is a functionalisation reaction, usually undertaken by a cytochrome P450 (CYP) enzyme. Phase II reactions are responsible for chemically altering the resulting metabolites into more soluble compounds for their removal from the body (95). These are catalysed by a number of

different transferase enzymes. The biotransformation of drugs occurs predominantly in the peri-central region of the liver lobule with CYP3A4 and CYP3A5 being responsible for the majority of prescription medications (95). Table 2 describes the most common CYPs and transferases.

Drug metabolism and clearance can vary greatly person to person and so care must be taken when considering dosage requirements. A wide range of factors including age, sex and genetic polymorphisms can all impact the rate at which drugs are metabolised. If clearance is too slow, there may be toxicity, whereas too fast and the drug will not exert its affect (95).

Table 2. Phase I and Phase II Drug Metabolising Enzymes

Enzyme	Protein Family	Biotransformation	Expression	Reference
CYP3A4 and CYP3A5	Cytochrome P450 Group 3	30-50% of medications	Most abundant CYP in the body, expressed primarily in liver	(95)
CYP2E1	Cytochrome P450 Group 2	Paracetamol, ethanol and endogenous products such as steroids and unsaturated fats.	Predominantly expressed in liver, higher rates of expression have been linked with cancers such as HCC and colorectal cancer	(95–97)
CYP2D6	Cytochrome P450 Group 2	25% of medications	Predominantly expressed in liver, has the highest number of genetic variants which affect metabolism of about 50% of drugs it interacts with	(95)
UGT1A1	UDP-glucurono-syltransferase Group 1	Only UGT able to transform bilirubin. Along with other family members UGT contribute most to phase II reactions	Among most important UGT enzymes in the liver	(98)
SULT1A1	Sulfotransferase subfamily 1	Phase II xenobiotic-conjugating	Major role in substance detoxification in	(98)

		enzyme with a broad range of substrates	foetal liver and exhibits wide tissue distribution in adults	
GST-alpha	Glutathione S-transferases	Major phase II drug metabolising enzyme which protects against oxidative stress	Soluble GST can be identified in many tissues around the body including the liver, kidney and brain	(98)

Pre Existing Conditions

It is important to recognise that whilst a novel therapeutic may be tolerable to the liver in a healthy individual, or at least in a patient where the liver is not the primary concern, in those with pre-existing liver conditions, tolerance will likely be reduced. A prime example of this is the development of HCC which more often than not, develops on a background of CLD (99). Sorafenib is a multi-kinase inhibitor approved for HCC treatment in patients with an inoperable tumour/advanced stage cancer. Whilst sorafenib is considered to have an acceptable safety profile in patients with a functioning liver, it has been shown to cause serious liver toxicity in 0.06% of treated patients and is generally not prescribed for those with severe liver damage/terminal stage HCC (100,101). The INSIGHT clinical trial found that the efficacy of sorafenib was reduced in patients with pre-existing severe liver damage, and that time to disease progression and overall survival were also greatly reduced compared to those with a healthier liver (101). The mechanism that causes sorafenib associated liver toxicity is not currently well understood, but studies in rat and human cell lines have suggested that this small molecule inhibitor causes mitochondrial dysfunction leading to cell death (102). They also suggested that patients with reduced CYP3A4 activity, would be more at risk of sorafenib induced hepatotoxicity (102,103).

Genetic Factors

There is a high degree of polymorphism in the CYP genes in families 1-3, the families most involved in phase I drug metabolism and the metabolism of procarcinogens (104,105). Genetic variants can be categorised by metabolic phenotypes: poor, normal, intermediate, rapid and ultra-rapid metabolisers. Genotyping patients who are receiving treatments, particularly long term, is a useful tool identify those more at risk of toxic side

effects (poor metabolisers) and those who require higher therapeutic doses (ultra-rapid metabolisers) (106). A study examined the functional effect of CYP3A4 polymorphisms in healthy volunteers. Volunteers were placed in different groups, with each group given a different drug that is metabolised by CYP3A4. Drug plasma concentration was determined after a single dose and each participant was genotyped to ascertain whether clearance rate was affected by any polymorphisms in CYP3A4. Overall, the polymorphisms detected did not have a pronounced effect on metabolism and clearance compared to the wild type enzyme. There were a few instances of a difference in clearance between wild type and a variant but these were not statistically significantly different or the variant only occurred in one patient so you could not draw firm conclusions. The study design only looked at the clearance rate after a single dose, there is a possibility that a more obvious impact of the genetic variants would be seen where a prolonged dose was administered (104).

Combination Therapies

Some patients may require a multi-drug approach for treatment of one or more conditions. In these cases, it is important to consider how each of these drugs are metabolised as one may affect the other. Drug-drug interaction studies are designed to look at how co-administration of two or more different drugs will affect the pharmacokinetics of each other (107,108).

Imatinib is a tyrosine kinase inhibitor used in the treatment of chronic myeloid leukaemia (CML). Patients with CML are at a higher risk of contracting infections due to their compromised immune system and so may be given prophylactic treatment alongside their chemotherapy to reduce this risk. Some drugs used to prevent/fight these infections are known inducers/inhibitors of CYP3A4 and so will affect the efficacy of imatinib, a substrate of CYP3A4, and the overall haematological response (107,108).

Rifampicin is an antibiotic that acts as an inducer of CYP3A4. This upregulation has been shown to increase the clearance rate of imatinib. A clinical study using healthy volunteers showed that the C_{max} and area under the curve were greatly reduced when imatinib was taken alongside rifampicin compared to when used as a single agent. As a result, it was suggested that when used in tandem, the plasma concentrations of imatinib would be sub-therapeutic and remission would not be achieved. It would be interesting to have

seen this study where a steady state C_{max} was achieved and see if clearance was different as this is what CML patients would experience during treatment (109).

Alongside prescribed medications, there are some herbal remedies/foods that can alter the normal pharmacokinetics of imatinib. St John's Wort is a herbal remedy that is widely available over the counter that can induce CYP3A4 and reduce the half-life of imatinib. It is also known that grapefruit juice an inhibit the activity of CYP3A4 and so those receiving higher doses of imatinib need to be aware in case of side effects caused by the reduced clearance (107).

1.5 Pre-Clinical Modelling

Preclinical testing of novel therapeutics has been historically modelled using 2D *in vitro* experiments and animal models. Whilst there is merit in both platforms, there are significant drawbacks associated with each. Figure 4 provides a summary of models currently available for drug discovery including some of the pros and cons of each.

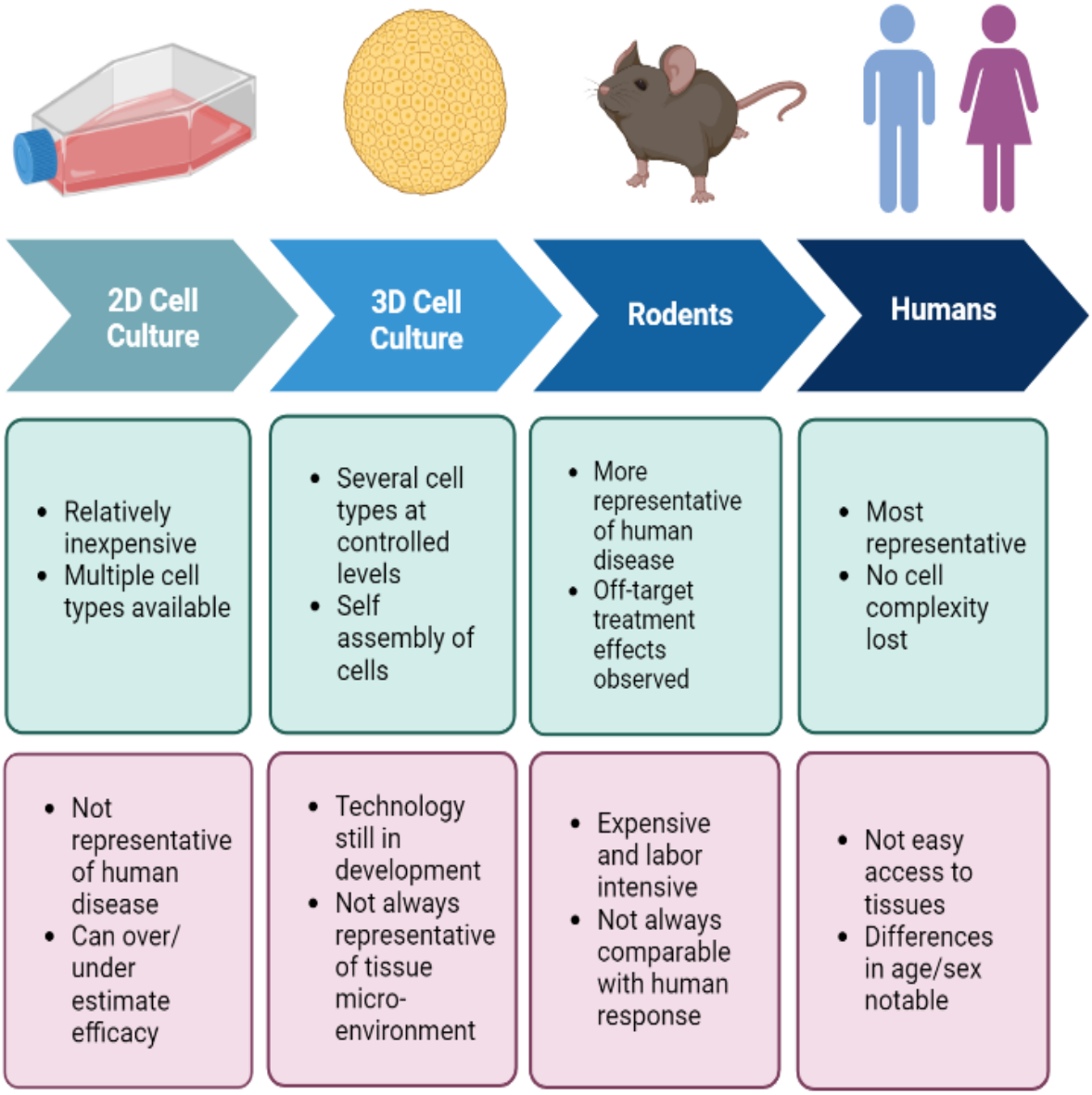

Figure 4. Current Modelling Options for Drug Discovery
Pros (green) and cons (red) of current drug discovery modelling platforms in increasing complexity from 2D cell culture to humans. Adapted from Oakley et al, 2019.

1.5.1 Two Dimensional Models

Cell Lines and Primary Cells

2D cell culture modelling is relatively cheap and time efficient and is a good starting point to test novel compounds (110). There are a large variety of cell lines commercially available produced from humans and animals, encapsulating cell types from organs, blood and tumours. Experimental setups using 2D cell culture are highly customisable, with the ability to grow cells as a single population or in co-culture with another cell type. Culture plates can also be chosen to produce high throughput systems, making screening for lead compounds using multiple concentrations very easy. However, this is not representative of the human tissue microenvironment and so results are not guaranteed to be translatable to humans (110). Alongside a low complexity environment, the cell lines used have been immortalised and will have lost a number of features commonly found in their cell of origin. For example, HepG2 is a frequently used human liver cell line. Derived from a HCC biopsy, HepG2s have been shown to have an altered gene and protein expression profile compared to both primary human hepatocyte lines and human liver tissue (111–113).

An alternative to immortalised cell lines are primary cells produced from human biopsy. These cells are more phenotypically similar to the native cell type, however they have a finite number of passages and there is not a steady supply and they can be quick to dedifferentiate when in culture (111). The young's modulus (a measure of mechanical stiffness) of tissue culture plastic is ~1000 fold higher than the cells being grown upon it, this difference results in changing of cell phenotype and the monolayer that it creates, even when multiple cell types are grown in co-culture, is not reflective of the normal architecture (114). This phenomenon can be observed when culturing HSCs. When in the liver, HSC are in a quiescent state, they differentiate to myofibroblasts in response to paracrine signalling. Experimental work to determine the signalling pathways that induce this activation, found that when grown on a hard plastic surface HSC would spontaneously activate into myofibroblasts and so the process could not be tightly controlled with this method (115). It has been shown that HSC activated in culture, have different gene expression profiles to HSC activated *in vivo*. This is likely due to the reduction in complexity and lack of one or more factors that would normally drive the trans-differentiation in the 2D model (115). We also see controversies from the use of in vitro models in renal fibrosis

research, where cell based experiments have shown EMT to be more significant source of myofibroblasts than is seen in lineage tracing experiments with human cell lines (69).

Studies that challenge cell lines are often studying efficacy rather than toxicity. Assay set up would commonly only use monoculture to map the drug response and so no data is gained reflecting how these compounds will affect the rest of the body (116). An example of this is a study using HepG2 and Huh7 cells, which identified that sorafenib (a HCC therapeutic) is toxic to some patients limiting its use, and reducing its dosage and prescribing another drug in combination may reduce the side effects whilst maintaining efficacy. Whilst this did show synergy between the two drugs, this was only performed on two HCC cell lines and did not provide any toxicity data other than apoptosis/viability assays so we do not know how this new combination would affect whole organ systems. This physiologically irrelevant environment fails to provide the wider picture of the efficacy and toxicology of potential drugs (117).

HepG2 cells have been used to model hepatotoxicity. A comparison of 2D monoculture and a more complex 3D spheroid (discussed in more detail later) made of the same cell type showed that 2D cells were less susceptible to drug toxicity (118). Four known hepatotoxicants were used at a range of concentrations, and in all cases the less complex 2D modelling showed higher cell viability at the end of treatment. It was suggested that this loss in sensitivity could be due to the loss of cell-cell contacts in monolayer culture (118). Similar findings were found in other studies comparing the two modelling systems using either other hepatotoxic drugs or liver cell lines, for example Li *et al* tested 100 drugs on 2D and 3D models and found greater sensitivity in the spheroid model (119).

Induced Pluripotent Stem Cells

Induced pluripotent stem cells (iPSCs) are an alternative to cell lines and primary cells grown from tissues. The reprogramming of mature human somatic cells to a pluripotent state was a technique discovered in 2007. Patient specific iPSCs can be generated to produce genetically diseased cells which can be used for drug screening or gene editing. They are able to proliferate indefinitely when cultured correctly whilst maintaining stable transcriptomic profiles, making them more reliable than immortal cell lines or primary cell lines. One issue that remains with iPSCs after the years of development in the field is that the reprogrammed cells display features more akin to foetal cells than mature adult cells and so is still not yet an optimal platform for drug screening (120–123).

One study that compared cell lines, primary cells and iPSCs to model toxicity of known compounds in hepatocytes found that the iPSC model was comparable to the primary derived hepatocytes, however they found that one of the drugs tested did not perform the same in the iPSCs. It was suggested that it this was due to an insufficient level of drug metabolising enzymes being produced by the cells, confirming these cells were more foetal like, as early human cells do not have the same expression profile for drug metabolising enzymes as mature adult cells (121,123,124).

1.5.2 Animal Models

Several animal species are used for safety and efficacy testing of both new and repurposed chemicals/therapeutics. These preclinical trials provide a much more representative model of drug interactions including the toxicological effect on off target organs. Animal testing for toxicity studies was introduced in the 1920's and remains the best predictor of adverse effects. Industry standards require rigorous testing in a variety of species before drugs can be introduced to the market, investigating adverse effects including amongst others, liver/kidney/reproductive damage in response to dose and exposure time. The importance of meticulous testing was highlighted in the 1950's when thalidomide, untested in pregnant animal species, was given to pregnant women with devastating consequences (116,125).

Animal models are however, more expensive and labour intensive than *in vitro* cell cultures and there are ethical implications of using animals to model human diseases with efforts now being made to reduce the number of animals used for medical science. Even though this platform is more complex, it still may not replicate adverse events accurately. Basic biological differences, including having a much shorter average life span and being smaller, give rise to scaling difficulties and a lack of longitudinal study opportunities. Small rodents are able to eliminate drugs from their body at a faster rate than humans when normalised for weight differences, as they have a higher CYP/body weight ratio. CYP isoform differences between species also confer significant differences in drug metabolism. These variations in clearance may hide or exacerbate potential toxicities or under/over exaggerate efficacy of drugs/chemicals which would only be identified much later on in the development process (116,126,127).

Fibrosis of the liver can be modelled reproducibly using either CCl_4 or bile duct ligation (BDL) methods. These methods are commonly used to induce central zone or portal zone

fibrosis of the liver in rodents, mimicking alcohol and cholestatic injury. There are mechanistic studies of therapeutics with anti-fibrotic potential which can demonstrate prevention of disease development. Whilst undoubtedly a useful model, there are some limitations with regard to how well this translates to human disease. The mice are usually very young, fibrosis development is very fast and may not display any other features associated with CLD in humans (128–131).

Induction methods vary greatly between research groups and as such the outcomes of studies not always comparable. The less extensive liver damage observed in rodents has been explained by factors including, a higher metabolism, a reduced timeline of disease progression and rodents tend to not voluntarily regularly consume high percentage amounts of ethanol (132).

Modelling CKD in rodents is more complex as there are numerous root causes and pathways of its development. Kidney fibrosis modelling in rodents is commonly induced by unilateral ureteral obstruction (UUO). This technique involves the blocking of urine flow through the kidney resulting in loss of proximal tubule cells, infiltration of leukocytes and the presence of fibroblasts which together lead to the development of tubulointerstitial fibrosis. The blockage can be removed after scar development to study the recovery and the impact of anti-fibrotic drugs. In a number of studies, therapeutics were added before and immediately after so we do not get to see the reversal for fibrosis in these instances. Further problems with this type of fibrosis model is are that the collection of clinical samples for monitoring the development of CKD is not possible and the removal of the blockage is not always successful (133,134).

A second model that can be used to demonstrate a more complex kidney disease state, is diabetic nephropathy (DN). DN begins with glomerular injury, causing structural abnormality of the whole glomeruli across the whole cortex region, and ends with tubulointerstitial damage and renal failure. DN can be induced in mice using different methods including dietary, genetic and chemical. Whilst chemical induction of DN is the quickest and easiest, toxicity related side effects of the chemicals used can limit the comparison with humans (135–137).

1.5.3 Three Dimensional Models

3D cell culture platforms for preclinical testing have gained traction in recent years as they are more comparable with the human cellular niche than 2D cell culture and animal

models. Organoids, microfluidics and bioprinting techniques have all been developed to address the drawbacks seen in 2D/animal models, making drug screening more physiologically relevant to the cellular environment in humans (126).

Spheroids

The self-organisation of spheroids, particularly heterogeneous spheroids, is what makes this model more representative of the tissue microenvironment than a 2D platform. Cells grown in this way are able to build up a more complex ECM in which efficient cell signalling can occur. Limitations associated with this model include cellular complexity and hypoxic cores (138).

As mentioned previously, immortalised cell lines may have different gene/protein expression profiles to somatic cells and so toxicity data may be skewed as a result (111–113). Kang *et al* immortalised primary cells isolated from mouse and human kidney which were able to maintain the characteristics of the original cell type and did not undergo epithelial-like to fibroblast-like transition like primary cells of the same type when in spheroid form. This model was then used to compare drug nephrotoxicity between the cells in 2D and 3D spheroid form where sensitivity to the drugs was markedly different in the 3D model. A second study looked at forming spheroids representative of the glomerulus. These spheroids could be modulated with pro-fibrotic agents to induce excess ECM production and podocyte loss. These could be subsequently treated with drugs to attenuate fibrosis development. These studies are still not complex enough to recapitulate the whole nephron, and instead focus on either the glomerular of tubular portions. For effective modelling of human disease, it is important that drug effects across the whole nephron are studied (139,140).

A further issue noted with spheroids is hypoxia and the observation that the larger a spheroid grows over the culture period, the greater the size of the necrotic core. This correlation was not only as a result of a high initial seeding level, as spheroids with a lower initial seeding volume developed a necrotic core towards the end of a 7-day culture period. Lacking the cells to develop a vasculature system, hypoxia and cell death is inevitable as the spheroid grows. Whilst a reduced oxygen environment is seen in the kidney medulla, it is not a feature in normal liver and so may not provide an accurate representation of drug interaction in healthy liver tissue. To navigate this, a shorter culture period or lower initial seeding would need to be considered (141).

Organoids

Organoids are an alternative to spheroids, more complex and produced from human biopsy, they can recapitulate (to some extent) the architectural complexity and cell type diversity of the native organ. Organoids can be produced from tissue resident stem cells, embryonic stem cells, iPSCs and tumour biopsy from cancer patients. Grown from single cells or small groups of cells, organoids are cultured within a specialised niche providing the essential factors required by the organ they are mimicking. iPSC derived organoids are preferred in cases where the model organ is difficult to biopsy, the brain for example, however adult stem cells taken are considered to be easier to propagate. Drug screening studies have been performed on cancer organoids, grown from patient tumour biopsies. One study produced breast cancer organoids which proved to be not only genetically consistent with the original tumour but were sensitive to the same therapeutics when cells were used in alternative models (142–144).

Limitations associated with this technology are similar to that of many other modelling systems. There is no vasculature developed in most cases, limiting the lifespan of the organoid as they grow larger and they generally fail to mature beyond a foetal phenotype meaning not all features of the adult cell are present. Culture is also very elaborate and expensive due to the requirement of a range of growth factors to push the stem cells towards specific differentiation pathways (142,143).

Organ-On-Chip

Organ-on-chip platforms using a microfluidic system was labelled as one of the top 10 emerging technologies in 2016 by the world economic forum. Media flow, concentration gradients and, in more recent developments, cell patterning, can be tightly controlled by the user to recapitulate the stresses experienced by tissues in the body (145).

There are several set up methods available for generating an organ-on-chip, with the ability to include multiple cell types. Prodanov et al developed a 3D model of a liver sinusoid by stacking multiple monolayers of different cell types. Primary human hepatocytes alongside representative non-parenchymal cells were used to develop the model which was shown to remain functional over a culture period of 28 days. It was noted that replacing the cell lines with primary non-parenchymal cells may provide a more accurate model of the human liver microenvironment (146).

Bioprinting

Bioprinting is a relatively new technique in 3D cell culture, using bioinks to build a tissue-like architecture. Bioinks consist of a hydrogel scaffold, the composition of which will vary across platforms, and the cells being used to build the tissue structure. There are a number of different printing techniques, but the more basic cheaper models can print as either a continuous filament (extrusion-based) or in droplets (inkjet). The cell types and relative concentrations can be user defined to produce a model of an organ that is similar to the *in vivo* microenvironment. As with any emerging technology, there are some drawbacks which include blockage of the printing nozzles due to viscosity of the bioink and cell death due to mechanical stresses (110,147).

A study from 2021 demonstrates the use of bioprinting to produce reproducible kidney organoids which contained cell types from across the nephron. They were printed as a paste which did not contain any hydrogel components and were able to self-organise into functional units. The resulting organoids were then tested for their ability to respond to known nephrotoxic substances which proved to respond in a dose dependent fashion. An interesting future development for this technology would be the use of patient derived primary cells in place of programmed pluripotent stem cells (148).

1.5.4 Precision Cut Tissue Slices

Precision cut tissue slices (PCTS) offer an *ex vivo* alternative for 3D disease modelling. Initially devised in 1920s-1930s to study liver function, PCTS are now being used to also study extra-hepatic organs such as the kidney, heart and lung. PCTS can be used to study organ function, disease development or therapeutic efficacy and toxicity. The main attraction of this system is that the tissue origin can be human, cutting out the need for less representative tissue sources such as rodents and immortalised cell lines. The resulting slices used in culture, contain all the cell types of the intact organ in the correct proportions and positions so have the complexity required to produce data that is more physiologically relevant than other 2D and 3D models. The main limitation of this system, is accessing human tissue of sufficient quality for processing and culturing, and there is a limited window from removal from the body to culture (149).

Bigaeva *et al* used the technique to predict the efficacy of anti-fibrotic drug candidates which have shown promise in animal and 2D culture models. They compared the results

of precision cut kidney slices (PCKS) from non-diseased and fibrotic human and murine kidneys. They found species differences in response to drugs, where murine PCKS responded faster to pharmacological intervention than human PCKS. For example, galunisertib (a TGFβ inhibitor) was able to reduce mRNA levels of all tested ECM markers in the non-diseased and fibrotic mouse kidney slices, however, in humans only collagen 1α1 levels were significantly affected. They also saw similar differences with imatinib treatment, where a greater number of ECM markers were decreased with treatment in the mouse slices (8 out of 14 genes) than in humans (3 out of 14 genes). This highlights the danger of over reliance on animal models for drug screening. As the culture period in this instance was only over 48h, it is not known whether a greater effect would have been seen had the tissue been in longer contact with the various drugs. Accessing human tissue for research is difficult and so the development of models within the slices would be attractive rather than having to wait for organs with a specific disease background as was the case in this paper (150).

The development of a bioreactor to allow longer term culture of precision cut liver slices (PCLS) has been described by Paish *et al*. Using specialised plates and a rocker system to mimic circulation, something missing in *in vitro* systems, the slices remained viable to 96h. They found that the *ex vivo* tissue could be modulated using pro-fibrotic stimulants to generate fibrosis within the slices and these responses could be attenuated with TGFβ inhibitors, demonstrating the potential as a drug discovery tool. The major pitfall with this model was the low throughput nature of the system. In order to test a large number of novel therapeutics at different doses per donor, multiple plates would be needed which would require a large amount of tissue, something not always available with human biopsy (151).

One of the limitations identified in current drug screening models, is the mismatch in phase I and phase II drug metabolising enzymes between the native tissue and cell model. In numerous cases, these enzymes are either not expressed in the correct proportions when compared to normal adult cells or not expressed at all. Studies using human PCLS have demonstrated the stable expression of functional phase I and phase II enzymes over a 5 day culture period. This is crucial to the use of PCTS as a platform for pre-clinical drug screening (152,153).

Both direct and idiosyncratic liver toxicity models have been developed by different groups with most focussing on genetic profiling post drug treatment to identify toxicity. Zarybnicky *et al* investigated direct hepatotoxicity of constituent parts of mint containing 'natural' products which have been implicated in human poisoning at high levels with paracetamol as a comparator. They managed to generate dose dependent responses in their PCLS and also demonstrated inter-patient variability, with some donor livers showing greater sensitivity than others. The PCLS used in this study were only cultured for 24h so it would have been interesting to see whether the non-responders would have shown signs of hepatotoxicity with further treatment. Also the inclusion of more donors would have potentially helped to identify trends in the responders versus non-responders. Idiosyncratic DILI was modelled by Hadi *et al* in human PCLS. Their hypothesis was that providing the correct stimuli was present in the tissue, idiosyncratic DILI could be identified as part of pre-clinical drug screening. They induced inflammation in the slices using LPS and co-incubated with drugs known to cause idiosyncratic DILI. They found some drugs synergistically increased DILI with the inflammatory background but others did not suggesting a different mechanism of action, and a requirement for further model development when investigating this type of DILI (154–156).

1.6 Aims of Project

It is clear that new models are required for preclinical testing which can provide physiologically relevant data on the efficacy and toxicity of novel therapeutics. *Ex vivo* 3D modelling of human disease has the potential to offer the complexity that is lacking in 2D models, without the ethical dilemma and continual expense linked to animal work. We will focus on precision cut tissue models, where previously this lab has previously demonstrated the use of bioreactor technology for the extended culture of rat and human liver tissue in a low throughput format (151).

Overall our project aims are:

- Scale the current 12 well bioreactor PCTS model to a 96 well format and optimise culture conditions
- Design and test a robot system to automate the set-up of the bioreactor
- Validate disease models of fibrosis development and acute inflammation in the PCLS and PCKS
- Demonstrate 96 well bioreactor as a platform for efficacy drug screening in PCLS and PCKS
- Demonstrate use of bioreactor for toxicity screening in PCLS and PCKS

1.6.1 Scale the current 12 well bioreactor PCTS model to a 96 well format and optimise culture conditions

Optimisation experiments will be performed using the newly designed 96 well culture plate, altering media volumes ensuring the air-liquid interface remains in the plate, and the slices do not suffer under hypoxic conditions. Next, a comparative study will be set up to ensure that reducing the size of the tissue slices from 3mm to 8mm in diameter does not have a negative impact of their lifespan, measuring functionality and viability across the culture period. This bioreactor system will be fully customisable for the needs of the user, capable of testing numerous drug doses both on its own and in combination, with and without a background of induced fibrosis or inflammation. The hope is for precision cut tissue technology to be used as a tool for drug discovery to reduce attrition rates in clinical trials.

1.6.2 *Design and test a robot system to automate the set-up of the bioreactor*

The potential of introducing robotics to aid in the setup of the 96 well bioreactor will be assessed using a custom designed automated system. The robot would be designed to punch out the PCTS from 250µM thick tissue sheets and then load single slices into individual wells which could be overseen by a trained individual. The aim being that the automation of the bioreactor set up process would produce more plates in a faster time, increasing productivity and starting health of the slices.

1.6.3 *Validate disease models of fibrosis development and acute inflammation in the PCLS and PCKS*

Models of fibrosis development and inflammation in both human kidney and liver tissue, will be validated, demonstrating disease features within the slices and reproducibility between multiple donor types including age, sex and any underlying disease in the organ. These models have previously been validated in the 8mm PCLS bioreactor and our aim is to show that these treatments are as potent in the 3mm slice system, without causing significant impact on viability and functionality of the tissue.

1.6.4 *Demonstrate 96 well bioreactor as a platform for efficacy drug screening in PCLS and PCKS*

The then validated disease models will be used to show proof of concept for efficacy studies. Current mouse models are treated with drugs in the presence of induced disease to determine their effectiveness, and we hope to recapitulate this in our PCTS models. Known anti-fibrotic and anti-inflammatory drugs will be used to demonstrate that disease progression can be inhibited within the slices.

1.6.5 *Demonstrate use of bioreactor for toxicity assessment of drugs/chemicals*

Lastly the ability of these models to predict toxicity of therapeutics will be assessed. Drugs with known toxicity in liver and kidney tissue will be selected and methodologies developed to accurately predict drug toxicity. Drugs will also be tested on both donor tissue and disease-induced tissues, to see if this platform can uncover differences in drug metabolism and toxicity seen between a comparatively healthy and diseased organ.

Chapter 2. Materials and Methods

2.1 Tissue Processing and Culture

2.1.1 Animal and Human Tissue

Sprague-Dawley rats housed in RC2 cages were used for animal work. For environmental enrichment, bedding, chew sticks and cardboard tubes were provided with free access to RM3 diet (DBM diets, Broxburn, UK) and water. Animals were maintained on a 12 hour light/dark cycle. They received humane care with experiments approved by the Newcastle Animal Welfare and Ethical Review Board. Animals were humanely killed under AWERB approval.

Human liver tissue was obtained from adult patients with informed consent undergoing surgical liver resection at the Freeman Hospital (Newcastle Upon Tyne, UK). Tissue was from the normal resection margin, and obtained under full ethical approval from the NovoPath Biobank Newcastle, (REC reference: 22/NE/0054) or the CEPA Biobank (17/NE/0070) and used subject to patients' written consent. Human kidney tissue was collected from donor kidneys declined for transplantation and accepted for research, through the Newcatle Transplant Biobank under project IOT054.

2.1.2 Materials for Liver Tissue Culture

Williams E media was purchased from Sigma and supplemented with 2% FBS (Gibco, 10500-064), 2% Glutamine/Pyruvate (Sigma, G7513-100ml/S8636-100ml), 1% Insulin (Gibco, 51500-056), 1% Penicillin/Streptomycin (Sigma, P0781—100ml) and 100nM dexamethasone (Cerilliant, D-085-1ml). Low gelling temperature agarose was purchased from Sigma and made to a 3% solution with phosphate buffered saline (Gibco, D8537-500ml). Krebs buffer was made up using 1L sterile water (Baxter, UKF7114), with a bottle of Krebs Ringer Powder (Sigma, K4002-10X1L), 15mM sodium bicarbonate (Sigma, S-6014) and 1.4ml D-glucose (Sigma, G8769-100ml).

2.1.3 Generating Precision Cut Liver Slices

The liver resection tissue was placed in cold Krebs buffer on collection and kept on ice upon arrival at the lab. For 12 well plates PCLS cultures, 8mm cores were punched out of the liver using a skin biopsy punch, and blotted dry before placing into a sterilised biopsy

dish, with a maximum of 6 cores per dish. For the generation of 96 well plates, a 1cm x 1.5cm block of tissue was cut, blotted dry and placed in a sterilised biopsy dish. Cooled, 3% agarose (Sigma, A9414-100g) was then poured over the cores/tissue block and the dish placed on ice at 4°C for 15 minutes until set. A VT1200S Vibratome (Leica) magnetic stage disk was covered with a strip of tape, then the agarose block was cut from the biopsy dish, glued to the magnetic stage and left to set. The disk was attached to the stage and the cutting basin was filled with Krebs buffer. Tissue slices were cut at a speed of 0.3mm per second at a thickness of 250μm with a 15° blade angle.

For set up of the 8mm slice system, sterile 12 well bioreactor plates containing transwell inserts, were loaded with 3ml Williams E plating media plus supplements including 10mM NAC (Sigma, A0737) per paired well and a single 8mm slice was placed in each well. To set up the 3mm slice system, 300μl Williams E plating media plus supplements including 10mM NAC was added to each paired well of the 96 well bioreactor plate, the 8µm pore *96 well* transwell insert (Corning) was placed in the bioreactor and 150μl media was added to each well (totalling 600μl per paired well). Tissue sheets were placed on a silicone mat and slices were punched out using a 3mm biopsy punch. The resulting slices were placed into the transwells and visually checked they had all settled to the bottom. Bioreactor plates were placed on rockers in a 37°C incubator with 5% CO_2. Depending on the study requirements, slices would be taken at T0 for histology, RNA, protein and resazurin assays (these processes are described below). Media was changed daily, with culture media being collected and stored at -80°C.

2.1.4 Materials for Kidney Tissue Culture

Kidney media was made up using DMEM F-12 minus glutamine (Gibco, 11320033) supplemented with 2% Glutamine/Pyruvate (Sigma, G7513-100ml/S8636-100ml), 1% Penicillin/Streptomycin (Sigma, P0781—100ml) and a Renal Epithelial Cell Growth Medium SingleQuots Kit (Lonza, CC-4127). Low gelling temperature agarose was purchased from Sigma (A9414-100g) and made to a 3% solution with phosphate buffered saline (Gibco, D8537-500ml).

2.1.5 Generating Precision Cut Kidney Slices

The kidney was collected on ice and kept on ice until processing started. The 8mm cores and the 1cm x 1.5cm blocks of tissue were cut exclusively from the cortex of the kidney. Slicing and plate set up for the kidney is the same as described in 2.1.2 with the exception of the use of Krebs buffer which was replaced with Kidney media for slicing. Kidney media (described in 2.1.3) is also used in place of Williams E media.

2.1.6 Culture and Harvest of Precision Cut Tissue Slices

Specific culture times and conditions are noted within each separate chapter. Media and treatments were made up fresh each day immediately prior to their use for the duration of the culture period. In the 12 well system, 1ml culture media was collected from each pair of slices daily during the media change and the remaining media discarded. In the 96 well system, the transwell insert was placed on sterile gauze to drain the media from the wells and the media from the bioreactor plate was transferred to a 96 well plate for freezing and storage (about 450μl). New media/treatments were added to the slices in the same volumes as noted in 2.1.2.

At the end of the culture period, a number of slices were harvested for various end points as required by the study. Slices taken for histology were placed between layers of sponge and paper in a histology cassette. Cassettes were placed in 10% formalin for 24 hours, then placed in 70% ethanol for at least 24 hours. Slices were then processed using the HistoCore Pearl tissue embedder (Leica), paraffin infiltrated slices were then embedded in paraffin blocks. Histology slides were produced using a microtome, cut at 5μm for staining. Slices for RNA and/or protein were placed in Eppendorfs and snap frozen. Slices for resazurin assay were transferred to a 96 well culture plate with 90µl fresh media and 10µl resazurin dye (Abcam, ab145513) at 4.5mM. After incubating in the dark at 37°C for 1 hour, 50µl media/dye mix was transferred to a white opaque flat bottom plate (Greiner Bio-One) and read using FilterMax 5, fluorescence setting with excitation at 535nm and emission at 595nm.

2.2 Analysing Soluble Outputs

2.2.1 *Lactate Dehydrogenase (LDH) Assay*

The CyQUANT LDH assay kit (Invitrogen, C20301) was used to assess the level of cellular cytotoxicity. 25µl media from each of the conditions was placed in a Corning ½ area, flat bottom, clear 96 well plate. 25µl LDH substrate mix, made up according to the manufacturer's instructions, was added to each of the sample wells alongside a positive control (provided in the kit) and a negative control (fresh media). The plate was protected from light and incubated for no more than 30 minutes, until a colour change was seen in the positive control and sample wells. The plate was then read on a Tecan plate reader at 490nm with a reference of 680nm.

2.2.2 Aspartate Amino Transferase (AST) Assay

The AST activity assay kit (Sigma, MAK055-1KT) was used to assess the level of hepatocyte damage. 12.5µl media at a 1:4 dilution was added to a Corning ½ area, flat bottom, clear 96 well plate. The substrate mixture and standards were made up according to the manufacturer's instructions. 2.5µl of each standard concentration was added to the relevant wells with 10µl assay buffer. 25µl substrate mixture was added to all wells in the plate which was then protected from light and incubated at 37°C for 3 minutes. The plate was read using a FilterMax F5 plate reader at 450nm, then read again every 5 minutes for 20 minutes, returning the plate to the 37°C incubator in between readings.

2.2.3 Albumin ELISA

The Human Albumin DuoSet ELISA kit (R&D Systems, DY1455) was used to assess the level of secreted albumin in the culture media and was performed according to the manufacturer's instructions. Greiner Bio-One ½ area, flat bottom, medium binding, clear 96 well plates were coated with 25µl capture antibody in PBS by incubating overnight at room temperature on a plate rocker. The capture antibody was aspirated and the plate washed 3 times with 150µl PBS plus (Sigma) 0.05% TWEEN 20 (Sigma, P2287-500ml) then the excess tapped out on to paper (from here this will be referred to as 'washing'), plates were blocked with 150µl reagent diluent (RD) buffer (PBS plus 1% BSA (Sigma)) per well for 1 hour at room temperature before washing. A standard curve was set up starting at 1600pg/ml (point A) diluted 1:2 in RD buffer to point G with a blank at point H. 25µl for

each standard curve point was added in duplicate to the plate alongside 25µl of each sample (samples were diluted to a pre-determined concentration in RD buffer) in duplicate and incubated at room temperature for 2 hours. After washing, 25µl detection antibody in RD buffer was added to each well and incubated for 2 hours at room temperature. After washing, 25µl 1x streptavidin in RD buffer was added to each well and incubated in the dark at room temperature for 20 minutes. The plate was given a final wash and 25µl of substrate solution (1:1 of A:B) (R&D Systems, DY999) was added to each well. Once a pronounced blue colour change was seen, 25µl H_2SO_4 was added to the wells, on top of the substrate solution. The plate was read on a FilterMax F5 plate reader at 450nm with a reference of 570nm.

2.2.4 Collagen ELISA

The Human Collagen 1A1 DuoSet ELISA kit (R&D Systems, DY6220-05) was used to assess the level of secreted Collagen 1A1 in the culture media and was performed according to the manufacturer's instructions. The protocol remains the same as described in 2.2.3 with the exception of the standards which start at 2000pg/ml.

2.2.5 KIM1 ELISA

The Human TIM-1/KIM1/HAVCR DuoSet ELISA Kit (R&D Systems, DY1750B) was used to assess the level of secreted KIM1 in the culture media and was performed according to the manufacturer's instructions. The protocol is the same as described in 2.2.4.

2.2.6 IL-8 ELISA

The Human IL8 DuoSet ELISA kit (R&D Systems, DY208) was used to determine the amount of secreted IL8 in the culture media and was performed according to the manufacturer's instructions. The protocol is the same as outlined in 2.2.3 with the exception of the standards which started at 500pg/ml.

2.2.7 Dilution ELISA Test

Dilution tests were performed with each study to determine the appropriate amount to dilute samples so that they fit within the standard curve of the respective ELISA. The basic

protocol is the same as described in 2.2.3, with the top of the standard altering depending on the specific kit being used (this is detailed within the methods for each kit type). The samples added to a dilution test plate are selected based on an expected highest and lowest amount of what is being quantified. Starting with a 1:2 dilution of each sample at point A, samples were serially diluted by half in RD buffer to point H. 25µl of the serial dilution was added to the plate alongside the standards for incubation for 2 hours as in the normal protocol. Once the plate had been read, the dilution factor chosen encompassed both the expected highest and lowest samples making sure neither exceed the top of the standard or are lower than the bottom.

2.2.8 *Meso Scale Discovery Assay*

A 110 U-Plex Immuno-Oncology Group 1 (human) assay kit (Cat No. K15342K) was purchased from Meso Scale Discovery. Samples were diluted 1:4 with either Kidney or Liver media as appropriate, apart from selected plates where the kit recommended a 1:100 dilution. The assay was performed according to the manufacturer's instructions. The plates were read using the MESO QuickPlex SQ 120mm with Methodical Mind software.

2.2.9 Urea Assay

The Quantichrom Urea Assay Kit (DIUR-100) from BioAssay Systems was used to quantify urea levels in the culture media. 25µl of neat sample was added to individual wells in a 96-well plate. The standard from the kit was diluted to give 5mg/ml in William's E culture media and 25µl added to the plate. The blank was 25µl Williams E culture media. The working reagent was made by mixing equal volumes of reagent A and reagent B from the kit (1:1 ratio). 100µl of the working reagent was then added to the samples, standard and blank. The plate was incubated in the dark at room temperature for 50 minutes. Absorbance was read at 430nm in a FilterMax F5 plate reader.

2.3 Histology

2.3.1 Haematoxylin and Eosin Staining

Paraffin embedded tissue sections were de-waxed by submerging in Clearene (Leica, 3803600E) twice, for 4 minutes each time. The tissue was then rehydrated by placing the slides through a sequential ethanol gradient (100%, 70%, 50%), standing in each

concentration for 4 minutes and then washed under cold running water. Sections were submerged in haematoxylin stain for 3 minutes before washing under cold running water and then placed in Scott's Water for 45 seconds, until a deep blue colour emerged in the tissue section. After further washing under cold running water the slides were placed in Eosin stain for 1 minute and briefly washed under running water to remove the excess stain. To dehydrate the sections, slides were placed in 100% ethanol for 4 minutes twice, then into Clearene twice for 4 minutes each. Slides were then cover slipped using Pertex mountant (Cell Path, UN1307).

2.3.2 Sirius Red Staining

Slides were dewaxed and rehydrated as previously described and then washed in distilled water for 3 minutes. They were then submerged in 0.2% phosphomolybdic acid for 5 minutes and washed under running distilled water for 3 minutes. The slides were then placed into 0.1% Sirius red for 2 hours, protected from light by wrapping in foil, then washed under running distilled water for 3 minutes. They were then dipped in 0.01M HCl twice before returning under running distilled water for a further 3 minutes. The slides were then dehydrated and mounted as described above.

2.3.3 α-Smooth Muscle Actin (αSMA)

Paraffin embedded sections were de-waxed and rehydrated as above. Slides were placed in a blocking solution of 300ml:7ml Methanol to 30% w/w Hydrogen Peroxide (Sigma, H1009-500ml) for 15 minutes, then washed in PBS for a further 5 minutes. Sections were then microwaved for 18 minutes in antigen unmasking solution (Vector, H-3300), then washed in PBS for 5 minutes after cooling. Slides were individually loaded into a Sequenza staining rack and three drops of Avidin blocking reagent (Vector, SP-2001) were added for 25 minutes before washing out in PBS. Three drops of Biotin blocking reagent (Vector, SP-2001) was added per slide and incubated for 25 minutes before washing 3x in PBS. 100µl of 1x casein block (Vector, SP-5020) was added at a 1:10 dilution and incubated for 25 minutes before washing in PBS. 100µl of 20% pig serum diluted in PBS was added to each slide and incubated for 30 minutes. Immediately after, 100µl mouse anti-αSMA-FITC at a 1:3000 dilution was added to each slide incubated at 4°C overnight. The following

morning, the sequenza racks were equilibrated to room temperature and then the antibody washed out with PBS. 100µl of biotinylated goat anti-fluorescein antibody (Vector, BA-0601) was added 1:200 dilution for 60 minutes, then washed 3x with PBS. 3 drops ABC vector tertiary (Vector, PK-7100) was added to each slide and incubated at room temperature for 60 minutes before washing 3x with PBS. To visualised positively stained cells, 100µl DAB (Vector, SK-4100) (made up using manufacturer's instructions) was added to a slide and left until a brown colour develops (1-2 minutes). The slides were then PBS washed and removed from the Sequenza rack and submerged in a rack in PBS for 30 seconds. The sections were transferred into haematoxylin for 2 minutes, washed under cold running water and then placed in Scott's Water for 30 seconds. They were then washed under water, dehydrated and coverslips mounted as described previously.

2.4 Microscopy and Image Analysis

2.4.1 Image Capture

Representative images and images for thresholding analysis were taken using a Nikon Eclipse Ni-E microscope with a Nikon DS-F13 camera. NIS Elements software was used for image capture. Images were taken at 4x, 10x and 20x and brightness was manually adjusted. To ensure consistency of brightness across sets of images, each stain from a whole study was imaged in one sitting.

2.4.2 Thresholding Analysis

Thresholding of images was undertaken using NIS Elements software. A minimum of 5 images was taken per stain in each treatment condition at 10x magnification to achieve an accurate representation of the tissue. Where possible, care was taken to avoid areas containing large vessels and tears in the tissue to not skew the data. Separate thresholds were produced for different stains using the 96h control slices. Thresholds were built using the smallest crosshair tool on the thresholding window in the NIS Elements software. Positive staining was selected one area at a time, starting with the very strong staining areas, with the whole image being checked after each selection to make sure no background staining was also being highlighted. Once happy that the highlighted zones in the image only contained true positive staining, the threshold was saved and applied to all the images taken from one study. The binary area fraction was multiplied by 100 to

give a percentage of positive staining in each image. These values were then averaged for each treatment group and graphed.

2.5 Data Analysis and Statistics

Data analysis was carried out using Microsoft Excel 2016, with the exceptions of ELISA data which was interpolated using GraphPad PRISM 9.0, and MSD analysis using Methodical Mind Software. All graphs were produced using GraphPad PRISM 9.0. Statistical analysis was undertaken using GraphPad PRISM 9.0 with the exception of Student's T Tests for the MSD dynamic range determination being done in Microsoft Excel 2016. Statistical significance in Microsoft Excel was defined as a result of ≤0.05. Statistical significance in GraphPad PRISM 9.0 was represented by '*' symbols. * represented differences with a p value of ≤0.05, ** represented values of ≤0.01, *** represented values of ≤0.001 and **** represented values of ≤0.0001.

Chapter 3. Robot Development

3.1 Introduction

The development of novel therapeutics is estimated to cost as much as $2.8 billion due to high attrition rates amongst candidate drugs (83,85). Drug related injury to vital organs, such as the liver and kidney, is not always realised until human clinical trials, after years of preclinical development. It is clear that the current modelling systems used in the pipeline of drug discovery are not sufficient in terms of their predictive power of efficacy and toxicity, and new options must be explored (82,84). Key requirements for new preclinical systems must be that they are medium/high throughput and physiologically relevant to human biology.

3.1.1 Current Modelling Platforms

Most commonly, 2D cell culture and animal models are used to understand efficacy and toxicity of lead candidates in pre-clinical modelling. Whilst 2D culture can be adapted to high throughput and can imply efficacy or toxicity, a monolayer of an immortalised cell line is not translatable to the human tissue niche (91,116). Loss of cell-cell/ECM contacts and changes in the transcriptional profile of an immortalised cell line contribute to this mismatch (111–113). Animal models provide a more biologically representative system that can be high throughput and provide off target toxicity data. However differences in ADME between humans and rodents result in only 43% accuracy when repeated in human trials and the ethical considerations warrant a reduction in the number of animals used for these experiments (90). Replacement, reduction and refinement (the 3Rs) are important aspects for governance of ethics of animal use in experimental design. Refining methods and reducing the number of animals required to improve welfare standards, but also (and the focus of this project), replacing the use of animal models with alternative models which can provide quality data (157).

The development of 3D cell culture models provides an opportunity to produce high throughput screening platforms that are more related to the biological niche than currently used 2D models. Spheroids/organoids, microfluidic techniques such as organ-an-a-chip, and bioprinting have all been suggested as potential methods for preclinical

screening studies (91,116). The self-organisation and more complex cellular and matrix composition and interactions often creates conditions that are more physiological and therefore have the potential to provide more accurate data for drug screening than 2D models (116).

3.1.2 Precision Cut Tissue Slices as a Tool for Drug Discovery

PCTS offers an *ex vivo* tissue culture system with the potential to overcome problems currently associated with preclinical modelling systems. The tissue can be of human origin, so all the cell types are represented in the correct proportions within their natural architecture and have not been altered so the phenotype of the originating cell is not lost (158). This provides a more physiologically relevant background on which to study the efficacy and toxic potential of lead drug candidates. PCTS platforms have shown promise in the testing of currently available anti-fibrotic drugs, but the main drawback has been that PCTS can only be cultured for a short period (150). This has however been addressed in our lab with the use of a specialised bioreactor plate which successfully increases culture lifespan (158).

Our validated PCLS system uses 8mm diameter tissue slices, cultured for up to 144h with 6 pairs of slices per bioreactor. This ex vivo model can be manipulated to display features associated with various liver diseases such as fibrosis, inflammation or steatosis. This technology allows analysis of multiple outputs including soluble secreted proteins from media, RNA/protein level changes and histology from the cultured slice. Whilst an insightful system, the 12 well model is low-throughput and requires large volumes of tissue to be suited to large scale drug screening.

3.1.3 Chapter Aims

- Develop an automated system to enhance bioreactor set up
- Optimise culture conditions for 96 well bioreactor

It was recognised that the manual plating of PCTS into the 96 well bioreactor is time and labour intensive, taking much longer than the 12 well bioreactor currently in use. Development of a robot that could automate the generation of 3mm tissue slices and plate set up, could reduce time and the number of people required to produce full plates

for medium throughput studies. Working with an engineering firm to build the robot, design requirements included an attachment to hold a biopsy punch, and the ability to move between a tray containing sheets of tissue to punch out slices, and the bioreactor culture plate into which the slice could be expelled.

After development of the robot, culture conditions will be optimised. Media volumes will be adjusted to support the culture of the smaller 3mm slices in the new bioreactor plate. It will be important to maintain the liquid-air interface whilst recovering enough media to complete soluble outputs to assess viability and functionality of slices throughout the treatment process.

3.2 Methods

3.2.1 Tissue Processing

Sourcing of tissue from both humans and rodents is described in methods chapter 2.1.1. General methods for the generation of liver and kidney slices are described in section 2.1. The exception to this chapter is in the plating of the PCTS. Here the generated tissue sheets were placed into the tissue trays containing a bed of 10% agarose, with 3mm slices being punched out and plated using the robot's attached biopsy punch. In instances where slices had to be punched out manually, this was done in a petri dish containing Krebs buffer for the liver and kidney for the kidney tissue.

3.2.2 Culture and Harvest of Precision Cut Tissue Slices

General methods for the culture of liver and kidney slices are described in 2.1.6. These studies were run for 96h from set up, replacing the media every 24h. Volumes of media added were altered through the optimisation process, specific volumes used are noted within the relevant results sections. To induce fibrosis, 3ng/ml TGFB (Peprotech, UK) and 50ng/ml PDGFBB (Peprotech, UK) both reconstituted according to manufacturer's instructions, were included in the media before adding to the bioreactor. All slices were taken for resazurin assay (described in 2.1.6).

3.2.3 Analysis of Soluble Outputs

General methods are described in 2.2. For this chapter we carried out Human Albumin DuoSet ELISAs (R&D Systems) and CyQUANT LDH assays (Invitrogen).

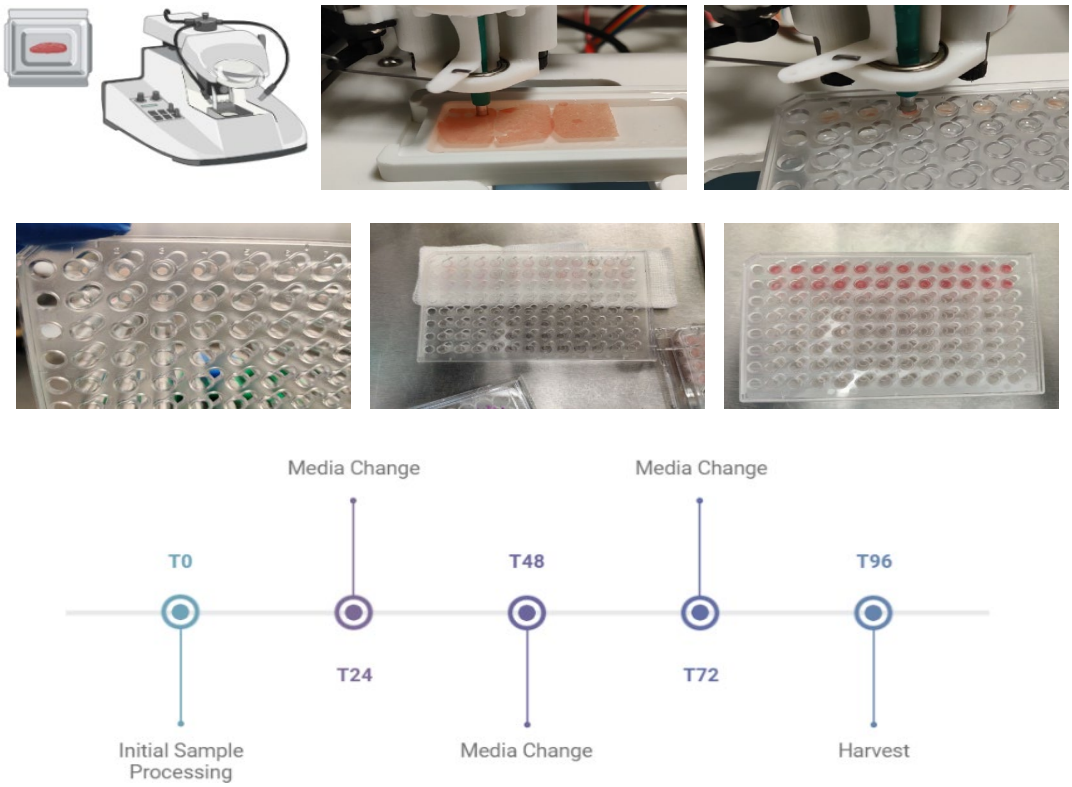

Figure 5. Bioreactor Set Up and Culture with Robot
Representative images of automated plate set up using the robot and treatment plan for plates cultured in this chapter. Tissue sheets are placed on the agarose bed in and the biopsy punch, attached to a moving arm, punches out a slice from the larger sheet. The attachment arm moves to the bioreactor plate containing 150µL media in each transwell and an individual slice is placed within the well. This process is repeated until single slices have been placed in all 96 wells. The media is then drained on sterile fabric to check that all wells contain slices. The plate is then filled with fresh, sterile media and placed in an incubator. Media is changed every 24h, storing the used culture media at -80°C, until the culture endpoint at 96 post processing when the slices are then harvested for relevant outputs which could include, resazurin assay, FFPE and snap freezing.

3.3 Results

3.3.1 Initial Set Up and Hardware Optimisation

Software Adjustments

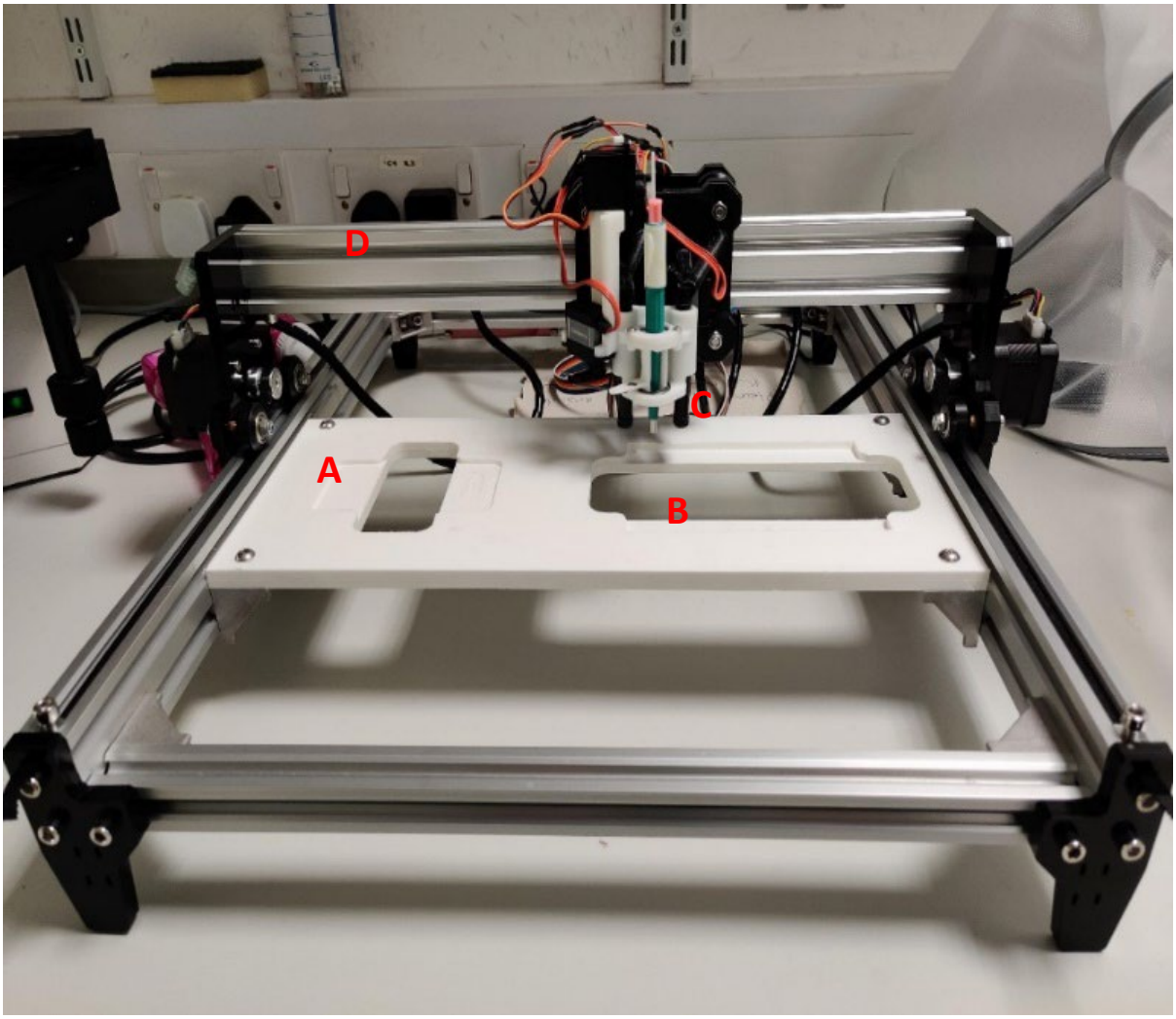

Figure 6. Robot Set Up
Section A is the tissue tray holder, section B is the Bioreactor plate holder, section C is the 3mm Biopsy punch and attachment arm and section D is the runner along which the biopsy punch holder moves in an X, Y and Z direction.

Our initial robot set up is shown in figure 6, we worked with an engineering firm to produce and further develop the machine. Using the base of a 3D printer, we designed a holder for the biopsy punch to sit in which could be moved in both X and Y directions, between a tray containing 250uM tissue sheets and the 96 well bioreactor plate. The biopsy punch itself could also be moved in a Z direction, the punch depth could be altered to account for the height differences between the tissue tray and the culture plate. The robot was controlled via a custom software program on a tablet, and the communication

between the two was achieved through a Raspberry Pi with a WiFi signal. A dry run of the movement sequence suggested one punch and plate cycle would take 11 minutes.

Initial tests to optimise the robot system were performed on rat liver tissue. For this, a 1cm x 1cm section of liver lobe was sliced to generate sheets which were placed in the tissue tray. At the start of each run the biopsy punch was manually aligned with well A1 and after stopping the run, the punch would need to be realigned to this starting position. It was swiftly realised this would be a problem for automatic plate loading if the robot had to be stopped mid run and so software was updated to include a pause button.

There were also problems with drift from the centre of the wells as the biopsy punch moved between the tissue tray and the transwell plate. It was believed that this was because of the manual positioning to A1 at the beginning of each run. A second version of the robot was designed that would be able to self-determine its starting point upon initialising.

Tissue Tray Adjustments

The biopsy punch struggled to cut against the plastic tray to cut out and pick up a slice, the result being blunting of the tool and damage to the tray. To prevent this damage and aid pickup of the slices, it was hypothesised that the addition of a layer of agarose to the tray would provide a softer surface and improve the punching process. To determine the best gel thickness and density, different concentrations of agarose were tested with increasing stiffness ranging from 3% (soft) to 10% (stiff) agarose, and tray depths from 2mm to 10mm (Figure 7). Where there was no agarose (well 1), the slices cut well but blunting of the punch occurred quickly. Wells 2, 3 and 4 punched out and picked up slices much more reproducibly. In wells 5 and 6, the tissue tended to get pushed down into the agarose bed, causing distortion in some of the slices and loss of tissue. This set up was repeated with different percentage weights of agarose and from this we decided on a 10% agarose gel at a depth of 3-4mm thick.

In order to accommodate this new addition we developed new biopsy trays with a deeper base. This made a significant difference to plating with a success rate of cutting out the slices and placing them in the tray of about 70-80%. It was noted that when placing the sheets in the tray, it was difficult to know where the biopsy punch would be cutting so tissue trays were further modified to include a sheet placement guide which could be seen through the agarose gel layer.

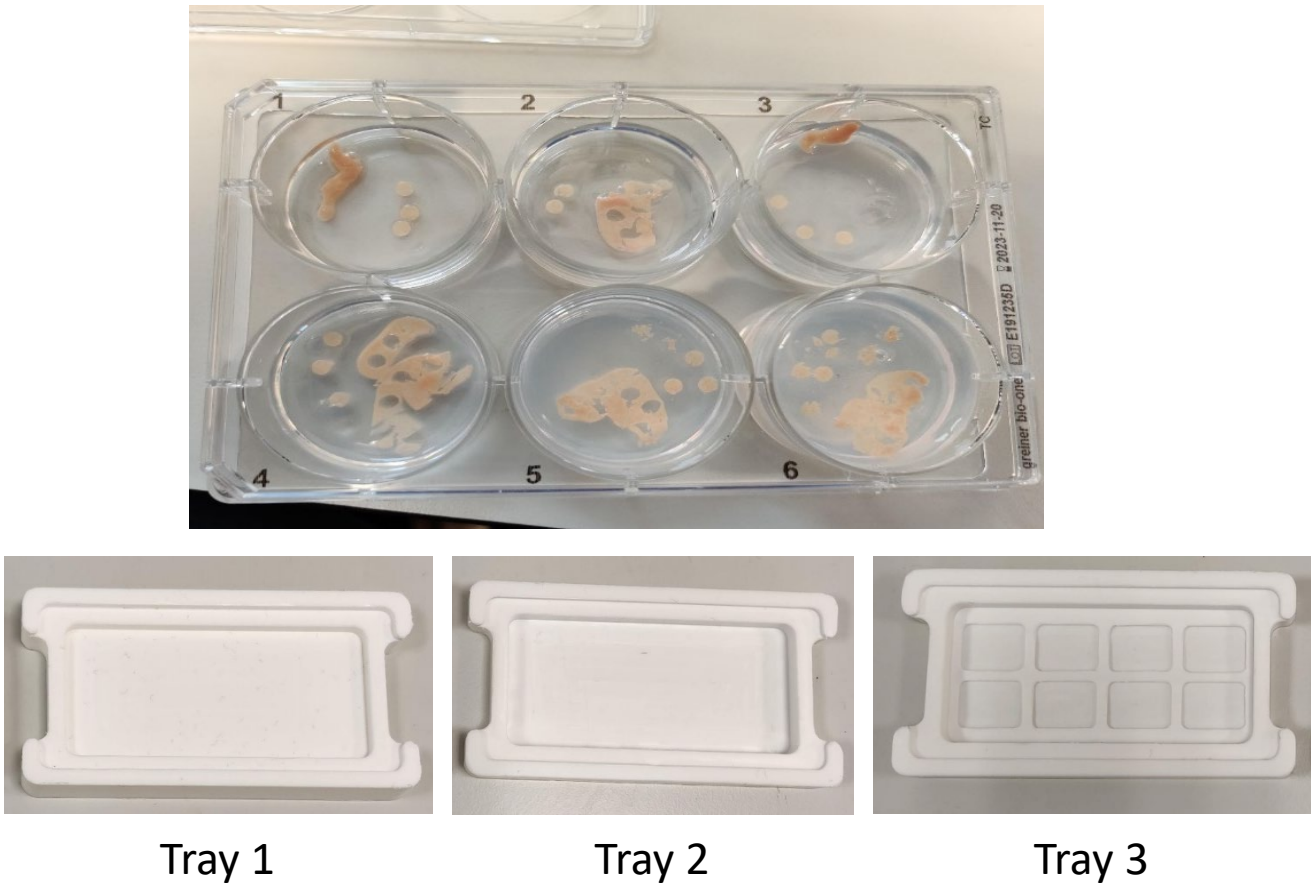

Figure 7. Tissue Tray Development
The top picture is a representative image of how we tested a range of thicknesses and percentage weights of agarose when determining the best cutting conditions for our tissue sheets.
The bottom image series shows the development of the tissue tray from a shallow (tray 1) to a deeper base (tray 2) and the addition of a tissue placement guide (tray 3).

3.3.2 Optimisation of Culture Conditions for 96 Well Format

For a first run with a look to culture 3mm PCLS in the 96 well bioreactor plate, liver tissue from a Sprague-Dawley rat was used. The resulting 1cm^2 sheets were placed side by side in the version 3 tissue tray on a 10% agarose bed. In order to get the tissue sheets into position, Krebs buffer was added to the tray and then 90% of the solution was removed of it once happy with the layout. This remaining buffer kept the slices from drying out whilst the robot was running and kept the off-cut tissue stuck to the agarose so it didn't lift away with the slice. The pickup and plating success rate of the rat liver tissue was around 70%.

After plate set up, culture conditions were then optimised. The plate was split into thirds, adding 625µl, 650µl and 675µl to each paired well of the bioreactor plate, plus 100µl into

each transwell, giving total volumes of 825µl, 850µl and 875µl. When changing media each day, a large volume of media had escaped, overflowing into neighbouring paired wells as the plate was rocked. A second rat liver plate was set up with reduced media volumes to try and prevent media spillage, with total volumes tested at 650µl, 625µl and 600µl. No media was observed to spill out from the plate, therefore a resazurin assay was carried out on the cultured rat slices at T96 to assess their metabolic activity post-culture (Figure 8A). The slices in the lower media volumes of 600µl and 625µl were more metabolically active than those in the higher media volumes at the end of the culture period.

Our second culture using the lower volumes suggested by the rat liver experiment was performed using human kidney, however the media started to move at T48. It was observed that once the media had escaped the paired wells, wetting the plate and transwell insert, leakage at later time points could not be prevented. The bioreactor system did support the culture of the kidney slices as assessed by resazurin, with the cultured slices remaining viable after the 96h culture period (Figure 8B). As observed with the rat liver tissue, the lower total media volumes seemed to support the slices better than higher volumes over the culture period to T96. For all other 96 well bioreactor tissue culture, a maximum volume of 600µl (300µl in the outer chamber of the paired well of the bioreactor base plate plus 150µl in each transwell) was used.

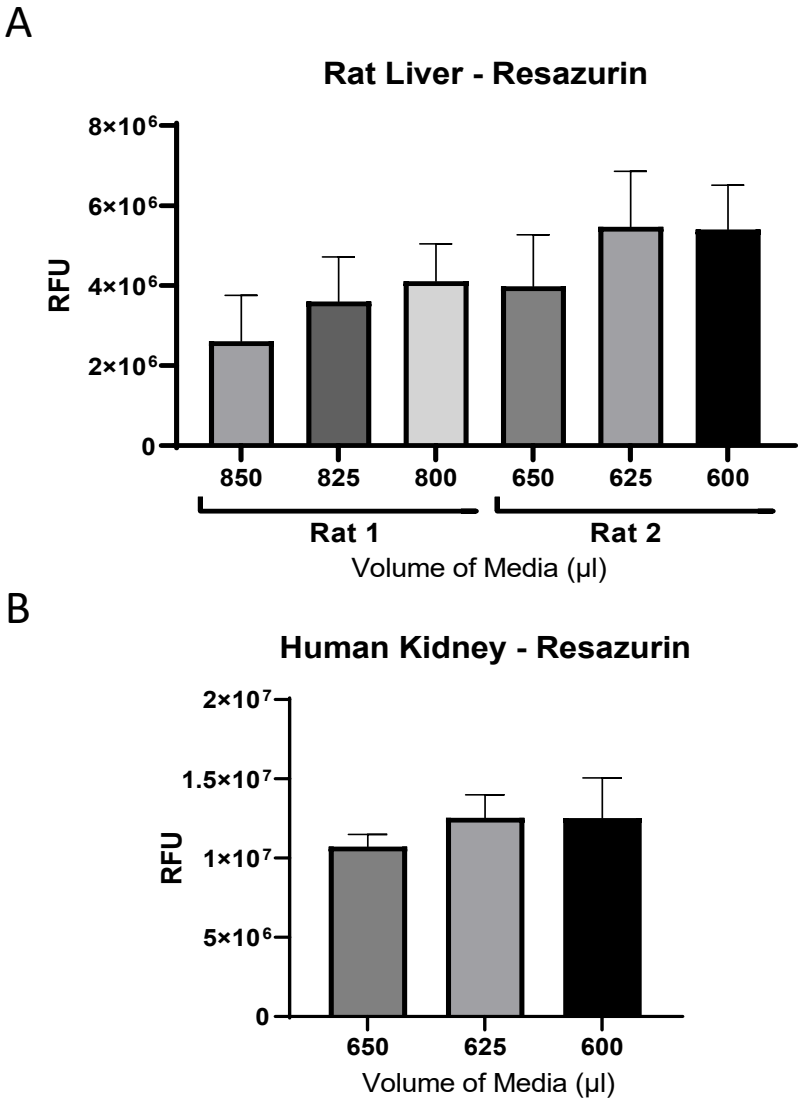

Figure 8. Optimisations of Culture Conditions for 3mm Slices
A. *Resazurin output from 3mm rat PCLS cultured in the 96 well bioreactor at 96h post processing in different media volumes.* ***B.*** *Resazurin output from 3mm PCKS cultured in the 96 well bioreactor at 96h post processing in different media volumes. Data shown are mean +/- SEM.*

3.3.3 Culturing with Optimised Conditions and Hardware

The newly optimised system was then tested using human liver and kidney to determine the usability and scalability of the system, with the hope that an individual would be able to monitor the running of several robots in parallel. Beginning with a kidney which, like rat liver, produced a large number of uniform tissue sheets with no major vessels or tears, slices were generated and then cultured for 96h and a resazurin assay was undertaken at harvest. This showed that the metabolic activity (Figure 9A) of the tissue slice had decreased over time but still appeared to be viable at the end of the culture period. Importantly there was no media transfer with the chosen media volume of 600µl. An LDH

assay was performed (Figure 9B) to check for any unexpected cytotoxicity as a result of necrotic death in the slices. This showed a high amount of LDH being released into 24h rest period media as a result of the mechanical slicing process, but quickly dropped off during the culture and by T96, was less than 5% of a positive control.

Next, a human liver was used to test the set up process as the other organ of interest for this project. Unlike the previous set ups, the resulting tissue sheets were not uniform and contained a number of vessels and tears. Sampling of the human liver is dictated by the tissue sample received from the liver resection. This made punching the slices with the robot significantly more challenging and so most of the plate was instead cut by hand. For culturing we included the Fibrosis Stimulation (Fib Stim) conditions alongside a control. All slices were harvested at T96 and metabolic activity was assessed by resazurin assay (Figure 9C). As was observed with the human kidney, the viability of the slices had dropped from T0 to the harvest point but they were alive and viable at the end of the culture period. To check that the PCLS were not just metabolically active, but were functional and healthy, Albumin ELISA (Figure 9E) and an LDH assay (Figure 9D) were run on the collected media. The Albumin ELISA demonstrated that the PCLS remained functional across the duration of the culture period. Output rose between the initial 24h rest media and 48h, then began to drop off again to 96h. The LDH showed a similar profile to the kidney (Figure 9B), initially high output in the 24h rest media, followed by a drop off after this time ending at less than 10% of positive control for (1x solution from the CyQuant kit) both the control and Fib Stim slices.

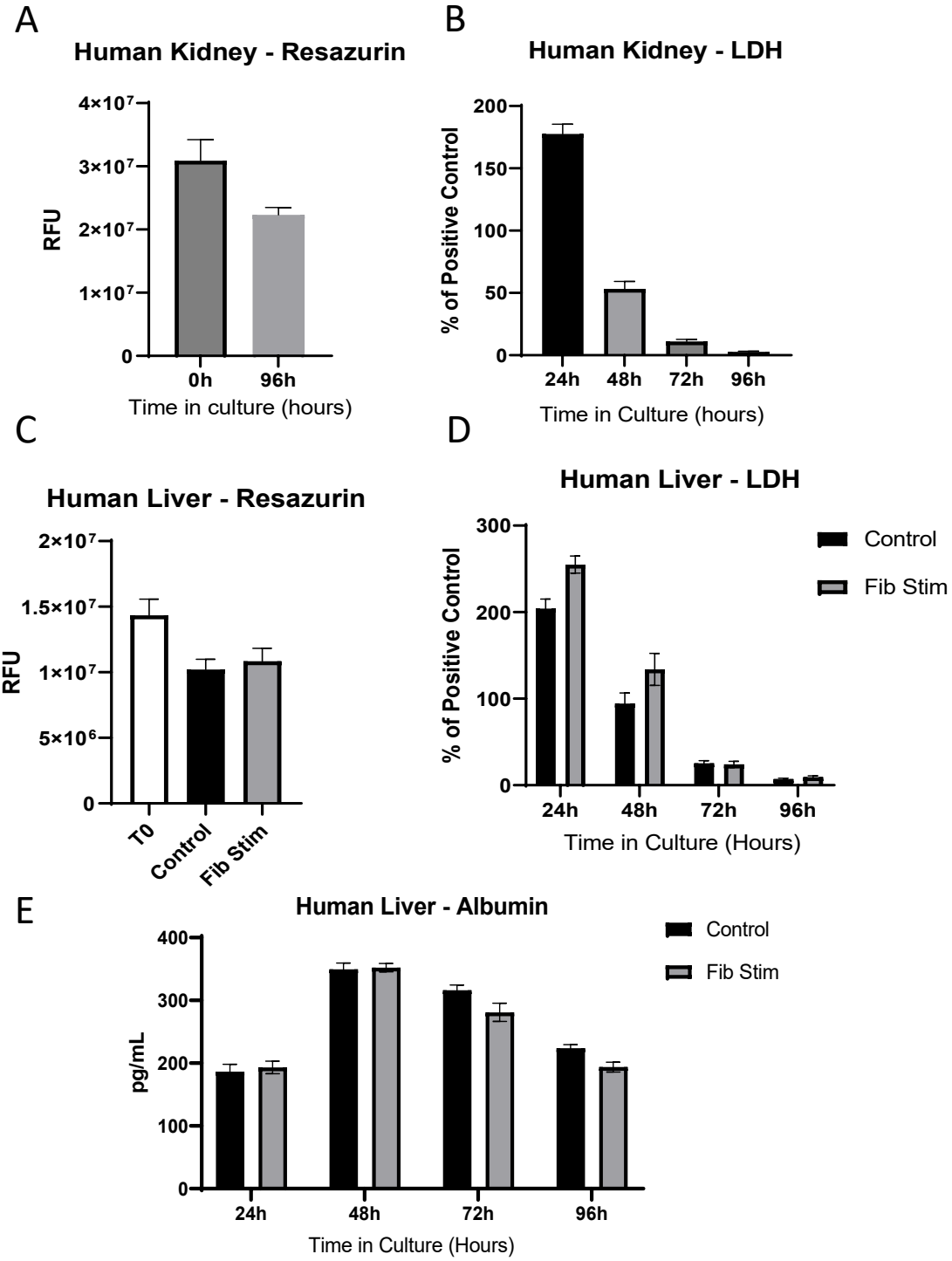

Figure 9. Culture of Human PCTS with Optimised Conditions

A. *Comparison of PCKS viability at processing (T0) and after 96h in culture.* ***B.*** *LDH release by same PCKS from A measured every 24h to 96h post processing.* ***C.*** *Comparison of PCLS viability between T0 and T96 slices treated +/- fibrosis treatment.* ***D.*** *LDH release by same PCLS as in C, measured every 24h to 96h post processing. Data is shown as percentage of positive control. The positive control used was a 1x stock taken from the kit.* ***E.*** *Comparison of soluble albumin release from PCLS between treated and untreated slices measured every 24h to T96. Data shown are mean +/- SEM. N=1 liver donors and N=1 kidney donors, n=5 technical replicates were averages for each of the treatment groups per donor.*

3.4 Discussion

3.4.1 Optimisation of Hardware

It was hypothesised that the development of a robotic system would increase efficiency of culture plate set up, producing more 96 well plates in a shorter time. Decreasing the time between biopsy collection and the end of tissue processing results in a greater slice viability.

With a first run, it was found that the biopsy punch was causing damage to the tray where tissue sheets were loaded and that the punch was unable to pick up a slice once it had been cut out for transfer into the 96 well plate. To prevent this damage and look for a solution to picking up slices, agarose was added to the tray, testing different percentage weights of agarose, increasing in firmness from 3% to 10%, and different thicknesses of each ranging from 2mm to 10mm. It was found that a firmer set agarose (at 10%) was able to more reliably cut out and pick up the tissue slices at a thickness of 3-4mm. When the agarose was thicker or less firm than these conditions the force of the biopsy punch would push the tissue into the agarose rather than cutting it. Agarose poured too thin, resulted in the punch cutting all the way through, and picking up a core of agarose with the slice. With these new conditions in mind, new tissue trays milled to a depth of 6mm to allow for this new addition.

3.4.2 Optimisation of Culture Conditions

Using our optimised tissue tray, a full plate set up was completed with the robot and cultured the resulting slices. Using a rat liver, there was a pickup and plate rate of around 70%. It was recognised however, that this tissue was healthy and uniform and so the slices being generated were likely to be of a much higher quality than expected with human tissue and so set up on human liver was expected to be more difficult. This plate was cultured for a period of 96 hours, using different media volumes to determine the optimum culture conditions for this size of slice in these plates.

The resazurin data at 96 hours post slicing showed there were small, but not significant, differences between the slices kept in different media volumes, with slices in the smaller volumes being more viable at 96h. This suggests the slices were experiencing more hypoxic conditions where there is too much media, the reduced movement in the over

full well, preventing effective oxygen penetration in the media to be utilised by the tissue slice. The increased volumes, particularly where there is media transfer increasing the volume of liquid in a well further, removed the media-tissue-air interface reducing the oxygen levels around the slice and caused the tissue to die.

The second set up and culture attempt used a human kidney. The lower media volumes reduced media escape but did not completely prevent it, suggesting the smallest volume of 600µl was most suitable. The data from the resazurin assay showed the same trend at 96h as that seen for the first rat experiment. It again suggests that the lower media volumes placed in the well and transwell, the more waste products are moved away from the slice providing oxygenation which in turn increased the longevity of the tissue. A similar finding to this was noted in the Paish (158) study.

3.4.3 Initial Runs Using Optimised Conditions

With the chosen setup and culture conditions, full runs from plating to 96h culture was attempted using human kidney and then human liver. The kidney produced uniform tissue sheets, much like the rat liver tissue, but the slice pick up was not as high, so many were manually punched and plated. The space between punched out slices on the tissue sheet was limited, resulting in some slices not being whole where the edges had been pressed into the agarose gel bed. To combat this, the user had to move the tissue around on the agarose bed to make sure whole slices would be generated. To rectify this, fewer slices would need to be punched out of a single tissue sheet and make the tissue tray larger to be able to produce the required number of slices. The subsequent PCKS culture showed that the bioreactor system could support the tissue to the 96h harvest point under our optimised culture conditions. Alongside the slices remaining alive and functional, the drop in LDH over the culture period shows the slices recover from the processing trauma after the T24 rest period and that they don't suffer further apoptosis/necrosis because of being cultured in the bioreactor plate.

The generation of PCLS using the robot proved to be more challenging than initially anticipated. As the robot could not differentiate between uniform tissue and where there were holes due to vessels, some of the slices were not perfect which would result in discrepancies between data points within treatment groups. To overcome this, the user needed to move the tissue around in the tray to ensure only whole slices were punched

which resulted in tissue wastage. Slices were also frequently not picked up and had to be manually placed in the wells. An alternative suggested approach would be to use the robot to generate the punched slices and deposit them into a 10cm dish containing media, however, it was decided that this would still not overcome the difficulties involving imperfect slices and that manual processing would be quicker.

At 96h, the PCLS were still metabolically active and functional. The 24h rest media contained lower albumin and higher LDH levels compared to the later time points, showing that the slices were able to recover from the trauma of the slicing process quickly in this system. By 96h, the albumin levels had dropped back down to near 24h. This decline in functionality is expected based on previous work but proved that the 96-well bioreactor can support functional, active slices (158). The addition of the pre-established fibrosis stimulation treatment had no effect on the viability of slices compared with the control across all 3 assays performed on the slices and media.

3.5 Conclusion

The aims for this chapter were:

- Develop an automated system to enhance bioreactor set up
- Optimise culture conditions for 96 well bioreactor

I have successfully optimised the culture conditions and demonstrated viability of 3mm precision cut tissue slices up to 96h in the 96 well bioreactor plate. The purpose of introducing a robotic system for the setup of the bioreactor was to speed up the slicing process through automation, producing more plates in a shorter time resulting in higher quality input tissue slices. In the case of the liver, there is a limit of 3 hours from biopsy to a completed slicing process, and so reducing tissue processing time is crucial to preserve cellular viability and reduce ischemia (158). The hope was that several machines could be run in tandem, setting up multiple plates in one go with each run taking just under 12 minutes per plate.

When testing this machine, it was realised that a user would need to sit and monitor the robot as it punched out each of the slices to check each well received a slice. It would also require a trained user making a judgement on what areas of the tissue are cut, potentially needing to move the tissue sheets on the tray to ensure that vessels and tears were missed, making it unfeasible for an individual to monitor multiple machines in tandem. Currently the robot can only punch predefined spaces out of the tissue tray, resulting in a difference in the quality of tissue being loaded into the plates and therefore of the end result of a study, reducing reproducibility and reliability. To allow the robot to be able to make this judgement call and increase the quality of the slices being loaded into plates, cameras and machine learning would need to be included in the software and set up of the system.

The way in which the software was set up, one sheet would have 12 slices punched and the tissue sheets that could reliably be produced were not big enough for this. It was suggested that the tissue tray could be made larger to hold more sheets but only punch 4-6 slices. Pinning the tissue into place to prevent the tissue moving around was also suggested. These changes would allow for multiple machines to run at once without the need for a dedicated individual to monitor each plate set up. A major consequence of this however, would be that the tissue wastage would increase significantly. It was decided

human tissue is too precious a resource to justify this extra tissue being discarded and so this would not be a reasonable change.

During the development of a robot which was hoped would make the set-up of 96 well plates more efficient, problems were encountered which were felt could not be resolved over the course of this project. The time/cost benefit could not be justified and so it was decided it would be more efficient for the purpose of this 3 year PhD to cut out the plates by hand. The way in which we cut sheets by hand was refined, reducing the time taken to set up plates, making further development towards automation less desirable.

Chapter 4. Fibrosis Modelling

4.1 Introduction

Whilst not in itself a disease, fibrosis is a common feature of multiple pathologies that can affect any organ. It is a dynamic process that has the potential to resolve as well as progress, however chronic injury leads to aberrant wound healing and slowly over time, the development of a fibrotic scar. This distorts local tissue architecture, compromising the functionality of the organ. In 'one-off' and minor instances of tissue/cellular injury, fibroblasts local to the area become activated, secreting inflammatory mediators and ECM components, creating a temporary scar to facilitate wound repair. Once healed, the scar is remodelled and the organ returns to normal tissue functionality. Where there is repeated injury or major insult, the deposition of ECM becomes excessive and is never fully resolved, forming fibrotic tissue (60,62,63).

4.1.1 Pathogenesis

There are a range of causative agents in the development of hepatic fibrosis and chronic liver disease, these can be grouped into 2 types, hepatotoxic injury and cholestatic injury. Hepatotoxic injuries are wide ranging and encompass anything that causes injury to hepatocytes. These can include amongst others, drugs and alcohol, infections, and metabolic syndromes such as NAFLD. Cholestatic injury occurs as a result of the blockage of bile flow. These blockages can result from large structures such as gallstones or tumours or as a result of progressive autoimmune disorders such as primary biliary cirrhosis or primary sclerosing cholangitis (159,160). A key concept in the development of liver fibrosis is reversibility following removal of the source of injury (61–63).

Kidney fibrosis, like liver fibrosis, is a feature of end stage CKD which is described as the loss of kidney function over time and can be caused by a number of underlying aeitiologies. These can include diabetes, chronic inflammation of the glomeruli and tubules, high blood pressure and recurrent infection. Fibrotic scars can develop within any of the 3 distinct kidney regions, the glomerulus, the tubular interstitium or the vasculature (161,162).

4.1.2 Myofibroblast Recruitment and Fibrotic Scar Development

Resident HSC are the main source of myofibroblasts in hepatotoxic-driven liver fibrosis. When damage to hepatocytes occurs, normally quiescent HSCs are activated and differentiate to myofibroblasts (7,71). The origins of myofibroblasts in the development of kidney fibrosis is less clear, with multiple cell lineages being implicated. Single cell RNA sequencing has suggested that pericytes and fibroblasts both contribute the most to fibrous scar formation. Epithelial cells and injured proximal tubule cells have also been implicated alongside bone marrow derived macrophages (70,163).

This activation is driven in part by the pro-fibrogenic cytokine TGFβ via SMAD signalling, which acts as an autocrine positive feedback loop. PDGF is also an important driver of myofibroblast proliferation and recruitment to damaged areas. In instances of removal of the injury inducer, activated myofibroblasts either undergo apoptosis, revert back to a quiescent phenotype (similar to, but not the same as, their original state) or become senescent (7,61,164).

After myofibroblasts have been activated, they express large amounts of ECM proteins which form a scar. Consisting mostly of type I and III collagens, fibrotic tissue, under physiological conditions, would then be remodelled and dissolved by MMPs. In the case of chronic disease and injury however, the deposition of ECM becomes continuous and the resulting scars distort local architecture, negatively impacting the functionality of the organ (60,62,78,79).

4.1.3 Current Models of Fibrosis

Liver Fibrosis

There are numerous models used in the study of liver fibrosis and the development of therapeutics. These can include 2D cell culture of cell lines and primary cells, complex 3D culture systems and rodent models. Common 2D models include the use of immortalised cell lines such as LX-2 (human HSC) or primary cell lines produced from human or rodent biopsy. Although they are relatively cheap and produce results quickly, there are a number of issues with this as a model for the study of liver fibrosis including the transcriptional differences between immortalised cell lines and primary cell lines and that HSCs when

grown in culture undergo spontaneous activation due to the adherence to the plastic culture dish (111–113,115).

The use of rodent models provides a more accurate representation of the biology of fibrosis development in the liver. Common methods of hepatic fibrosis induction include CCl_4 and BDL, both methods are able to reproducibly induce liver fibrosis and numerous studies have shown mechanistically how potential anti-fibrotic therapies can prevent disease progression (131,165,166). Alongside the common problems associated with animal modelling such as expense and ethical considerations, there are model specific problems with this type of disease induction. The major factor is the development of fibrotic disease is very different to what is observed in humans. Typically mice are very young and the development of fibrosis occurs over a matter of weeks and have no comorbidities associated, whereas CLD patients tend to be on average 50 ± 10 years of age, with more complex and systemic disease features (167). Also, in the case of the CCl_4 model, anti-fibrotic drugs are given prophylactically in combination with the insult so the capability of a drug to reduce pre-existing fibrosis is not always assessed.

3D cell culture systems have been proposed as an alternative for the study of human disease, providing the complexity that is lacking in 2D experimental models whilst negating the ethical dilemma of animal models. Microfluidic 'organ-on-a-chip' designs and 3D bio-printed models of liver fibrosis have been developed where the user can dictate the cell types and percentage of population to mimic the position of cells within a fibrotic liver. Whilst undoubtedly a more physiologically relevant system than 2D monoculture, the cell types being used are typically immortalised cell lines and the technology of bio-printing is still developing and not ready for imminent incorporation into a drug discovery pipeline (168,169).

Kidney Fibrosis

2D cell models of renal fibrosis have limited capability to recapitulate the biology of disease progression as they are usually mono cultures and are not able to retain the spatial properties of the whole tissue. Not only are there a large number of cell types with in the kidney which contribute to the fibrogenic process including mesenchymal cells, epithelial and endothelial cell and fibroblasts, the biology of individual cell types, such as tubule cells vary greatly from each other depending on their spatial location within the nephron

(20,66,69,70). The environment in which these cells live is also different depending on their placement within the cortex or medullary region. The translational value of 2D models has been shown to be questionable in the argument of the origin of myofibroblasts in the progression of renal fibrosis, where evidence gathered from these models cannot be confirmed in whole organ models (69,134).

A range of animal models exist to study the development of kidney fibrosis, these can include genetically engineered models, chemically induced models and acquired injury models. UUO, is a common method for the induction of renal fibrosis in rodents, causing physical injury to the kidney which results in fibrotic scar development. Drug treatments can be given post injury to better understand their therapeutic value to patients with CKD. The main problems identified with the UUO model is the lack of outputs that are clinically relevant in humans such as glomerular filtration rate, protein urea and normal serum creatinine levels. Success or failure of a novel therapeutic is mostly reliant on histological output (133,134,170). Alongside physical injury models, chemical injury can be used to induce renal fibrosis. High dose folic acid treatment is widely used to induce kidney disease in rodents. A single intraperitoneal injection of a single high dose (250mg/kg) of folic acid can cause acute kidney injury which can develop into CKD if left untreated (171). This model does allow for the measurement of clinically relevant outputs unlike the UUO model, however it is only an experimental model because such high levels of folic acid are not observed in patients with CKD (172). Genetic models of type 1 diabetes can also be used to study CKD and renal fibrosis via development of diabetic nephropathy. The non-obese diabetic (NOD) mouse for example develops autoimmune destruction of islet cells or the Akita/*Ins2* mouse which has a mutation in the gene for insulin causing improper folding of the tertiary structure and hyperglycaemia (173). There are however problems associated with each of these, including inconsistent disease onset in NOD mice and modest disease alteration to the kidney compared to humans in the Akita/*Ins2* mice (173).

3D cellular models of the kidney are also being developed to model disease progression. Organoids produced using pluripotent stem cells from multiple cell lineages are able to reproduce some kidney disease features but more resemble the kidney in early foetal development rather than adults and lack a vasculature system (174). Methodology for the decellularisation of kidney tissue and repopulating with primary cell lines was described by He *et al.* They recellularised the scaffold with primary renal cells and primary

mesenchymal cells resulting in well dispersed cellular engraftment across the kidney scaffold featuring 'glomerular-like' structures (175,176). The major drawback of this model was that it was based on using rat tissue and primary cells rather than from humans. Further development of this model to use human tissue rather than animals would make this more attractive for preclinical modelling (175).

4.1.4 Precision Cut Tissue Slices as a Model for Fibrosis Development

Model development is usually a trade-off between a high throughput system and physiological relevance, PCTS have the potential to offer both without compromise. Studies using this technology have become more commonplace, with a variety of animal models and human models being tested among groups. These studies have shown that there is predictive value in the model for the testing of anti-fibrotic therapies, particularly when human tissues are used. However, historically the major hurdle for most is the very short culture period, often only 48h before the tissue slices are no longer viable (150,177,178). A study from our lab sought to extend the lifespan of PCTS culture using a specialised bioreactor system (151). This has had a significant impact on their longevity, where culture periods can be as long as 144h hours. The improvement to this platform allows time for fibrosis to develop within the disease control slices, something that other studies have not been able to achieve.

More recently, the problems associated with this technique for modelling fibrosis are tissue availability and a low throughput system. The larger 8mm cores that are punched out from the liver resection tissue or unused donor kidneys can leave large amounts of waste tissue, both from the biopsy and initial slicing. Complex studies, where there are a range of different experimental groups, can also require a large number of slices for analysis including, histology, viability assessment and technical replicates of each drug dose, making the treatment process cumbersome.

4.1.5 Chapter Aims

- Validate the fibrosis model in the 96 well bioreactor in both human liver and kidney.

- Demonstrate use of the bioreactor as a suitable platform for efficacy testing anti fibrotic drugs.

I aim to develop a medium throughput system for the modelling of fibrosis and demonstrate its ability to accurately predict the efficacy of anti-fibrotic therapies. The optimised 96 well bioreactor will be used to culture 3mm slices produced from human kidney and liver tissue in the presence of pro-fibrotic stimuli to produce a fibrotic disease state, and use well described inhibitors to demonstrate its ability as a prognostic indicator.

4.2 Methods

4.2.1 Materials

Sourcing of tissue and general materials for tissue culture are described in 2.1. TFGβ1 and PDGFββ were purchased from Peprotech and each made up to a stock solution of 20mM according to manufacturer's instructions. ALK5 inhibitor SB-525334 (Alk5i) was purchased from Sigma was made to a stock solution of 10mM in DMSO (Sigma). Pirfenidone was purchased from Cambridge Bioscience (CAY13986-100mg) and dissolved in DMSO to a stock concentration of 100mM.

4.2.2 Culture Conditions for Development of Fibrotic Liver Slices

Production of the 8mm and 3mm liver slices is described in 2.1.3. After a 24h rest period following the slicing process, slices were stimulated with 3ng/ml TGFβ1 and 50ng/ml PDGFββ ± 10µM Alk5i. Relevant controls ± drug vehicles were also included. Treatments were refreshed every 24h with supernatants collected as previously described (2.1.6) until the end of the culture period at 96h post tissue processing. Slices were harvested for histological and biochemical assays and the methodology for this is described in the Methods chapter.

4.2.3 Culture Conditions for Development of Fibrotic Kidney Slices

Production of the 3mm kidney slices is described in 2.1.5. Following a 24h rest period after the slicing process, slices were stimulated with 3ng/ml TGFβ1 and 50ng/ml PDGFββ ± 10µM Alk5i. Relevant controls ± drug vehicles were also included. Treatments were refreshed every 24h with supernatants collected as previously described (2.1.6) until the end of the culture period at 96h post processing. Slices were harvested for histological and biochemical assays, methodology for this is described in the Methods chapter.

4.2.4 Analysis of Soluble Outputs

Soluble outputs from the cultured slices, including the CyQUANT LDH assay, the AST activity assay, a number of ELISA kits including Albumin, KIM1 and Collagen as appropriate

and a MSD U-Plex assay to measure inflammatory markers were used. The specific protocols for each of these is described in 2.2 of the Methods chapter.

4.2.5 Histological Analysis

A number of different stains were performed on tissue sections, protocols for these are described in 2.3 of the Methods chapter. These include H&E, Sirius Red and αSMA.

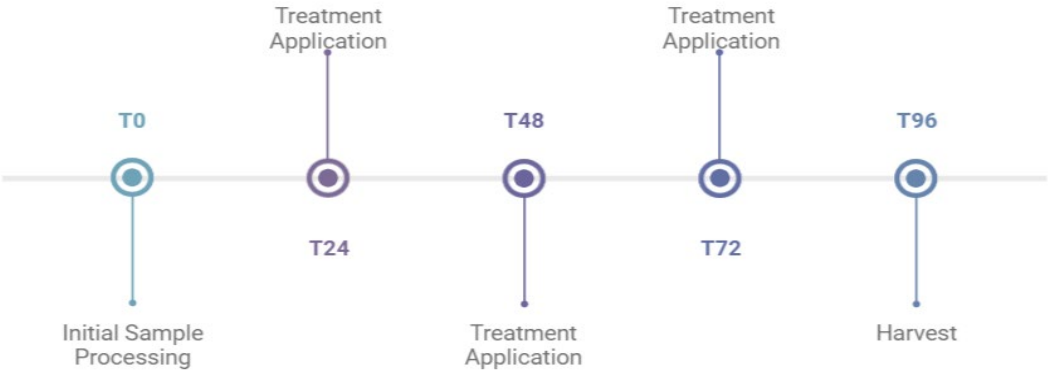

Figure 10. Treatment Plan for Fibrosis Model
Treatments refreshed every 24h, with media collected and stored at -80°C

4.3 Results

4.3.1 Comparison of PCLS Fibrosis Model in 8mm and 3mm Tissue Slices

It has been previously shown from our lab that with the use of a specialised bioreactor system the life span of 8mm PCLS can be extended to at least 96h (151). I hoped to further develop this system to create a medium throughput platform using smaller diameter PCLS in a 96 well bioreactor.

To validate the fibrosis stimulation model in the 3mm PCLS, a comparative study between the existing 12 well bioreactor and the newly developed 96 well bioreactor using the same donor was performed. To generate 3mm PCLS, 250uM thick sheets of tissue were produced and 3mm disks of tissue were punched out and then set in a transwell insert placed in a newly designed 96 well bioreactor plate.

To ensure 3mm slices did not behave differently compared to their larger counterparts, slice viability at the start (T0) and end (T96) of the culture period, measured by resazurin assay, confirmed that viability was comparable between the two different slice sizes (Figure 11A). There was a decrease in viability in both slice sizes from T0 but the drop was comparable with an average of 37% of T0 in the 3mm slices and a 50% drop from T0 in the 8mm slices. These same trends are observed between the two groups, where the addition of the Fib Stim (TGFβ1 + PDGFββ) treatment did not negatively impact PCLS viability. After finding that the slices remained metabolically active over the culture period, soluble factors in the collected media across all time points were characterised to evaluate tissue health. Soluble albumin is a biomarker for functioning hepatocytes in liver tissue and is an indicator of tissue health and functionality. Figure 11B shows albumin production over time in both the 3mm and 8mm slices. In both bioreactor set ups, levels of albumin increase from 24h to 48h and remain stable to 72h, with the 3mm slices appearing to secrete more than the 8mm counterparts. At 96h in the 3mm slices, albumin production decreases again to levels similar to the 24h rest media. Levels in the 8mm slices do not drop off at 96h and remain at least as high as those seen at 72h. Albumin production also does not significantly vary between the control and treatment groups at any of the time points in the 3mm slices.

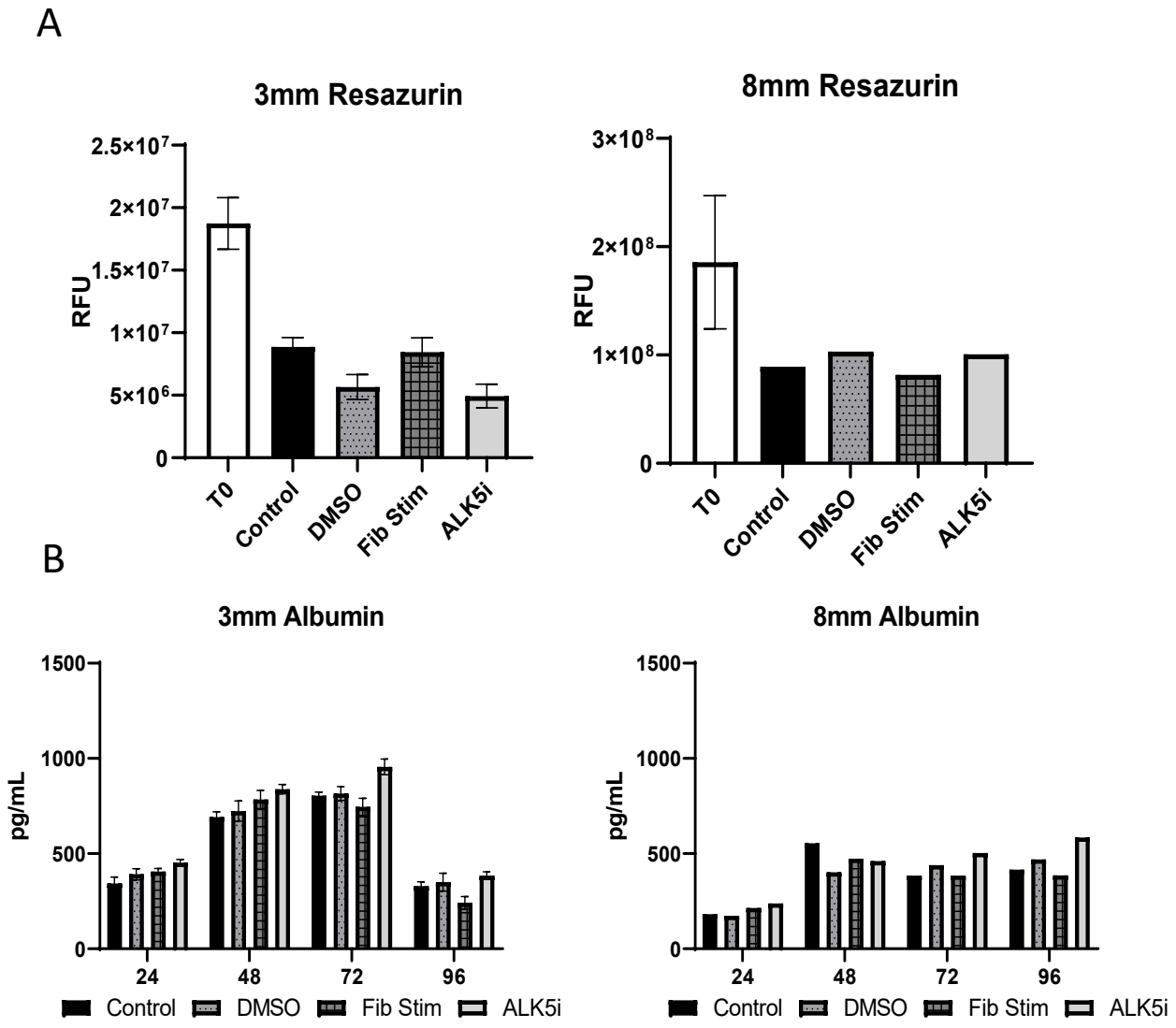

Figure 11. Comparison of Fibrosis Model in 8mm and 3mm PCLS
A – *Resazurin output at T0 and 96h culture from 3mm PCLS (left) and 8mm PCLS (right).* ***B –*** *Soluble albumin from culture media saved at 24h intervals from 3mm PCLS (left) and 8mm PCLS (right). Data shown as mean +/- SEM. N=1 liver donor, n=5 technical replicates for 3mm PCLS treatment groups and n=1 technical replicates for 8mm slices.*

Alongside monitoring metabolic output and measuring functionality of the tissue slices, levels of treatment-induced cytotoxicity were examined. LDH is a marker of cell injury, released as a result of damage to the membrane of a cell. AST is used clinically as a measure of liver function, it is released from hepatocytes as a result of hepatocyte injury. Figure 12A shows the AST levels measured from culture media. Both bioreactor set ups follow a similar trend where AST output is highest at 24h, due to post-cutting stress, but then falls by about half at 48h and then remains stable to 96h. The 8mm slices produce

more AST across all time points and treatment groups than the 3mm slices. Figure 12B shows LDH release from cultured slices as a percentage of a positive control. At 24h, the levels of LDH are raised, due to post-slicing trauma, but these reduce and level off to between 1% and 2% of the positive control by 96h in both the 3mm and 8mm slices. The 3mm slices had a higher amount of LDH release at 24h compared to the 8mm slices, however from 48h onwards the average levels across the treatment groups were the same at between 1-3% of the positive control.

Finding that the 96 well bioreactor was able to support the culture of 3mm slices for 96h, and the addition of the Fib Stim challenge showed no greater detrimental effect when

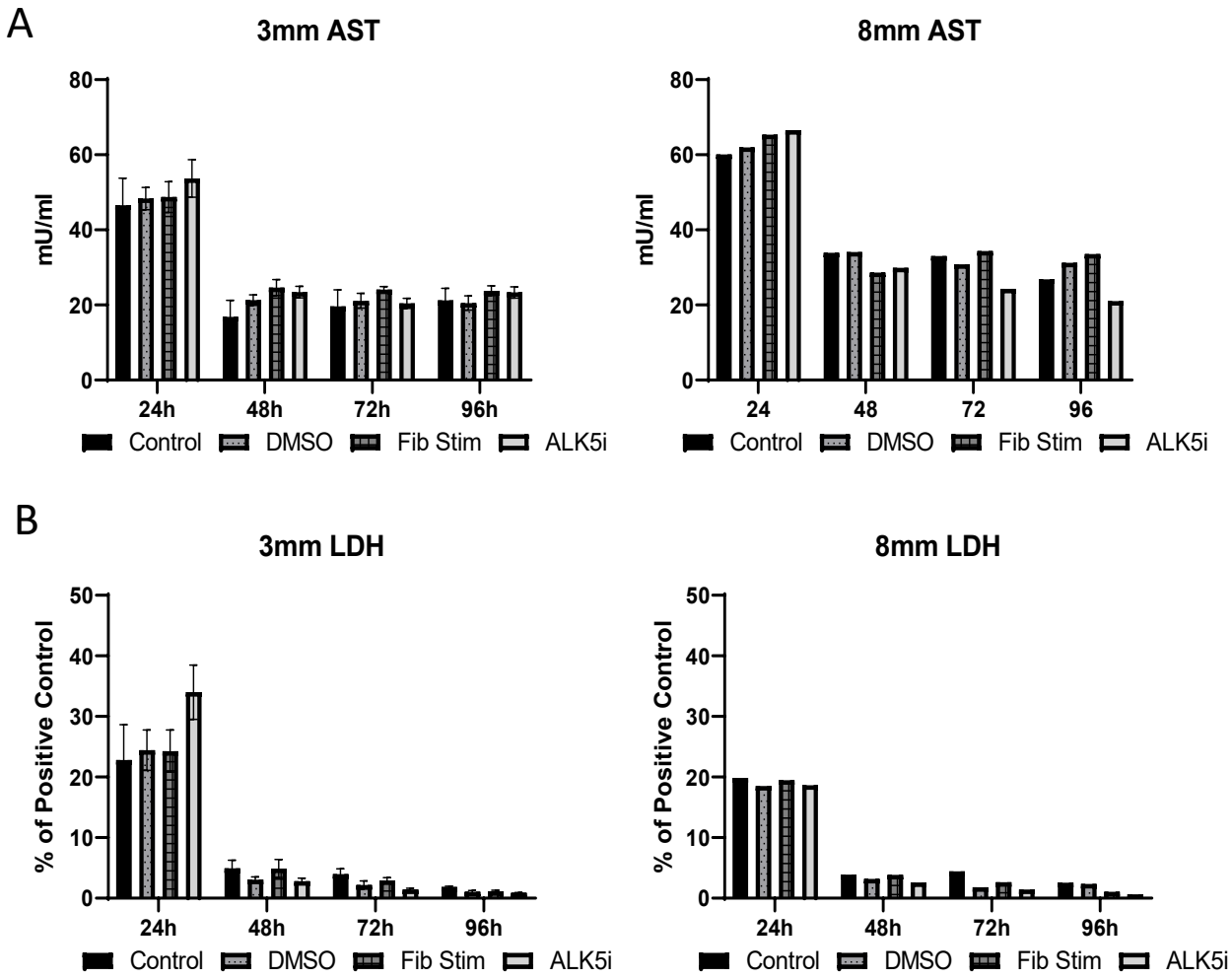

Figure 12. Comparison of Fibrosis Model in 8mm and 3mm PCLS
A – *AST output from culture media saved at 24h intervals from 3mm PCLS (left) and 8mm PCLS (right).*
B – *LDH output from culture media saved at 24h intervals from 3mm PCLS (left) and 8mm PCLS (right). Data shown as mean +/- SEM. N=1 liver donor, n=5 technical replicates for 3mm PCLS treatment groups and n=1 technical replicates for 8mm slices.*

directly compared to the existing model, more donor livers were collected to further validate this model.

4.3.2 Validation of the Fibrosis Model in the Liver

A total of 7 donors were collected to validate the fibrosis model in human PCLS in the 96 well format, using 3mm slices. Information about these donors is included in Table 3. The average age of the donors was 64 years, with 57% being male and 43% being female. All patients had liver fibrosis to some extent, with 43% being grade 2, and grade 1 and 3 fibrosis each being represented by 28.5% of the cohort. There was limited inclusion of patients with significant steatosis, with 86% categorised as grade 0 or grade 1, and patients were not type 2 diabetic. As before, several methods were used to characterise the model and monitor viability, health and damage alongside the amount of collagen as a marker for the development of fibrosis within the tissue. The potential use of histological analysis on these much smaller tissue slices was also investigated.

Table 3. Demographics of Donors used in Fibrosis PCLS Validation

Donor Number	Age	Sex	Fibrosis Score	Steatosis Score
Donor 1	58	M	1	0
Donor 2	80	F	2	1
Donor 3	76	M	3	0
Donor 4	56	F	2	1
Donor 5	62	F	3	0
Donor 6	58	M	2	2
Donor 7	62	M	1	0

Figure 13A displays the metabolic activity of the 3mm PCLS at 96h normalised to an individual donor's T0 value. There were no significant differences between the treatment groups by one-way ANOVA and all of the slices remained viable. The LDH output (Figure 13B) showed the same trends observed in previous studies, where the 24h post processing media contained high amounts of LDH release which dropped by more than half at 48h and then by more than half again at 72h. There were no significant differences between the different treatment groups at any of the time points measured. Albumin production (Figure 13C/13D) increased from 24h to 48h and then decreased slowly to 96h. Functionality of the slices drops to between 62-78% of T48 at the end of the culture period and there were no statistical differences between treatment groups. I was confident these

methods to induce fibrosis didn't have a significant impact on the overall health of the PCLS, so moved to assess the disease features induced by inclusion of TGFβ and PDGFβ.

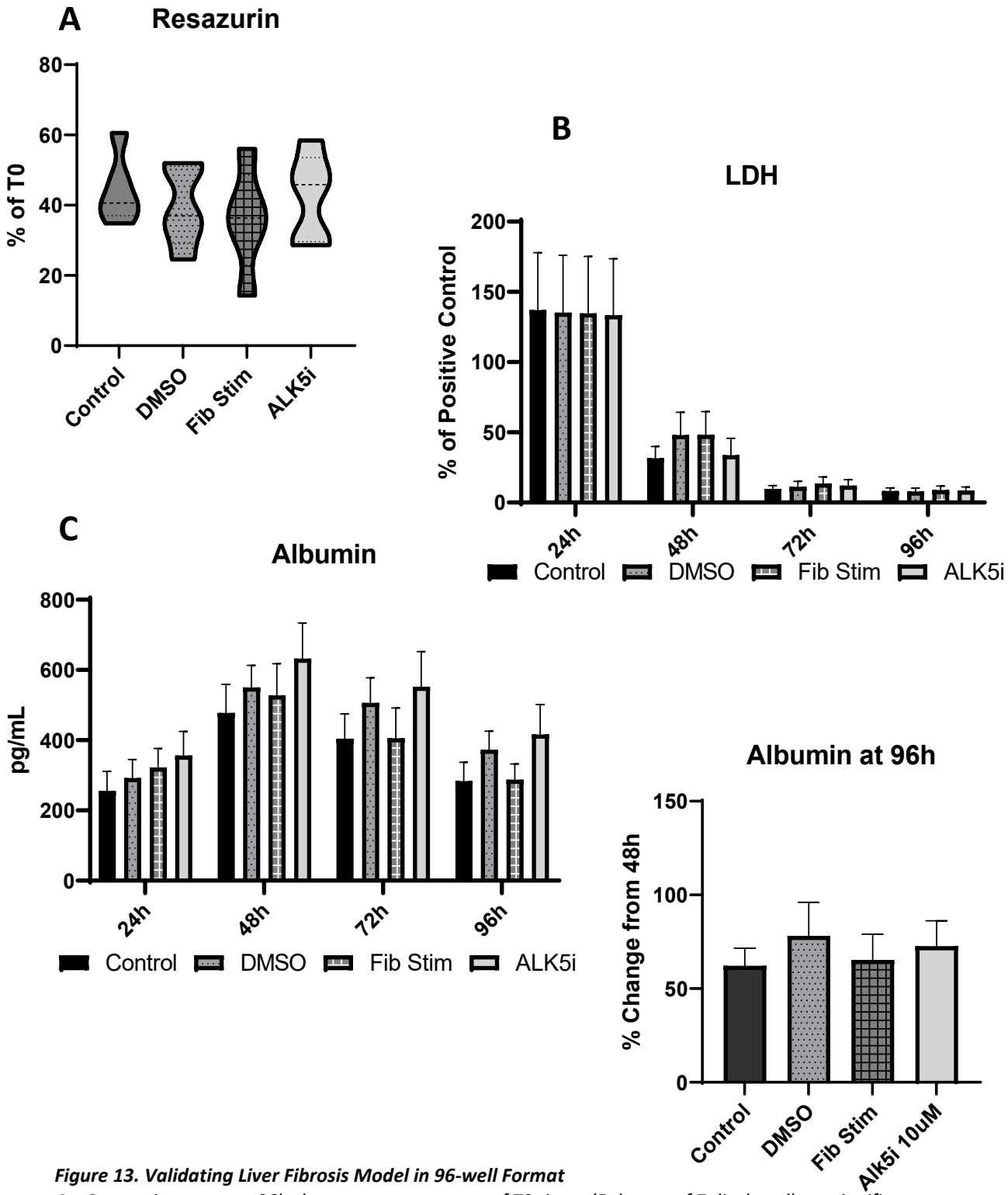

Figure 13. Validating Liver Fibrosis Model in 96-well Format

A – *Resazurin output at 96h shown as a percentage of T0 tissue (5 donors of 7 displayed), no significant differences by one-way ANOVA.* ***B –*** *LDH output measured at 24h intervals to the end point at 96h post slicing.* ***C –*** *Soluble albumin shown at all time points with absolute values.* ***D –*** *Soluble albumin output at 96h post processing, shown as percentage decrease from 48h, there were no statistically significant differences by one-way ANOVA. Data shown as mean +/- SEM. N=7 liver donors, with n=5 technical replicates per donor.*

An important soluble biomarker to monitor the development of fibrosis was Collagen 1A1, a pro-fibrogenic ECM component. By ELISA, there were no significant differences in collagen output between the control and stimulated treatment groups until 96h in culture (Figure 14A/14B). At 72h, the Fib Stim group appeared higher, but it was not enough to be classed as significant. Soluble collagen levels increased over the course of the culture period in the control slices, suggestive of spontaneous matrix remodelling and fibrogenesis. Alk5i was included to determine if, like the 12 well plate, induction of fibrosis could also be attenuated in the 3mm slices in the 96 well plate. The inhibitor did reduce the levels of soluble collagen after challenge with profibrotic stimuli, inferring the potential of this bioreactor system for use as a medium throughput, anti-fibrotic target validation platform.

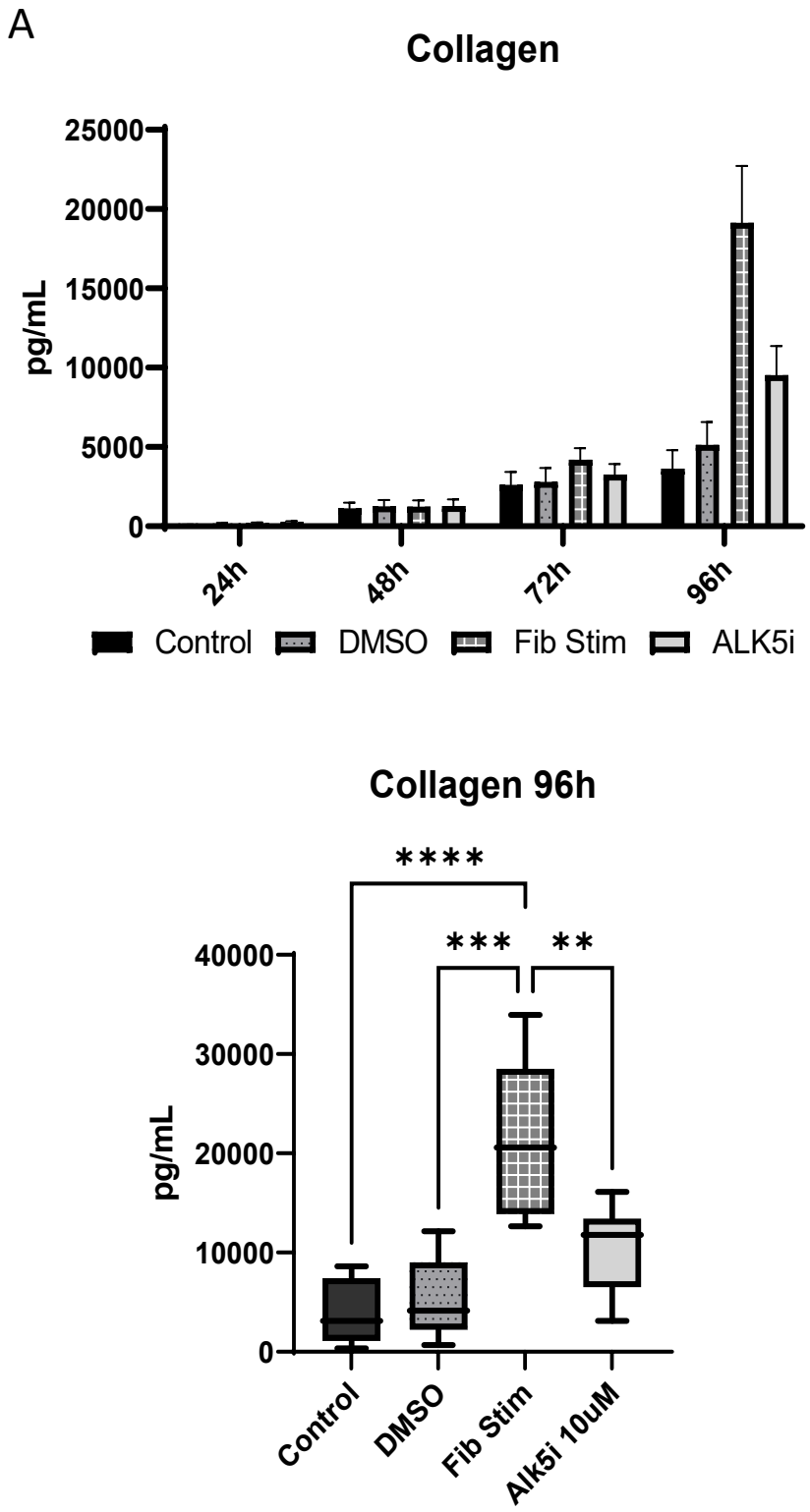

Figure 14. Validating Liver Fibrosis Model in 96-well Format

A – *Soluble collagen measured from culture media across all time points. No statistical significance for samples from 24h-72h but there is significance at 96h by one-way ANOVA (shown in B). Data shown as mean +/- SEM.* ***B-*** *Soluble collagen measured from culture media at 96h, statistical analysis by one-way ANOVA. ** p=≤0.01, *** p=≤0.001, **** p=≤0.0001. Data shown as min to max box and whisker. N=7 liver donors, n-5 technical replicates per donor.*

Histological analysis was performed on FFPE liver slices to further validate the development of fibrotic disease in the tissue (Figure 15). Starting with 8mm PCLS, slices were embedded flat, to assess the overall tissue architecture, and upright to view a cross-section of the slice. Haematoxylin and Eosin (H&E) staining was conducted to look at general morphology, Sirius red was chosen to assess collagen fibre deposition and fibrosis and immunohistochemistry with an αSMA-targeting antibody was used to identify activated myofibroblasts.

Confirming the ELISA findings, there was a small degree of spontaneous fibrosis occurring in the control culture slices. There were more collagen fibres and thicker regions of collagen deposition (stained red) across the 96h cultured control slice and a greater number of αSMA positive cells compared to the T0 tissue. The inclusion of the Fib Stim treatment increased both collagen deposition and hepatic stellate cell activation further still. There was more collagen branching out across the slice with a greater thickness in areas surrounding central veins and an increased number of αSMA positive staining in both slice orientations. This also demonstrated that the treatments added to the media penetrate through the whole slice and do not just have a surface level effect.

The same stains were then performed on the 3mm slices, representative images of these slices are shown in Figure 16B. Using NIS-Elements, thresholding was applied to a series of images taken from each stain (Figure 16A). Both the Sirius Red and the αSMA are higher in the Fib Stim treated slices than the Alk5i attenuated and control slices, but statistical significance was only achieved between the Fib Stim and Alk5i groups. Comparing the appearance of the 8mm and 3mm slices, the smaller slices were more difficult to get whole images from due to the nature of the embedding process, where placing multiple slices in one block meant they would often not all be at the same depth when cut on the microtome. There was greater shrinkage of the slices over the culture period and during the fixation/processing stage in the 3mm slices more than their larger counterparts, and they would fold in on themselves, resulting in overlapping tissue and tearing in the images.

I have shown that this fibrotic disease model is reproducible across multiple donors with a range of backgrounds (age/sex/background liver state) and next aimed to show this methodology could be used in other organs using this platform.

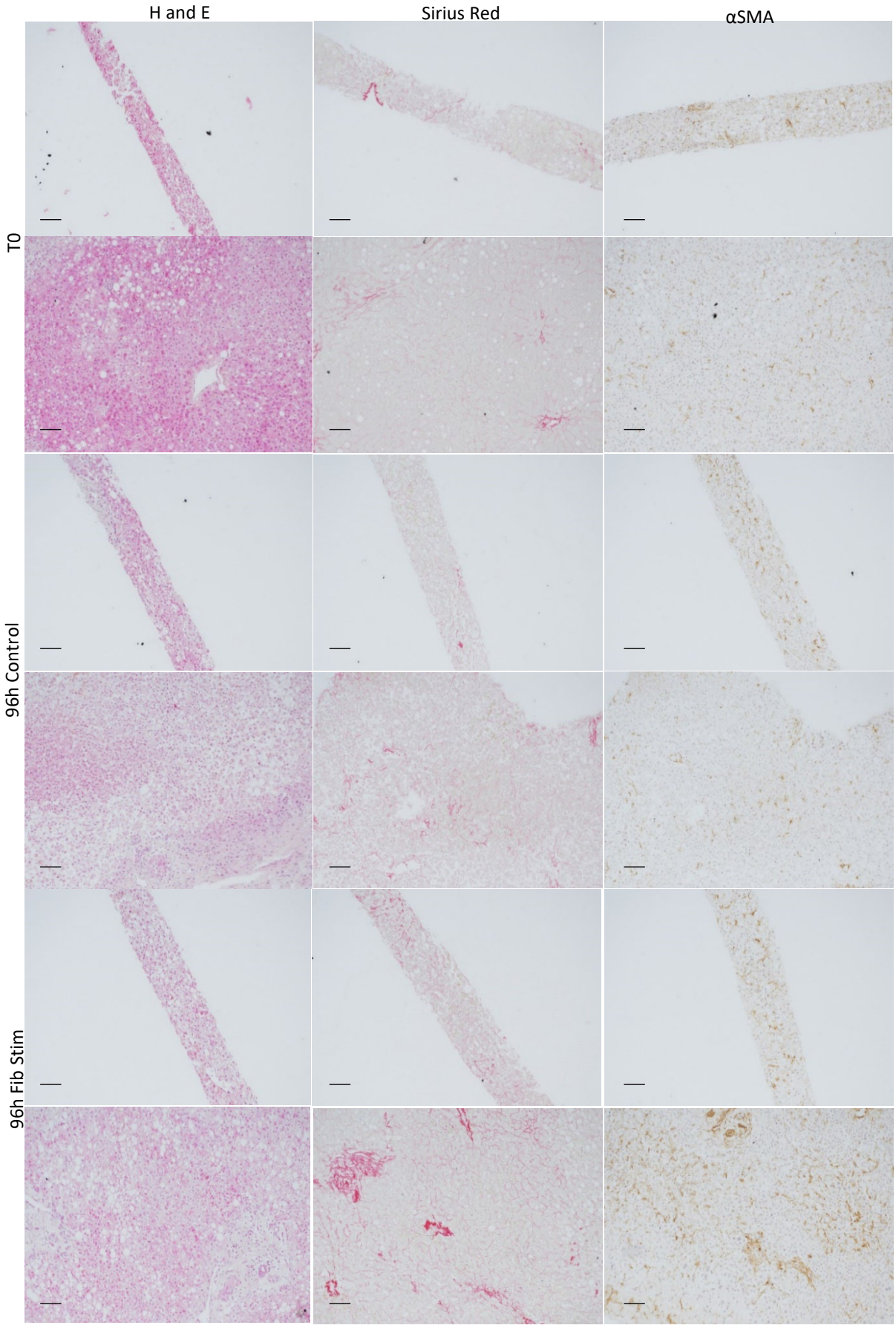

Figure 15. 8mm PCLS Histology

Representative images of PCLS taken at T0 and then 96h of culture with and without the Fib Stim treatment. In each pair, the top images show a cross sectional view of the slice stood upright and the bottom image is a top down view of the slice laid flat. Images taken at 10x magnification, the scale bar represents 100µm. n=1

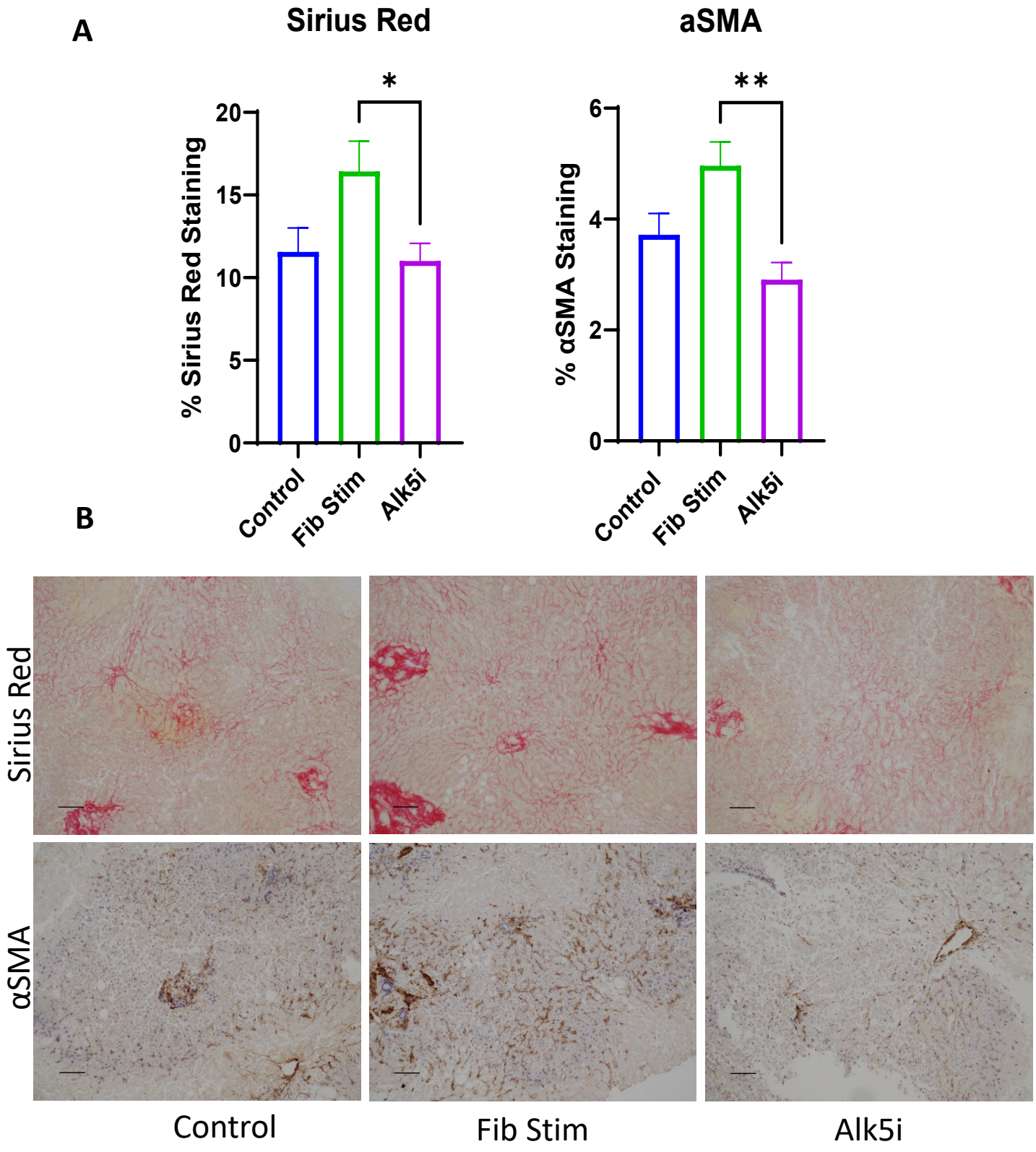

Figure 16. 3mm PCLS Thresholding and Histology

A- *Graph showing thresholding of 3mm slices stained with Sirius Red and αSMA. Statistical analysis by one-way ANOVA * p=≤0.05, ** p=≤0.01. N=2 liver donors (donors 5 and 6, Table 3), n=5 images taken per treatment group. Data shown as mean +/- SEM.* ***B-*** *Representative images of PCLS taken 96h of culture with and without the Fib Stim +/- Alk5i. Images taken at 10x magnification, the scale bar represents 100μm.*

4.3.3 Validation of the Fibrosis Model in the Kidney

I next set out to validate the PCKS model using similar methods as the liver. A total number of five donors were collected to validate the fibrosis model in human PCKS. Information about these donors is included in Table 4. All of the donors for this study were between the ages of 65-75 years of age, with an average age of 67.5 years and 60% of the donors were female. Every donor was measured by BMI as at least overweight with one donor classed as obese. Unlike the liver, during the processing stage fat is not macroscopically visible within the kidney tissue, excess fat is situated around the organ.

Table 4. Demographics of Donors Used in PCKS Fibrosis Development Validation

Donor Number	Age	Sex	BMI
Donor 1	69	M	27
Donor 2	63	M	32
Donor 3	68	F	25
Donor 4	75	F	25
Donor 5	63	F	27

As before, a resazurin assay was used to assess the viability of the PCKS at the end of the culture period. This is shown in Figure 17A as percentage change from T0. There were no significant differences between the treatment groups and all the slices were viable at the end of the culture period which in this instance was 96h post processing. There was one donor (donor 3) that was less metabolically active at the end of the culture period compared to the others, but it did still prove to be viable.

LDH release, a measure of cytotoxicity, followed the same trend in the kidney as it has done in the liver (Figure 17B). High amounts of LDH were secreted into the 24h post processing media, and then a constant reduction over time in all treatment groups to 96h. There were no significant differences in LDH release between the treatment groups at any time across the culture period.

Soluble collagen was used as an indicator of fibrogenesis, the result of which is shown in Figure 17C. Statistical significance between the vehicle control (DMSO) and the Fib Stim treatment group was achieved at 96h. Whilst each donor responded to the treatments applied, there was a larger degree of biological variation between the donors than was seen in the liver, therefore the data was normalised to the individual donor's vehicle control (Figure 17D). This showed a greater significance and reproducibility across the

donors. There was one replicate that failed to induce fibrosis as effectively as the others (donor 3), the same donor with the lower metabolic output.

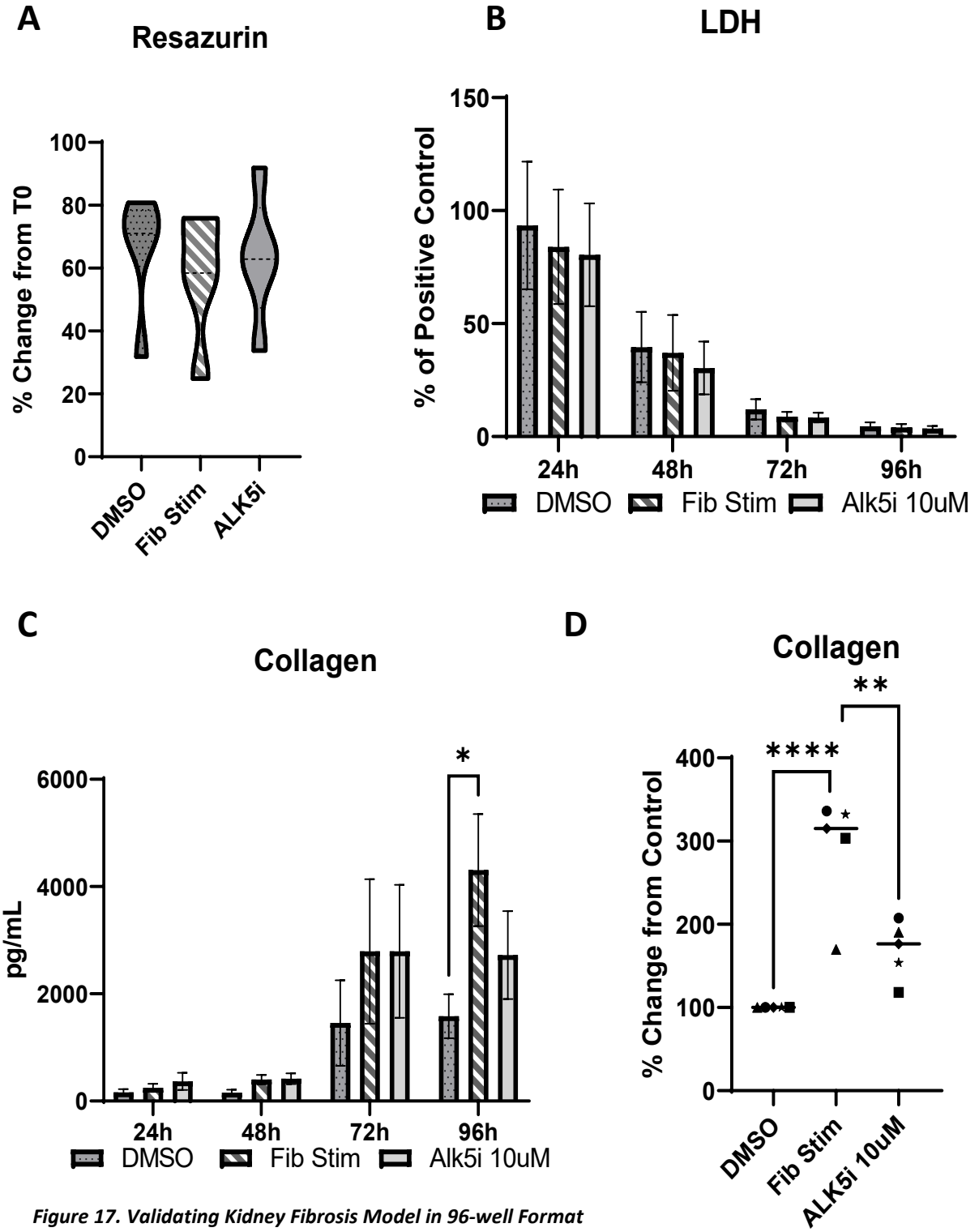

Figure 17. Validating Kidney Fibrosis Model in 96-well Format

A – *Resazurin output at 96h shown as a percentage of T0 tissue* ***B –*** *LDH output measured at 24h intervals to the end point at 96h post slicing.* ***C –*** *Soluble collagen shown at each time point with absolute values, a statistically significant difference was only observed at 96h by ANOVA. D – Soluble collagen as percentage of control. All p values were calculated using a one-way ANOVA. * p=≤0.05, ** p=≤0.01, **** p=≤0.0001. N=5 kidney donors, n=5 technical replicates per donor.*

The 96h cultured, 3mm PCKS were then examined histologically for collagen deposition and HSC activation (Figure 18). Sirius red staining revealed thickening of the tubular basement membrane and an increase in collagen in the tubular interstitium in the Fib Stim slices. There was a large amount of αSMA positive staining across the whole tissue in the DMSO and Fib Stim slices but this was reduced in the Alk5i treated slices with the staining more concentrated around small groups of tubules. Thresholding was applied to a series of images taken from each stain. The same trend in both stains was observed, where the sections from the Fib Stim treated slices had a higher percentage of αSMA positive regions and Sirius red positive regions than both the DMSO and Fib Stim plus Alk5i treated PCKS.

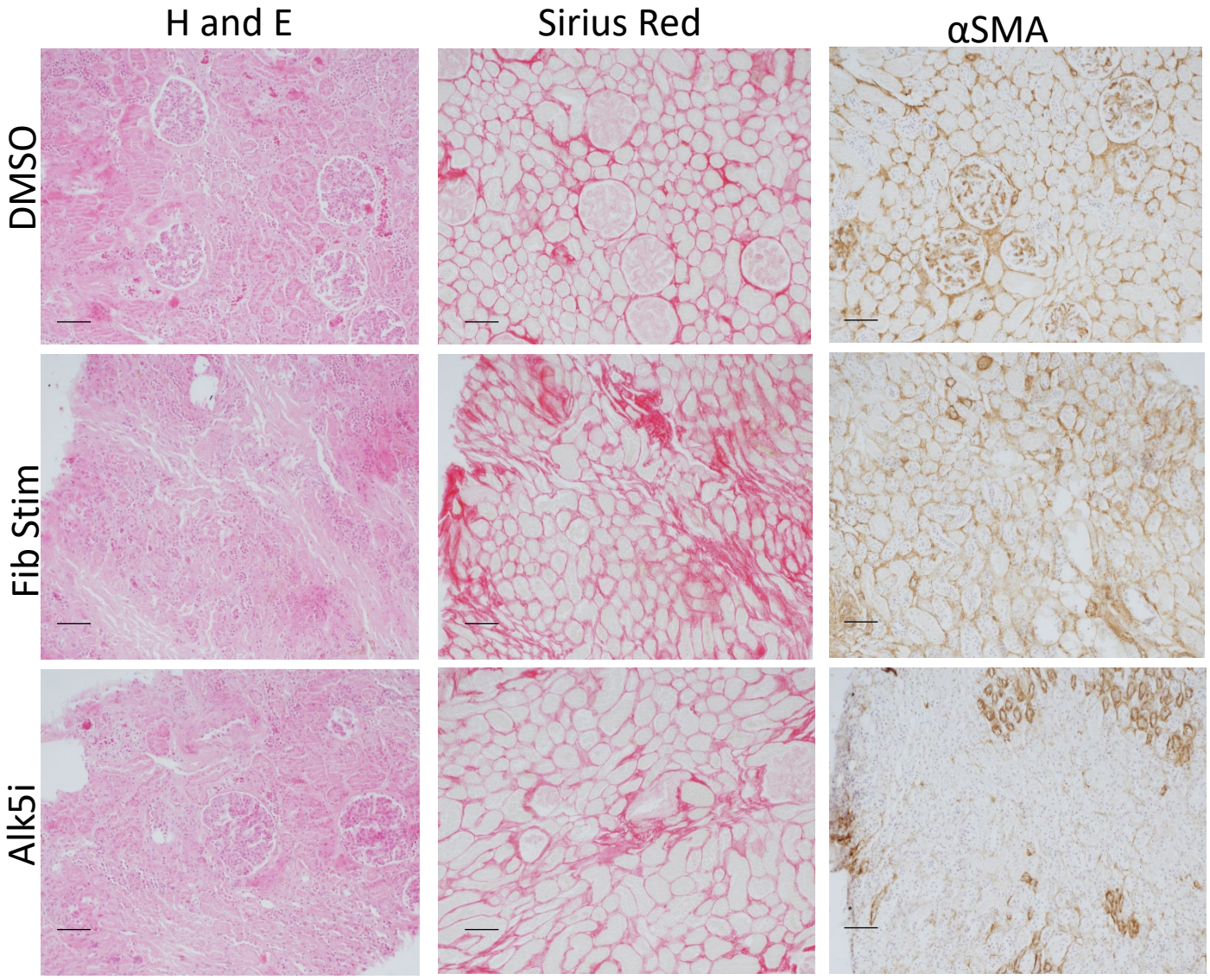

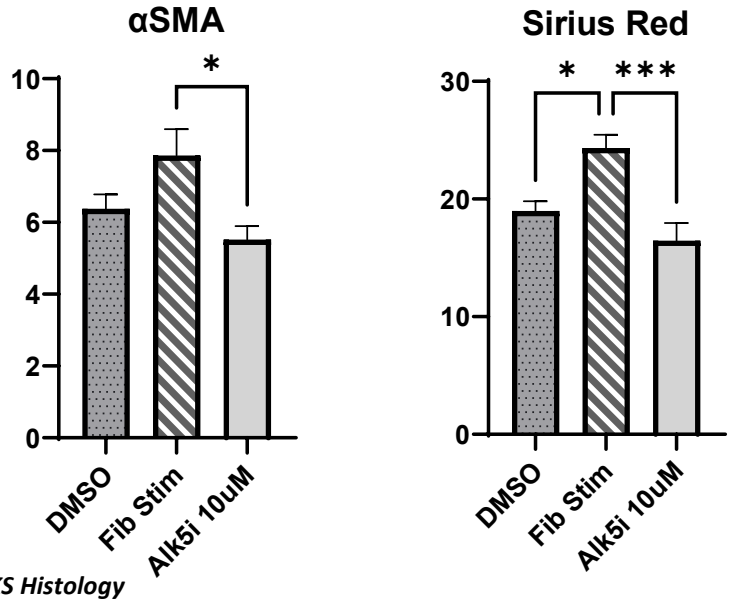

Figure 18. 3mm PCKS Histology

*Representative images of PCKS taken 96h of culture with and without the Fib Stim +/- Alk5i, the αSMA Alk5i image is not representative of the average section, due to technical issues with slice quality and large vessels in the other images. Images taken at 10x magnification, the scale bar represents 100µm. Thresholding of 10x magnification images stained with αSMA and Sirius Red. Statistical significance calculated using one-way ANOVA. * p=≤0.05, *** p=≤0.001. Data shown as mean +/- SEM. N=2 kidney donors (donors 1 and 2 from Table 4).*

4.3.4 Identification of Fibrosis Associated Markers

The markers that had been selected for the validation of this model were targeted fibrosis indicators, and were used to assess the dynamics of the fibrogenic markers in this disease model. To capture a broader and unbiased biomarker data set to characterise the *ex vivo* model, culture media samples were run on a 111-plex Meso-Scale Discovery (MSD) assay to profile inflammatory and fibrotic markers. A total of three liver and four kidney donors that had been treated with the Fib Stim Alk5i treatments were selected for this panel, this information is shown in Table 5 and Table 6. The liver donors were predominantly female with an average age of 50. All of the donors used in this study had a degree of pre-existing fibrosis but only one was steatotic. The kidney donors were also predominantly female with the entire cohort being over the age of 60. Each of the donors were also classified as overweight by BMI measurement with one being classed as obese.

Table 5. Demographics of Liver Donors Used in MSD Panel Screening

Donor Number	Age	Sex	Fibrosis Score	Steatosis Score
Donor 1	58	M	2	2
Donor 2	31	F	2	0
Donor 3	60	F	3	0

Table 6. Demographics of Kidney Donors Used in MSD Panel Screening

Donor Number	Age	Sex	BMI
Donor 1	63	M	32
Donor 2	68	F	25
Donor 3	75	F	25
Donor 4	63	F	27

Of these 111 markers, 35% were undetectable and 54% were not dynamic in the liver, and in the kidney 34% were undetectable and 60% were not dynamic. The ‘undetectable’ threshold was set at any protein concentrations under 1pg/ml in each of the treatment groups and the ‘not dynamic’ category included proteins where there were no significant differences between DMSO control slices and Fib Stim treatment groups as determined by t-test.

The dynamic soluble proteins identified in the PCLS after 96h in culture are shown in Figure 19. Vascular Endothelial Growth Factor A (VEGF-A), IL-6 and Placental Growth

Factor (PIGF) were significantly upregulated when the Fib Stim treatment is applied, and subsequently attenuated by the inclusion of the Alk5i. The inverse of this was observed with gp130, Macrophage Inflammatory Protein 1β (MIP-1β) and Macrophage Derived Chemokine (MDC) where the Fib Stim treatment suppressed the secretion of these proteins and the inclusion of Alk5i reversed this.

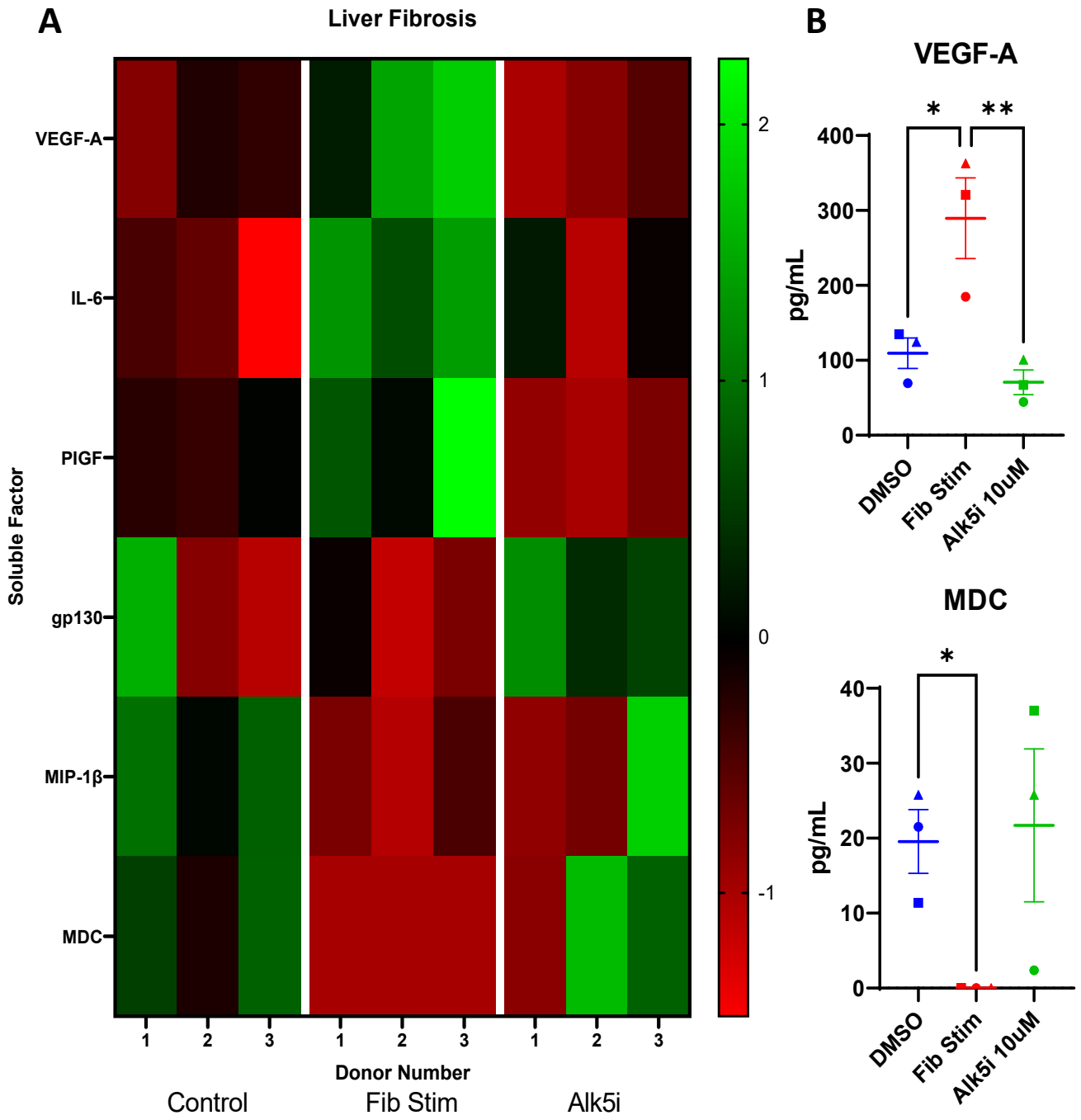

Figure 19. MSD Outputs from PCLS Fibrosis Model

A- *Heat map showing all dynamic proteins identified in the MSD panel, dynamic proteins identified by student's t-test comparing control and fib stim groups. Data shown as z transformed.* ***B-*** *Individual examples of dynamic proteins identified in MSD screening using absolute values, statistical analysis by one-way ANOVA * p=≤0.05, ** p=≤0.01. Data shown as mean +/- SEM. N=3 liver donors (donors 1, 2 and 3 from Table 3). 5 technical replicates per treatment condition were pooled for each donor to run on the MSD panel.*

The secretory profile of the kidney with the Fib Stim treatment was very different (Figure 20), with only 4 of the screened factors identified as dynamic and only 2 of these are in common with the liver. Granulocyte-Macrophage Colony Stimulating Factor (GM-CSF), Monocyte Chemoattractant Protein-1 (MCP-1) and IL-6 were significantly increased in response to the Fib Stim treatment. PIGF expression was varied between donors in the DMSO and Fib Stim groups but was attenuated in all donors with the addition of Alk5i.

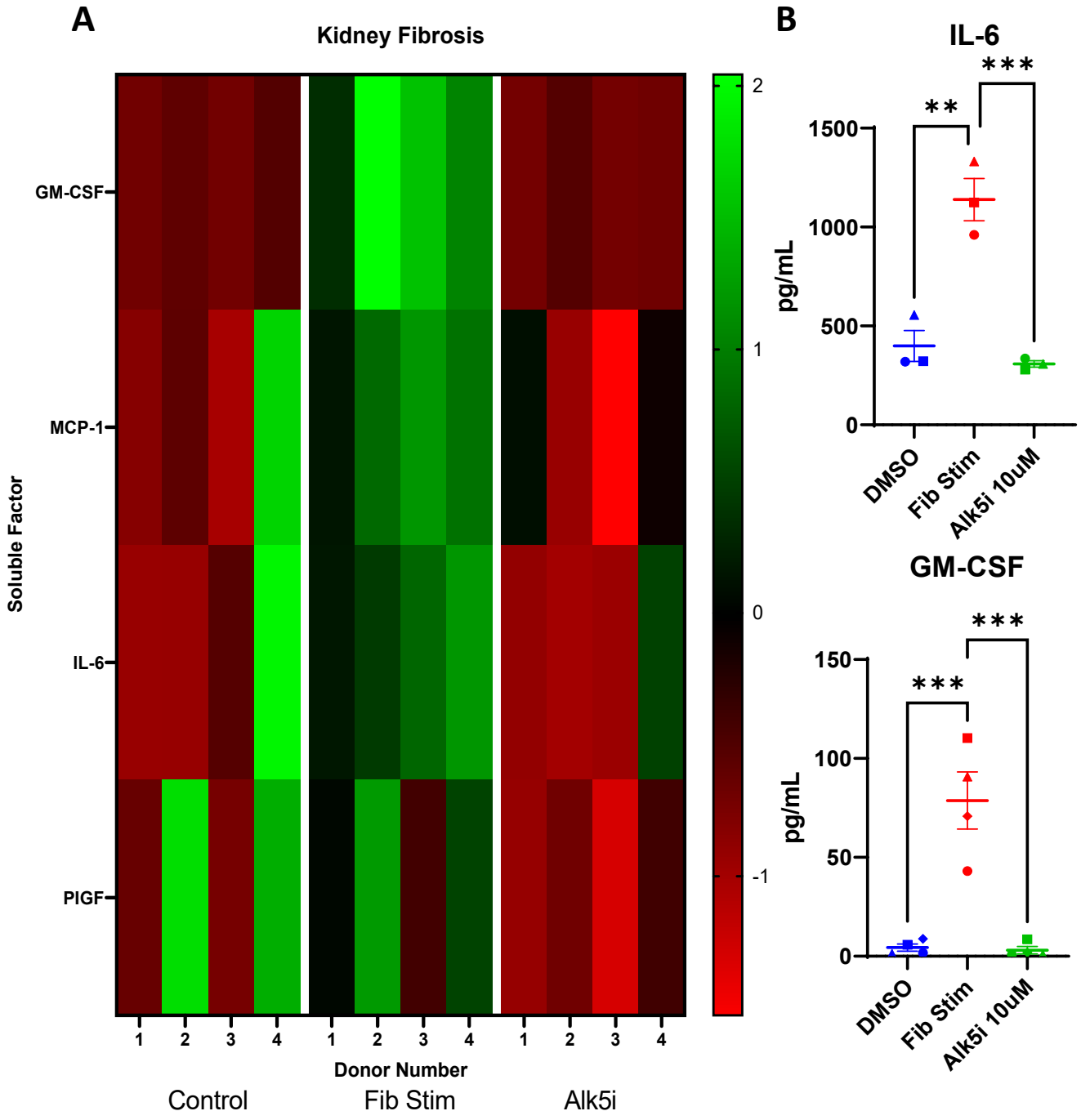

Figure 20. MSD Outputs from PCKS Fibrosis Model

A- *Heat map showing all dynamic proteins identified in the MSD panel, dynamic proteins identified by Student's T test comparing control and fib stim groups. Data shown as z transformed.* ***B-*** *Individual examples of dynamic proteins identified in MSD screening using absolute values, statistical analysis by one-way ANOVA ** p=≤0.01, *** p=≤0.001. Data shown as mean +/- SEM. N=4 kidney donors (donors 1, 2, 3 and 4 from Table 4). 5 technical replicates per treatment condition were pooled for each donor to run on the MSD panel.*

4.3.5 Feasibility of Efficacy Testing Drug Screens with Novel Bioreactor

One of the main aims of this project was to determine the feasibility of using this modelling platform for the screening of lead candidates in drug discovery. I have so far shown that this 96-well bioreactor system can reproducibly generate fibrotic disease features across multiple organs and donors. The next step was to show that this platform can be used to test the efficacy of anti-fibrotic inhibitors and therapeutics. The Alk5i SB-525334 is a potent and selective inhibitor of TGFβ signalling and this type of inhibitor is used as a positive control in several anti-fibrotic therapy studies (151,179,180). This Alk5i was used in a dose dependent manner with the addition of the validated Fib Stim treatment to demonstrate the potential of this model to be used to not only screen compounds for their anti-fibrotic efficacy, but also to identify suitable doses.

A top concentration of 10µM of the inhibitor, shown by previous studies in this project to sufficiently attenuate the development of fibrosis in both the liver and the kidney, alongside a 10-fold serial dilution to a bottom concentration of 0.001µM formed the dosage scale. PCLS and PCKS were cultured in the presence of the Fib Stim treatment to 96h post processing and fibrogenesis in the slices was assessed by collagen ELISA, shown in Figure 21. Using the Fib Stim treated slices as the benchmark of total fibrosis development, the reduction in fibrosis from the inhibitor was calculated as a percentage of this level. There was a similar trend in both the PCLS (Figure 21A) and PCKS (Figure 21B), where the three lowest concentrations (0.001µM, 0.01µM and 0.1µM) did not have a reductive effect of fibrosis development but 1µM and 10µM did demonstrate therapeutic efficacy. 1µM Alk5i reduced collagen output compared to the Fib Stim group more in the PCLS than the PCKS, and the 10µM dose was able to reduce the collagen output by around 50% in both organs, almost to the DMSO vehicle control (with no Fib Stim treatment).

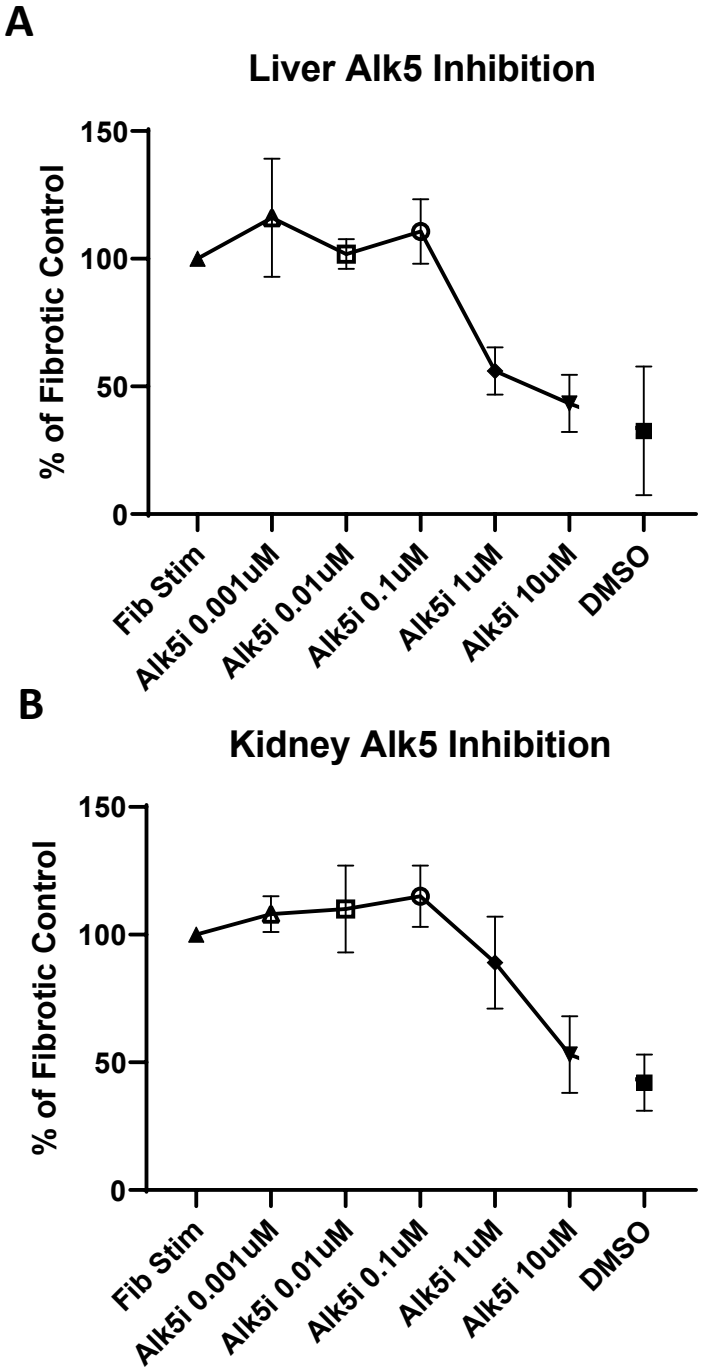

Figure 21. Dose Dependent Inhibition of Fibrosis Measured by Collagen Output

*Addition of Alk5 inhibitor to attenuates the development of fibrosis both PCLS **(A)** and PCKS **(B)** in a dose dependant manner. Technical replicates for each treatment group averaged for each individual donor, in each organ there is an n=2 donors (donor 6 and 7 from table 3 and donor 4 and 5 from table 4) and 5 technical replicates per treatment condition for each donor. Data is shown as mean +/- SEM.*

αSMA and Sirius Red staining and thresholding was performed on the PCKS to assess fibrotic changes, and the data is shown in Figure 22 and Figure 23 respectively. Each treatment group had 5 slices embedded in the same formalin fixed paraffin embedded (FFPE) block, and at least 5 images were taken from different fields of view. Thresholding of these images was performed using NIS-Elements software. The initial threshold was created using the vehicle control slices, and this was then applied to all of the images that were taken. Representative images are shown for each treatment group, alongside a graph displaying the percentage of positive staining across the slices. The number of the embedded PCLS were not sufficient to perform this type of analysis. On a larger dataset, more time would have allowed me to fully optimise the embedding and processing methods.

The levels of positive staining in both αSMA and Sirius Red slices showed a similar trend to the soluble collagen ELISA data, where an increase in the concentration of the Alk5i reduced the levels of collagen deposition and activated myofibroblasts. Numbers of αSMA positive cells peaked in the Fib Stim and lowest concentration of Alk5i (0.001µM). There was then an overall decrease in the numbers of activated HSCs as the concentration of Alk5i increased to 10µM. There was a difference in the number of αSMA positive cells between the Fib Stim control and slices treated with 0.01µM and 1µM Alk5i. There was a reduction in the positive staining in the 10µM and 0.1µM compared to the Fib Stim control. Further donors should be obtained to apply statistical analysis.

Collagen deposition, indicated by the deep red colour in the representative images of Sirius Red stained PCKS, was highest in the lowest concentration of Alk5i, but gradually decreased with increasing doses of Alk5i. The glomerular basement membrane thickened, and the interstitial space became more fibrotic. The Fib Stim and 0.001µM Alk5i slices harboured the most fibrotic features, with the other treatment groups developing progressively less fibrosis as the concentration of Alk5i increased. In both stains, the 0.01µM slices appeared to have significantly less fibrosis development than the Fib Stim control and were both more on par with the vehicle control.

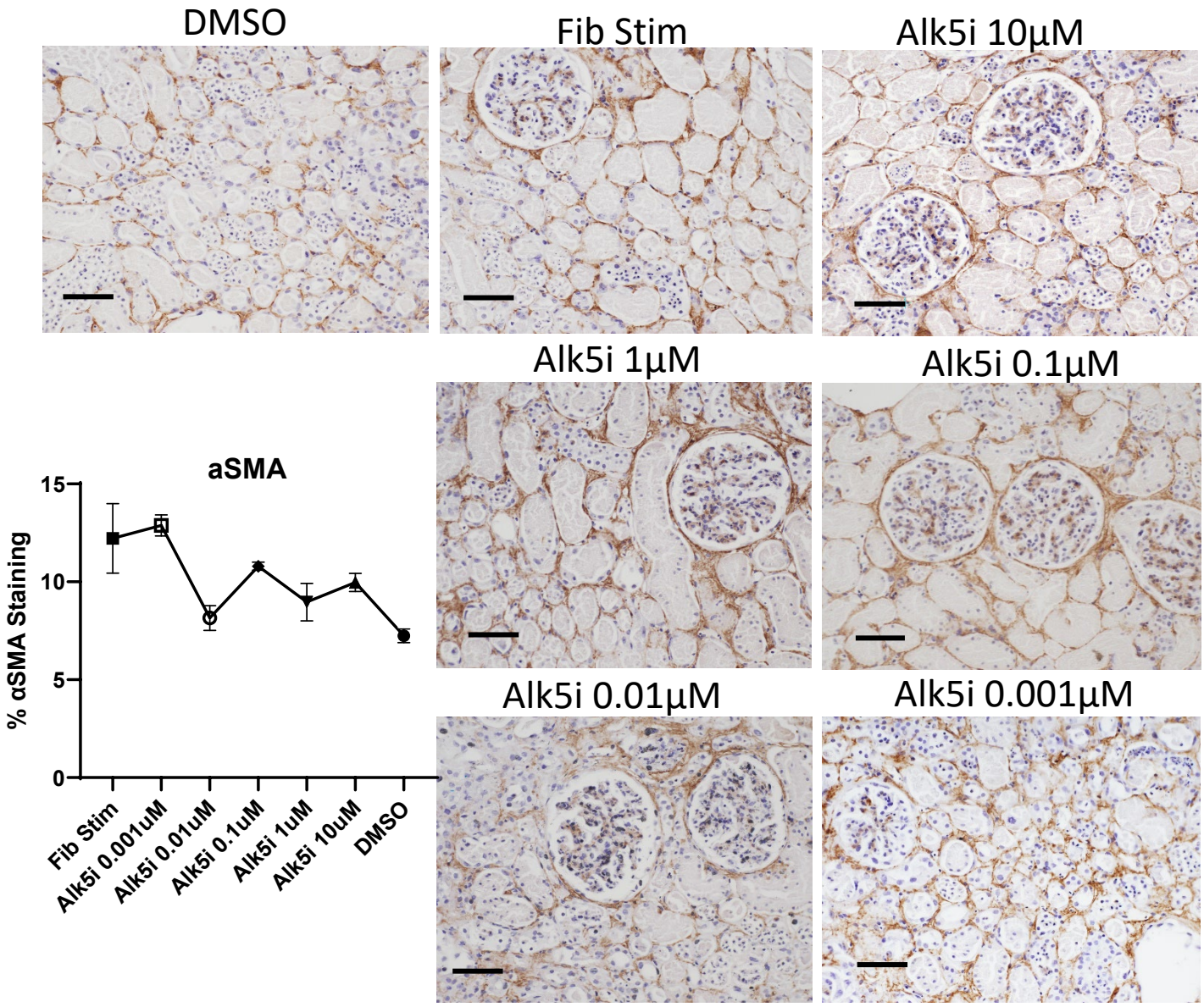

Figure 22. αSMA Positive Staining in 3mm PCKS
Representative images of αSMA staining performed on 3mm PCKS harvested at 96h post processing, cultured with Fib Stim treatment and Alk5i doses. Scale bar represents 100µm. Percentage of positive staining across the treatment is shown on the graph, 1 donor (donor 4) with a minimum of 5 images taken per treatment group. Data shown as mean +/- SEM.

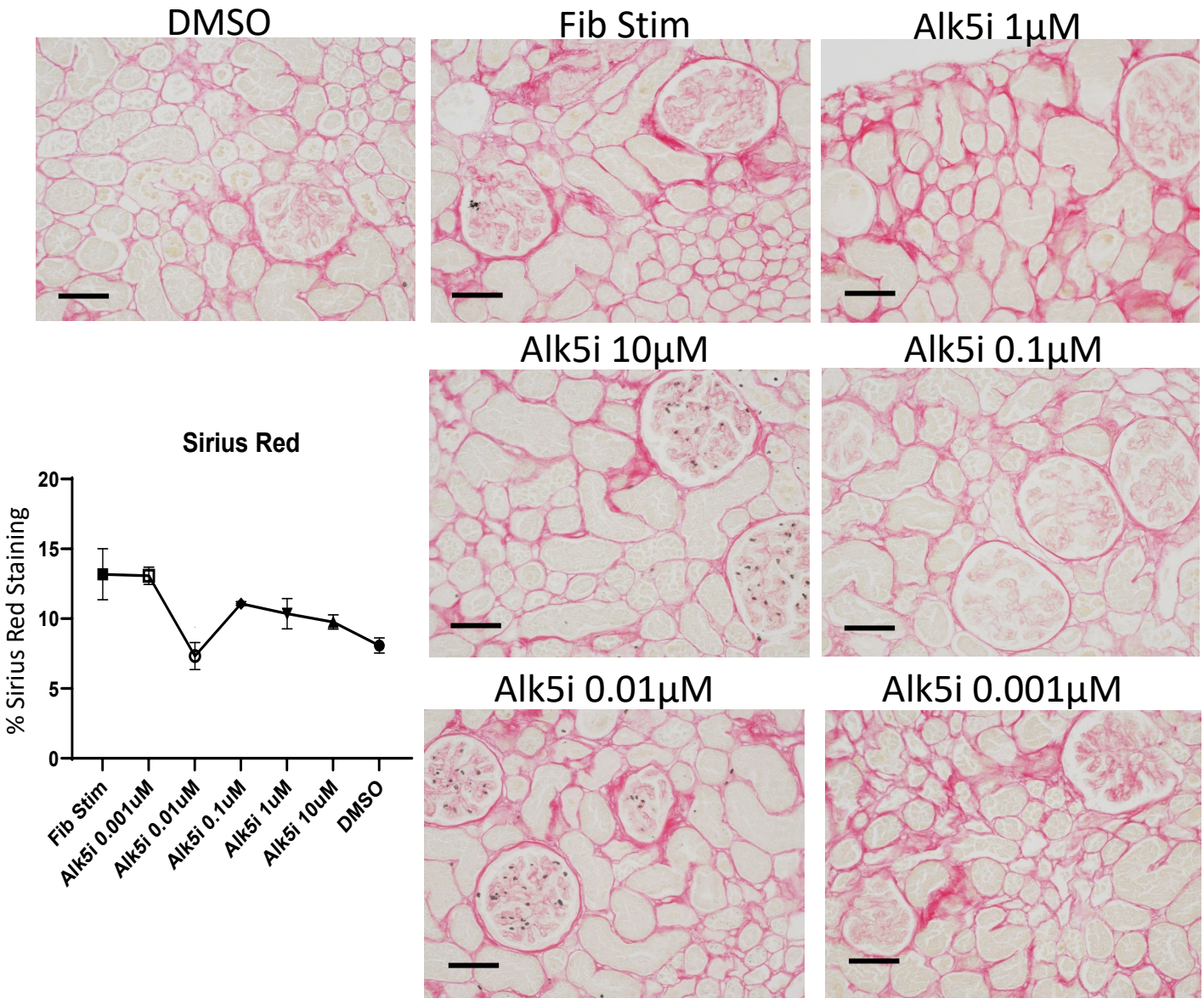

Figure 23. Sirius Red Staining in 3mm PCKS
Representative images of Sirius Red staining performed on 3mm PCKS harvested at 96h post processing, cultured with Fib Stim treatment and Alk5i doses. Scale bar represents 100µm. Percentage of positive staining across the treatment is shown on the graph, 1 donor (donor 4) with 5 images taken per treatment group. Data shown as mean +/- SEM.

After demonstrating the use of small molecule inhibitors in modulating disease progression in the 96 well format, a clinically approved anti-fibrotic was selected to test the system. Pirfenidone is one of two licensed anti-fibrotic drugs for clinical use. The dose range in the PCLS was similar to the range used in the Alk5i dose response studies (Figure 24A). Only the top concentration of Pirfenidone was able to successfully reduce collagen secretion by the slices, with the lower two appearing higher than the Fib Stim treated slices. In the kidney (Figure 24B), a 2-fold dilution dose series was chosen after exploratory

studies in the PCLS revealed that concentrations lower than 0.25µM produced no anti-fibrotic effects. Therefore, Pirfenidone concentrations ranging from 2.5µM to 0.6µM were selected. All three doses were able to reduce fibrosis within the PCKS to some degree, but none of the groups achieved statistical significance compared to the Fib Stim control.

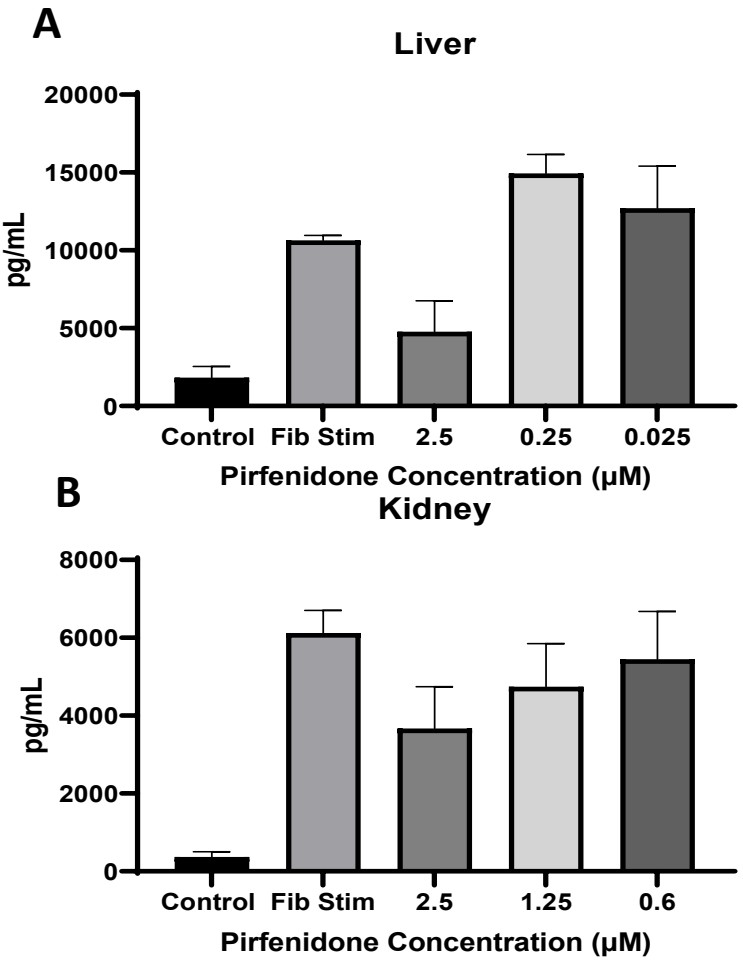

Figure 24. Collagen Secretion from PCTS in response to Pirfenidone Treatment
A- *Soluble collagen output from PCLS media treated with Fib Stim and a range of Pirfenidone doses from 2.5µM to 0.025µM.* ***B-*** *Soluble collagen output from PCKS media treated with Fib Stim and doubling dose of Pirfenidone from 2.5µM to 0.6µM. n=1 kidney donor and n=1 liver donor with 5 technical replicates per donor. Data shown as mean +/- SEM.*

4.4 Discussion

I set out to show that the 96 well bioreactor system is able to reproducibly generate a fibrotic phenotype across multiple organs, which can be cultured over several days for the purpose of target identification/validation and preclinical drug testing. Using a combination of live slice outputs, soluble factors and histology, I have built a picture describing fibrotic disease within donor liver and kidney tissue.

4.4.1 Comparison of PLCS Fibrosis Model in 8mm and 3mm Tissue Slices

First, the culture of 3mm PCLS including the Fib Stim treatment, was compared with the already validated 8mm PCLS model. A comparative study was used to assess the scalability of the system from a low throughput to a medium throughput bioreactor. It is possible to maintain the viability of PCLS in the 96 well bioreactor however, as expected, the smaller slices had a lower RFU value in the resazurin assay as there are fewer cells present to oxidise the non-fluorescent resazurin and produce the fluorescent resorufin. To bring these to a more comparable level, the 3mm slices would need to be incubated for significantly longer in the resazurin dye. Importantly, the difference in the drop in metabolic activity from T0 and 96h between the 3mm and 8mm slices was not significantly different, suggesting that the novel bioreactor can be utilised to culture PCLS in both 12-well and 96-well formats. AST levels were higher in the 8mm PCLS but the LDH levels were the same, suggesting these differences are due to a higher number of hepatocytes being present in the larger slices, rather than cellular injury induced by their culture. It was interesting that higher amounts of albumin were being produced in the 3mm slices in the 3 earlier time points, potentially due to the differences in tissue: media volume ratios. As there was only one technical replicate per condition in the 8mm PCLS, it is not possible to draw firm conclusions about these differences. However, it is clear that the optimised 96 well bioreactor is as capable at supporting the culture of PCLS using the same treatment regime as the 12 well version, and this does not have significant detrimental impact on the smaller slices. I then set out to demonstrate the reproducibly of the platform in replicating a fibrotic disease state within both liver and kidney tissues.

4.4.2 Validation of Fibrosis Disease Model in PCLS and PCKS

Seven liver donors were used for this study which encompassed a relatively diverse range. There was a fairly even split of sexes and background fibrosis across the study, but was lacking in age range and steatotic livers. The nature of the liver resection surgery means we are less likely to receive younger donors, and so have not been able to investigate this demographic in the validation of this model. It would be of interest to add additional donors which fit this category to confirm this method of fibrosis induction is reproducible in younger and potentially less diseased liver, and the development of fibrosis using TGFβ/PDGFββ does not require a pre-existing low level of background disease. Only donors with little/no steatosis were used in this study. Resected tissue samples with large amounts of fat were not always suitable for the preparation of 3mm slices (data not shown).

Five kidney donors were obtained for the fibrosis development study which, whilst well balanced for males and females, only involved older adults with an age range of 63-75, all of whom were overweight by measurement of BMI. Further donors that were younger or were within the normal weight BMI range would provide a more rounded picture of reproducibility between donors and allow identification any conditions that are more or less likely to respond to the Fib Stim treatment or modulation with drugs.

Viability of the slices was assessed at the end of the culture period by reseazurin assay. This was a direct way of evaluating the effects of culture and treatment on the tissue. All slices were still metabolically active at 96h post processing and the Fib Stim treatment did not significantly negatively impact the lifespan of the slices. It was also interesting that the kidney slices appear to cope better in this format than the liver slices. The PCKS had dropped to 60-70% of their T0 compared to the PCLS that had dropped to 40-50%. This is likely due to the tissue being removed from the body and the starting quality. The liver tissue has been shown by previous work to quickly decline in health after removal from the body, requiring processing ideally within 2 hours (151). These samples are surgical biopsies and can often arrive with portions that have been cauterised before being placed in the cold Kreb's solution. Kidney tissue on the other hand, is usually immediately perfused upon retrieval in a solution to extend their life as they are initially to be used for transplant. They are also less likely to have incidental disease development, even though

they are typically from older donors, and have an ideal processing time of 48h post retrieval, ultimately producing higher quality and more metabolically active slices.

Viability of the PCTS was further assessed by measuring LDH as an indicator of cellular damage, and albumin as a biomarker for hepatocyte health and functionality (in the PCLS). LDH release in both the PCKS and PCLS show the same trend, being very high at 24h, accounted for by the transient post-processing stress the tissue is under, and then a fast decline to 96h, indicating the culturing conditions are not cytotoxic or causing significant necrosis.

There was an increase across all treatment groups in the amount of albumin being produced by hepatocytes from 24h to 48h. This increase in functionality was likely a return to what would be normal levels after recovery from processing stresses. There was a steady decline in albumin secretion by the PCLS after 48h, suggesting that there were either a proportion of cells are being lost between time points, or the hepatocytes overall, whilst still alive, were not able to maintain normal albumin output as a result of the culture conditions which, while as close as can reasonably be made, are not the same as conditions in the body. To account for inter slice variability, some soluble outputs at 96h have been normalised to an individual treatment group's 48h level, demonstrating that the Fib Stim treatment regime didn't have a significantly different impact on the slices than the controls.

A pro-fibrotic response can be generated in both organs with the TGFβ/PDGFβ stimulation. Soluble collagen secreted into the surrounding media was quantified by ELISA, and histological analysis was conducted using αSMA and Sirius Red staining to measure fibrosis development. Collagen output was significantly increased with the application of the fibrosis stimulants in both organs at 96h suggesting an increase in ECM deposition and fibrotic scar formation within the slices. There was also a level of spontaneous fibrosis within the controls with a significant increase in both the media only and vehicle control from 48h to 96h. It has been well established that the culturing of hepatic stellate cells leads to a degree of spontaneous fibrosis and so it is not surprising that this would occur within the bioreactor (111,115).

To further confirm the fibrotic phenotype, FFPE slices were stained looking for markers associated with fibrotic disease. αSMA expression is a feature of activated myofibroblasts which are a key driver of fibrosis, secreting excess ECM components as part of a wound

healing response. Activated by TGFβ and PDGFβ, higher numbers of these cell types were present in the Fib Stim slices, compared with the controls. Sirius Red staining was performed to highlight collagen deposition within the slice, which increases significantly in the Fib Stim slices. The 8mm slices were imaged not only the flat surface of a slice, but also as a cross section of the centre of the slice where it was observed that the Fib Stim treatment is not localised to the external 'media facing' portion of the slice, but was able to permeate the whole tissue section and exert a biological effect.

For further work with the tissue slices, I would look to extend the culture period to see how much longer the bioreactor could continue to support viable slices and identify donor types that are more likely to support this extended culture. It would also be interesting to see how much further the TGFβ/PDGFβ induced fibrosis could develop and at what point, if at all within the bioreactor, does this begin to have a negative impact on the health of the slices. Identification of more biomarkers to identify cytotoxicity and functionality within the kidney slices would be useful, providing a greater panel of evidence with which to understand the outcomes of a study.

4.4.3 Identification of Fibrosis Associated Markers

The approach to this point was narrow and biased, in that only assessed a limited number of biomarkers that gave a basic 'yes/no' answer to the question of disease development. Therefore, wider screening of the soluble factors in the media was conducted with an MSD panel. Due to limited sample spaces on the panel, only a small number of donors from each study were run. This meant that both the liver and kidney studies included mostly female donors and almost all were over 60. It would be preferable to increase the number of male donors in both studies to determine how much of an impact sex had on the rate and intensity of fibrosis progression in future MSD screens. It would also be of interest to obtain more younger/pre-menopausal females to establish whether or not the menstrual cycle influences disease progression in any way.

From the 111-plex assay, 35% were undetectable and 54% were not dynamic in the liver and in the kidney, 34% were undetectable and 60% were not dynamic. There was very little overlap in the biomarkers that were identified as dynamic between the liver and the kidney in response to the Fib Stim treatment, with PIGF and IL-6 being the only markers that were significantly affected in both organs.

The addition of the Fib Stim treatment to PCKS increased GM-CSF and MCP-1 significantly, but this was not observed in the PCLS. Whilst well documented for its role in inflammation, the role of GM-CSF is not well defined in the development of fibrosis. The kidney data correlated with what has been shown by Xu *et al* in their kidney model, where GM-CSF, released by proximal tubule cells in response to stress and injury, induced MCP-1 expression via macrophage recruitment, producing a sustained fibrotic and inflammatory niche both *in vivo* and *in vitro.* The development of fibrosis in the PCKS, induced by incubation with TGFβ and PDGFβ, is causing injury to the proximal tubule cells. As the fibrotic scar develops, GM-CSF is released producing a pro inflammatory environment which can attract immune cells, suggesting that while an important mediator of a pro-inflammatory environment, GM-CSF itself does not constitute a common pathological feature of fibrosis (181–183).

PIGF and VEGF are increased in response to the Fib Stim treatment and this is attenuated by Alk5i treatment in PCLS. The same trend was observed in the PCKS for PIGF but not for VEGF. It is possible that with further donors, a significant dynamic range could be achieved between the control and Fib Stim groups as the raw values suggest an upregulation of VEGF in response to fibrosis induction, however with the three donors in the study, significance is not achieved. PIGF is a member of the VEGF family which promotes angiogenesis, a key process accompanying fibrosis. There have been studies in mice and humans showing significantly upregulated PIGF and VEGF levels in fibrotic/cirrhotic livers and it is understood that excess VEGF is pathogenic, resulting in faster disease progression. Within the slices, the developing scar distorts local architecture causing capillary rarefaction and hypoxia resulting in an increase in pro-angiogenic factors (184–186).

The other common upregulated protein in both the PCLS and PCKS systems in response to Fib Stim treatment, is IL-6. IL-6 is a cytokine which drives chronic inflammation and fibrogenesis secreted by activated myofibroblasts. This data adds to the other evidence showing the Fib Stim treatment is able to produce a disease state within the PCLS that is comparable with fibrosis development in patients (56,187,188).

MIP-1β (also known as CCL4) expression was significantly decreased in the fibrosis induced PCLS. Similar findings were observed by Sadeghi *et al* in their study involving liver cirrhosis, where healthy patients had significantly higher serum levels of MIP-1β than

patients with cirrhosis. MDC (also known as CCL22) was also significantly decreased in the fibrosis induced PCLS. I suggest this reduction is because TGFβ is activating macrophages to an M2b subtype rather than the MDC producing M2a subtype (189).

This fibrosis model is not only able to produce significant architectural changes within the tissue from excess ECM deposition but can also replicate the changes in inflammatory and fibrotic biomarkers observed in clinical samples. The panel that was selected was geared towards inflammatory markers, and so a panel more aimed towards pro and anti-fibrotic markers could potentially identify other dynamic soluble factors secreted into the media. Further donors for MSD screening would be beneficial to increase the power of statistical analysis. It would also allow us to understand if there is inter-donor variability depending on categories such as sex, age, or underlying disease state, and how significant this is. It has also been observed (data in chapter 5) that expression of inflammatory markers is usually highest earlier on in the culture period, therefore testing earlier 48h and 72h media samples, may identify other biomarkers affected by the addition of the Fib Stim treatment.

4.4.4 Feasibility of Efficacy Testing Drug Screens with Novel Bioreactor

After validating the reproducibility of the fibrosis model in the PCLS and PCKS I then set out to demonstrate the use of the 96 well bioreactor for efficacy testing of anti-fibrotic therapies. There are currently only two anti-fibrotic treatments available to patients, but these are both for lung fibrosis and are not very effective. Liver and kidney fibrosis have no approved anti-fibrotic therapies and are instead managed by treating the underlying cause of injury rather than inhibiting the progression of scarring. There have been several anti-fibrotic drugs that have shown promise in animal studies but these have not led to success in human clinical trials (190–193).

Alk5 inhibitors are commonly used to demonstrate the potential of newly developed drug screening tools. Fib Stim challenged PCLS and PCKS were cultured with a range of Alk5i doses to produce a dose dependent response. Both organs demonstrated a negatively correlated curve in the soluble collagen ELISA, and in the PCKS also demonstrated this effect in the αSMA and Sirius Red staining. The treatments are able to permeate the whole slice and do not just have surface level effects in both the liver and the kidney. Some slices will have tears in them during histology processing and cutting which could not be fully imaged, and this can skew the data. These factors have likely resulted in the lower

percentage of positive staining in both the αSMA and Sirius Red thresholding graphs (Figure 22 and Figure 23) in the 0.01µM Alk5i treatment group.

There were some problems identified with the potential use of histological analysis in the 3mm slices, particularly in the case of the liver. The majority of the PCLS had contracted during the culture period and had folded during processing, making embedding a challenge. The resulting sections cut from the FFPE block were not whole, but torn, limiting the number of representative images taken. Tweaks to the process will be made going forward. The PCKS were more successful as they did not shrink in culture. However, it was found that for successful imaging of stained sections, there should be a minimum of 5 slices per treatment group, to provide a good representation of the biology. To address this for future work, whole slices should be embedded individually which will more accurately represent the amount of αSMA and collagen expression within the tissue. Fewer slices would be required for gene and protein expression profiling, so in cases where a range of drugs and/or concentrations are to be tested on one plate, snap freezing tissue coupled with non-destructive soluble markers would be a better alternative to histology in these instances.

After demonstrating a dose response effect could be achieved with the bioreactor, Pirfenidone, a drug used in the clinic to treat patients with lung fibrosis, was selected to demonstrate the ability of the platform to predict efficaciousness. Pirfenidone inhibits fibrosis development by inhibiting TGFβ production, attenuating TGFβ/SMAD3 signalling which prevents myofibroblast activation and reduces TGFβ induced αSMA production. The exact mechanism behind this is not understood fully. It is metabolised by CYP1A2 to mainly 5-hydryoxypirfenidone and 5-carboxypirfenidone, which have been shown to have anti-fibrotic effects alongside the parent drug. Pirfenidone has been limited in use for other fibrotic diseases due to toxicity, but it has been suggested that dose alterations may extend its use to fibrotic diseases in other organs (194–196).

Concentrations of Pirfenidone lower than 0.25µM were not able to prevent fibrosis development in the tissue slices but the higher concentrations were able to reduce collagen deposition. There was limited tissue available when I had reached a point at which I could perform these studies due to surgery cancellations from COVID-19 and NHS blood shortages, resulting in only 1 donor per tissue type for these experiments with only a small number of concentrations tested. More concentrations of Pirfenidone should be

tested in both organs, including higher concentrations to investigate if this could reduce fibrosis development further in the PCTS without increasing toxicity.

4.5 Conclusion

The aims for this chapter were:

- Validate the fibrosis model in the 96 well bioreactor in both human liver and kidney
- Demonstrate use of bioreactor as a suitable platform for efficacy testing anti fibrotic drugs

I have successfully scaled and validated the fibrosis model in the liver and kidney in the novel 96 well plate bioreactor. The slices remain metabolically active and functional to the culture end point at 96h post processing, and can also be manipulated to develop features associated with fibrotic disease and the treatments applied are able to permeate the whole slice. This method of disease modelling was also reproducible across multiple donor types including sex, age and underlying pathologies, and is suitable for modulating with inhibitors. In the donor pool that was available for the validation study, even though there were a broad range of donor types, it would be useful to build these numbers further to better identify the most suitable candidates for this kind of study. This would allow understanding of whether differences in fibrosis development within the PCTS are donor dependent (sex/age/underlying disease) or independent (resection retrieval time). The suitability of this modelling platform for the efficacy testing of anti-fibrotic drugs and target validation in both the kidney and liver has also been demonstrated. A minimum of three paired wells (6 slices) were used per condition to provide sufficient technical replicates for both viability assessment and soluble factor examination to evaluate efficacy. Data obtained then suggested a smaller, 2-fold dilution series should be performed between concentrations that have demonstrated the most significant effect and the first concentration that has no or limited anti-fibrotic effects with 6 paired wells (12 slices) per condition. This would allow the user to identify the optimal concentration of the drug that generates a significant reduction in fibrosis development. The large number of slices would also allow for more representative histological analysis and extra slices for unbiased multi-omic interrogation of disease biology such as proteomics or transcriptomics or multiplex image analysis, for example Hyperion imaging mass cytometry.

Chapter 5. Inflammation Modelling

5.1 Introduction

Inflammation is feature of almost all human disease, and is a hugely complex process involving numerous cell types and proteins which either drive or supress the inflammatory response (40,41). Under physiological conditions, inflammation is considered protective, removing dead/damaged cells or invading pathogens and aiding in tissue remodelling and repair. In cases of chronic illness however, inflammation can become pathological, and in the context of fibrotic disease, promotes fibrosis development and a decline in organ function (40). NASH in the liver and glomerulonephritis in the kidney are examples of chronic conditions where inflammation is a key feature, which both can develop into end stage CLD or CKD respectively when allowed to remain unresolved (43,50).

5.1.1 Development of Inflammation and Common Features

Inflammation transpires in most cases from loss of local tissue structure and subsequent loss of function which can occur from physical injury, infection or from a chemical source such as alcohol, toxicants, glucose or fatty acids (40). Damage to the parenchymal cells releases DAMPs (or PAMPs where microorganisms are present) which are detected by PRRs such as members of the TLR family on the surface of (most commonly) antigen presenting cells such as macrophages (40,41). This binding event triggers an intracellular signalling cascade to promote and regulate the immune response. The three main pathways that control this are NF-κB, MAPK and JAK-STAT (41).

Each of these three major inflammatory signalling pathways is capable of upregulating a wide range of both pro and anti-inflammatory genes, and so there is some specificity built into the system to prevent all genes being activated in response to all stimuli (197). NF-κB for example, has 5 family members which form either homo- or hetero-dimers to regulate distinct sets of genes. Loss of one of these transcription factors affects the response to immune challenge (198). There are also many inhibitory proteins within the cytoplasm and nucleus to prevent activation of pathways to terminate the inflammatory response.

Cytokines are small proteins produced by numerous cell types which regulate the immune and inflammatory response. Their effects depend on the type of cell they are influencing and multiple cytokines may have the same effect on a cell (199). IL-6, IL-1β,

TNF-α and IL-8 have been identified as crucial cytokines in the development of inflammation caused by infection, autoimmune diseases and injury (53,56,199,200).

5.1.2 Current Models of Inflammation

Many 2D cell culture models of inflammation and cytokine production in response to challenge often use primary cells. Differences in the inflammatory response to mediators such as LPS have been observed between mice and humans (201). For example, GM-CSF differentiated primary mouse monocytes have a different secretory output in response to LPS compared to primary human cells. There were 2 common cytokines (TNF-α and IL-6) but 5 others that were species specific (201). This could be as a result of species differences but could also be as a result of an incomplete picture from only using one cell type.

Animal modelling of inflammatory diseases provides a more complete picture of response to challenge compared to 2D cell culture. All immune cells are present, unlike in *in vitro* models, and those that would normally disappear soon after removal from the body, are naturally replaced. Knockout animal models for mechanistic study of inflammation has highlighted contradictions that would not be apparent with *in vitro* monoculture. Blocking IL-6 for example, has been shown to reduce inflammation in a diet-induced model of NASH and chronic signalling exerts a pro-inflammatory effect, however IL-6 release from other tissues has a beneficial effect on glucose control and insulin resistance (202).

Human PCTS have, as a model of inflammation, the ability to negate the issues of species differences and lack of tissue context. There have been several studies which have modelled inflammation in precision cut lung slices using bacterial and/or viral products (203). Kolbe *et al* applied both live and heat-killed *Pseudomonas aeruginosa* to lung slices, and found that the tissue was able to mount a robust immune response to these bacterial products. This response could also be modulated with the use of inhibitors (204). The main limitations with PCTS as a model for the inflammatory response is the variation in immune cells within slices and lack of a blood supply. Each slice will only contain cells that were present at the time of slicing and some primary immune cells such as neutrophils, can deplete soon after removal from the body. Manually adding in an immune component is a strategy should be considered, however in order to maintain

physiological relevance, the balance of different immune cells and volumes added to slices would need to be taken into account. Donor matching would be important, as the addition of non-compatible white cells may themselves cause an immune response, skewing data and exhausting certain cell types.

5.1.3 Chapter Aims

- Validate the inflammatory model in the 96-well bioreactor in both human liver and kidney slices.
- Demonstrate the use of the bioreactor as a suitable platform for efficacy testing anti-inflammatory drugs.

I aim to validate a model of inflammation in the PCLS and PCKS using the 96-well bioreactor. LPS, IL-1α and IL-1β will be used first to optimise the induction of the inflammatory response in the tissue, and variables including stimulant concentration and culture time will be tested to determine which mediator induces the strongest and most reliable inflammatory response in the PCTS. Then known anti-inflammatory compounds will be tested to demonstrate the use of the bioreactor as a suitable platform for efficacy testing of novel inhibitors of the immune response.

5.2 Methods

5.2.1 Materials

Sourcing of tissue and general materials for tissue culture are described in 2.1. IL-1α, IL-1β were purchased from Peprotech and reconstituted according to manufacturer's instructions. LPS was purchased from Sigma and dissolved in PBS to 5mg/ml. IKK2VI inhibitor was purchased from Cayman Chemical Company and reconstituted in DMSO to 100mM.

5.2.2 Culture Conditions for PCLS Inflammation Model Optimisation

Production of the 3mm liver slices is described in 2.1.3. After a 24h rest period following the slicing process, slices were stimulated with IL-1α or IL-1β at 1000pg/ml, 250pg/ml, 100pg/ml and 25pg/ml or LPS at 100ng/ml, 25ng/ml and 10ng/ml. Relevant vehicle controls were also included. Treatments were refreshed every 24h with supernatants collected as previously described (2.1.6) until the end of the culture period at 96h post processing. Slices were harvested for biochemical assays and the media was frozen, methodology for this is described in the Methods chapter.

5.2.3 Culture Conditions for PCKS Inflammation Model Optimisation

Production of the 3mm kidney slices is described in 2.1.5. Following a 24h rest period after the slicing process, slices were stimulated with IL-1α or IL-1β at 1000pg/ml, 250pg/ml, 100pg/ml and 25pg/ml or LPS at 100ng/ml, 25ng/ml and 10ng/ml. Relevant vehicle controls were also included. Treatments were refreshed every 24h with supernatants collected as previously described (2.1.6) until the end of the culture period at 96h post processing. Slices were harvested for biochemical assays and the media was frozen for ELISAs and LDH assays. The methodologies for these assays are described in the Methods chapter.

5.2.4 Culture Conditions for PCLS and PCKS for Inflammatory Inhibition

Production of the 3mm slices is described above. Following a 24h rest period, slices were treated for a further 24h with 1000pg/ml IL-1β + IKK VI in a 10 fold dilution series from 10µM to 0.001µM. Controls included were a vehicle control equivalent to the top drug

concentration, a 10µM IKK VI only control and a 1000pg/ml IL-1β only control. At 48h post processing, all slices were harvested for either biochemical assay or freezing. Media samples were also collected for ELISAs and AST and LDH assays. The methodology for these is described in the Methods chapter.

5.2.5 Analysis of Soluble Outputs

Several methods were used to analyse the soluble outputs from the cultured slices, and they included; the CyQUANT LDH assay, a number of ELISA kits including Albumin, KIM1 and IL8 as appropriate and a MSD U-Plex assay. The specific protocols for each of these is described in 2.2 of Materials and Methods.

A

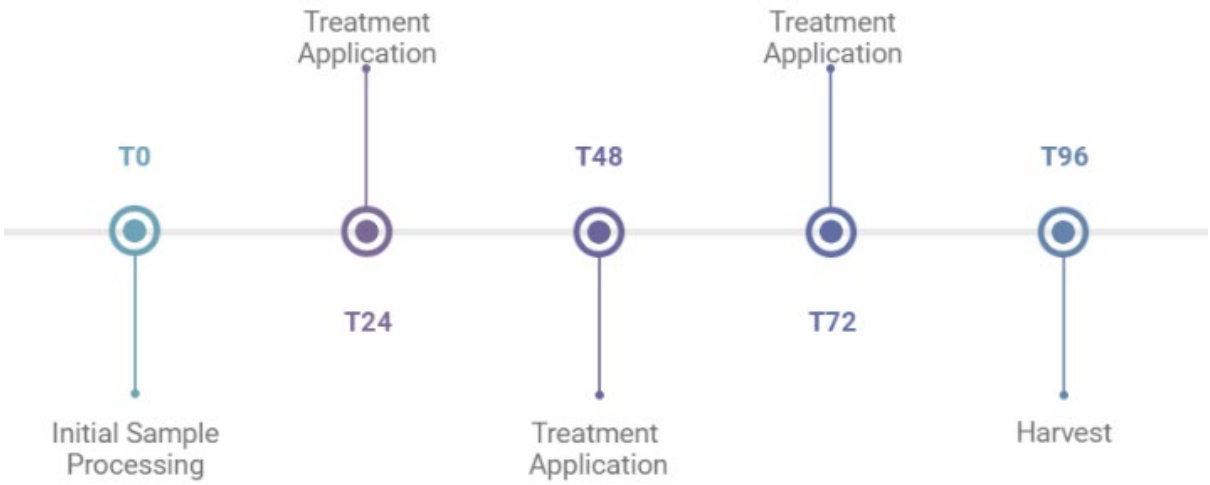

B

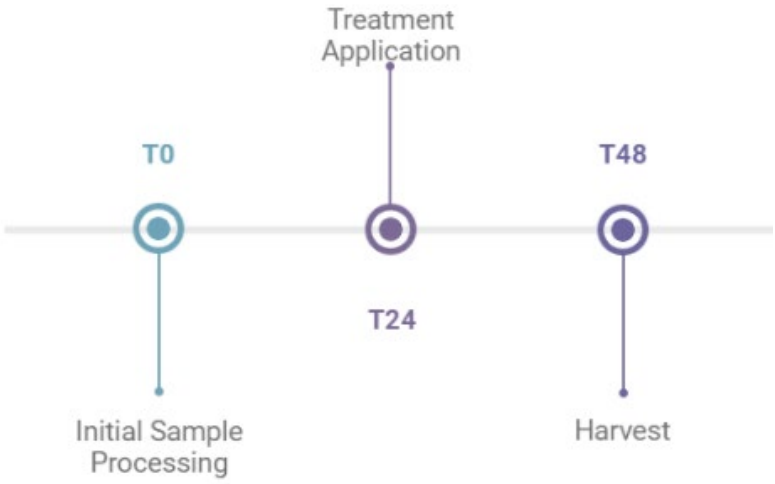

Figure 25. Treatment Plans for Inflammation Model
A- *Inflammation model optimisation protocol ran for 96h from initial sample processing.* ***B-*** *Optimised protocol for generating inflammation in the PCTS. Slices received one cycle of treatment after a 24h rest period, slices harvested 48h post processing.*
Treatments refreshed every 24h where appropriate, with media collected and stored at -80°C

5.3 Results

5.3.1 Optimisation of Inflammation Model

For the development of a model to study inflammation in the tissue, we selected 3 pro-inflammatory mediators. IL-1α and IL-1β are cytokines involved in regulating the immune and inflammatory response in injured tissues and LPS is produced by gram negative bacteria and as a result triggers an immune response. Initial optimisation for this model involved selecting the most potent activator for our model and identifying the best concentration and culture time.

The protocol was optimised using five liver donors shown in Table 7, and four kidney donors shown in Table 8. The average age of the liver donors was 54 with the youngest patient being 23 years of age. 60% of the five donors were female and 40% were male. 80% had pre-existing fibrosis development to some degree but only one of these donors also had steatosis. There was one patient who had developed neither fibrosis nor steatosis according to their resection sample grading. The average age of the kidney donors was 64 with the youngest being 54 years of age and 75% were female. Three of the four donors in this study were also classed as overweight by their BMI.

Table 7. Liver Donors in Inflammation Optimisation

Donor Number	Age	Sex	Fibrosis Score	Steatosis Score
Donor 1	59	F	1	0
Donor 2	23	F	1	0
Donor 3	73	M	2	0
Donor 4	57	F	0	0
Donor 5	58	M	2	2

Table 8. Kidney Donors in Inflammation Optimisation

Donor Number	Age	Sex	BMI
Donor 1	63	M	32
Donor 2	75	F	25
Donor 3	63	F	27
Donor 4	55	F	23

Metabolic output at 96h in the PCLS treated with IL-1α (Figure 26A), IL-1β (Figure 27A) and LPS (Figure 28A) has been normalised to an individual donor's T0. Slices incubated with higher concentrations of each of the inflammatory stimulants, on average, had a higher metabolic output than the control, but this increase was not statistically significant in any case. The results for donor 2 (the very young female), however, showed the inverse of all the other donors across all three stimulants, where the higher concentrations had a lower metabolic output.

LDH release from the PCLS was measured to confirm that the inflammatory stimuli were not cytotoxic (Figure 26B, Figure 27B and Figure 28B). The pattern of LDH release to each of the stimulants was as expected in both organs, high at 24h due to post processing recovery and significantly reduced after this time. The treatments applied did not cause an increase in LDH at any point during their application when compared to the control group. After finding that the slices had remained viable across all conditions, and that the inflammatory mediators were not exerting an immediate and obvious toxic effect on them, soluble factors in the media linked with an inflammatory response were analysed.

IL-8 was used as the starting measure of activation of an inflammatory response within the tissues. Unlike our fibrosis model, repeated treatment with any of the chosen stimulants did not progressively increase the inflammatory response. Both the IL-1α (Figure 26C) and IL-1β (Figure 27C) readouts showed a well-defined stepwise increase in IL-8 release in response to higher stimulant concentration at each time point in the PCLS. 100ng/ml LPS elicited the greatest IL-8 response, and this remained higher than the control across the culture period. The lower two concentrations were as effective as each other at inducing an inflammatory response at 48h, however after this time, IL-8 production in the slices dropped to a similar level of the untreated control. Only the top concentrations of the chosen inflammatory mediators could induce a statistically significant inflammatory response in the liver as inferred by the production of IL-8 by the tissue slices. Whilst LPS and IL-1β achieved this with the first treatment, it took a further 24h of treatment to achieve statistical significance between the control and top concentration in IL-1α. LPS (Figure 28C) appeared to be unable to sustain a more chronic response in the liver tissue, with IL-8 levels dropping over the culture period across all concentrations. It also required a much higher concentration to exert the same effect as IL-1β and IL-1α.

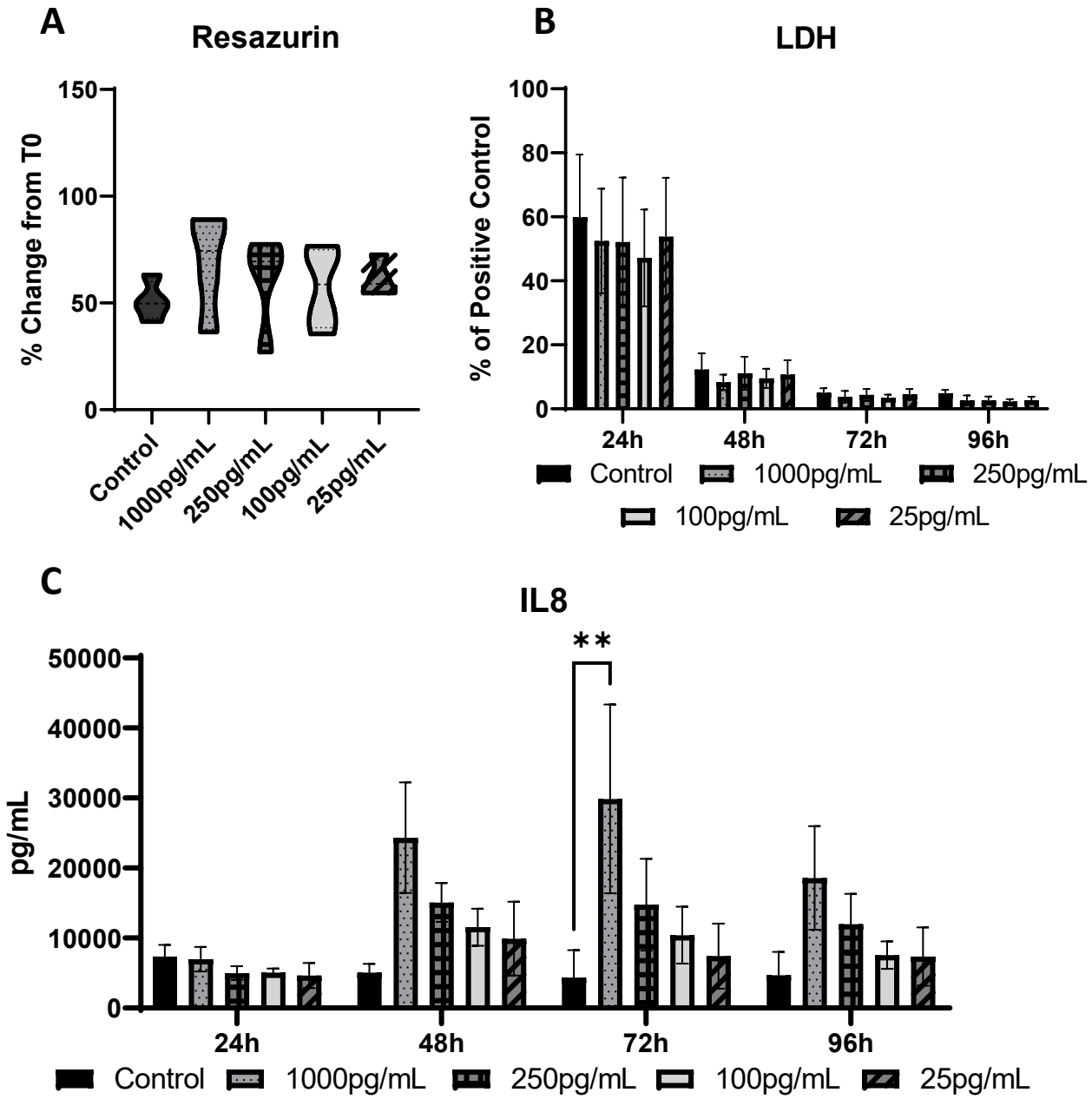

Figure 26. Optimisation of IL-1α Inflammatory Stimulation in PCLS

A- *A resazurin assay was performed on slices at 96h, shown here as percentage of T0 slices, no statistically significant differences seen by ANOVA. Data shown as average and min/max values.* ***B-*** *LDH output was measured from culture media saved at 24h time points, data shown as percentage of positive control, mean +/- SEM.* ***C-*** *Soluble IL-8, measured by ELISA from culture media saved at 24h time points, absolute values with mean +/- SEM. Statistical significance between treatment groups measured within time points by 2-way ANOVA, ** p=≤0.01. N=5 liver donors with 5 technical replicates per treatment group per donor.*

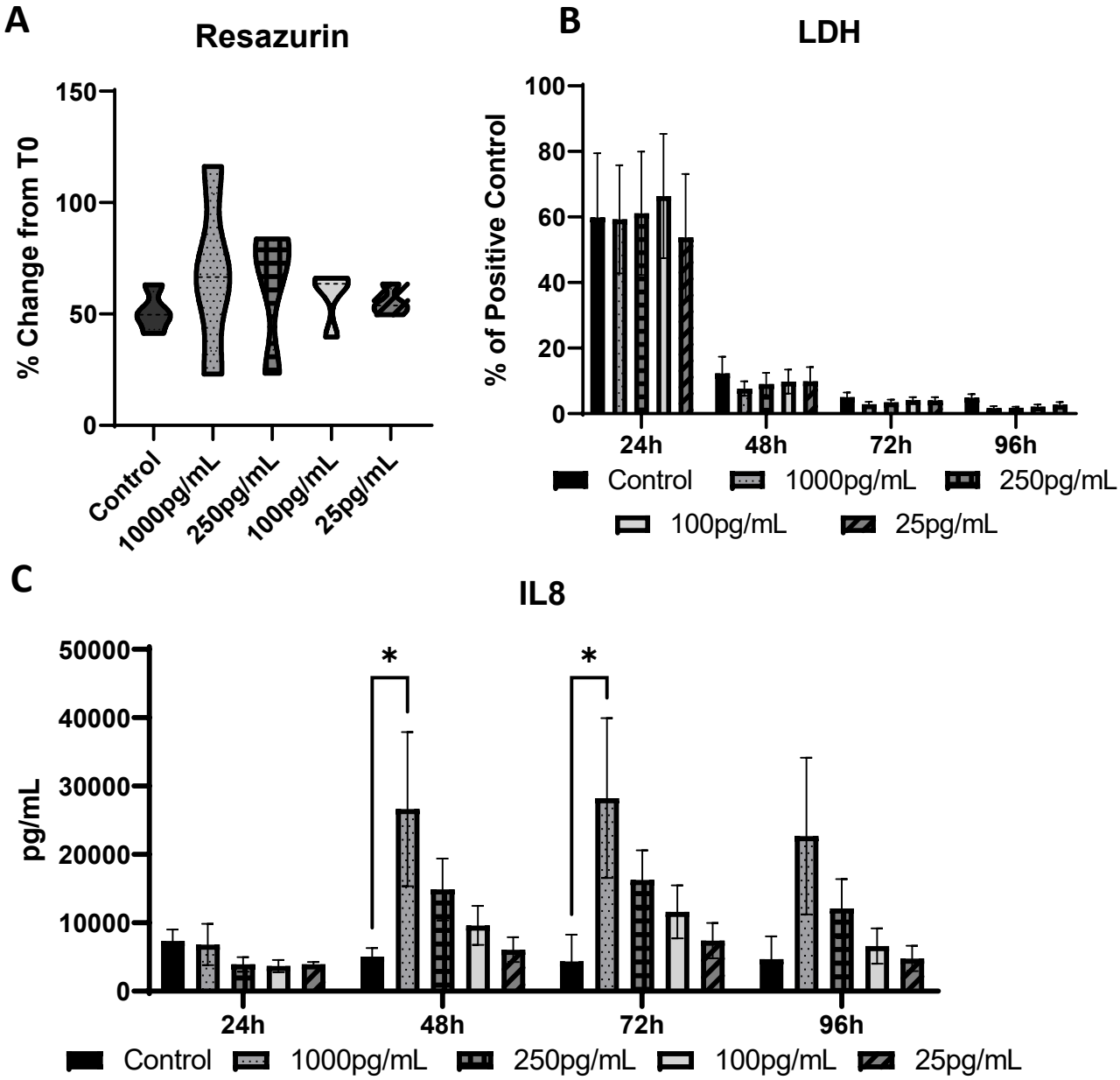

Figure 27. Optimisation of IL-1β Inflammatory Stimulation in PCLS

A- *A resazurin assay was performed on slices at 96h, shown here as percentage of T0 slices, no statistically significant differences seen by ANOVA. Data shown as averages plus min/max values.* ***B-*** *LDH output was measured from culture media saved at 24h time points, data shown as percentage of positive control, mean +/- SEM.* ***C-*** *Soluble IL-8, measured by ELISA from culture media saved at 24h time points, absolute values with mean +/- SEM. Statistical significance between treatment groups measured within time points by 2-way ANOVA* p=≤0.05. N=5 liver donors with 5 technical replicates per treatment group per donor.*

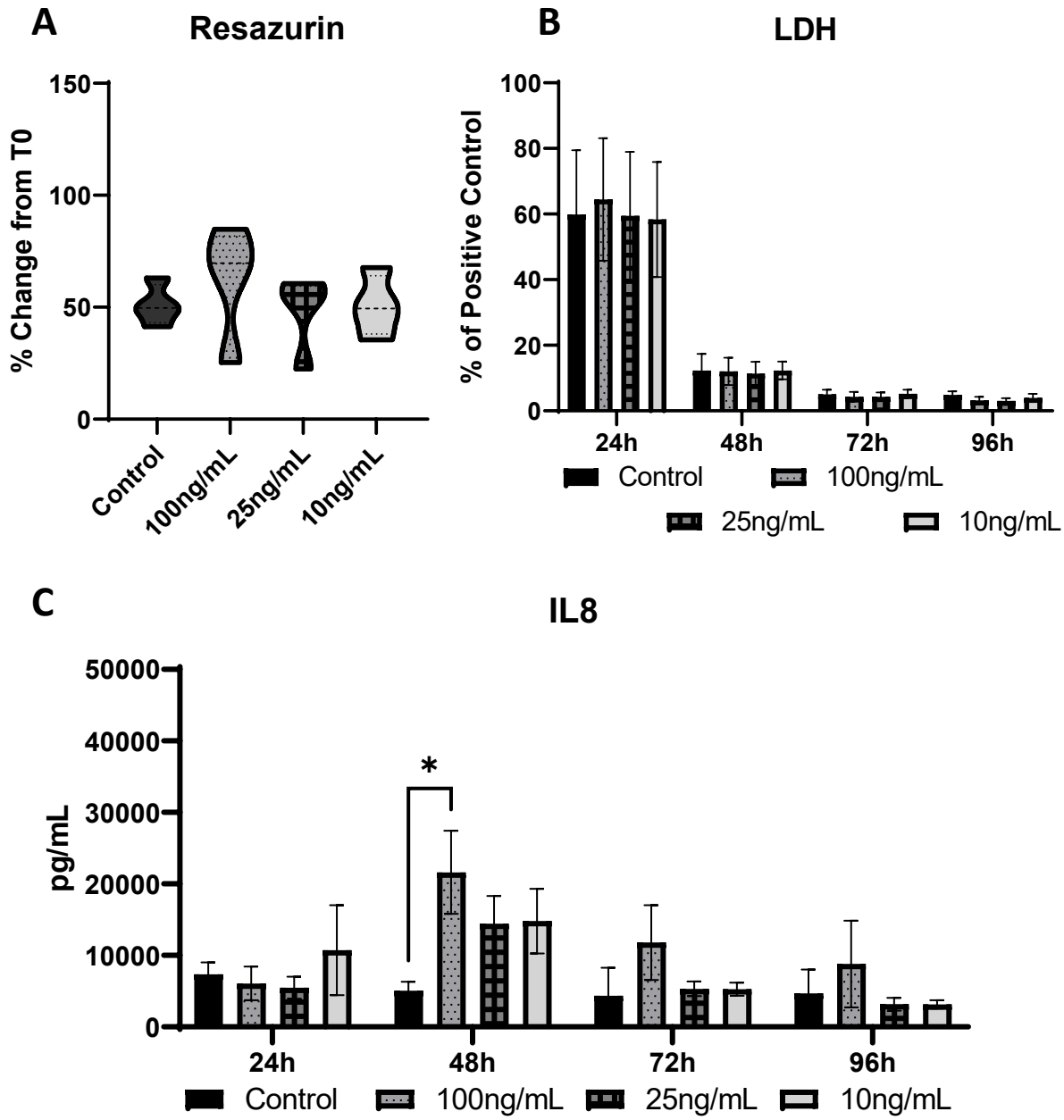

Figure 28. Optimisation of LPS Inflammatory Stimulation in PCLS

A- *A resazurin assay was performed on slices at 96h, shown here as percentage of T0 slices, no statistically significant differences seen by ANOVA. Data shown as average plus min/max values.* ***B-*** *LDH output was measured from culture media saved at 24h time points, data shown as percentage of positive control, mean +/- SEM.* ***C-*** *Soluble IL-8, measured by ELISA from culture media saved at 24h time points, absolute values with mean +/- SEM. Statistical significance between treatment groups measured within time points by 2-way ANOVA, * p=≤0.05. N=5 liver donors with 5 technical replicates per treatment group per donor.*

In the PCKS, the higher concentrations of IL-1α appeared to have a negative effect on metabolic activity as measured by resazurin assay (Figure 29A), but this difference was not calculated to be statistically significant by one-way ANOVA. A similar trend was also seen in some the IL-1β treated PCKS donors (Figure 30A), but not to the same degree as

with the IL-1α treated slices. Overall there were no significant differences between the control and stimulated slices at any concentration. The addition of all of the LPS concentrations had, on average, a negative effect on slice health compared to the control, but like the other stimulants, this difference was not significantly different (Figure 31A). Incubation of the PCKS with the individual stimulants did not cause an increase in LDH release across the culture period. In the IL-α (Figure 29B), IL-1β (Figure 30B) and LPS (Figure 31B) treated slices, LDH release was highest at 24h then there is a steady decrease in all concentrations of the respective stimulants to 96h.

IL-1β produced the most statistically significant response in PCKS at the top concentration at 48h compared to the control (Figure 30C). A stepwise decrease was seen as the stimulant concentration decreases, and the inflammatory response to repeated IL-1β treatment, was never as high as the initial exposure. The response to IL-α was more variable (Figure 29C), where 1000pg/ml and 100pg/ml were able to induce a significant response to the stimulant compared to the control at 48h. The top concentration (1000pg/ml) was able to induce significantly higher IL-8 production again at 96h compared to the control. The response to the LPS stimulant was different in the PCLS compared to the other stimulants used (Figure 31C). At 48h, 25ng/ml LPS and at 96h, 10ng/ml LPS were able to produce a statistically significant increase in IL-8 in the PCLS compared to the control, but it was observed that the spread of data is much greater in these conditions compared to others at the same time points and if more donors were gathered for this analysis, the outliers may not have such an influence. There is no stepwise increase in IL-8 secretion as the concentration of LPS increases, and there were no statistically significant differences between any of the treatment groups relative to each other within the time points.

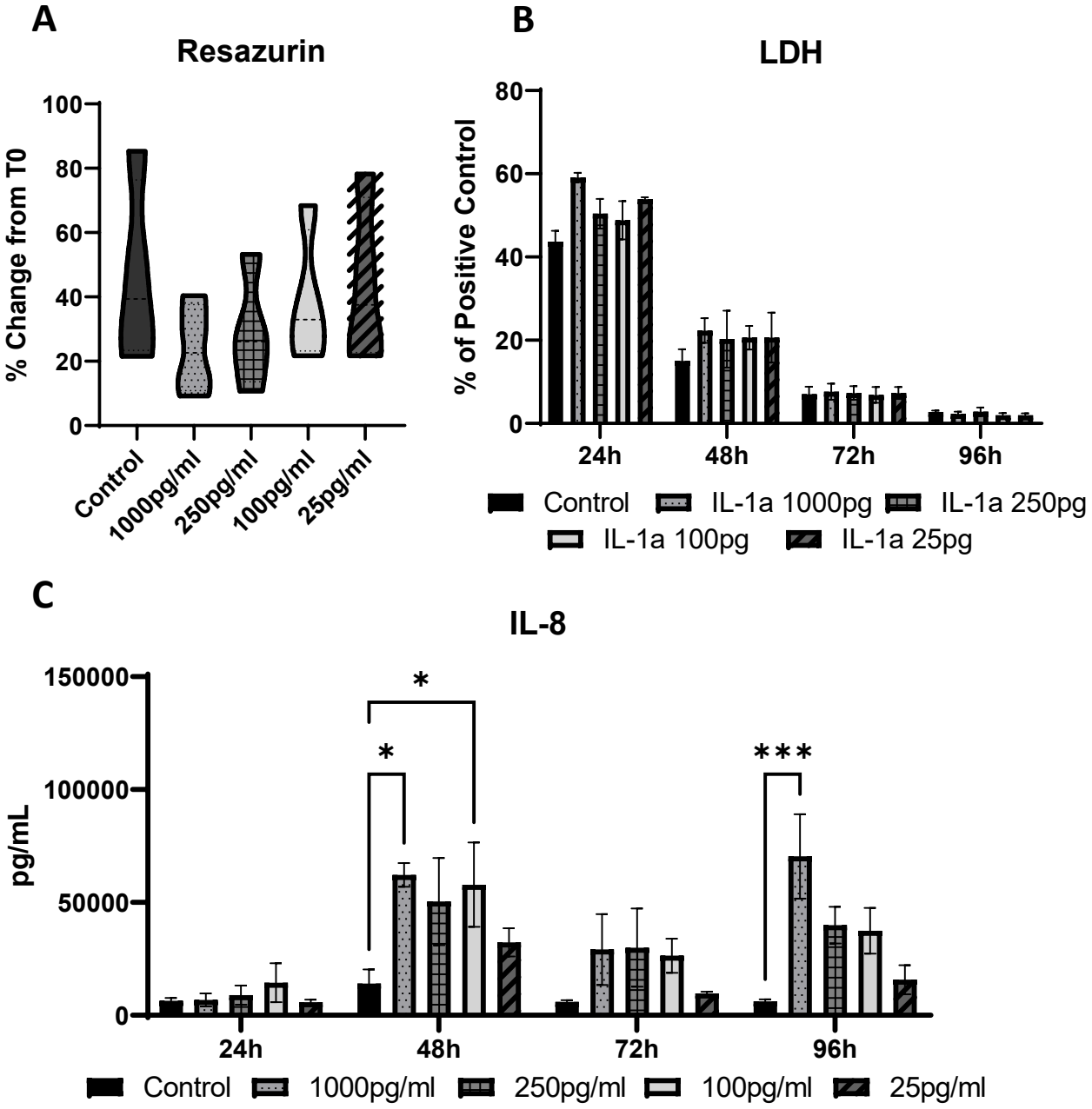

Figure 29. Optimisation of IL-1α Inflammatory Stimulation in PCKS

A- *A resazurin assay were performed on slices at 96h, shown here as percentage of T0 slices, no statistically significant differences seen by ANOVA. Data shown as averages plus min/max values.* ***B-*** *LDH output was measured from culture media saved at 24h time points, data shown as percentage of positive control, mean +/- SEM.* ***C-*** *Soluble IL-8, measured by ELISA from culture media saved at 24h time points, absolute values with mean +/- SEM. Statistical significance between treatment groups measured within time points by 2-way ANOVA* p=≤0.05, *** p=≤0.001. N=4 kidney donors*

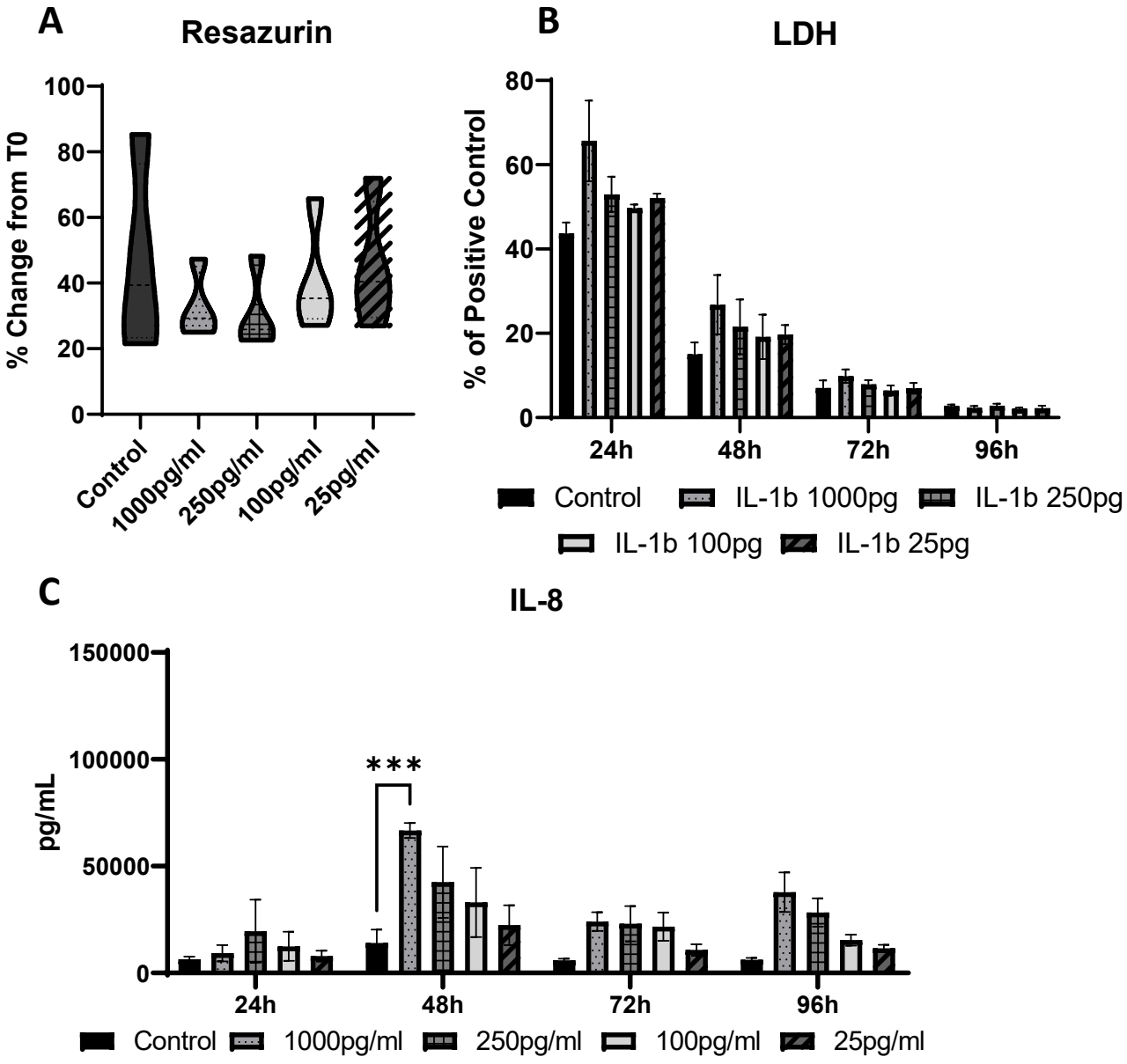

Figure 30. Optimisation of IL-1β Inflammatory Stimulation in PCKS

A- *A resazurin assay were performed on slices at 96h, shown here as percentage of T0 slices, no statistically significant differences seen by ANOVA. Data shown as averages plus min/max values.* ***B-*** *LDH output was measured from culture media saved at 24h time points, data shown as percentage of positive control, mean +/- SEM.* ***C-*** *Soluble IL-8, measured by ELISA from culture media saved at 24h time points, absolute values with mean +/- SEM. Statistical significance between treatment groups measured within time points by 2-way ANOVA, *** p=≤0.001. N=4 kidney donors*

The inflammatory response in the slices, measured by IL-8 release, did not increase over time and that in most cases, the most significant response was seen only after the first treatment cycle at 48h. Also, only the top concentration of each stimulant was able to reliably achieve a significant response in the tissues. For these reasons, it was decided that for future work, the acute inflammatory response model was best kept to 48h total culture time, with one treatment cycle, using the top concentration of the stimulant. To determine the best stimulant for anti-inflammatory drug screening testing, a number of inflammatory factors were measured in the PCTS using a 111-plex MSD panel.

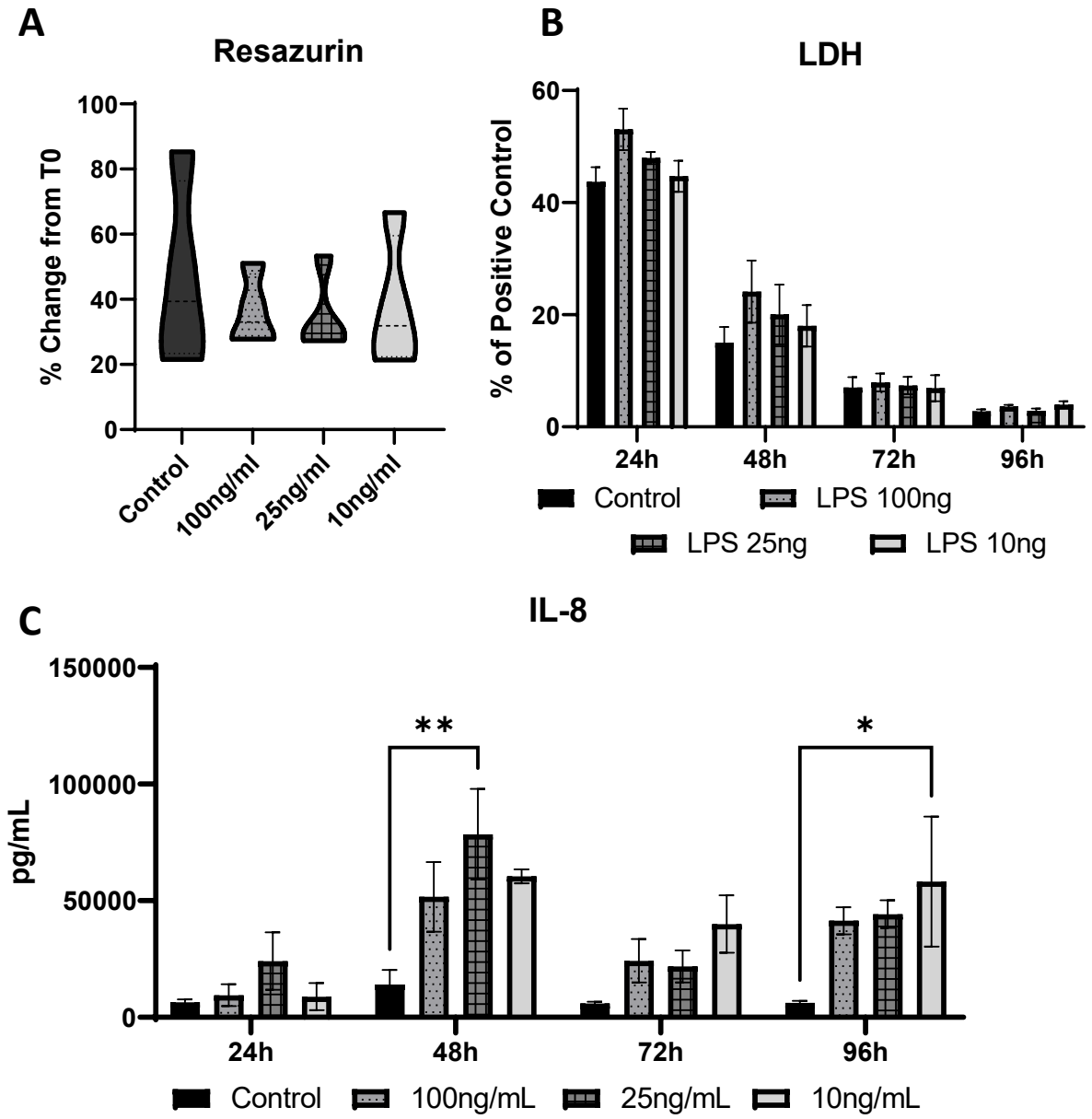

Figure 31. Optimisation of LPS Inflammatory Stimulation in PCKS

A- *A resazurin assay were performed on slices at 96h, shown here as percentage of T0 slices, no statistically significant differences seen by ANOVA. Data shown as averages plus min/max values.* ***B-*** *LDH output was measured from culture media saved at 24h time points, data shown as percentage of positive control, mean +/- SEM.* ***C-*** *Soluble IL-8, measured by ELISA from culture media saved at 24h time points, absolute values with mean +/- SEM. Statistical significance between treatment groups measured within time points by 2-way ANOVA, * p=≤0.05, ** p=≤0.01. N=4 kidney donors*

5.3.2 Identification of Inflammatory Biomarkers

The same 111-plex MSD assay as was used to characterise the fibrosis model was performed on the top concentrations of each inflammatory stimulant after one treatment cycle (48h media) as described previously. As before, the 'undetectable' category included any proteins under 1pg/ml in each of the treatment groups and the 'not dynamic' category included proteins where there were no significant differences between control and IL-1β or LPS treatment groups as determined by Student's T-test. In the liver, 33% of tested proteins were undetectable, and 54% were not dynamic. In the kidney 24% were undetectable and 45% were not dynamic. Proteins categorised as dynamic from this panel in response to either IL-1β or LPS stimulation in the PCLS and PCKS are shown in Figure 32 and Figure 33 respectively. Due to limited space on the MSD panel, only two donors treated with LPS in the PCLS were included, and IL-1α treated slices were not included.

The expression profiles of IL-1β and LPS induced inflammation are very different, showing the response in the PCLS is not generic, but stimuli specific. Twenty two factors were identified from the MSD panel as significantly increased in response to either LPS or IL-1β stimulation. 45% of these factors were common, including IL-6, IL-8, MCP-1 and MCP-2. 41% of this dynamic group were increased only in response to LPS including epithelial neutrophil activating protein 78 (ENA78) and interferon gamma-induced protein 10 (IP-10), and 14% were increased only in response to IL-1β including cutaneous T cell-attracting chemokine (CTACK), CD40L and IL-1β. MIP-1α, MIP-1β, TNF-α and MCP-4 are significantly increased in both LPS and IL-1β challenged PCLS compared to the control, but there are also significant differences between the stimuli, where LPS was able to elicit a much stronger response in upregulating these factors.

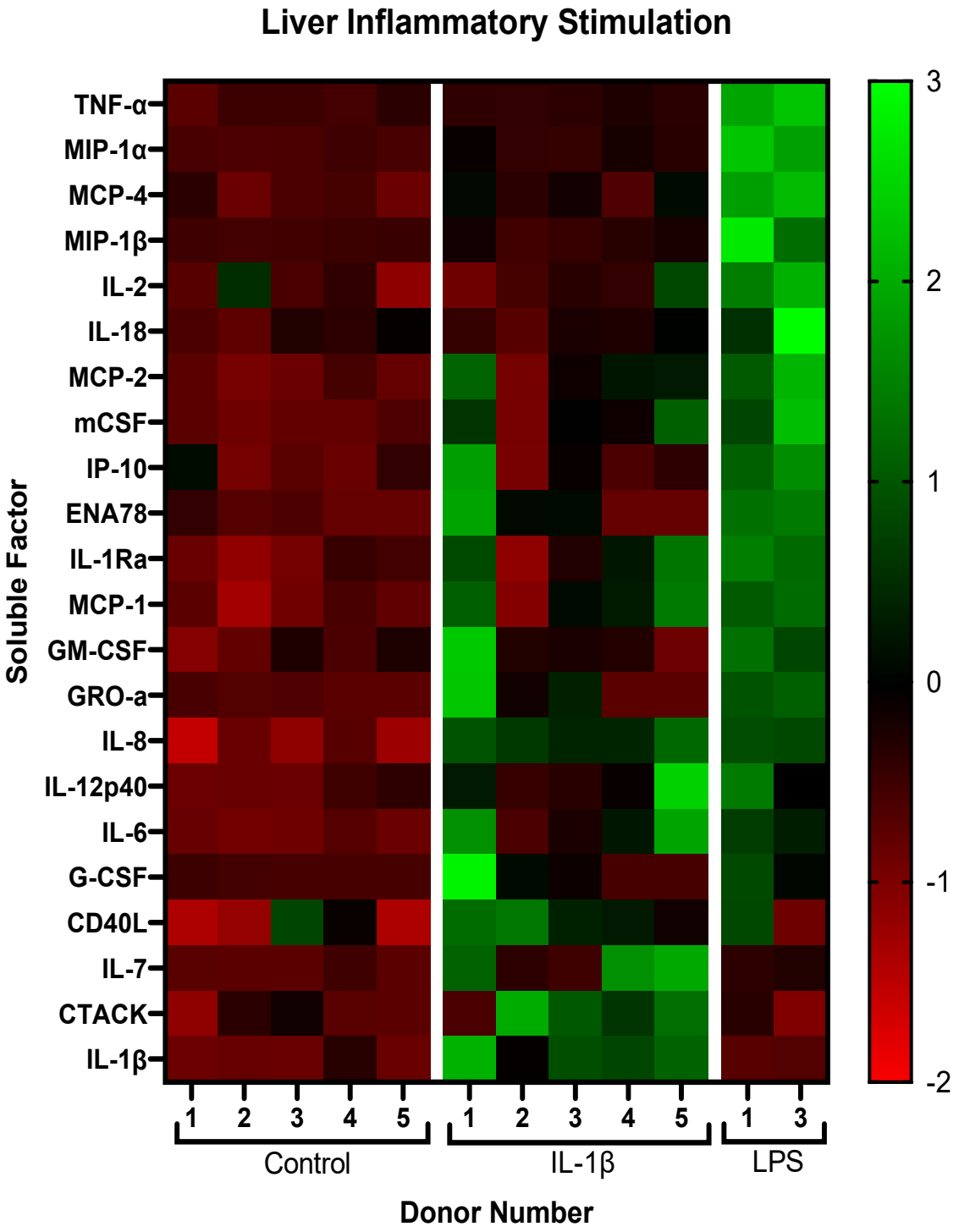

Figure 32. MSD Outputs from Inflammatory Stimulation in PCLS
Heat map shows proteins identified as significantly different between the controls and one or both of the inflammatory stimuli by Student's T-Test were Z-transformed. Higher expressed proteins are green and lower expressed proteins are red. Media from technical repeats within donors were pooled and 5 donors (donors 1-5 in Table 7) were run on the panel. Due to space limitations, only 2 donors treated with LPS were run (donors 1 and 3 from Table 7)

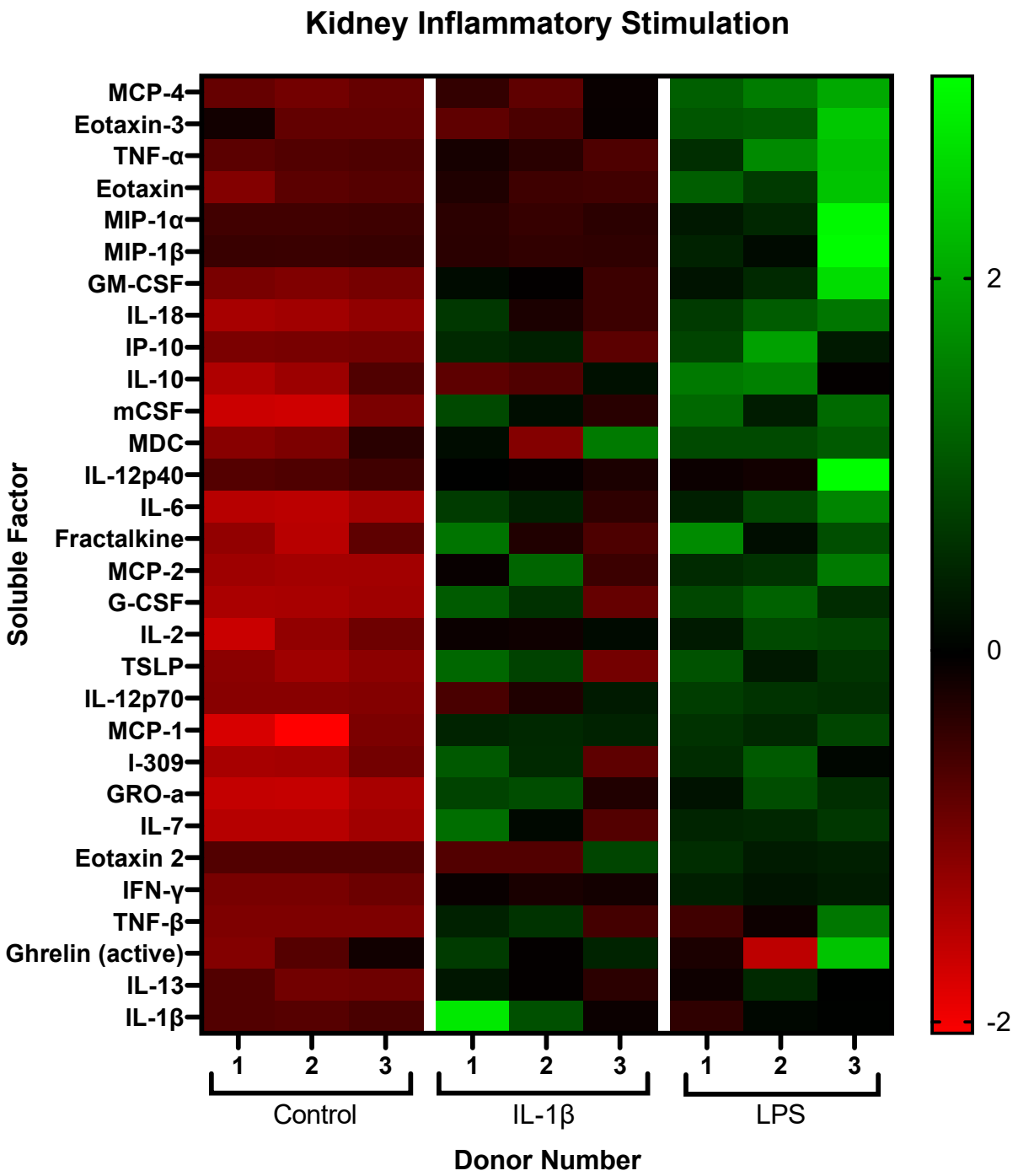

Figure 33. MSD Outputs from Inflammatory Stimulation in PCKS

Heat map shows proteins identified as significantly different between the controls and one or both of the inflammatory stimuli by Student's T-Test were Z-transformed. Higher expressed proteins are green and lower expressed proteins are red. Media from technical repeats within donors were pooled and 3 donors (donors 1, 2 and 3 from Table 8) were run on the panel.

Similar to the PCLS, there are differences between the expression profiles of LPS challenged and IL-1β challenged PCKS. Thirty dynamic proteins were identified in the PCKS in response to IL-1β and LPS treatment. 17% were increased exclusively by IL-1β including MIP-1α and MIP-1β, 40% by LPS including Eotaxin, Eotaxin 2 and Eotaxin 3. Both stimuli

were able to exert effects on 43% of the dynamic soluble factors including IL-6, MCP-1 and MCP2. LPS induced a significantly stronger response in upregulating TNFα, MCP-4, IL-2, IL-12p40 and IFNγ production compared to IL-1β.

There were differences between the inflammatory responses observed in the kidney and liver slices. There were 17 commonly upregulated proteins in response to LPS or IL-β challenge in the PCLS and PCKS with 6 upregulated in the same manner. For example, IP-10 was upregulated in both organs by LPS only and IL-6 is upregulated in both organs by IL-1β and LPS. Thirteen proteins identified as dynamic in the PCLS were not statistically significant in the PCKS including Eotaxin, Eotaxin-2 and Eotaxin-3, whereas five proteins identified in the PCLS were not statistically significant in the PCKS including ENA78 and CTACK.

Having completed these optimisation studies for modelling acute inflammation, it was decided that the best stimulant for further work would be IL-1β. This study confirmed that IL-1β could reliably induce inflammation in both the PCLS and PCKS, and in the case of the PCKS, IL-1β induced secretion of more dynamic inflammatory proteins compared to IL-1α. Whilst LPS was able to induce more dynamic proteins in both the PCLS and PCKS, our aim was to produce a model more similar to inflammation caused by chronic disease from cellular damage and metabolic dysregulation rather than pathogen invasion.

5.3.3 Using the Bioreactor for Drug Efficacy Studies

Having optimised the inflammatory model in the 96-well system, the next step was to determine if the response to IL-1β in the slices could be modulated using therapeutics. IKK2 is an essential to the activation of canonical NF-κB signalling, a key pathway in the development of inflammation. IKK2 inhibitor VI (IKK2VI) was selected to block the downstream events of activated NF-κB dimers to demonstrate that our model of acute inflammation could be modulated with drugs.

Three liver donors (Table 9) and five kidney donors (Table 10) were obtained to test the inhibitor treatment protocol. In this study, 66% of the liver donors were female and the average age was 50. All of the donor tissue had some degree of fibrosis but none showed any steatosis. 75% of the kidney donor tissue was from female patients with an average

age of 62. Only one donor was classed as being a healthy weight by BMI, with 40% of the pool being obese.

Table 9. Demographics of Liver Donors used in IKK2VI Study

Donor Number	Age	Sex	Fibrosis Score	Steatosis Score
Donor 1	58	M	1	0
Donor 2	31	F	2	0
Donor 3	60	F	3	0

Table 10. Demographics of Kidney Donors used in IKK2VI Study

Donor Number	Age	Sex	BMI
Donor 1	63	M	31
Donor 2	68	F	25
Donor 3	63	F	27
Donor 4	55	F	23

To demonstrate the use of the 96 well bioreactor as a platform for testing anti-inflammatory drugs, a 10-fold serial dilution from 10µM to 0.001µM IKK2VI was performed. After a 24h rest period post slicing, 1ng IL-1β +/- the dose range of IKK2VI was applied for a further 24h, and the inflammatory response in the slices was initially assessed by IL-8 ELISA. The top concentration of IKK2VI (10µM) was most successful in reducing inflammation in both the liver (Figure 34A) and the kidney (Figure 34B), attenuating IL-8 production in the slices to near to, if not below, that of the control slices with no IL-1β exposure. 1µM IKK2VI also reduced IL-8 production in both the PCLS and PCKS compared to the IL-1β control, but not as successfully as the higher concentration. The remaining three concentrations of IKK2VI tested here were not able to significantly reduce IL-8 secretion in either organ.

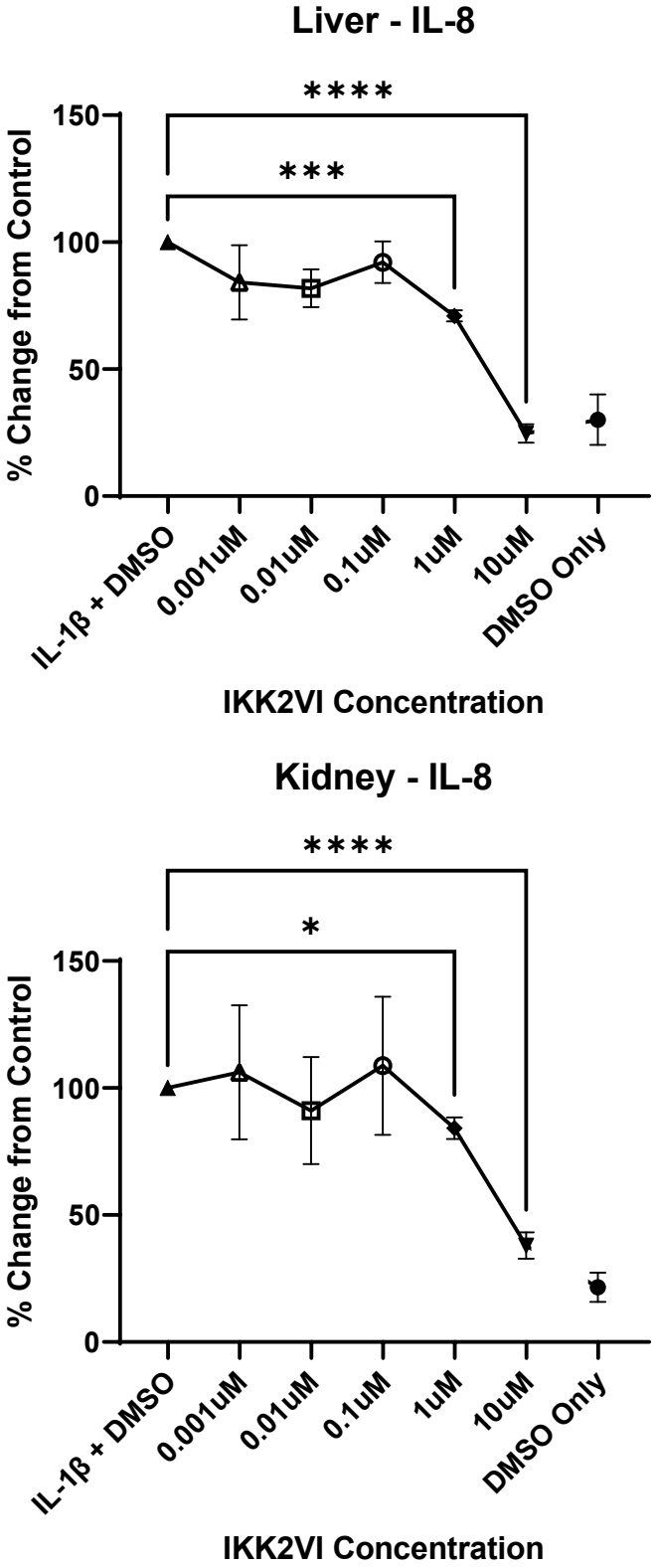

Figure 34. Dose Dependent Inhibition of Inflammation using an IKK2VI Inhibitor

*Addition of IKK2VI inhibitor to attenuates the development of inflammation both PCLS **(A)** and PCKS **(B)** in a dose dependant manner. Technical replicates for each treatment group averaged for each individual donor. We collected N=3 liver donors and N=4 Kidney, 5 technical replicates were averaged per treatment group per donor. Data is shown as mean +/- SEM. Statistical analysis completed by one-way ANOVA, * p=≤0.05, *** p=≤0.001, **** p=≤0.0001.*

Thirteen proteins from the MSD panel were statistically significantly different (analysed by Student's T-test) between the DMSO control and IL-1β in the PCLS (Figure 35). The top ten of these in the heat map are also significantly reduced, compared to the IL-1β treated slices, when IKK2VI is included. Of the three that are not statistically significant (IL-1β, CD40L and TNF-α), IL-1β has been manually added to the media in the IKK2VI treatment group, and CD40L and TNF-α would likely become significant with further donors as they are reduced in response to the IKK2VI addition.

There were eight proteins from the MSD panel that were identified as dynamic between the DMSO control and IL-1β groups in the PCKS (Figure 36). CD28, IFNα2α, programmed death ligand 1 (PD-L1) (Epitope 1), I-309 and IL-1α (not shown) were identified as significantly reduced between the IL-1β and IKK2VI inhibitor treated slices but not between the IL-1β and DMSO control slices. The trend of upregulation in response to challenge and subsequent attenuation with the inhibitor, is however still observed and with further donors would likely result in these achieving statistical significance between the DMSO control and IL-1β treated slices.

Five proteins (MCP-1, MCP-2, MCP-4, IL-6 and IL-1β) were commonly increased in both the PCLS and PCKS in response to IL-1β. Gro-α, IL-1α and Fractalkine exhibited a dynamic change only in the kidney and 8 (IL-8, MIP-1α, MIP-1β, CTACK, CDL40, IL-7, mCSF and TNF-α) were only in the liver. Some of these have a large spread of data (Gro-α, IL-1α, MIP-1α/β) and could benefit from further donors, whilst others could potentially change after being re-run due at different dilutions. For example, IL-8 data points from the MSD were almost all over the standard curve so the resulting numbers in the PCKS were all very similar.

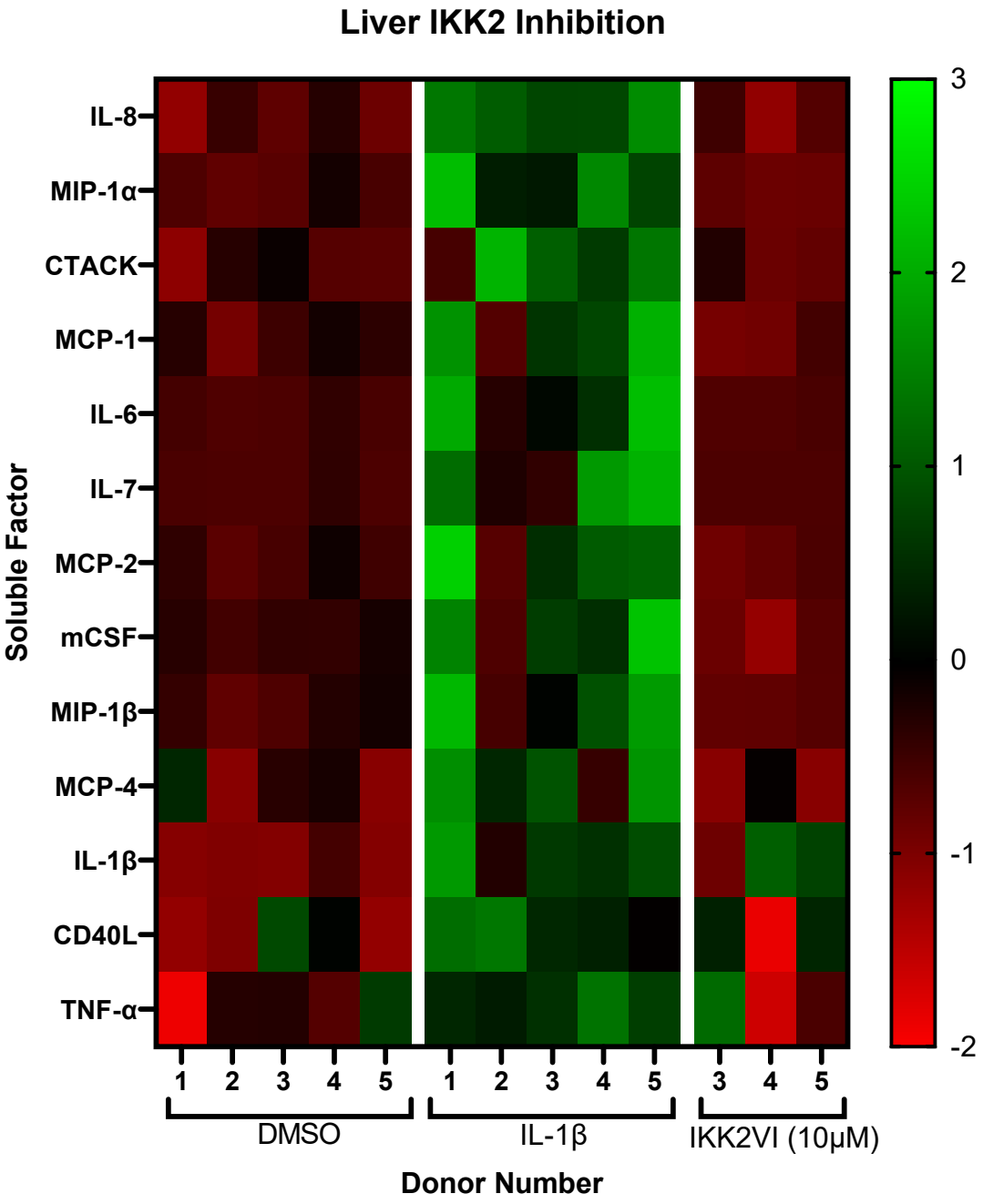

Figure 35. MSD Outputs from IKK Inhibitor Testing in PCLS

Heat map showing proteins identified as being significantly different between the control and IL-1β by Student's T-Test were Z-transformed and graphed. Higher expressed proteins are green and lower expressed proteins are red. Media from technical repeats within donors were pooled and 5 donors were run on the panel (donors 1-5 from Table 9). Due to space constraints, only 3 of the 5 donors (donors 3, 4 and 5 from Table 9) were run with the IKK inhibitor.

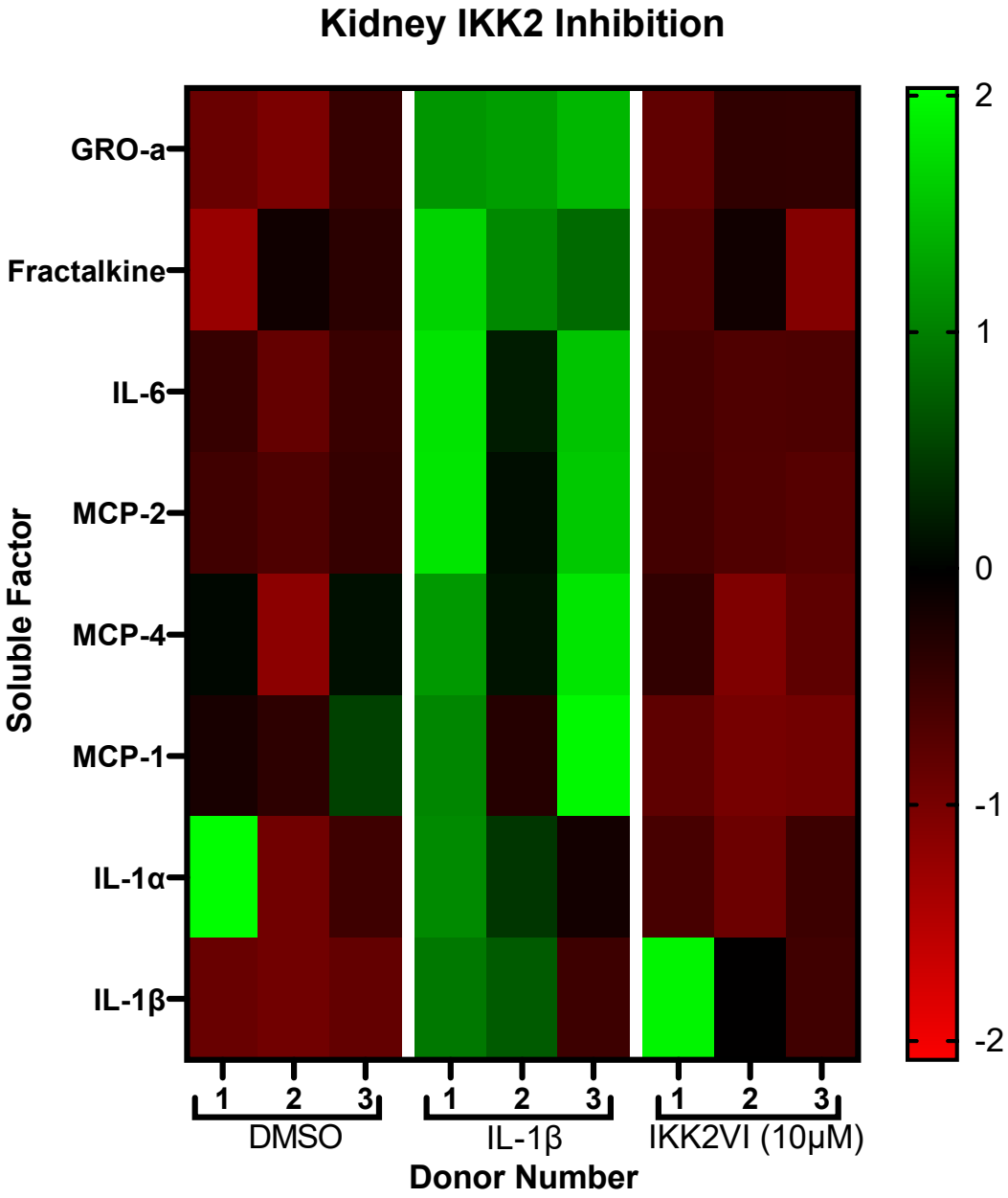

Figure 36. MSD Outputs from IKK Inhibitor Testing in PCKS

Heat map shows proteins identified as being significantly different between the control and IL-1β by Student's T-Test were Z-transformed and graphed. Higher expressed proteins are green and lower expressed proteins are red. Media from technical repeats within donors were pooled and 3 donors were run on the panel (donors 1, 2 and 3 from Table 10).

5.4 Discussion

5.4.1 Optimisation of Inflammation Model

Inflammation is a feature of multiple diseases and when left unresolved, can contribute to local tissue damage and ultimately organ failure. The ability to effectively model the inflammatory response and subsequently modulate with therapeutics is an important step in preventing further organ damage in patients with chronic inflammation. Three drivers of inflammation were selected to optimise our PCLS and PCKS model of this phenomenon, and determine which of these inflammatory stimulants produces the most significant and reproducible response in comparison with a control in both the liver and the kidney.

1000pg/ml IL-1β reliably produced the most significant rise in IL-8 in both liver and kidney slices during our culture optimisation across multiple donors. It also had the least detrimental impact on the slices at T96, where in the PCKS, IL-1α appeared to be having a greater negative effect on the slices, with a reduced metabolic activity, particularly at the top concentration. Interestingly, unlike the fibrosis model described previously, the activation of inflammatory pathways did not increase with subsequent treatment cycles, and IL-1β was the only stimulant tested that was able to prolong a significant inflammatory response from the first cycle with recurrent treatment. For acute inflammatory studies, the culture period was limited to 48h, but if chronic inflammation modelling was ever appropriate, the same stimulant could be used in both allowing for direct comparison between the two.

5.4.2 Identification of Inflammatory Markers

The inflammatory biomarker panel was diversified with the use of a 111-plex MSD panel, providing a more complete picture of the acute inflammatory model we had been optimising to select the best stimulant for further studies. The 48h time point media samples were selected for each of the stimulants, pooling together the technical repeats from individual donors, and ran at the dilution recommended by the manufacturer on the screening panel. Increased levels of a number of inflammation-associated proteins were observed in response to tissue slice culture with LPS, IL-1α and IL-1β, and the inflammatory profile of these slices was different depending on the stimulant used.

LPS is a major component of the cell surface of gram negative bacteria and is used in numerous models to induce an immune response and inflammatory reaction (205–207). In the PCLS and PCKS, there was a significant increase in proteins such as Eotaxin family members (PCKS only), IP-10/CXCL10 and GM-CSF and ENA78/CXCL5 (PCLS only) in response to LPS. These proteins have all been identified as key in the immune response. Eotaxin, Eotaxin-2 and Eotaxin-3 are potent eosinophil chemoattractants produced in response to infection and allergic reactions by a number of cell types including tissue resident macrophages and fibroblasts, and have been shown previously to be induced by LPS in *in vitro* models (206,208). These family members were found to be significantly upregulated in response to LPS in our model in the PCKS but not the PCLS. Whilst this appears to suggest that the Eotaxin family are kidney specific, it is more likely that this lack of statistical significance could be due to reduced donor numbers of LPS treated PCLS (n=2) resulting in an under-powered statistical analysis. Eotaxin-2 secretion by these PLCS for example, has a P value of 0.057, marginally over the 0.05 limit.

High levels of IP-10 have been observed in patients with bacterial infections and it has been implicated in chronic inflammatory diseases and cancer (209). IP-10/CXCL10 is increased in response to LPS in the PCLS and PCKS, complying with what is found clinically. It is not however, significantly increased in response to IL-1α and IL-1β. As IP-10 has been associated with more chronic inflammatory diseases, it would be interesting to see if levels begin to increase with prolonged IL-1α or IL-1β treatment.

GM-CSF is another cytokine that was identified in this study as significantly upregulated in response to LPS stimulation in both the PCLS and PCKS. It is also significantly increased compared to the control in the IL-1α and IL-1β treated PCKS but not PCLS. GM-CSF is released from proximal tubule cells in response to stress and injury and has been documented by Xu *et al,* which could account for this significant increase in the kidney slices in response to acute inflammation (183).

IL-1β is a pro inflammatory cytokine associated with the innate immune response. Expression of IL-1β, induced by DAMPS and PAMPS, upregulates production of other cytokines and chemokines to produce a local inflammatory response (53). CTACK, also known as CCL27, was found to be upregulated in the PCLS in response to IL-1β stimulation, but not in the PCKS. CTACK was also shown to be regulated by IL-1β in some cell types,

and a clinical study by Beudeker *et al,* CTACK levels were reported to be elevated in patients with chronic liver diseases (210,211).

Numerous factors in the inflammatory response were identified that were significantly increased upon challenge with the stimulants in both the PCLS and PCKS including IL-6, IL-7, MCP-1, M-CSF and TNFα. IL-6 has been well documented as a key regulator of inflammation, induced by IL-1β and TLR ligands (such as LPS) via NF-κB signalling (56). IL-7 has been detected in the liver and kidney cells by other groups in response to activation with inflammatory stimulants including IL-1β (212). MCP-1 (also known as CCL2) is a chemokine that recruits immune cells to sites of injury and is expressed by numerous cell types in response to cytokines and LPS (213,214). M-CSF is a growth factor released during an inflammatory response that polarises macrophages to anti-inflammatory, pro-fibrotic M2 class macrophages (215). TNFα is another major regulator of the inflammatory response that has pleiotropic effects on many cell types, perpetuating inflammation via NF-κB and MAPK signalling (200,216). The upregulation of all of these genes in our model demonstrate that we can successfully induce an acute response within the bioreactor cultured tissue slices. There are some other proteins that are important inflammatory mediators that either appear as significantly increased compared to the control only in one organ or in response to one stimulant. For a number of proteins including G-CSF, GROα, MCP-4, MIP-1α and MIP1-β, this lack of statistical significance was due to a spread in the data between donors and either removing the donors which are obvious outliers or increasing the number of donors within the study would improve the validation of these proteins. Surprisingly, IL-8, which during the initial optimisation studies was significantly increased upon challenge to stimuli, was not significantly increased in the PCKS when analysed with the MSD panel. When reviewing the raw data from the MSD, the IL-8 values from the PCKS media are all above the curve, and the upper limit of the assay, so the concentrations for the treatment groups are not accurate. This would need to be repeated at a much higher dilution of the culture media than the 1:4 recommended by the manufacturer to obtain more precise results.

The purpose of this model is to replicate the features seen in chronic diseases of the liver and kidney to test potential anti-inflammatory compounds. It was clear from the MSD panel that we can generate different inflammatory-associated profiles in the slices depending on the stimulant used. Challenge with LPS upregulated proteins associated

with the immune response and infection, as well as common inflammatory pathways. Alongside activation of signalling pathways that are not common in chronic liver and kidney conditions such as NASH or glomerulonephritis, in order to elicit the same level of response, LPS concentrations were 100x higher than IL-1β. Based on this, I elected to use IL-1β as the inflammatory stimulant for subsequent studies.

5.4.3 Modulating the Inflammatory Response in the PCTS

After selecting IL-1β as the inflammatory stimulus to advance to future studies, I then set out to demonstrate the use of this model as a tool for efficacy testing anti-inflammatory compounds. Blocking components of the inflammatory response and/or their signalling pathways to reduce chronic inflammation has been clinically successful with drugs such as infliximab and golimumab approved by the FDA (217). IKK2 is a regulatory kinase in the NF-κB signalling pathway (activated by IL-1β ligand binding) which phosphorylates IκBα and promotes its degradation by the proteasome, releasing NF-κB dimers for translocation to the nucleus. Blocking this interaction using IKK2 inhibitors has been shown in 2D, single population cell culture to reduce the level of NF-κB target genes in culture (218).

A negative correlation between IKK2VI concentration and IL-8 production was found in both the PCLS and PCKS, inferring that inflammation can be successfully modulated in the 96-well bioreactor. Whilst 1μM of the inhibitor could statistically significantly reduce inflammation within the slices, 10μM had a much greater effect, therefore was selected as the top concentration of IKK2VI to run more extensive analysis.

In the MSD panel, there were 13 proteins that were significantly increased in response to IL-1β in the PCLS and 8 in the PCKS. Common factors increased in both bioreactor cultured tissue slices were IL-6, MCP-2, M-CSF, MCP-1 and IL-1β. As discussed previously, these are all important factors in the perpetuation of the inflammatory response (52,53,56,215). Interestingly IL-1β levels are reduced in slices treated with IKK2VI, suggesting that the slices are generating more IL-1β as a result of the inflammatory state of the tissue. IL-8, MIP-1α, MIP-1β, CTACK, CDL40, IL-7, M-CSF and TNFα were all successfully modulated in the PCLS but not the PCKS. For the majority of these, either including more donors or repeating the MSD at a different dilution would likely result in significance as the values were either too low in some groups, over the top of the standard curve (IL-8) or had outlying values/high degree of variance for meaningful statistics. CTACK however, appears

to be tissue specific, as expression could be modulated in the PCLS but did not significantly change in any treatment group in the PCKS. Fractalkine is dynamic in the PCKS but not the PCLS. Also known as CX3CL1, Fractalkine can be anchored to the cell membrane or released as a soluble protein. It has been implicated in kidney disorders such as glomerulonephritis and tubulointerstitial inflammation where it is expressed on the apical membranes of proximal tubule cells. Fractalkine is also found on biliary epithelial cells in biliary cirrhosis and on endothelial cells of small vessels within the liver (219). This more established role in renal inflammation may account for the increased levels seen in the PCKS compared to the PCLS and for the more dynamic range observed in the treatment groups. Possibly repeating this with a lower dilution factor and increasing donor numbers may reveal a relationship between IL-1β stimulation and Fractalkine upregulation in the liver.

The next step would be to develop some alternative methods for identifying inflammation within the tissue slices. Harvesting slices at the culture endpoint for histological analysis or proteomic/RNA-sequencing may provide alternatives to the MSD screen when assessing novel therapeutics. MSD panels are expensive to perform and may not be appropriate for testing large numbers of novel anti-inflammatory compounds. It would also be beneficial to further test the efficacy predictive ability of the bioreactor by using clinically relevant compounds. This could include a mixture of small molecule inhibitors and antibodies that will inhibit both IL-1β signalling and also other inflammatory mediators that are induced by IL-1β.

5.5 Conclusion

The aims of this chapter were:

- Optimise and validate the inflammatory model in the 96-well bioreactor in both human liver and kidney slices.
- Demonstrate the use of the bioreactor as a suitable platform for efficacy testing anti-inflammatory drugs.

I have successfully validated a model of acute inflammation using IL-1β in human PCLS and PCKS in the 96-well bioreactor, and have optimised the system for the best stimulant, concentration and culture time to develop an acute inflammatory response that is comparable to a biological response to injury. 1000pg/mL IL-1β challenged slices remained metabolically active to the end of the culture period and the addition of the stimulant did not have any negative impact of the health of the slice compared to the control. Using the MSD panel, it was possible to identify significant increases in several crucial inflammatory cytokines and chemokines in the tissue, suggesting this model would not only be appropriate for efficacy and toxicity testing, but is also a useful tool for mechanistic studies. The model was reproducible across multiple donors including a range of ages and underlying pathologies. For the kidney optimisation study, I would have liked to have obtained more male donors/donors within the normal BMI range to understand if any of these factors had an effect of the lower metabolic output (measured as a percentage of T0) at 96h compared to the PCLS. It would have also been beneficial to have obtained more replicates of the LPS treatment group in the PCLS, as only an n=2 could fit on the MSD panel that was run.

The potential for this platform to be used as a tool in efficacy testing of anti-inflammatory compounds in the setting of acute liver/kidney inflammation was successfully validated. The use of IKK2VI confirmed that IL-1β-induced inflammation in PCLS and PCKS can be supressed by anti-inflammatory compounds. It would have been useful to also test this model with a clinically approved anti-inflammatory but due to time constraints and tissue availability it was not possible to carry out this study. A greater variety of donors should be used when using this as a screening tool, including a wider range of ages and be more balanced with male and female donors. Most of the donors used here were female and in the case of the kidney, were all older patients. Utilising different outputs such as

proteomics or transcriptomics using frozen slices at the end of the culture period could increase the confidence in the results that were obtained and reveal new and interesting mechanisms or biological targets for future investigation.

Chapter 6. Predicting Toxicity

6.1 Introduction

The development of a single novel therapeutic has been estimated to cost up to $2.8 billion (85). A major setback with the current drug discovery pipeline, is that identifying toxic effects of novel therapeutics during the preclinical phase is very poor. 20-40% of candidates are recalled because of unforeseen drug induced injury to organs (84,85).

6.1.1 Key Elements for Successful Preclinical Modelling

Whether or not a compound will exert a toxic affect is not always a straightforward yes or no question. When considering the development of a suitable model for pre-clinical assessment of lead candidate compounds, alongside building in complexity of the native organ microenvironment, inter-patient variability must also be considered. Genetics, age and underlying pathological conditions impact the speed at which drugs are metabolised, altering efficacy and potentially inducing toxic side effects.

Pharmacogenetics will influence how individuals are able to metabolise drugs. CYPs are phase I drug metabolising enzymes which can be studied as part of a patient's genetic profile, and are categorised into 4 groups, including poor metabolisers, intermediate metabolisers, extensive metabolisers and ultra-rapid metabolisers (220). These groups range from functionally poor and/or complete deletion of alleles in poor metabolisers, to having two or more functionally competent alleles in ultra-rapid metabolisers. Where a drug has an intrinsic toxicity to an organ, poor metabolisers are more likely to suffer adverse effects, however ultra-rapid metabolisers may not receive any therapeutic benefit before the drug is metabolised and cleared from the body (221). Xu *et al*, found that age also leads to variable CYP expression, although it should be noted this work was in rodents. In general, expression of CYPs increased from infancy to adulthood and then slowly decreased again in aged animals. Regulation of CYP enzymes is similar in humans and animals and so is an important feature to consider when testing novel therapeutics and suggesting toxic and non-toxic doses (222). Paracetamol for example, must be given in much lower doses to infants and children compared to adults who have a higher CYP2E1 availability in their livers.

Alongside genetic variation in drug metabolising enzymes, underlying pathological conditions such as liver cirrhosis can alter the expression patterns of CYP enzymes, making

these patients more likely to suffer adverse effects than healthy individuals. Duthaler *et al* showed that in a group of 400 patients with liver cirrhosis, incorrect dosages in prescription medication led to adverse drug reactions which, in some cases, resulted in hospitalisation. They identified, using a cocktail of drugs, that the activity of some CYP enzymes including CYP1A1 and CYP3A4, were reduced in patients with severe cirrhosis, but others such as CYP2C9 were not (223). When testing lead candidates for toxicity studies, it is therefore important to consider all of these factors in the modelling system.

Current limitations of *in vitro* models include difficulties in long-term toxicity assessment, particularly in 2D monoculture. Lack of other cell types such as immune cells result in indirect toxicity not being identified and these platforms are typically not suitable for studies spanning months to identify this difficult to predict adverse reaction.

6.1.2 2D Pre-Clinical Models

As previously discussed, 2D cell culture does have many benefits in early pre-clinical testing, including its relatively cheap running costs and easy scalability for adapting to high throughput testing (110). An ideal starting point for testing therapeutics, compounds will typically be screened using a panel of cell lines and those that show efficacy are progressed to animal models (224). Cui *et al* used a range of cell lines including a human liver, lung and brain cancer cells to test the potential of a combination therapy of sorafenib and dihydroartemisinin. They identified variation in sensitivity across the different cancer types to the combination treatment, with HepG2 (liver cancer) and SW480 (colon cancer) cell lines being most sensitive (225). Whilst this format is a useful first step in identifying drug efficacy in different cancers, there is no information gained about off target toxicity either within the target organ or other areas of the body. Also, commercially available cell lines do not have the same transcriptional profiles as the native cell type. This phenotypic change may over or under exaggerate the potential of the therapeutic(s) being tested (111–113). Patient derived primary cells or iPSCs may provide an alternative for a more accurate representation of cell-drug interactions, however the lack of structure and presence of other organ specific cell types reduce physiological relevance and mean results are not guaranteed to be replicated in more complex systems (91,110,118).

6.1.3 Animal Pre-Clinical Models

Industry standards require the testing of drug candidates to be rigorously tested in numerous animal species before they can be prescribed for humans. Alongside efficacy testing, these animal studies are key to identifying adverse effects due to long term administration or high dosage (116,125). Animal models are able to demonstrate the complexity required when investigating drug efficacy and toxicity, however they still have drawbacks including differences in lifespan, metabolism and genetic variation in CYPs can all contribute to the mismatch between animals and humans, resulting in often unpredictable translation to humans (127,226). Paracetamol metabolism in rats is a good example of why caution should always be taken when interpreting data from animal studies. Walubo *et al* investigated the use of CYP inhibitors for prevention of hepatotoxicity post paracetamol overdose with rats. They found that CYPs were key to paracetamol induced hepatotoxicity and their inhibition interrupted the mechanism by which paracetamol causes liver injury and suggested that their use could aid in the recovery of patients suffering overdose. It is known however, that rats are more resistant to paracetamol induced hepatotoxicity than humans and other animal models due to a high anti-oxidant capacity and so this research may not be directly translatable to a human experience of this treatment (94,227).

6.1.4 3D Pre-Clinical Models

Recent progress in model development for toxicity prediction have been in the field of 3D cell culture. These systems include organoids/spheroids, microfluidics, sandwich cultures and bioprinting of 3D tissues (228). Tuffin *et al* developed a spheroid model of kidney glomeruli using immortalised podocyte and glomerular endothelial cell lines. They were able to demonstrate expression of key glomerular cell markers and histological features within the spheroid. They also showed that TGFβ1 treatment was able to induce collagen production and that this could be modulated with anti-fibrotic compounds such as Nintedanib, and the system could be adapted for medium throughput compound screening (140). The main outputs of this model were imaging of spheroids to identify podocyte loss, however there was limited identification of toxicity associated biomarkers. Further testing with toxic compounds would be required to validate its use for rapid drug screening. Organ-on-chip microfluidic systems have been developed for the kidney and

liver for the purposes of toxicity testing. Ewart *et al* designed a liver-on-chip system and tested a range of toxic drugs and non-toxic analogues to demonstrate the predictive value of the system. They found the system to be a suitable tool for predicting DILI, showing improved sensitivity compared to spheroid and animal models (229). The cells used in this model were cryopreserved primary cell lines and they incorporated the major cell types in the liver including, hepatocytes, sinusoidal endothelial cells, Kupffer cells and HSC. It would be useful to confirm that the cells used are able to express both drug metabolising enzymes and drug transporting enzymes throughout the culture period and that levels are comparable with human liver tissue. Whist this system was only cultured for a number of days, there have been similar models developed proven to remain viable for 28 days (146).

6.1.5 Precision Cut Tissue Slice Pre-Clinical Models

PCTS offer an alternative to cell line based 3D modelling. This *ex vivo* system retains all of the histological features and cell phenotypes of the organ being studied (151). The use of PCLS for drug toxicity prediction has been established by other research groups, using, among others, Troglitazone, paracetamol and diclofenac. These studies were able to demonstrate inter-patient variability, dose dependency and synergy between therapeutics (154,156). The main drawback of this platform for safety profiling studies compared to rodent models is that it is not suitable for long term culture. Where mice or rats can be treated for several weeks/months, the PCTS only remain viable for up to 144h post-slicing, limiting the platform for use to early phase pre-clinical screening study.

6.1.6 Chapter Aims

- Optimise the methodology for predicting drug toxicity in the 96-well bioreactor.
- Demonstrate potential of the 96-well bioreactor for prediction of adverse drug reactions using clinically relevant compounds.
- Demonstrate the potential of the 96-well bioreactor as a platform for identification of differences in DILI between healthy patients and those with underlying pathologies.

I aim to explore the potential of bioreactor cultured PCTS to be used as a tool for predicting adverse effects of lead candidates in the drug discovery process. The

methodology development will investigate length of application time and the point at which drugs should be applied to the slices over the culture period to develop a reproducible system for testing novel therapeutics. Once protocols have been developed, drugs known to cause hepatotoxicity or nephrotoxicity will be tested on the PCTS to demonstrate the predictive value of the platform.

6.2 Methods

6.2.1 Materials

Sourcing of tissue and general materials for tissue culture are described in 2.1. TFGβ1 and PDGFββ were purchased from Peprotech and each made up to a stock solution of 20mM according to manufacturer's instructions. Rotenone was purchased from Sigma (R8875-1G) and dissolved in DMSO to 0.5mg/ml. Paracetamol was purchased from Sigma (A5000-100G) and the powder was weighed out as required and dissolved directly into the media. Troglitazone (3114), Rosiglitazone (5325) and Cisplatin (2251) were all purchased from Tocris and made up in DMSO to their solubility limits as recommended by the manufacturer.

6.2.2 Culture Conditions for Toxicity Modelling in PCLS

Production of 3mm liver slices is described in 2.1.3. After a 24h rest period following the slicing process, treatments were applied. In cases where drugs were applied for less than 24h, media was changed daily to the point of application then all media was changed in the plate (including controls), for application of the drug treatment. DMSO was added to the control at the same point at which drugs were used. Where drugs were applied for 24h or more, media was changed daily then all slices were harvested at the end of the culture period. For disease induced versus normal cultured drug studies, Fib Stim treatment was applied throughout the culture period and drugs were added at either 96h only or 96h and 120h. During acute response studies, drugs were added at 24h then harvested at 48h. Before drugs were added at the 24h time point, all slices were first washed in new media to remove any remaining NAC from the wells, which may interfere with the interaction between the drug and the slice. Slices were harvested for biochemical assays, methodology for this is described in the Methods chapter.

6.2.3 Culture Conditions for Toxicity Modelling in PCKS

Production of 3mm liver slices is described in 2.1.3. After a 24h rest period following the slicing process, treatments were applied. DMSO was added to the control at the same point at which drugs were used. Where drugs were applied for 24h or more, media was changed daily and all slices were harvested at the end of the culture period. For disease

induced versus normal cultured studies, Fib Stim treatment was applied throughout the culture period and drugs were added at either 96h only or 96h and 120h. During acute response studies, drugs were added at 24h then harvested at 48h. Before drugs were added at the 24h time point, all slices were first washed in new media to remove any remaining NAC from the wells, which may interfere with the interaction between the drug and the slice. Slices were harvested for biochemical assays, methodology for this is described in the Methods chapter.

6.2.4 Analysis of Soluble Outputs

I used several methods to analyse the soluble outputs from the cultured slices. These include the CyQUANT LDH assay, Urea assay, the AST activity assay and a number of ELISA kits including Albumin and HSP70 as appropriate. The specific protocols for each of these is described in 2.2 of the Methods chapter.

6.3 Results

6.3.1 Analysis of Cytochrome P450s and Drug-Associated Transmembrane Proteins

The primary goal of this chapter is to assess if the 96-well bioreactor system can be used as a pre-clinical drug screening tool to predict efficacy and toxicity of lead candidates in drug discovery. Having demonstrated its use in predicting efficacy of anti-fibrotic and anti-inflammatory compounds, I next aimed to validate methodology for the identification of potentially toxic compounds. The cytochrome P450 family of enzymes are responsible for phase I drug metabolism, introducing a reactive or polar moiety to the drug by oxidation, reduction or hydrolysis reactions. This initial reaction can produce several metabolites some of which exert a therapeutic effect. Some 2D cell culture models that use immortalised cell lines have altered CYP expression profiles, and therefore the efficacy and/or toxic effects of candidate compounds may not be correctly predicted.

To demonstrate the cultured slices were able to continually express both metabolic enzymes and drug transporters on the surface of cells, RNA sequencing, proteomics and histological analysis were performed. RNA sequencing and proteomics was completed in collaboration with others in the Newcastle Fibrosis Research Group, and part of the data set was used for this chapter. Figure 37 shows the levels of four major CYP enzymes in 96h cultured PCLS +/- Fib Stim treatment. RNA sequencing data is on the left of the panel (patterned) and proteomic data is on the right (solid colour). The RNA levels of each of the four CYP enzymes were significantly reduced in the Fib Stim treated slices at the end of the culture period. The protein levels however, did not change significantly with the addition of the Fib Stim treatments. CYP2E1 was the most abundant CYP in the PCLS that was investigated. Interestingly CYP3A5 had the highest RNA levels in both the control and fibrosis treated slices but was the least abundant of the CYPs looked at in this study.

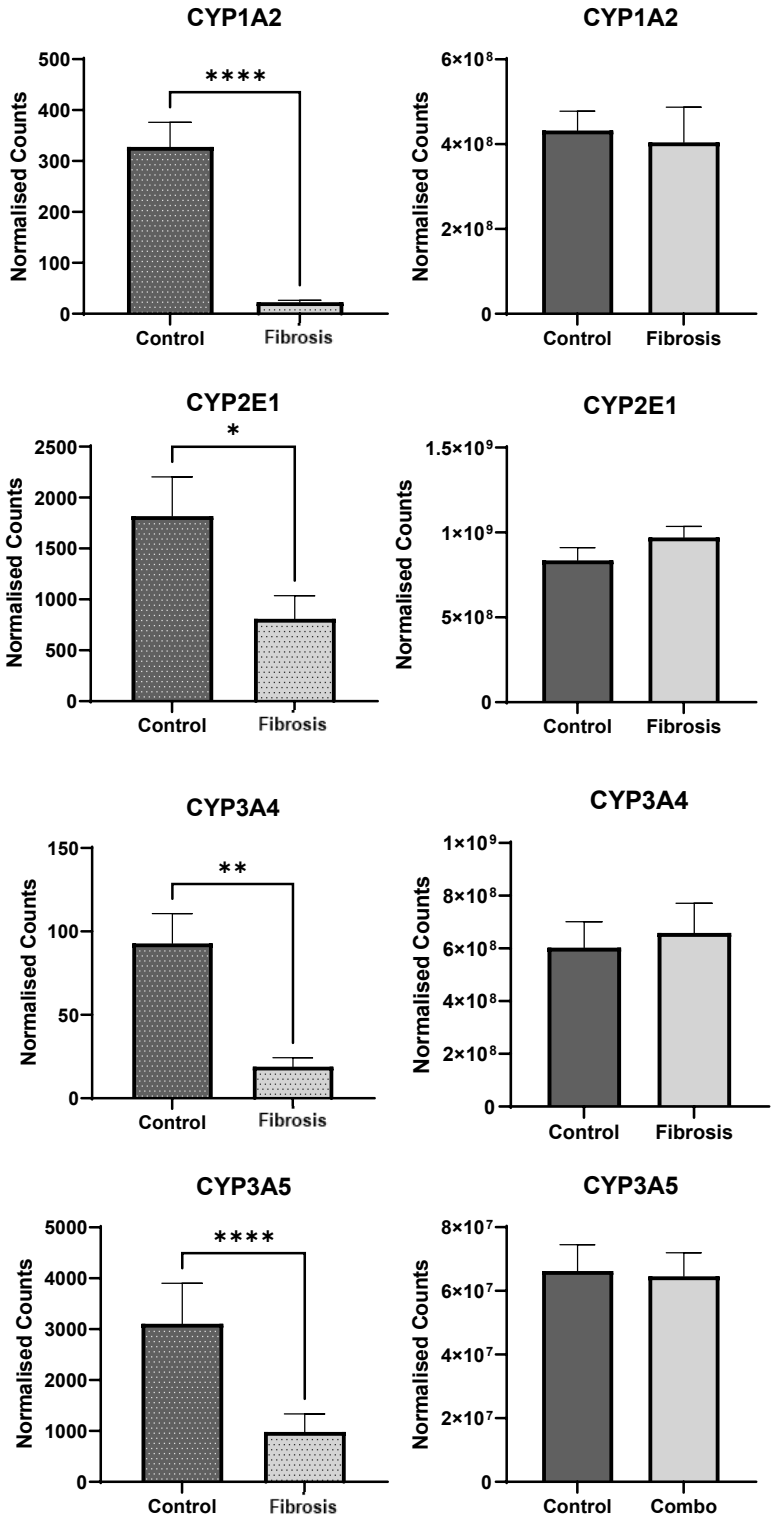

Figure 37. RNA Sequencing and Proteomics of Cultured PCLS

RNA sequencing and proteomic analysis performed on PCLS cultured for 96h hours +/- Fib Stim treatment. From the data set, some key CYP450 enzymes have been identified. Graphs on the left hand side (patterned) display RNA sequencing data and graphs on the right display proteomic data (solid colour). Statistical analysis calculated using Student's T test, * p=≤0.05, ** p=≤0.01, **** p=≤0.0001. RNA sequencing used n=12 liver donors and proteomics used n=6 liver donors.

RNA sequencing data from 96h cultured PCKS +/- Fib Stim treatment is shown in Figure 38. Solute Carrier Family 47 Member 1 (SLC47A1 or MATE1) and Solute Carrier Family 47 Member 2 (SLC47A2 or MATE2) were significantly decreased where fibrogenesis had been induced in the slices. There were no significant changes in RNA levels of Solute Carrier Family 22 Member 1 (SLC22A1 or OCT1) with the inclusion of the Fib Stim treatment in the PCKS, however RNA levels of Solute Carrier Family 22 Member 2 (SLC22A1 or OCT2) significantly increased with Fib Stim treatment.

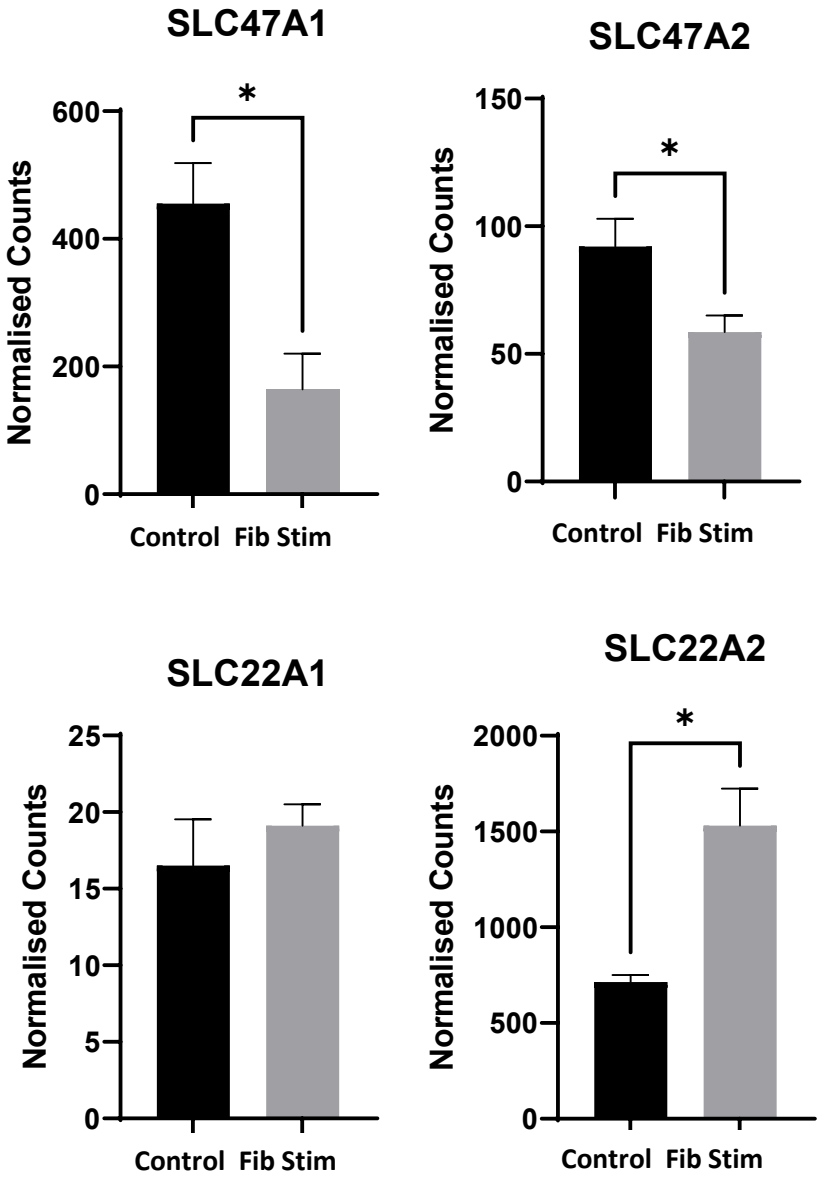

Figure 38. RNA Sequencing of Cultured PCKS

*RNA sequencing analysis was performed on PCKS cultured for 96h hours +/- Fib Stim treatment. From the data set, some key drug transporting proteins have been identified. Statistical analysis calculated using Student's T test. * p=≤0.05. N=5 Kidney Donors.*

After demonstrating that key drug transporters and metabolic enzymes are expressed in the tissue at the end of the culture period, I hypothesised that drugs may be taken up and may be effectively metabolised by the tissue and so moved on to optimise PCTS culture for predictive drug toxicity.

6.3.2 Methodology Development

Rotenone, whilst not a clinical therapeutic, is a compound with known cytotoxicity. It inhibits complex I of the mitochondrial electron transport chain resulting in reduced ATP generation and necrosis, with the liver a major site of drug induced damage (230). A short incubation of 6 hours was initially tested to determine the speed with which metabolic activity of the slices would decline with the addition of toxic compounds. The result of rotenone addition to PCLS is shown in Figure 39. The addition of both concentrations of rotenone decreased the viability of the slices assessed by resazurin assay in comparison with the control. Functionality of hepatocytes was assessed by measurement of soluble albumin, where there was also a drop in production in both the 5µM and 10µM treated slices. There was very little difference in LDH output post rotenone application between the treatment concentrations or the control. Interestingly AST levels appeared to drop significantly in the slices treated with rotenone compared to the control, potentially as a result of the short culture time.

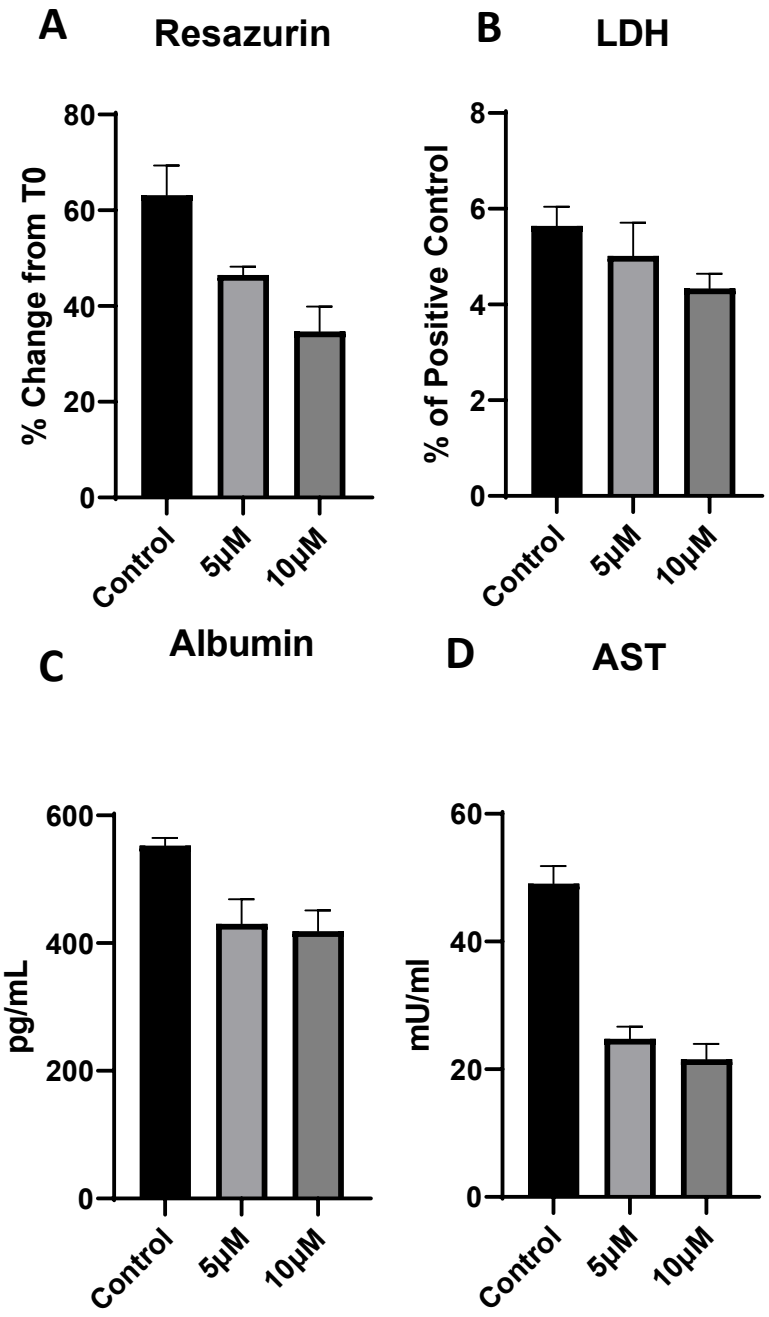

Figure 39. PCLS culture with Rotenone

Rotenone was added at 90h post slicing for 6 hours. ***A****- A reaszuin assay was performed at 96h shown here as a percentage decrease from T0.* ***B****- An LDH assay was carried out on the 96h media, shown as a percentage of control.* ***C****- Soluble albumin measured by ELISA using the 96h media, absolute values.* ***D****- AST levels were measured from the 96h media. Data shown as mean +/- SEM. N=1 liver donor, 5 technical replicates were averaged per treatment group.*

After identifying that we could negatively impact the PCLS with known toxic compounds, I next chose paracetamol as a clinically relevant hepatotoxic drug to further define the best methods for toxicity modelling studies (Figure 40). Paracetamol is an example of a drug that causes direct hepatotoxicity. Also known as acetaminophen, paracetamol is the most common cause acute liver failure in the UK, accounting for around 65% of total cases. Overdosing, particularly regularly exceeding the recommended dosage, or taking paracetamol in combination with other drugs, can ultimately result in liver failure and death (231).

When metabolised in the liver, 55-60% of the total paracetamol is converted to acetaminophen-glucuronide and 20-30% has a sulphate group added by sulfotransferase. These products become more water soluble and are excreted in the urine. The remaining 10% is converted to the active metabolite N-acetyl-p-benzoquinone imine (NAPQI) by CYP isoform 2E1 (CYP2E1). NAPQI is then conjugated with glutathione to detoxify the metabolite, where it leaves the liver to be further degraded by other organs (231–233).

In a case of paracetamol overdose, the levels of NAPQI outstrip the levels of available glutathione. The free NAPQI is then able to bind to mitochondrial proteins on cystine residues. The NAPQI-mitochondrial protein adducts then enter the mitochondria, causing mild oxidative stress by electron transport chain interference. Through a number of intermediates, c-jun N-terminal kinase (JNK) is activated and translocates into the mitochondria where it exacerbates oxidative stress. The generation of peroxynitrite by superoxide and nitric oxide, increases the permeability of the mitochondrial membrane releasing endonucleases and apoptosis inducing factor into the cytosol. These proteins migrate to the nucleus where they cause DNA damage and induce apoptosis (232,234,235).

The only currently available antidote for treating paracetamol overdose is N-acetylcysteine (NAC). It must be delivered very quickly after the overdose as protein adducts will form within the first 30 minutes. It promotes the synthesis of glutathione and supports the mitochondria by enhancing ATP levels, preventing the downstream effect of NAPQI (235).

The 6 hour incubation of rotenone was able to reduce the viability of the cells but did not increase cytotoxicity biomarkers. In order to identify these features within the paracetamol-treated PCLS, I extended the treatment time to 24h. The PCLS were treated

at 24h post processing to determine if the slices could recover from the treatment, or if they continue to be impacted even after the initial insult has been removed. The viability of the slices was significantly lower than the control at the end of the culture period measured by resazurin assay. Albumin output fell faster in the paracetamol treated slices compared to its control throughout the culture period, although this drop was not calculated to be statistically significant by two-way ANOVA. LDH and AST were used to measure cytotoxicity in the PCLS. LDH release in the controls was as expected, dropping quickly over the culture period as the slices recover from the slicing process. Interestingly LDH release in the paracetamol challenged PCLS plummets immediately, and then begun to increase from 72h. By 96h LDH release from the drug treated slices was higher than the control. AST production in the control PCLS decreases from 48h as the slices had recovered from post-cutting trauma. Paracetamol treatment did not cause an immediate increase in AST production in hepatocytes, but peaks instead at 72h post processing. Levels reduce slightly at 96h in the paracetamol challenged slices from 72h, but they remained above those secreted by the control slices.

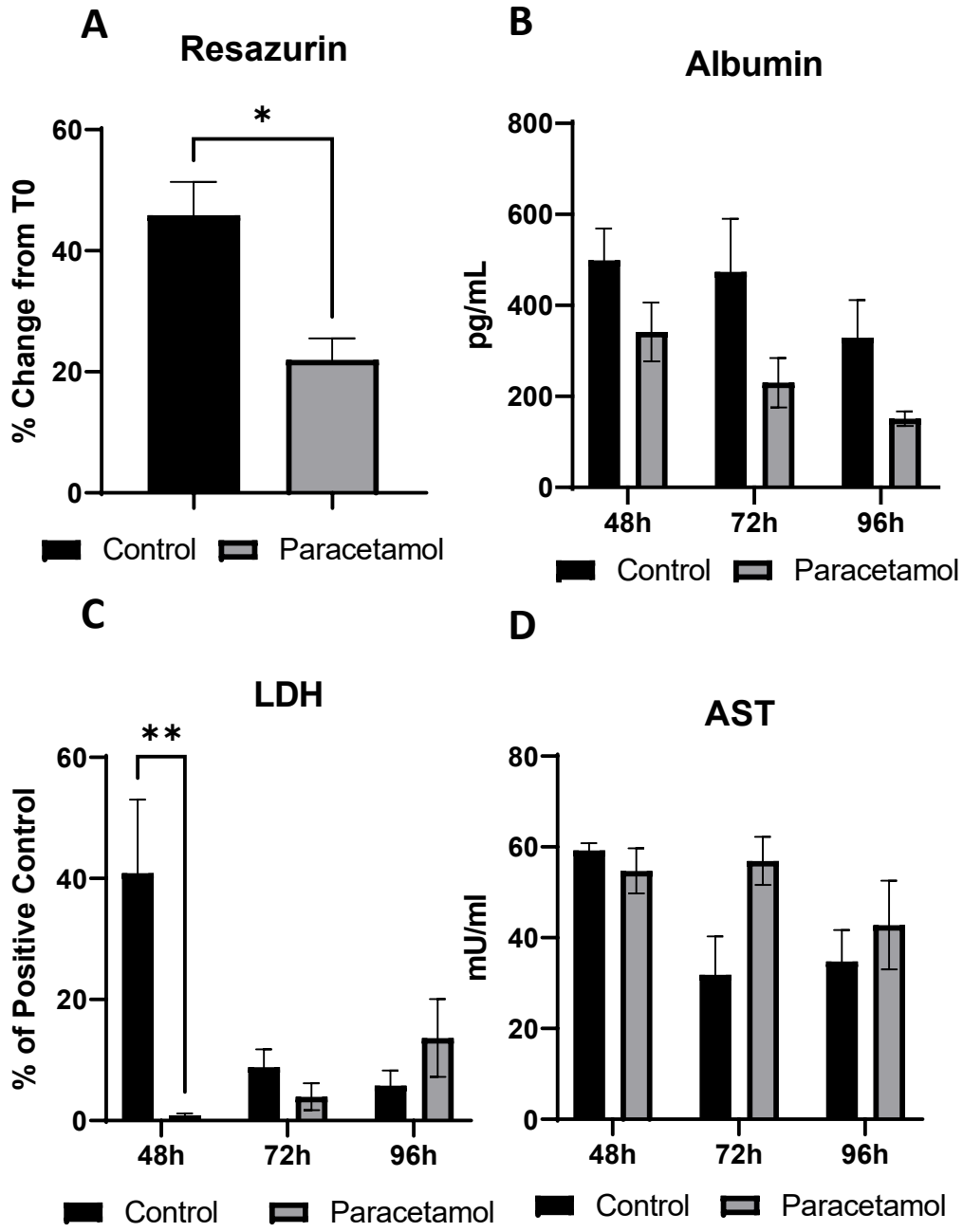

Figure 40. PCLS Culture with Paracetamol

A- *A resazurin assay was performed at 96h shown here as a percentage decrease from T0.* ***B-*** *Soluble albumin was measured from culture media from 48h onwards. Shown as absolute values* ***C-*** *LDH levels were determined from culture media at 48h, 72h and 96h post slicing* ***D-*** *AST levels were determined from culture media at 48h, 72h and 96h post slicing. Data shown as mean +/- SEM and statistical analysis calculated using one-way ANOVA. * p=≤0.05, ** p=≤0.01. N=6 donor livers, n=5 technical replicates per treatment group were averaged per donor.*

6.3.3 Predicting Acute Toxicity in the PCTS

The 24-hour treatment cycle used in the paracetamol challenge was preferred to the 6-hour rotenone challenge. For the remaining optimisation and testing of the system, all drugs were applied for a full media change cycle. Drugs with known hepatotoxicity and nephrotoxicity were selected to demonstrate acute drug injury in the PCLS and PCKS respectively. After a 24h rest period, drugs were added to the culture media for a further 24h before harvesting.

Troglitazone and Rosiglitazone are both thiazolidinediones developed for the treatment of type 2 diabetes (236). Troglitazone was approved for use in the late 1990's and withdrawn shortly after by the FDA and European medicines agency (EMA) due to liver injury, acute liver failure and fatality associated with its usage (236). Rosiglitazone was approved for use shortly after as an alternative to Troglitazone in 2000. It was then banned for use in 2010 by the EMA for its association with DILI but remained on sale in the United States with restrictions placed on its usage. PCLS were treated for 24h with Troglitazone (Figure 41) and Rosiglitazone (Figure 42) concentrations ranging from 75µM to 300µM. They were applied 24h post processing, with all the slices being washed in fresh media before the drugs were applied to remove any traces of NAC. Troglitazone was able to significantly reduce the metabolic activity in the slices at all concentrations tested (Figure 41A), but there were no differences between concentrations. Rosiglitazone however (Figure 42A), only induced a significant decrease in the metabolic activity of the slices at the highest drug concentration. There was then a step-wise increase in metabolic activity as the concentration decreased, with the resazurin levels of the lowest concentration of the Rosiglitazone treatment group being comparable with the vehicle control. Due to procurement issues for the Albumin ELISA kits, for this work, urea output was measured instead as a gauge of tissue functionality. Media from the harvest point at 48h was assessed for urea output. Expressed as a percentage of the control slices, both Troglitazone (Figure 41B) and Rosiglitazone (Figure 42B) were able to negatively impact the functionality of the slices. Both drugs showed a dose dependent effect, where the highest drug concentration of 300µM reduced urea output most, and addition of 75µM of either drug showed the smallest decrease compared to the control. Interestingly, the drugs showed similar reductive effects in functionality as metabolic activity. All tested concentrations of Troglitazone were significantly reduced in both assays, whereas the

75µM dose of Rosiglitazone did not significantly reduce either functionality of activity within the slices. AST levels were increased in response to the addition of Troglitazone (Figure 41D) and Rosiglitazone (Figure 42D) at each of the concentrations tested compared to the control, however, statistically significantly increases in AST production were only observed in the 300µM Troglitazone treated slices. Correlating with the markers indicative of slice health and functionality, the highest concentration of each drug causes the largest increase in this liver damage marker which decreased as the drug concentration was reduced. This pattern was also observed in the release of LDH in Troglitazone treated slices (Figure 41C). It was noted however, that the increases in LDH from slices incubated with the three drug concentrations were not statistically significant. LDH released was slightly raised in all response to Rosiglitazone at all concentrations tested, however none were calculated to be significant compared to the control by one-way ANOVA the increase was very similar in each of the concentrations of Rosiglitazone that had been applied (Figure 42C).

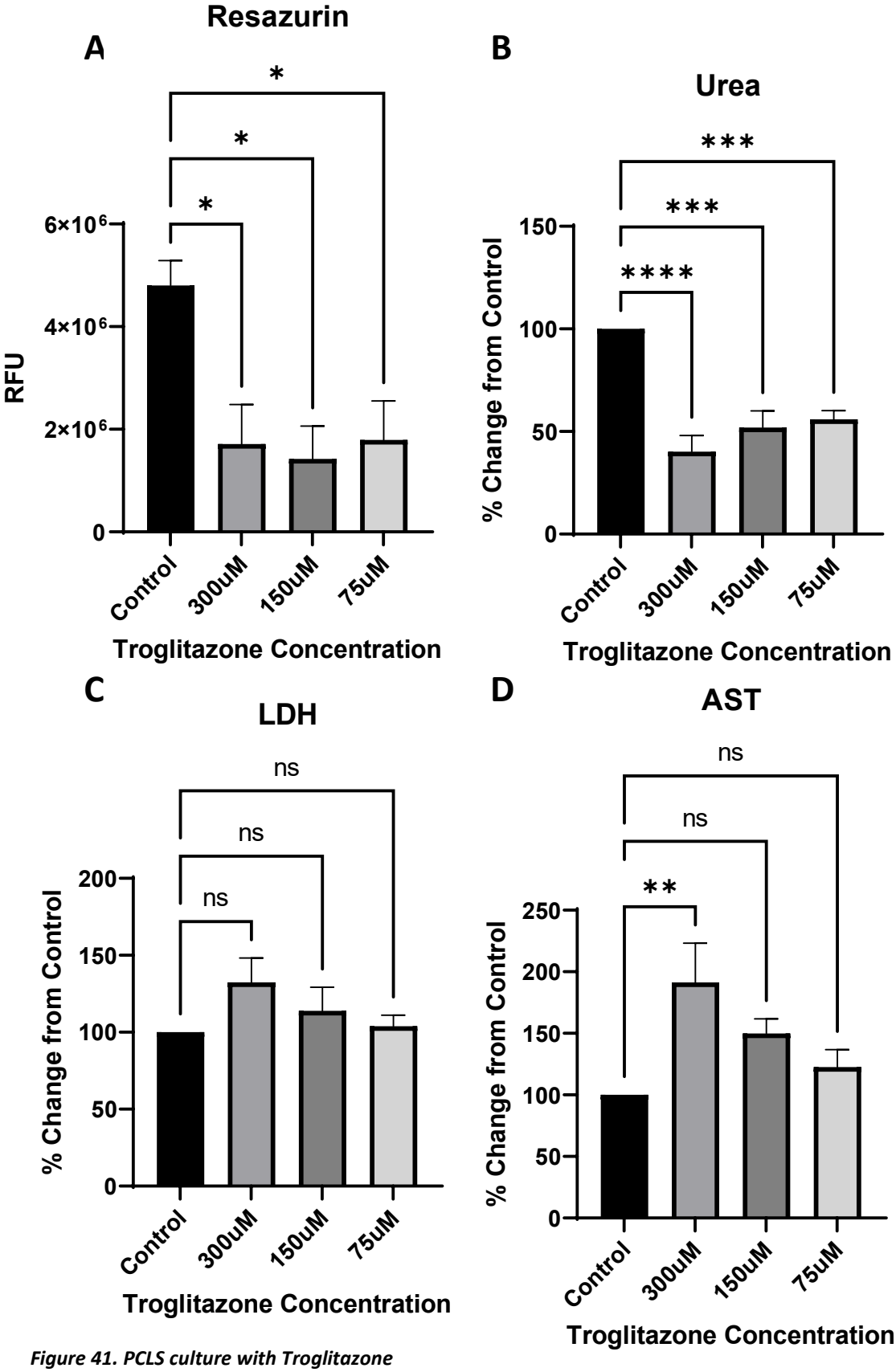

Figure 41. PCLS culture with Troglitazone

Troglitazone was added for a single 24h treatment cycle. ***A-*** *A resazurin assay was performed at 48h, shown as RFU.* ***B-*** *Urea levels were measured from 48h culture media. Shown as percentage change from control* ***C-*** *LDH levels were determined from culture media at 48h, shown as percentage of control* ***D-*** *AST levels were determined from culture media at 48h and shown as percentage of control. Data shown as mean +/- SEM and statistical analysis calculated using one-way ANOVA. Ns= not significant* p=≤0.05, ** p=≤0.01, *** p=≤0.001, **** p=≤0.0001. n=2 Liver Donors, n=5 technical replicates per treatment group were averaged per donor.*

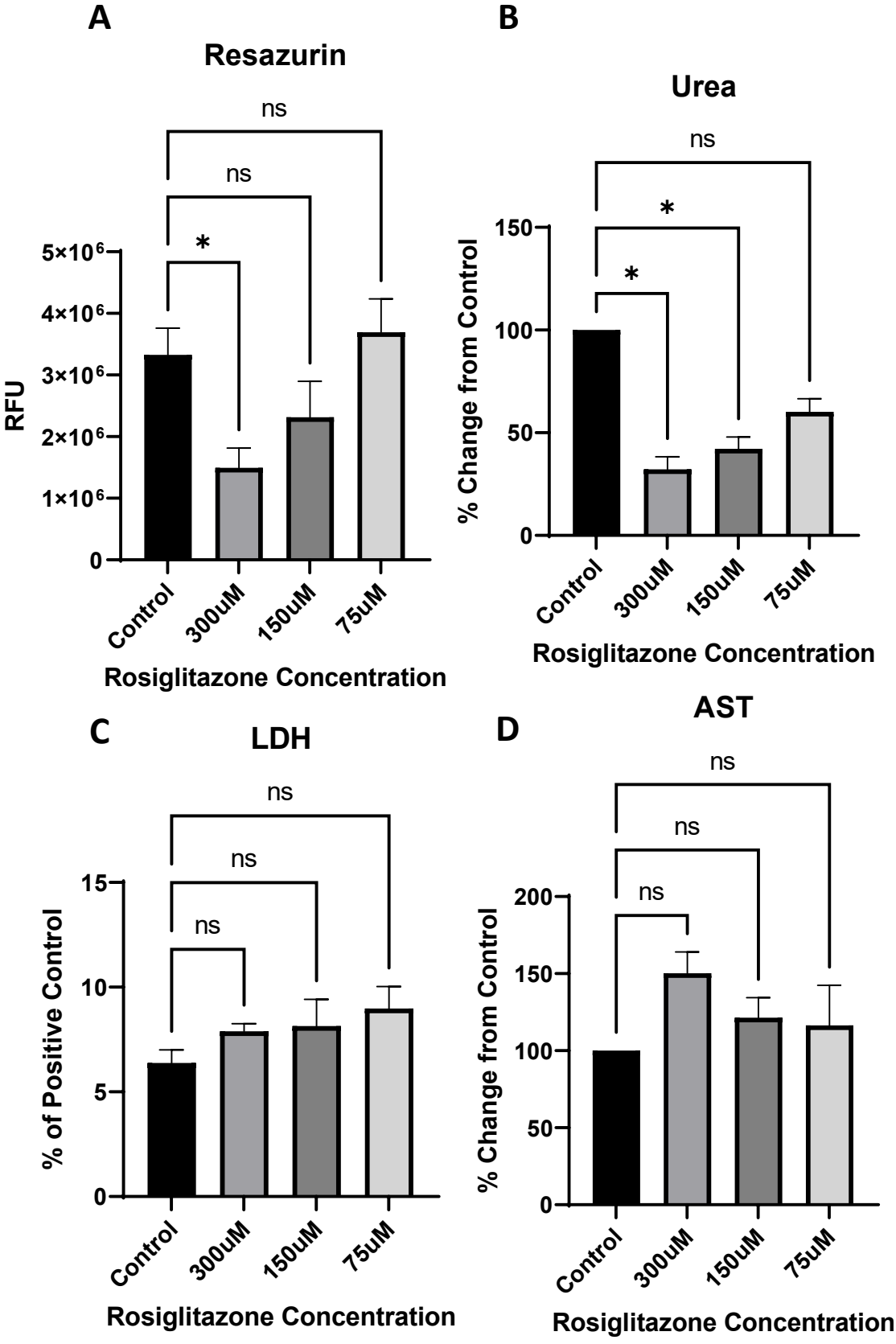

Figure 42. PCLS culture with Rosiglitazone

Rosiglitazone was added for a single 24h treatment cycle. ***A-*** *A resazurin assay was performed at 48h, shown as RFU.* ***B-*** *Urea levels were measured from 48h culture media. Shown as percentage change from control* ***C-*** *LDH levels were determined from culture media at 48h, shown as percentage of positive control* ***D-*** *AST levels were determined from culture media at 48h and shown as percentage of control. Data shown as mean +/- SEM and statistical analysis calculated using one-way ANOVA. Ns= not significant, * p=≤0.05. n=2 Liver Donors, n=5 technical replicates per treatment group were averaged per donor.*

Cisplatin is a chemotherapeutic agent used to treat solid cancers. Although it is an effective drug, adverse effects in normal tissues limit its usage in some patients. Nephrotoxicity in particular has been identified as a common side effect (237). We used 300x Cmax of cisplatin, as described by Ikeda *et al*, as a top concentration, with a two-fold dilution series to test the ability of the PCKS to predict drug injury in the kidney (Figure 43) (238). 1000µM and 500µM cisplatin were able to significantly reduce metabolic activity in the slices after 24h of treatment compared to the vehicle control (Figure 43A). The lowest concentration was able to reduce metabolic activity but this was not calcuated to be significant by one-way ANOVA. Unexpectedly, there was a significant drop in LDH release compared to the control in all concentrations (Figure 43B). Heat shock protein 70 (HSP70) is considered to be an alarmin or danger signal, produced in response to pathological or physiological stress (239). It was hypothesised that HSP70 could be a useful biomarker in identifying drug induced damage in the PCKS. In response to the top concentration of cisplatin, HSP70 secretion was significantly increased compared to the control (Figure 43C). The lower concentrations were raised compared to the vehicle control but this increase was not calculated to be significant by one-way ANOVA.

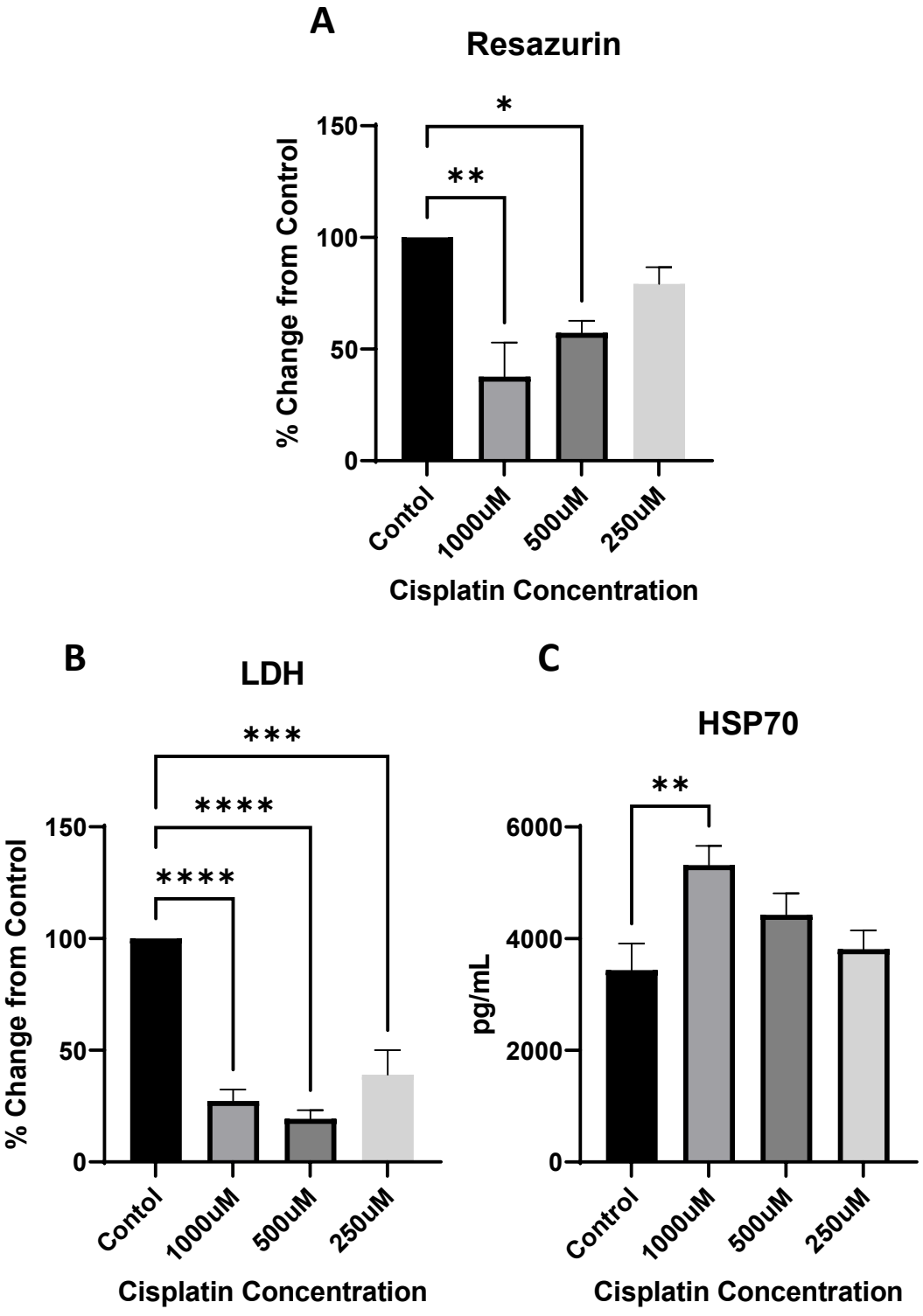

Figure 43. PCKS Culture with Cisplatin

Cisplatin was added for a single 24h treatment cycle. ***A-*** *A resazurin assay was performed at 48h, shown as percentage of control.* ***B-*** *LDH levels were determined from culture media at 48h, shown as percentage of control* ***C-*** *Soluble HSP70 levels were determined from culture media at 48h and shown as absolute values. Data shown as mean +/- SEM and statistical analysis calculated using one-way ANOVA. * p=≤0.05, ** p=≤0.01, *** p=≤0.001, **** p=≤0.0001. n=3 Kidney Donors with n=5 technical replicates per treatment group were averaged per donor.*

6.3.4 Predicting Acute Drug Injury in Fibrotic and Non-Fibrotic Tissue

Alongside the acute injury on PCTS, I also investigated whether the addition of fibrotic disease into the slices could influence the toxicity outcomes. Slices were cultured +/- the validated Fib Stim treatment for 3 treatment cycles and then a single drug dose applied for a further 24h. 300µM Troglitazone was added in the PCLS after acute injury studies showed it to be the most efficient at inducing toxicity in the slices. There was a significant drop in metabolic activity between the vehicle controls and their drug treated counter parts calculated by one-way ANOVA (Figure 44A). There were however, no significant differences in metabolic activity between the normal cultured slices and disease induced slices with the addition of Troglitazone. Functional assessment by soluble albumin ELISA (Figure 44B) produced a similar pattern, where Troglitazone had a significant negative impact on hepatocyte functionality when comparing with the relevant controls. Calculated by one-way ANOVA, there was no difference in albumin output between the groups that were treated with Troglitazone. Data was normalised to the pre-drugged slice media and it was observed that the addition of Troglitazone caused an increase in both LDH and AST markers (Figure 45). There was a rise in LDH release and AST production in both the control and fibrosis induced slices, however the spread of data between the two donors meant that these differences were not calculated to be statistically significant.

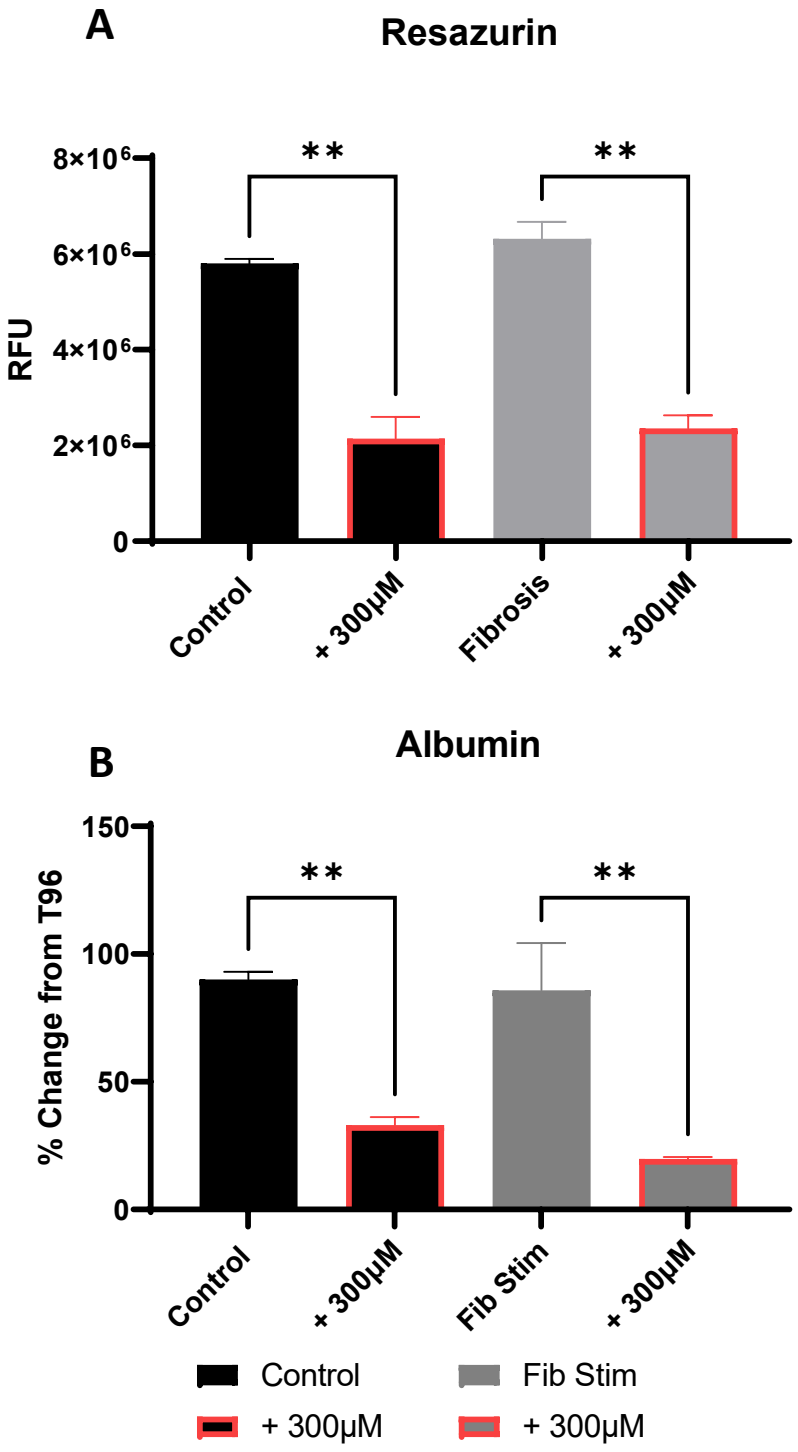

Figure 44. Normal Cultured versus Disease Induced Response to Troglitazone
A- *A reaszuin assay was performed at 120h, shown as RFU.* ***B-*** *Soluble albumin levels were determined from culture media at 96h and 120h, shown as percentage change of 96h. Data shown as mean +/- SEM and statistical analysis calculated using one-way ANOVA. ** p=≤0.01. n=2 liver donors with n=5 technical replicates per treatment group were averaged per donor.*

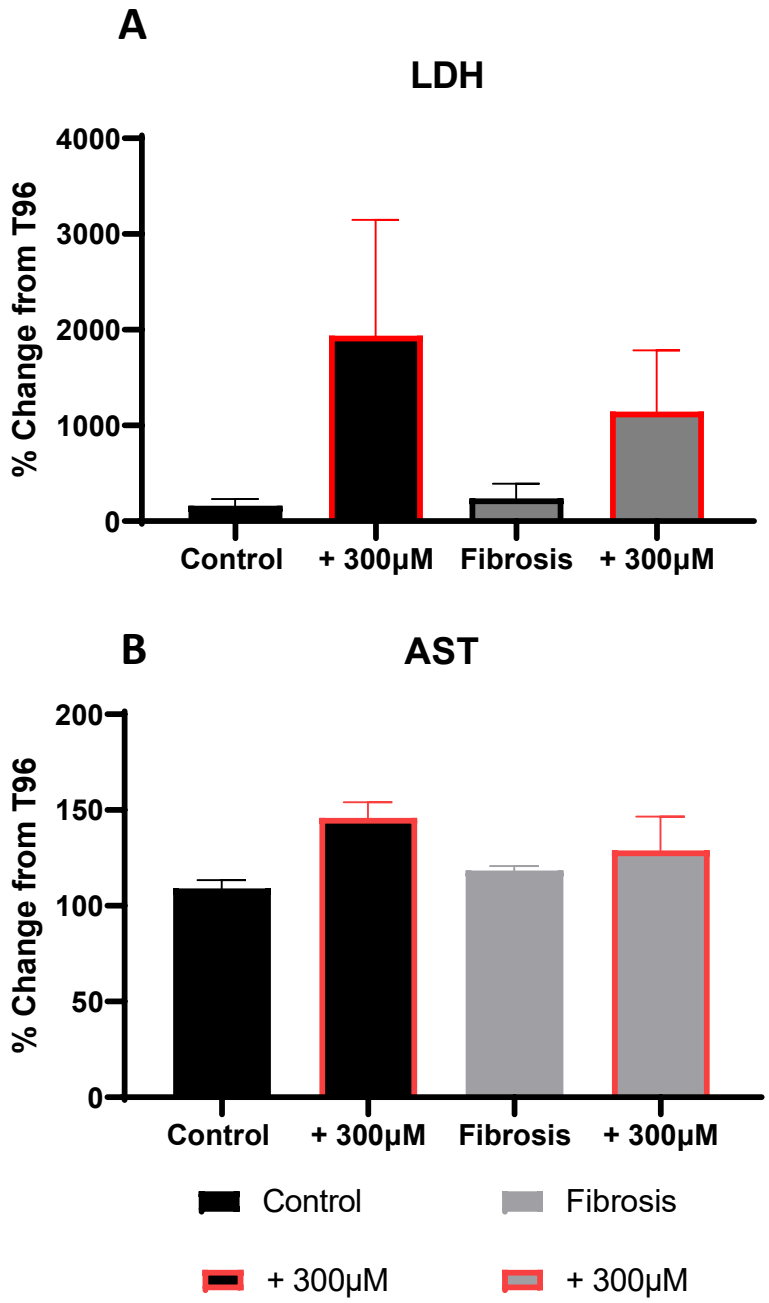

Figure 45. Normal Cultured versus Disease Induced PCLS Response to Troglitazone
A- *LDH release was measured in the 96h and 120h and is shown as a % change from 96h.* ***B-*** *AST levels were determined from culture media at 96h and 120h, shown as percentage change of 96h. Data shown as mean +/- SEM and statistical analysis calculated using one-way ANOVA. n=2 Liver Donors with n=5 technical replicates per treatment group were averaged per donor.*

1mM Cisplatin was used to replicate this study in the PCKS (Figure 46). As expected the addition of cisplatin significantly reduced metabolic activity in the slices compared to the relevant control. There was also a drop in slice viability between the diseased induced and the normal controls but not between the two drug treated groups. LDH and HSP70 were used to identify damage signals from the cultured PCKS. There was a significant increase in LDH release in both groups with the addition of cisplatin compared to their respective controls at 96h (pre-application) and 120h (post application). The non-drugged slices for both the normal and disease-induced controls reduced LDH from 96h to 120h but not significantly. There were no significant differences in LDH release between the normal and disease induced slices at any of the time points, with or without the addition of cisplatin. HSP70 however produced a different picture. Challenge with cisplatin increased HSP70 levels in the media compared to the relevant 120h control but this was only calculated as significant in the disease induced slices. The inclusion of the Fib Stim treatment significantly increased the secretion of HSP70 from 96h to 120h, but where the PCKS were cultured with no additional treatments the level instead dropped slightly. Comparing the normal cultured slices and the disease induced slices at each time point, there was no difference in HSP70 levels at 96h but there was a significant increase at 120h in both the cisplatin treated and non-drugged slices.

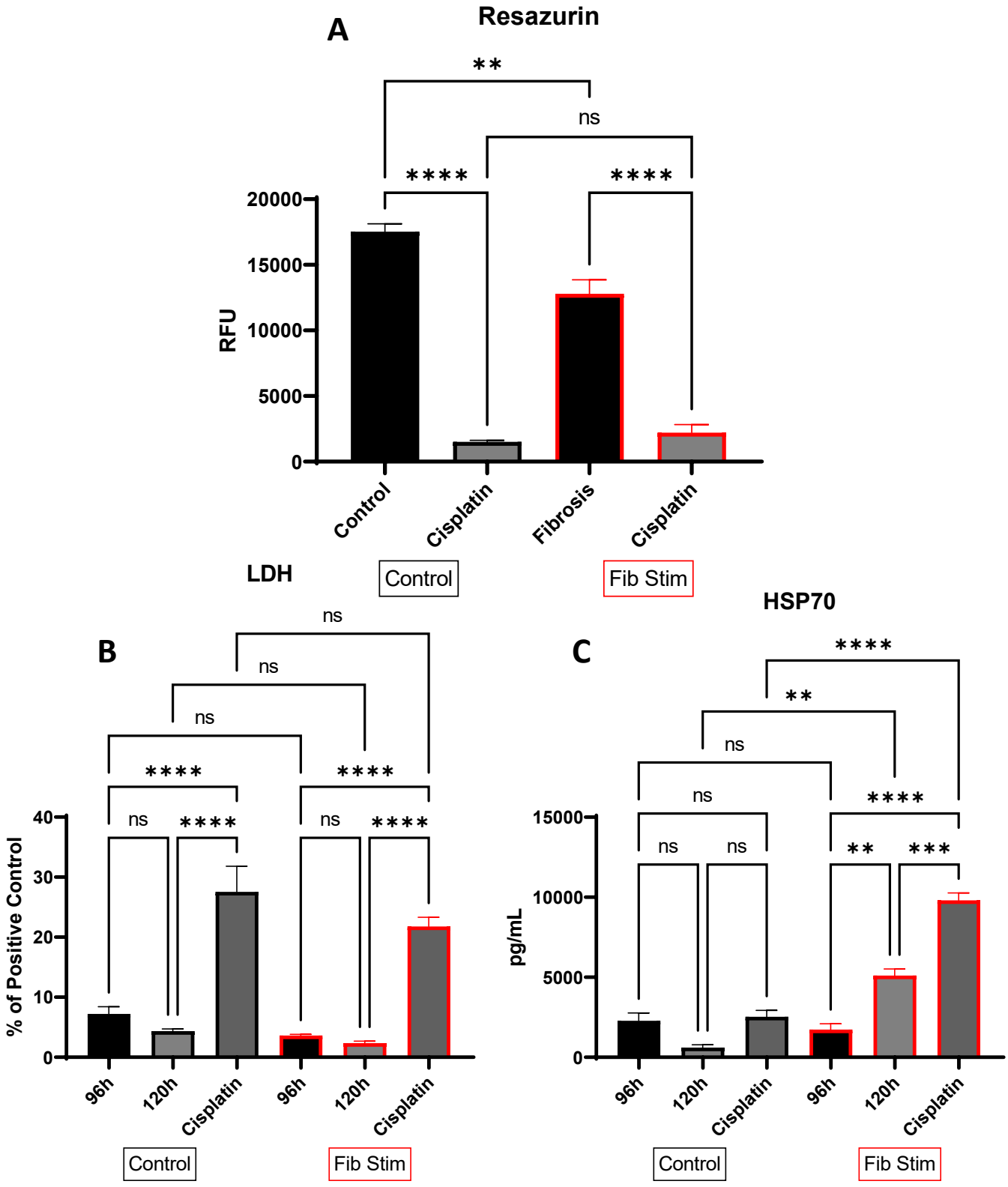

Figure 46. Normal Cultured versus Disease Induced PCKS Response to Cisplatin

A- *A resazurin assay was performed at 120h, shown as RFU.* ***B-*** *LDH levels were measured in the 96h and 120h culture media and shown as percentage of positive control.* ***C-*** *Soluble HSP70 levels were measured in the 96h and 120h culture media and are shown as absolute values. Data shown as mean +/- SEM and statistical analysis calculated using one-way ANOVA (black). Ns= not significant, ** p=≤0.01, *** p=≤0.001, **** p=≤0.0001. n=3 Kidney Donors with n=5 technical replicates per treatment group were averaged per donor.*

6.4 Discussion

The international consortium for innovation and quality in pharmaceutical development (IQ) microphysiological systems affiliate (MPS), is a cross-pharma collaboration that has developed a series of criteria that new pre-clinical models should meet. They suggest that models that are able to meet their guidelines are more likely to exhibit a high predictive ability than those that do not (229). These guidelines include, the model should replicate key histological structures and functions of the organ being studied, it should be able to distinguish between toxic small molecules and a non-toxic analogue and the model should be able to demonstrate predictive clinical responses of six additional drugs (229). I have shown previously that this platform displays key features of the whole organ, where the cells remain viable and functional across the culture period. Before the predictive ability of the platform could be tested with drugs known to cause toxicity, the methodology of application first had to be developed.

6.4.1 Analysis of Cytochrome P450s and Drug-Associated Transmembrane Proteins

To be suitable for assessment of therapeutics, it is important that a model is able to express proteins relevant to the transport and metabolism of drugs. RNA sequencing and proteomic analysis was performed on liver and kidney slices cultured for 96h +/- Fib Stim treatment. In the PCLS, RNA sequencing suggested there was a significant decrease in some of the CYPs crucial to the metabolism of xenobiotics. Disease states typically have a negative impact on metabolic capacity, with loss of tissue architecture resulting in a reduction in functional hepatocytes leading to reductions in CYP levels (221,240). Interestingly in the PCKS there were variations in the drug transporter RNA levels that were not just reduction in response to fibrogenesis. SLC22A2 for example, was significantly increased compared to the control group. Whilst there were significant differences at the RNA level, this was not translated to the protein level. There was some variation observed between groups but it is not significant in any case. Despite a relationship between RNA and protein levels, increases to one cannot always infer increases to the other, as protein levels are regulated by more than just messenger RNA (mRNA) levels. Post translational modification to proteins and a short half-life/fast turnover of messenger RNA mean that copy numbers of mRNA rapidly become independent of protein level

(233,234). The crucial result from this analysis was that both metabolic enzymes and drug transporters are constitutively expressed throughout the culture period, implying drugs cultured alongside the slices could be taken up by cells and metabolised. Additional work that I would like to undertake for further analysis, would be to conduct CYP activity assays and measure metabolite levels of known compounds.

6.4.2 Methodology Development

Rotenone is a naturally occurring molecule used in some countries as a pesticide. It exhibits cytotoxicity via its ability to interfere with the electron transport chain in mitochondria, resulting in reduced ATP generation and necrosis (230). For initial testing of the potential of the 96-well bioreactor to predict toxicities, rotenone was added to the PCLS for 6 hours prior to harvesting. The compound was able to reduce viability and functionality of the tissue slices, assessed by resazurin assay and soluble albumin ELISA respectively. Increases in cytotoxicity were not observed in either LDH or AST, and in the AST there were significant reductions in levels in the drug treated slices compared to the untreated control. It was suspected that the rotenone in the media was possibly interfering with the AST assay, as this decrease was not observed in any other treatment groups on the bioreactor plate. It was suggested that prolonged incubation with rotenone may allow for further release of LDH in the drug treated slices, and that 6 hours was not sufficient time for this to increase significantly.

Paracetamol was chosen to develop methodologies to model hepatotoxicity, as it is a clinically relevant drug known to cause significant toxicity to hepatocytes in patients that take a paracetamol overdose (93). After a 24h rest, a single high dose of paracetamol was added to the PCLS for 24h and then allowed to recover to 96h. The addition of the paracetamol had a significant, negative impact on the viability of the slices and also reduced the functionality of the slices. Albumin secretion by the slices fell much quicker across the culture period than the control, suggesting that the slices don't recover from the toxic insult. LDH levels dropped very quickly after the introduction of paracetamol and slowly increased again to 96h where they were higher than the control. This is potentially due to the paracetamol in the media used interfering with the assay, rather than being a genuine drop. As new media is added to the slices, the paracetamol and its metabolites are washed from the plate, and by 96h there is no interference with the assay. The AST levels did not change compared to the control immediately, taking an extra treatment

cycle to be notably different to the control. In clinical cases of paracetamol overdose, liver function test analysis finds that liver transaminases begin to increase 12 hours after ingestion, peaking at 18-72h post ingestion (227). This suggests the modelling of drug toxicity in the 96-well bioreactor can predict toxicity of drugs and mirror clinical outcomes.

6.4.3 Acute Induction of Drug Induced Injury

The 24 hour treatment cycle proved a better method for drug administration than a 6 hour cycle. The addition of the drugs at 90 hours meant that the last media change before the application of the drugs was 6 hours short of the previous time point, and 18 hours longer than the culture media with the drug included. This made comparing the levels of soluble markers pre and post drug addition more complex. To test the system for its predictive abilities, we selected three drugs with known either hepatotoxicity or nephrotoxicity, using a single treatment cycle with a small dosage range.

Thiazolidinediones, Troglitazone and Rosiglitazone, were initially developed to treat patients with type 2 diabetes (236). After being approved for use in the late 1990's, Troglitazone was withdrawn from sale shortly after by both the FDA and EMA due to severe hepatotoxicity and fatality (236). Rosiglitazone, although withdrawn for sale in Europe for similar toxicity issues, is still available in the United States but with restrictions on prescriptions. The mechanism of Troglitazone toxicity is not fully understood but it is thought to be associated with mitochondrial dysfunction and has been shown to be both concentration and time dependent (243,244). Ewart *et al* assessed the predictive value of their 3D microfluidic organ-on-chip system with Troglitazone, where they used 300x average Cmax as a top concentration (229). Due to solubility limitations, we used a top concentration of 50 fold average Troglitazone Cmax as defined by Ewart *et al,* and used the same concentration of Rosiglitazone to allow for direct comparison (229). We found that there were concentration dependent changes in metabolic activity, slice functionality and alterations in damage associated markers in response to both hepatotoxic drugs. Differences in toxicity between the two drugs could be observed, with the lower concentrations of Rosiglitazone not having such a significant detrimental impact on metabolic activity, and AST/LDH levels were not significantly increased at any concentration. Troglitazone however, demonstrated diminished metabolic activity and significantly increased AST production in response to the top concentration used. The

ability of a pre-clinical model to distinguish between structurally similar drugs is an important test according to the IQMPS, one which the 96-well bioreactor appears to do successfully. It should however, be noted that there were limited donor numbers involved in this study and should be repeated on more donors to confirm this ability.

Cisplatin is an effective chemotherapeutic agent for the treatment of solid tumours. Its ability to induce nephrotoxicity is a limiting factor in its usage for the treatment of cancer patients (237,238). Cisplatin is taken up into the proximal tubule cells where it causes DNA damage and mitochondrial stress (245). 300x Cmax cisplatin was used as described by Ikeda *et al*, lower concentrations were tested initially (data not shown) but we struggled to observe any significant impact on the viability and health of the slices until testing these much higher concentrations (238). There were concentration dependent changes in metabolic activity with the higher concentrations having the greatest negative impact. HSP70 was used as a marker of cell damage as it is increased in response to physiological stress/injury (239). This marker was successfully used in this model to demonstrate drug induced cellular injury in the PCKS, not only was HSP70 increased in response to cisplatin, it was dose dependent. LDH was unexpectedly, significantly lower than the control with the addition of the different concentrations of cisplatin. It is possible that the proximal tubule cells were killed by the treatment and therefore did not release LDH into the surrounding media, but considering the slices were still metabolically active this may not be the only contributing factor. It has been observed in other studies that LDH levels in the control are still high at 48h relative to levels at 72h and 96h, suggesting the slices are still recovering from the slicing process. To further develop this system, a comparative study using a single hit of the drug at 24h post slicing and 48h post slicing to see if this extra recovery time would produce more accurate LDH results. Also for future study, it would be interesting to see if there are further increases in AST/LDH production with subsequent treatment cycles and if these differences between structurally similar drugs become more pronounced with further culture. Other studies that have investigated the predictive ability of their organ models such as organ-on-chip systems will culture in the presence of a drug over several days, and so to demonstrate this model is also capable of longer culture periods would be beneficial.

6.4.4 Acute Drug Injury in Fibrotic and Non-Fibrotic Tissue

In human trials of novel therapeutics, the drugs will often be first given to healthy volunteers. The safety profile of that drug generated from these early studies is therefore not accurate for those with underlying health conditions such as CKD and CLD. It is known that with changes in tissue architecture as a result of disease, the ability of the organ to metabolise drugs and remove toxic products is altered (18,19). Modelling of drug-tissue interactions in the pre-clinical phase could provide further information for later phase trials and would remove candidates with unacceptable toxicity before they made it to human trials, saving time and money.

The addition of Troglitazone to normal cultured and diseased induced PCLS resulted in significant reduction in tissue health compared to their controls. There was variation in all the biomarkers that were analysed between the fibrosis-induced groups compared to the normal cultured slices, however none were calculated to be statistically significant. As there was only an n=2 here it is difficult to calculate meaningful statistical analysis and so further donors would be required to strengthen this.

In contrast to the acute drug injury in the short term cultured PCKS, the LDH assay looks more as would be expected with the addition of a nephrotoxic substance after the longer rest, suggesting the extra rest period could be beneficial for this type of study. LDH and resazurin assays were unable to identify any significant differences in slice health between normal slices and those cultured with fibrogenic stimuli, however there were differences in HSP70. Cisplatin is taken up by the transmembrane protein SLC22A2 into proximal tubule cells and moved out of cells into the tubule lumen by SLC41A1 (237,245). From the RNA sequencing, it was observed that SLC22A2 was increased and SLC47A1 was reduced in response to fibrogenesis in the slices. This could potentially explain the increased levels of HSP70 in the disease-induced slices in response to cisplatin treatment, where the over expressed SLC22A2 is able to uptake more cisplatin and the reduced SCL47A1 is not able to cope with the influx causing DNA damage and mitochondrial stress within the cells and the subsequent increase in HSP70 expression. This suggests this model has the potential to identify differences in drug toxicity in diseased versus non-diseased tissues, however a greater variety of biomarkers should be identified to better evaluate these differences.

6.5 Conclusion

The aims of this study were:

- Optimise the methodology for predicting drug toxicity in the 96-well bioreactor.
- Demonstrate potential of the 96-well bioreactor for prediction of adverse drug reactions using clinically relevant compounds.
- Demonstrate the potential of the 96-well bioreactor as a platform for identification of differences in DILI between healthy patients and those with underlying pathologies.

The methodology optimisation for culturing PCTS with drugs for toxicity prediction was successfully completed. A full 24 hour treatment cycle is able to induce significant decline in slice health and this decline can be dose dependent. For further development of the system, delaying the addition of the drugs a further 24h would be recommended, allowing the slices to fully recover from post-slicing trauma. In some of the biomarkers assessing tissue damage/stress the control group levels were still very high making the differences with the addition of the drugs less significant. It would be beneficial to allow full recovery of the slices before the addition of these compounds to generate more reliable data.

Next, I established that the addition of toxic compounds to the PCTS system was able to induce a number of markers indicative of tissue health decline, including loss of metabolic activity, reduction of albumin and urea in the PCLS and increases in HSP70 in the PCKS. IQMPS guidelines for the development of 3D cultured pre-clinical models state that a model should be able to distinguish between structurally similar drugs. For this Troglitazone, banned for sale due to severe hepatotoxicity, and Rosiglitazone, also a thiazolidinedione, were tested using the same concentrations. There were differences in their toxicity profiles in our studies, suggesting this platform can distinguish between chemically similar drugs. This was however, completed using a low number of replicates so more donors should be tested to confirm this. The platform should be tested, according to the IQMPS guidelines, on a minimum of 7 pairs of toxic and non-toxic compounds which due to time constraints I was unable to do here, but I have shown promise with one pair. The addition of further biomarkers to the current panel would also be useful for building a safety profile of novel compounds. It was observed that some drugs potentially interfere

with some of the colourimetric biomarker assays such as paracetamol and LDH. For the liver these could include diagnostic markers ALT, ALP and GGT, or creatinine and urea levels in the kidney. Candidate biomarkers such as cytokeratin 18 which is released from necrotic hepatocytes, clusterin which has been shown to identify nephrotoxicity or micro-RNAs which can be organ specific would also be good additional options for safety profile assessment (246,247). Drug concentrations for this study were selected based on similar work by other groups (229). Whilst we can identify toxicity in the slices at the top concentrations used, it should be recognised that these concentrations are much higher than plasma levels of these drugs in humans. A wider range of doses should be tested inclusive of therapeutic levels to determine if damage associated markers are present at these lower volumes, or if these increase with repeated treatments.

I then attempted to demonstrate differences in toxicity profiles between normal cultured and disease induced tissues using the top concentrations of drugs used previously in the PCLS and PCKS. There were differences in some biomarkers between the normal cultured and disease induced slices, suggesting this system with further development and testing could identify patients that are more at risk of adverse effects from the drug. As it stands however, more replicates using a wider range of therapeutics and dosages is required. One of the difficulties of this type of study is that the tissue used often comes from patients with underlying pathological conditions and slices may already show signs of fibrosis development or lipid accumulation, this may skew the control data as some donors may already have altered drug metabolism. A more suitable comparative study would be to obtain more donors that could be grouped by fibrosis and steatosis score and compared with each other, rather than inducing further fibrosis or inflammation in single donors.

Whist there are drawbacks with this platform that have been acknowledged, PCTS have the potential to be used in early pre-clinical screening of lead candidate drugs, reducing reliance on animal models for efficacy testing and early safety profiling studies.

Chapter 7. Discussion

The current drug discovery pipeline is not sufficient to identify toxicity of novel therapeutics resulting in 30-40% of drug attrition attributed to unforeseen adverse effects (84,85). To reduce this failure rate, and by extension the cost of therapeutic development, there needs to be investment in the improvement of complex, physiologically relevant organ models. 2D models are not complex enough to reveal drug-tissue interactions, and there is a move to reduce the number of animals used in scientific research, making way for the development of 3D cell culture models (110,118,169).

Efficacy testing in 2D cell culture is often the first screening tool for lead compounds. Whist relatively inexpensive and high throughput, they are far removed from the native tissue microenvironment, commonly missing cell types with lines that no longer express major features of the model cell (111,113). Animal modelling is a significant improvement for pre-clinical drug evaluation, but results should always be treated with caution as translation from rodents to humans is not guaranteed. For example, rats are much less susceptible to paracetamol induced hepatotoxicity than humans (94). An advantage of rodent models over 2D cell culture is that these efficacy studies can be tested on a background of disease, such as anti-fibrotic therapy development in CCl_4 challenged mice (128,129). 3D models have gained traction in recent years with advancements in microfluidic systems, organoids and bioprinting techniques being developed. Several organ-on-chip systems have been developed, incorporating the cell types of the native tissue into a layered structure with some models resembling native organ architecture (146,229). Some groups have also demonstrated the abilities of this technology to predict drug toxicity, although I found less evidence of disease modelling for drug efficacy (229). PCTS offer a 3D, complex model which retains the architecture and cell types (inclusive of their natural phenotypes) of the native organ. This model has shown promise for predicting efficacy and toxicity in numerous research groups, and this lab has developed a bioreactor plate which extends their life in culture to up to 144h (150,156,158,203).

This project aimed to develop a medium throughput platform for the pre-clinical screening of lead candidate drugs using human liver and kidney tissues. This novel 96-well bioreactor platform focusses on the use of PCTS from the liver and the kidney, both sites

exposed to ingested xenobiotics and therefore at risk of drug induced injury. The main aims were to optimise the bioreactor for successful culture of 3mm PCLS and PCKS, validate models for the study of fibrogenesis and inflammation, and demonstrate the usage of the platform for predicting drug efficacy and toxicity.

7.1 Robot Development and Bioreactor Optimisation

The aims for this section of the project were to optimise the culture conditions of the 96-well bioreactor for the culture of 3mm slices and investigate the potential of introducing robotics to aid the set-up. The culture conditions were successfully optimised, showing that both the PCLS and PCKS remain metabolically active and functional through 96h of culture. The development of a robot for the purpose of automating the cutting out and plating slices was not achieved. After making numerous alterations to the hardware and software, it was decided that too much additional work was required to fully automate the system that would not be within the scope of this project. Whilst the pickup and plating efficiency was improved with the alteration of the tissue trays and addition of agarose, other inclusions that would be required were not reasonable. These included reducing the number of slices cut from a single tissue sheet, and the addition of a camera driven artificial intelligence system to prevent the generation of partial slices from either overlapping of the cutting area with the biopsy punch or cutting in areas containing vessel holes or tears in the tissue. Without these changes, it was likely that the system would not be fully automated, as a trained user would be required to monitor progress, ensuing that good quality slices were consistently produced. However, it was noted that these changes would result in a large amount of wastage which, considering the precious nature of the tissue, was not feasible. Instead, we altered the way the slices were cut by hand which decreased plating time whist maximising the number of generated slices. I believe is not reasonable for an academic lab to further develop the robotic system, but it could potentially be useful in an industrial setting. Significant investment would be required to improve the robot to a stage where it overtakes the efficiency of a trained user.

7.2 Fibrosis Model Development

A comparison of the 3mm and 8mm PCLS bioreactors demonstrated similar levels of tissue viability, functionality, and disease features. The smaller slices proved to be just as functional as their larger counter parts, producing similar levels of albumin and

comparable levels of AST and LDH. Whilst the resazurin levels were much lower, the trends between the treatment groups mirrored each other. The bioreactor was successfully scaled with validation of the fibrosis model in both the liver and kidney slices. Multiple donors were collected, and I demonstrated the reproducibility of the Fib Stim treatment for the generation of fibrosis in the slices. Donors that were unsuitable for modelling were identified, these included those with high steatosis in the liver as these resections often did not slice well and had low metabolic activity at T0 compared to other resected tissue with no/little steatosis, and kidneys that had been perfused more than 48h before acceptance in the lab. Increases in fibrosis-associated features including collagen deposition and activated HSC were present in the treated slices and were significantly different to the non-treated controls. These were measured using several different methods including, histology and biomarker analysis by ELISA and MSD. Different expression patterns were observed between the organs within the MSD panel including upregulation of MCP-1 and GM-CSF in the kidney and downregulation of MIP-1β and MDC. This work, particularly the MSD panel, would benefit from increased donor numbers are there was some variation between the donors that were included. It would also be interesting to understand whether this variation in biomarker levels were as a result of a particular donor characteristic such as underlying disease, age or sex. Alongside this, I showed that the response to the pro-fibrogenic stimuli could be modulated. Using inhibitors and clinically available drugs, dosage dependent reductions in fibrogenesis were performed in both the PCLS and PCKS, demonstrating the use of the platform for efficacy testing of anti-fibrotic compounds.

Overall, this is a suitable model for the study of fibrosis development and medium throughput screening of anti-fibrotic compounds. The slice system is histologically accurate and contains the cell types present in the native organ in the right proportions, meaning compounds that target a range of pro-fibrotic pathways can be tested. The large number of slices in a single plate allow a range of testing conditions with technical replicates to provide accurate data. When comparing this platform to similar modelling systems by other groups, it was observed that the culture time was longer in most cases (up to 144h versus an average of 48h) resulting in a more fibrotic phenotype with TGFβ/PDGFββ induction using this bioreactor. Some groups also used rodent tissue,

rather than human tissue, with fibrotic induction methods that are not comparable to human pathophysiology (such as UUO and CCl_4 treatment) (150, 154-156, 203, 204).

7.3 Inflammation Model Development

A model of acute inflammation was validated within the PCTS. Starting with an optimisation study using three different inflammatory stimuli, it was found that IL-1β most reliably produced a dose dependent response across multiple donors in both the liver and kidney slices. There were differences in protein expression depending on the organ of origin and stimuli used, for example biomarkers associated with the inflammation in response to infection were only upregulated after challenge with LPS, suggesting that this model is highly specific in response to different challenges. It would be beneficial to undertake further replicates looking at expression profiles within the slices between LPS and IL-1β challenged slices as some data points showed large variation between donors, effecting statistical analysis. The methods used to identify inflammation within the tissue were largely soluble biomarker based, it would be interesting to expand the assessment of slices with, for example, histology or proteomics. Identifying different white cell populations within the tissue slices and evaluating protein levels within the tissue and not just soluble protein would provide a more complete picture of inflammation within the slices. I also demonstrated the use of this model for the assessment of anti-inflammatory compounds. Inflammatory biomarkers produced in response to IL-1β challenge were reduced with the addition of and IKK2 inhibitor. Furthermore, this response was observed to be dose dependent with a 10-fold dilution series of the inhibitor. Additional anti-inflammatory drugs should be tested using this methodology, as only one inhibitor was tested here.

Overall, this model is a useful tool for the study of the acute inflammatory response and for the testing of anti-inflammatory compounds. With such a large range of biomarkers proven to be altered in response to inflammatory challenge, drugs that target the major inflammatory signalling pathways can all be tested and studies to understand redundancy built into the inflammatory system could also be undertaken.

7.4 Modelling Toxicity in the PCTS

The first aim of this chapter was to optimise the methodology for the culture of slices with drugs. It was found that the PCTS were able to cope with a full 24h treatment cycle which allowed for better comparison with previous time periods. It was also realised that a 48h rest period post slicing before drug application was better for comparing a non-treated control with drug treated slices as the extra recovery time reduced the damage associated biomarkers to a lower baseline. Next, I showed that the system has potential for predicting toxicity using clinically relevant drugs and that it can distinguish between structurally similar drugs with different reported toxicities. For further work here, more pairs of toxic compounds and non-toxic analogues should be tested to ensure that the system can not only identify the toxic drug but that it does not over exaggerate toxicity in drugs with profiles that have been deemed acceptable by the FDA and EMA. Alongside this, the inclusion of additional biomarkers for toxicity assessment is important to generate a more definitive safety profile for test compounds. As well as literature searches for new damage associated biomarkers, MSD offer a toxicity multiplex panel which could be incorporated into analysis of the culture media. The last aim of this chapter was to determine whether or not the bioreactor could identify differences in toxicity in disease induced PCTS and normal cultured PCTS. Within the single liver donor, there were no significant differences between groups with the addition of the drug treatment, and within the single kidney donor, there was limited evidence in the HSP70 data that fibrosis development resulted in a greater toxic effect. A problem that was identified with this method of identifying different safety profiles between diseased and non-diseased tissue is that, especially for the liver studies, the tissue that is obtained is often from patients who already suffer from underlying pathologies and so may already display features of fibrosis or steatosis. A more accurate method of predicting differences between diseased and non-diseased organs would be to collect a wider range of donors and perform statistical analysis grouping patients by their pre-culture fibrosis and steatosis scores.

Overall, this 96-well bioreactor has the potential to become a useful tool for the screening of novel lead candidate drugs and the prediction of their toxicity, reducing reliance on less physiologically relevant 2D and animal pre-clinical models. Compared to similar modelling systems from other groups, this bioreactor system is as capable at identifying toxicity of compounds and distinguishing between toxic and non-toxic analytes. As we did not use

rodent tissue, it is not possible to determine differences between species. The major benefit of this modelling platform over others, is the medium throughput nature, as I have a single plate containing 96 slices while others tended to use larger slices in 12 and 24 well plates (150, 154-156). The major drawback of PCTS in either this system or those developed by other groups, is that this model would not be suitable for long term studies as the current lifespan of the slices (in our platform) is 144h, where as liver-on-chip platforms have been shown to remain viable after 28 days while producing acceptable safety profiles (145). I have shown however, that this platform is still capable of producing clinically relevant safety profiles for known toxic compounds in the shorter term.

Chapter 8. Future Direction

Additional work for each individual chapter has been identified within the relevant section. This broadly includes the addition of further donors and testing of other anti-fibrotic, anti-inflammatory and toxic compounds with non-toxic analogues.

- I would like to be able to further develop the slice model to include other features of CLD, for example the exploration of models of NAFLD, NASH or HCC and understanding how these models could be put to use for testing novel lead compounds for efficacy and toxicity profiling.
- It would also be interesting to study chronic inflammation as a result of senescent cells rather than by challenge with recombinant proteins, and if these cells could be induced in the slices.
- As I have shown that this platform is suitable for the culture of slices produced from the kidney and the liver (and others in the lab have shown its suitability in the culture of lung slices), this system could investigate multi-morbidity, using conditioned media from one organ to treat another and see if the factors released from the fibrotic/steatotic/inflamed tissue can influence development of similar conditions in other slices.

Chapter 9. Reference List

1. Abu Rmilah A, Zhou W, Nelson E, Lin L, Amiot B, Nyberg SL. Understanding the marvels behind liver regeneration. WIREs Dev Biol [Internet]. 2019 May [cited 2023 Mar 1];8(3). Available from: https://onlinelibrary.wiley.com/doi/10.1002/wdev.340

2. Schulze RJ, Schott MB, Casey CA, Tuma PL, McNiven MA. The cell biology of the hepatocyte: A membrane trafficking machine. J Cell Biol. 2019 Jul 1;218(7):2096–112.

3. Hundt M, Basit H, John S. Physiology, Bile Secretion. In: StatPearls [Internet]. Treasure Island (FL): StatPearls Publishing; 2022 [cited 2023 Mar 1]. Available from: http://www.ncbi.nlm.nih.gov/books/NBK470209/

4. Michalopoulos GK, Bhushan B. Liver regeneration: biological and pathological mechanisms and implications. Nat Rev Gastroenterol Hepatol. 2021 Jan;18(1):40–55.

5. Dutta S, Prasad Mishra S, Kumar Sahu A, Mishra K, Kashyap P, Sahu B. Hepatocytes and Their Role in Metabolism. In: Dunnington K, editor. Drug Metabolism [Internet]. IntechOpen; 2021 [cited 2023 May 16]. Available from: https://www.intechopen.com/chapters/78184

6. Khomich O, Ivanov AV, Bartosch B. Metabolic Hallmarks of Hepatic Stellate Cells in Liver Fibrosis. Cells. 2019 Dec 20;9(1):24.

7. Tsuchida T, Friedman SL. Mechanisms of hepatic stellate cell activation. Nat Rev Gastroenterol Hepatol. 2017 Jul;14(7):397–411.

8. Barry AE, Baldeosingh R, Lamm R, Patel K, Zhang K, Dominguez DA, et al. Hepatic Stellate Cells and Hepatocarcinogenesis. Front Cell Dev Biol. 2020 Aug 5;8:709.

9. Moreira RK. Hepatic Stellate Cells and Liver Fibrosis. Arch Pathol Lab Med. 2007 Nov 1;131(11):1728–34.

10. Zisser A, Ipsen DH, Tveden-Nyborg P. Hepatic Stellate Cell Activation and Inactivation in NASH-Fibrosis—Roles as Putative Treatment Targets? Biomedicines. 2021 Mar 31;9(4):365.

11. Troeger JS, Mederacke I, Gwak G, Dapito DH, Mu X, Hsu CC, et al. Deactivation of Hepatic Stellate Cells During Liver Fibrosis Resolution in Mice. Gastroenterology. 2012 Oct;143(4):1073-1083.e22.

12. Nguyen-Lefebvre AT, Horuzsko A. Kupffer Cell Metabolism and Function. J Enzymol Metab. 2015;1(1):101.

13. Ju C, Tacke F. Hepatic macrophages in homeostasis and liver diseases: from pathogenesis to novel therapeutic strategies. Cell Mol Immunol. 2016 May;13(3):316–27.

14. Wang C, Ma C, Gong L, Guo Y, Fu K, Zhang Y, et al. Macrophage Polarization and Its Role in Liver Disease. Front Immunol. 2021 Dec 14;12:803037.

15. Rappaport AM. The Microcirculatory Acinar Concept of Normal and Pathological Hepatic Structure. Beitr Zur Pathol. 1976 Jan;157(3):215–43.

16. Paris J, Henderson NC. Liver zonation, revisited. Hepatology. 2022 Oct;76(4):1219–30.

17. Jungermann K, Keitzmann T. Zonation of Parenchymal and Nonparenchymal Metabolism in Liver. Annu Rev Nutr. 1996 Jul;16(1):179–203.

18. Panday R, Monckton CP, Khetani SR. The Role of Liver Zonation in Physiology, Regeneration, and Disease. Semin Liver Dis. 2022 Feb;42(01):001–16.

19. Ghallab A, Myllys M, H. Holland C, Zaza A, Murad W, Hassan R, et al. Influence of Liver Fibrosis on Lobular Zonation. Cells. 2019 Dec 2;8(12):1556.

20. Skorecki K, Chertow GM, Marsden PA, Taal MW, Yu ASL, editors. Brenner & Rector's the kidney. 10th edition. Philadelphia, PA: Elsevier; 2016. 2 p.

21. Radi ZA. Kidney Pathophysiology, Toxicology, and Drug-Induced Injury in Drug Development. Int J Toxicol. 2019 May;38(3):215–27.

22. Sol M, Kamps JAAM, van den Born J, van den Heuvel MC, van der Vlag J, Krenning G, et al. Glomerular Endothelial Cells as Instigators of Glomerular Sclerotic Diseases. Front Pharmacol. 2020 Oct 6;11:573557.

23. Balzer MS, Rohacs T, Susztak K. How Many Cell Types Are in the Kidney and What Do They Do? Annu Rev Physiol. 2022 Feb 10;84:507–31.

24. Avraham S, Korin B, Chung JJ, Oxburgh L, Shaw AS. The Mesangial cell — the glomerular stromal cell. Nat Rev Nephrol. 2021 Dec;17(12):855–64.

25. Hall AM, Polesel M, Berquez M. The proximal tubule, protein uptake, and the riddle of the segments | Elsevier Enhanced Reader [Internet]. [cited 2023 Mar 8]. Available from: https://reader.elsevier.com/reader/sd/pii/S008525382100055 7?token=40B3BCF95CDF22E39AA258E2067E6AD5909FFAE97386CE9E146DB676E5CE5CEB1F43CAD55870A6DB701A590A7EDD6651&originRegion=eu-west-1&originCreation=20230308095837

26. Fujishiro H, Himeno S. Gene expression profiles of immortalized S1, S2, and S3 cells derived from each segment of mouse kidney proximal tubules. Fundam Toxicol Sci. 2019;6(4):117–23.

27. Capasso G, Trepiccione F, Zacchia M. The Physiology of the Loop of Henle. In: Critical Care Nephrology [Internet]. Elsevier; 2019 [cited 2023 Mar 13]. p. 42-48.e1. Available from: https://linkinghub.elsevier.com/retrieve/pii/B978032344942700008X

28. McCormick JA, Ellison DH. Distal Convoluted Tubule. In: Terjung R, editor. Comprehensive Physiology [Internet]. 1st ed. Wiley; 2014 [cited 2023 Apr 12]. p. 45–98. Available from: https://onlinelibrary.wiley.com/doi/10.1002/cphy.c140002

29. Cheemerla S, Balakrishnan M. Global Epidemiology of Chronic Liver Disease. Clin Liver Dis. 2021 Jun 4;17(5):365–70.

30. Younossi ZM, Stepanova M, Ong J, Trimble G, AlQahtani S, Younossi I, et al. Nonalcoholic Steatohepatitis Is the Most Rapidly Increasing Indication for Liver Transplantation in the United States. Clin Gastroenterol Hepatol. 2021 Mar;19(3):580-589.e5.

31. Piazzolla VA, Mangia A. Noninvasive Diagnosis of NAFLD and NASH. Cells. 2020 Apr 17;9(4):1005.

32. Rinella ME, Lazarus JV, Ratziu V, Francque SM, Sanyal AJ, Kanwal F, et al. A multi-society Delphi consensus statement on new fatty liver disease nomenclature. Hepatology [Internet]. 2023 Jun 24 [cited 2023 Sep 22];Publish Ahead of Print. Available from: https://journals.lww.com/10.1097/HEP.0000000000000520

33. Wiering L, Tacke F. Treating inflammation to combat non-alcoholic fatty liver disease. J Endocrinol. 2023 Jan 1;256(1):e220194.

34. Raza S, Rajak S, Upadhyay A, Tewari A, Sinha RA. Current treatment paradigms and emerging therapies for NAFLD/NASH. Front Biosci Landmark Ed. 2021 Jan 1;26:206–37.

35. Younossi ZM, Golabi P, de Avila L, Paik JM, Srishord M, Fukui N, et al. The global epidemiology of NAFLD and NASH in patients with type 2 diabetes: A systematic review and meta-analysis. J Hepatol. 2019 Oct;71(4):793–801.

36. Kalantar-Zadeh K, Jafar TH, Nitsch D, Neuen BL, Perkovic V. Chronic kidney disease. The Lancet. 2021 Aug;398(10302):786–802.

37. Kovesdy CP. Epidemiology of chronic kidney disease: an update 2022. Kidney Int Suppl. 2022 Apr;12(1):7–11.

38. Noble R, Taal MW. Epidemiology and causes of chronic kidney disease. Medicine (Baltimore). 2019 Sep;47(9):562–6.

39. Couser WG. Glomerulonephritis. The Lancet. 1999 May;353(9163):1509–15.

40. Medzhitov R. The spectrum of inflammatory responses. Science. 2021 Nov 26;374(6571):1070–5.

41. Chen L, Deng H, Cui H, Fang J, Zuo Z, Deng J, et al. Inflammatory responses and inflammation-associated diseases in organs. Oncotarget. 2017 Dec 14;9(6):7204–18.

42. Yang Y, Kim S, Seki E. Inflammation and Liver Cancer: Molecular Mechanisms and Therapeutic Targets. Semin Liver Dis. 2019 Feb;39(01):026–42.

43. Tanwar S, Rhodes F, Srivastava A, Trembling PM, Rosenberg WM. Inflammation and fibrosis in chronic liver diseases including non-alcoholic fatty liver disease and hepatitis C. World J Gastroenterol. 2020 Jan 14;26(2):109–33.

44. Haftcheshmeh SM, Abedi M, Mashayekhi K, Mousavi MJ, Navashenaq JG, Mohammadi A, et al. Berberine as a natural modulator of inflammatory signaling pathways in the immune system: Focus on NF-κB, JAK/STAT, and MAPK signaling pathways. Phytother Res. 2022;36(3):1216–30.

45. Yu H, Lin L, Zhang Z, Zhang H, Hu H. Targeting NF-κB pathway for the therapy of diseases: mechanism and clinical study. Signal Transduct Target Ther. 2020 Sep 21;5(1):209.

46. Gupta S, Paul WE, Steinman RM, editors. Mechanisms of lymphocyte activation and immune regulation X: innate immunity. New York: Springer; 2005. 163 p. (Advances in experimental medicine and biology).

47. Morris R, Kershaw NJ, Babon JJ. The molecular details of cytokine signaling via the JAK/STAT pathway. Protein Sci Publ Protein Soc. 2018 Dec;27(12):1984–2009.

48. Hu X, Li J, Fu M, Zhao X, Wang W. The JAK/STAT signaling pathway: from bench to clinic. Signal Transduct Target Ther. 2021 Nov 26;6(1):402.

49. Manzoor Z, Koh YS. Mitogen-activated Protein Kinases in Inflammation. J Bacteriol Virol. 2012;42(3):189.

50. Koyama Y, Brenner DA. Liver inflammation and fibrosis. J Clin Invest. 2017 Jan 3;127(1):55–64.

51. Singh S, Anshita D, Ravichandiran V. MCP-1: Function, regulation, and involvement in disease. Int Immunopharmacol. 2021 Dec;101:107598.

52. Irak K, Bayram M, Cifci S, Sener G. Serum levels of NLRC4 and MCP-2/CCL8 in patients with active Crohn's disease. Ojcius DM, editor. PLOS ONE. 2021 Nov 17;16(11):e0260034.

53. Dinarello CA. Overview of the IL-1 family in innate inflammation and acquired immunity. Immunol Rev. 2018 Jan;281(1):8–27.

54. Nelson JE, Handa P, Aouizerat B, Wilson L, Vemulakonda LA, Yeh MM, et al. Increased parenchymal damage and steatohepatitis in Caucasian non-alcoholic fatty liver disease patients with common IL1B and IL6 polymorphisms. Aliment Pharmacol Ther. 2016 Dec;44(11–12):1253–64.

55. Yamaguchi K, Nishimura T, Ishiba H, Seko Y, Okajima A, Fujii H, et al. Blockade of interleukin 6 signalling ameliorates systemic insulin resistance through upregulation of glucose uptake in skeletal muscle and improves hepatic steatosis in high-fat diet fed mice. Liver Int. 2015 Feb;35(2):550–61.

56. Hirano T. IL-6 in inflammation, autoimmunity and cancer. Int Immunol. 2021 Mar 1;33(3):127–48.

57. Lim YJ, Sidor NA, Tonial NC, Che A, Urquhart BL. Uremic Toxins in the Progression of Chronic Kidney Disease and Cardiovascular Disease: Mechanisms and Therapeutic Targets. Toxins. 2021 Feb 13;13(2):142.

58. Kopf M, Baumann H, Freer G, Freudenberg M, Lamers M, Kishimoto T, et al. Impaired immune and acute-phase responses in interleukin-6-deficient mice. Nature. 1994 Mar 24;368(6469):339–42.

59. Chen W, Yuan H, Cao W, Wang T, Chen W, Yu H, et al. Blocking interleukin-6 trans-signaling protects against renal fibrosis by suppressing STAT3 activation. Theranostics. 2019;9(14):3980–91.

60. Zhao X, Chen J, Sun H, Zhang Y, Zou D. New insights into fibrosis from the ECM degradation perspective: the macrophage-MMP-ECM interaction. Cell Biosci. 2022 Jul 27;12(1):117.

61. Kisseleva T, Brenner D. Molecular and cellular mechanisms of liver fibrosis and its regression. Nat Rev Gastroenterol Hepatol. 2021 Mar;18(3):151–66.

62. Henderson NC, Rieder F, Wynn TA. Fibrosis: from mechanisms to medicines. Nature. 2020 Nov 26;587(7835):555–66.

63. Sun YM, Chen SY, You H. Regression of liver fibrosis: evidence and challenges. Chin Med J (Engl). 2020 Jul 20;133(14):1696–702.

64. Zhou D, Liu Y. Understanding the mechanisms of kidney fibrosis. Nat Rev Nephrol. 2016 Feb;12(2):68–70.

65. Duffield JS. Cellular and molecular mechanisms in kidney fibrosis. J Clin Invest. 2014 Jun 2;124(6):2299–306.

66. Moeller MJ, Kramann R, Lammers T, Hoppe B, Latz E, Ludwig-Portugall I, et al. New Aspects of Kidney Fibrosis–From Mechanisms of Injury to Modulation of Disease. Front Med. 2022 Jan 12;8:814497.

67. Fogo AB. Causes and pathogenesis of focal segmental glomerulosclerosis. Nat Rev Nephrol. 2015 Feb;11(2):76–87.

68. Zeisberg M, Neilson EG. Mechanisms of Tubulointerstitial Fibrosis. J Am Soc Nephrol. 2010 Nov;21(11):1819–34.

69. Yuan Q, Tan RJ, Liu Y. Myofibroblast in Kidney Fibrosis: Origin, Activation, and Regulation. In: Liu BC, Lan HY, Lv LL, editors. Renal Fibrosis: Mechanisms and Therapies [Internet]. Singapore: Springer Singapore; 2019 [cited 2023 Apr 17]. p. 253–83. (Advances in Experimental Medicine and Biology; vol. 1165). Available from: http://link.springer.com/10.1007/978-981-13-8871-2_12

70. Kuppe C, Ibrahim MM, Kranz J, Zhang X, Ziegler S, Perales-Patón J, et al. Decoding myofibroblast origins in human kidney fibrosis. Nature. 2021 Jan 14;589(7841):281–6.

71. Higashi T, Friedman SL, Hoshida Y. Hepatic stellate cells as key target in liver fibrosis. Adv Drug Deliv Rev. 2017 Nov;121:27–42.

72. Berumen J, Baglieri J, Kisseleva T, Mekeel K. Liver fibrosis: Pathophysiology and clinical implications. WIREs Mech Dis [Internet]. 2021 Jan [cited 2023 May 23];13(1). Available from: https://onlinelibrary.wiley.com/doi/10.1002/wsbm.1499

73. Yan Y, Zeng J, Xing L, Li C. Extra- and Intra-Cellular Mechanisms of Hepatic Stellate Cell Activation. Biomedicines. 2021 Aug 14;9(8):1014.

74. Yu XY, Sun Q, Zhang YM, Zou L, Zhao YY. TGF-β/Smad Signaling Pathway in Tubulointerstitial Fibrosis. Front Pharmacol. 2022 Mar 24;13:860588.

75. Xue T, Yue L, Zhu G, Tan Z, Liu H, Gan C, et al. An oral phenylacrylic acid derivative suppressed hepatic stellate cell activation and ameliorated liver fibrosis by blocking TGF - β1 signalling. Liver Int. 2023 Mar;43(3):718–32.

76. Xu XY, Geng Y, Xu HX, Ren Y, Liu DY, Mao Y. Antrodia camphorata-Derived Antrodin C Inhibits Liver Fibrosis by Blocking TGF-Beta and PDGF Signaling Pathways. Front Mol Biosci. 2022 Feb 15;9:835508.

77. Mazhari S, Gitiara A, Baghaei K, Hatami B, Rad RE, Asadirad A, et al. Therapeutic potential of bone marrow-derived mesenchymal stem cells and imatinib in a rat model of liver fibrosis. Eur J Pharmacol. 2020 Sep;882:173263.

78. Guillamat-Prats R. The Role of MSC in Wound Healing, Scarring and Regeneration. Cells. 2021 Jul 8;10(7):1729.

79. Parola M, Pinzani M. Liver fibrosis: Pathophysiology, pathogenetic targets and clinical issues. Mol Aspects Med. 2019 Feb;65:37–55.

80. Acharya P, Chouhan K, Weiskirchen S, Weiskirchen R. Cellular Mechanisms of Liver Fibrosis. Front Pharmacol. 2021 May 6;12:671640.

81. Roehlen N, Crouchet E, Baumert TF. Liver Fibrosis: Mechanistic Concepts and Therapeutic Perspectives. Cells. 2020 Apr 3;9(4):875.

82. Maharao N, Antontsev V, Wright M, Varshney J. Entering the era of computationally driven drug development. Drug Metab Rev. 2020 Apr 2;52(2):283–98.

83. Simoens S, Huys I. R&D Costs of New Medicines: A Landscape Analysis. Front Med. 2021 Oct 26;8:760762.

84. Wagner JA, Dahlem AM, Hudson LD, Terry SF, Altman RB, Gilliland CT, et al. Application of a Dynamic Map for Learning, Communicating, Navigating, and Improving Therapeutic Development: Drug Discovery, Development, and Deployment Map. Clin Transl Sci. 2018 Mar;11(2):166–74.

85. Hartung T. Look back in anger – what clinical studies tell us about preclinical work. ALTEX. 2013;30(3):275–91.

86. Andrade RJ, Chalasani N, Björnsson ES, Suzuki A, Kullak-Ublick GA, Watkins PB, et al. Drug-induced liver injury. Nat Rev Dis Primer. 2019 Aug 22;5(1):58.

87. LiverTox: Clinical and Research Information on Drug-Induced Liver Injury [Internet]. Bethesda (MD): National Institute of Diabetes and Digestive and Kidney Diseases; 2012 [cited 2023 May 23]. Available from: http://www.ncbi.nlm.nih.gov/books/NBK547852/

88. Sales GTM, Foresto RD. Drug-induced nephrotoxicity. Rev Assoc Médica Bras. 2020;66(suppl 1):s82–90.

89. Daudon M, Frochot V, Bazin D, Jungers P. Drug-Induced Kidney Stones and Crystalline Nephropathy: Pathophysiology, Prevention and Treatment. Drugs. 2018 Feb;78(2):163–201.

90. Uhl EW, Warner NJ. Mouse Models as Predictors of Human Responses: Evolutionary Medicine. Curr Pathobiol Rep. 2015 Sep;3(3):219–23.

91. Brancato V, Oliveira JM, Correlo VM, Reis RL, Kundu SC. Could 3D models of cancer enhance drug screening? Biomaterials. 2020 Feb;232:119744.

92. Research NC for T. Drug Induced Liver Injury Rank (DILIrank) Dataset. FDA [Internet]. 2023 Sep 2 [cited 2023 May 10]; Available from: https://www.fda.gov/science-research/liver-toxicity-knowledge-base-ltkb/drug-induced-liver-injury-rank-dilirank-dataset

93. Rotundo L, Pyrsopoulos N. Liver injury induced by paracetamol and challenges associated with intentional and unintentional use. World J Hepatol. 2020 Apr 27;12(4):125–36.

94. Walubo A, Barr S, Abraham AM, Coetsee C. The role of cytochrome–P450 inhibitors in the prevention of hepatotoxicity after paracetamol overdose in rats. Hum Exp Toxicol. 2004 Jan;23(1):49–54.

95. Zhao M, Ma J, Li M, Zhang Y, Jiang B, Zhao X, et al. Cytochrome P450 Enzymes and Drug Metabolism in Humans. Int J Mol Sci. 2021 Nov 26;22(23):12808.

96. Harjumäki R, Pridgeon CS, Ingelman-Sundberg M. CYP2E1 in Alcoholic and Non-Alcoholic Liver Injury. Roles of ROS, Reactive Intermediates and Lipid Overload. Int J Mol Sci. 2021 Jul 30;22(15):8221.

97. Sharzehan MAK, Sito H, Abdullah N, Alexiou A, Papadakis M, Jamal R, et al. Association between CYP2E1 polymorphisms and colorectal cancer risk: a systematic review and meta-analysis. Sci Rep. 2022 Nov 23;12(1):20149.

98. Jancova P, Anzenbacher P, Anzenbacherova E. PHASE II DRUG METABOLIZING ENZYMES. Biomed Pap. 2010 Jun 1;154(2):103–16.

99. Couri T, Pillai A. Goals and targets for personalized therapy for HCC. Hepatol Int. 2019 Mar;13(2):125–37.

100. Shi Q, Yang X, Ren L, Mattes WB. Recent advances in understanding the hepatotoxicity associated with protein kinase inhibitors. Expert Opin Drug Metab Toxicol. 2020 Mar 3;16(3):217–26.

101. Ganten TM, Stauber RE, Schott E, Malfertheiner P, Buder R, Galle PR, et al. Sorafenib in Patients with Hepatocellular Carcinoma—Results of the Observational INSIGHT Study. Clin Cancer Res. 2017 Oct 1;23(19):5720–8.

102. Zhang J, Salminen A, Yang X, Luo Y, Wu Q, White M, et al. Effects of 31 FDA approved small-molecule kinase inhibitors on isolated rat liver mitochondria. Arch Toxicol. 2017 Aug;91(8):2921–38.

103. Mingard C, Paech F, Bouitbir J, Krähenbühl S. Mechanisms of toxicity associated with six tyrosine kinase inhibitors in human hepatocyte cell lines. J Appl Toxicol. 2018 Mar;38(3):418–31.

104. Saiz-Rodríguez M, Almenara S, Navares-Gómez M, Ochoa D, Román M, Zubiaur P, et al. Effect of the Most Relevant CYP3A4 and CYP3A5 Polymorphisms on the Pharmacokinetic Parameters of 10 CYP3A Substrates. Biomedicines. 2020 Apr 22;8(4):94.

105. Johansson I, Ingelman-Sundberg M. Genetic Polymorphism and Toxicology—With Emphasis on Cytochrome P450. Toxicol Sci. 2011 Mar;120(1):1–13.

106. Klomp SD, Manson ML, Guchelaar HJ, Swen JJ. Phenoconversion of Cytochrome P450 Metabolism: A Systematic Review. J Clin Med. 2020 Sep 7;9(9):2890.

107. Peng B, Lloyd P, Schran H. Clinical Pharmacokinetics of Imatinib: Clin Pharmacokinet. 2005;44(9):879–94.

108. Peng B, Hayes M, Resta D, Racine-Poon A, Druker BJ, Talpaz M, et al. Pharmacokinetics and Pharmacodynamics of Imatinib in a Phase I Trial With Chronic Myeloid Leukemia Patients. J Clin Oncol. 2004 Mar 1;22(5):935–42.

109. Bolton AE, Peng B, Hubert M, Krebs-Brown A, Capdeville R, Keller U, et al. Effect of rifampicin on the pharmacokinetics of imatinib mesylate (Gleevec, STI571) in healthy subjects. Cancer Chemother Pharmacol. 2004 Feb 1;53(2):102–6.

110. Ma L, Wu Y, Li Y, Aazmi A, Zhou H, Zhang B, et al. Current Advances on 3D-Bioprinted Liver Tissue Models. Adv Healthc Mater. 2020 Dec;9(24):2001517.

111. Gerets HHJ, Tilmant K, Gerin B, Chanteux H, Depelchin BO, Dhalluin S, et al. Characterization of primary human hepatocytes, HepG2 cells, and HepaRG cells at the mRNA level and CYP activity in response to inducers and their predictivity for the detection of human hepatotoxins. Cell Biol Toxicol. 2012 Apr;28(2):69–87.

112. Yokoyama Y, Sasaki Y, Terasaki N, Kawataki T, Takekawa K, Iwase Y, et al. Comparison of Drug Metabolism and Its Related Hepatotoxic Effects in HepaRG, Cryopreserved Human Hepatocytes, and HepG2 Cell Cultures. Biol Pharm Bull. 2018 May 1;41(5):722–32.

113. Hart SN, Li Y, Nakamoto K, Subileau E anne, Steen D, Zhong X bo. A Comparison of Whole Genome Gene Expression Profiles of HepaRG Cells and HepG2 Cells to Primary Human Hepatocytes and Human Liver Tissues. Drug Metab Dispos. 2010 Jun;38(6):988–94.

114. Skardal A, Mack D, Atala A, Soker S. Substrate elasticity controls cell proliferation, surface marker expression and motile phenotype in amniotic fluid-derived stem cells. J Mech Behav Biomed Mater. 2013 Jan;17:307–16.

115. De Minicis S, Seki E, Uchinami H, Kluwe J, Zhang Y, Brenner DA, et al. Gene Expression Profiles During Hepatic Stellate Cell Activation in Culture and In Vivo. Gastroenterology. 2007 May;132(5):1937–46.

116. Chaicharoenaudomrung N, Kunhorm P, Noisa P. Three-dimensional cell culture systems as an *in vitro* platform for cancer and stem cell modeling. World J Stem Cells. 2019 Dec 26;11(12):1065–83.

117. Morisaki T, Umebayashi M, Kiyota A, Koya N, Tanaka H, Onishi H, et al. Combining Celecoxib with Sorafenib Synergistically Inhibits Hepatocellular Carcinoma Cells In Vitro. ANTICANCER Res. 2013;

118. Tutty MA, Vella G, Prina-Mello A. Pre-clinical 2D and 3D toxicity response to a panel of nanomaterials; comparative assessment of NBM-induced liver toxicity. Drug Deliv Transl Res. 2022 Sep;12(9):2157–77.

119. Li F, Cao L, Parikh S, Zuo R. Three-Dimensional Spheroids With Primary Human Liver Cells and Differential Roles of Kupffer Cells in Drug-Induced Liver Injury. J Pharm Sci. 2020 Jun;109(6):1912–23.

120. Haake K, Ackermann M, Lachmann N. Concise Review: Towards the Clinical Translation of Induced Pluripotent Stem Cell-Derived Blood Cells— *Ready for Take-Off*. Stem Cells Transl Med. 2019 Apr 1;8(4):332–9.

121. Rowe RG, Daley GQ. Induced pluripotent stem cells in disease modelling and drug discovery. Nat Rev Genet. 2019 Jul;20(7):377–88.

122. Yamanaka S. Induced Pluripotent Stem Cells: Past, Present, and Future. Cell Stem Cell. 2012 Jun;10(6):678–84.

123. Corbett JL, Duncan SA. iPSC-Derived Hepatocytes as a Platform for Disease Modeling and Drug Discovery. Front Med. 2019 Nov 15;6:265.

124. Medine CN, Lucendo-Villarin B, Storck C, Wang F, Szkolnicka D, Khan F, et al. Developing High-Fidelity Hepatotoxicity Models From Pluripotent Stem Cells. Stem Cells Transl Med. 2013 Jul 1;2(7):505–9.

125. Goldberg AM, Frazier JM. Alternatives to Animals in Toxicity Testing. Sci Am. 1989 Aug;261(2):24–31.

126. Kitaeva KV, Rutland CS, Rizvanov AA, Solovyeva VV. Cell Culture Based in vitro Test Systems for Anticancer Drug Screening. Front Bioeng Biotechnol. 2020 Apr 9;8:322.

127. Martignoni M, Groothuis GMM, De Kanter R. Species differences between mouse, rat, dog, monkey and human CYP-mediated drug metabolism, inhibition and induction. Expert Opin Drug Metab Toxicol. 2006 Dec;2(6):875–94.

128. Ogaly HA, Aldulmani SAA, Al-Zahrani FAM, Abd-Elsalam RM. D-Carvone Attenuates CCl4-Induced Liver Fibrosis in Rats by Inhibiting Oxidative Stress and TGF-ß 1/SMAD3 Signaling Pathway. Biology. 2022 May 12;11(5):739.

129. Liu J, Kong D, Qiu J, Xie Y, Lu Z, Zhou C, et al. Praziquantel ameliorates CCl_4 -induced liver fibrosis in mice by inhibiting TGF-β/Smad signalling via up-regulating Smad7 in hepatic stellate cells. Br J Pharmacol. 2019 Dec;176(24):4666–80.

130. Yu B, Qin S yu, Hu B li, Qin Q yi, Jiang H xing, Luo W. Resveratrol improves CCL4-induced liver fibrosis in mouse by upregulating endogenous IL-10 to reprogramme macrophages phenotype from M(LPS) to M(IL-4). Biomed Pharmacother. 2019 Sep;117:109110.

131. Gao Y, Fan S, Zhao P, Li H, Cai C, Li X, et al. β-catenin/TCF4 inhibitors ICG-001 and LF3 alleviate BDL-induced liver fibrosis by suppressing LECT2 signaling. Chem Biol Interact. 2023 Feb;371:110350.

132. Nevzorova YA, Boyer-Diaz Z, Cubero FJ, Gracia-Sancho J. Animal models for liver disease – A practical approach for translational research. J Hepatol. 2020 Aug;73(2):423–40.

133. Martínez-Klimova E, Aparicio-Trejo OE, Tapia E, Pedraza-Chaverri J. Unilateral Ureteral Obstruction as a Model to Investigate Fibrosis-Attenuating Treatments. Biomolecules. 2019 Apr 8;9(4):141.

134. Yang HC, Zuo Y, Fogo AB. Models of chronic kidney disease. Drug Discov Today Dis Models. 2010 Mar;7(1–2):13–9.

135. Löwen J, Gröne EF, Groß-Weißmann ML, Bestvater F, Gröne HJ, Kriz W. Pathomorphological sequence of nephron loss in diabetic nephropathy. Am J Physiol-Ren Physiol. 2021 Nov 1;321(5):F600–16.

136. Alpers CE, Hudkins KL. Mouse models of diabetic nephropathy: Curr Opin Nephrol Hypertens. 2011 May;20(3):278–84.

137. Grange C, Tritta S, Tapparo M, Cedrino M, Tetta C, Camussi G, et al. Stem cell-derived extracellular vesicles inhibit and revert fibrosis progression in a mouse model of diabetic nephropathy. Sci Rep. 2019 Mar 14;9(1):4468.

138. Hurrell T, Kastrinou-Lampou V, Fardellas A, Hendriks DFG, Nordling Å, Johansson I, et al. Human Liver Spheroids as a Model to Study Aetiology and Treatment of Hepatic Fibrosis. Cells. 2020 Apr 14;9(4):964.

139. Kang HM, Lim JH, Noh KH, Park D, Cho HS, Susztak K, et al. Effective reconstruction of functional organotypic kidney spheroid for in vitro nephrotoxicity studies. Sci Rep. 2019 Nov 26;9(1):17610.

140. Tuffin J, Chesor M, Kuzmuk V, Johnson T, Satchell SC, Welsh GI, et al. GlomSpheres as a 3D co-culture spheroid model of the kidney glomerulus for rapid drug-screening. Commun Biol. 2021 Dec 2;4(1):1351.

141. Mukomoto R, Nashimoto Y, Terai T, Imaizumi T, Hiramoto K, Ino K, et al. Oxygen consumption rate of tumour spheroids during necrotic-like core formation. The Analyst. 2020;145(19):6342–8.

142. Hofer M, Lutolf MP. Engineering organoids. Nat Rev Mater. 2021 Feb 19;6(5):402–20.

143. Liu C, Qin T, Huang Y, Li Y, Chen G, Sun C. Drug screening model meets cancer organoid technology. Transl Oncol. 2020 Nov;13(11):100840.

144. Sachs N, De Ligt J, Kopper O, Gogola E, Bounova G, Weeber F, et al. A Living Biobank of Breast Cancer Organoids Captures Disease Heterogeneity. Cell. 2018 Jan;172(1–2):373-386.e10.

145. Wu Q, Liu J, Wang X, Feng L, Wu J, Zhu X, et al. Organ-on-a-chip: recent breakthroughs and future prospects. Biomed Eng OnLine. 2020 Dec;19(1):9.

146. Prodanov L, Jindal R, Bale SS, Hegde M, McCarty WJ, Golberg I, et al. Long-term maintenance of a microfluidic 3D human liver sinusoid: Maintenance of a Microfluidic 3D Human Liver Sinusoid. Biotechnol Bioeng. 2016 Jan;113(1):241–6.

147. Jain P, Kathuria H, Dubey N. Advances in 3D bioprinting of tissues/organs for regenerative medicine and in-vitro models. Biomaterials. 2022 Aug;287:121639.

148. Lawlor KT, Vanslambrouck JM, Higgins JW, Chambon A, Bishard K, Arndt D, et al. Cellular extrusion bioprinting improves kidney organoid reproducibility and conformation. Nat Mater. 2021 Feb;20(2):260–71.

149. Graaf IAD, Groothuis GM, Olinga P. Precision-cut tissue slices as a tool to predict metabolism of novel drugs. Expert Opin Drug Metab Toxicol. 2007 Dec;3(6):879–98.

150. Bigaeva E, Puerta Cavanzo N, Stribos EGD, de Jong AJ, Biel C, Mutsaers HAM, et al. Predictive Value of Precision-Cut Kidney Slices as an Ex Vivo Screening Platform for Therapeutics in Human Renal Fibrosis. Pharmaceutics. 2020 May 18;12(5):459.

151. Paish HL, Reed LH, Brown H, Bryan MC, Govaere O, Leslie J, et al. A Bioreactor Technology for Modeling Fibrosis in Human and Rodent Precision-Cut Liver Slices. Hepatology. 2019 Oct;70(4):1377–91.

152. Starokozhko V, Vatakuti S, Schievink B, Merema MT, Asplund A, Synnergren J, et al. Maintenance of drug metabolism and transport functions in human precision-cut liver slices during prolonged incubation for 5 days. Arch Toxicol. 2017 May;91(5):2079–92.

153. Elferink MGL, Olinga P, Van Leeuwen EM, Bauerschmidt S, Polman J, Schoonen WG, et al. Gene expression analysis of precision-cut human liver slices indicates stable expression of ADME-Tox related genes. Toxicol Appl Pharmacol. 2011 May;253(1):57–69.

154. Zárybnický T, Matoušková P, Lancošová B, Šubrt Z, Skálová L, Boušová I. Inter-Individual Variability in Acute Toxicity of R-Pulegone and R-Menthofuran in Human Liver Slices and Their Influence on miRNA Expression Changes in Comparison to Acetaminophen. Int J Mol Sci. 2018 Jun 19;19(6):1805.

155. Vatakuti S, Pennings JLA, Gore E, Olinga P, Groothuis GMM. Classification of Cholestatic and Necrotic Hepatotoxicants Using Transcriptomics on Human Precision-Cut Liver Slices. Chem Res Toxicol. 2016 Mar 21;29(3):342–51.

156. Hadi M, Westra IM, Starokozhko V, Dragovic S, Merema MT, Groothuis GMM. Human Precision-Cut Liver Slices as an *ex Vivo* Model to Study Idiosyncratic Drug-Induced Liver Injury. Chem Res Toxicol. 2013 May 20;26(5):710–20.

157. Sneddon LU, Halsey LG, Bury NR. Considering aspects of the 3Rs principles within experimental animal biology. J Exp Biol. 2017 Sep 1;220(17):3007–16.

158. Paish HL, Reed LH, Brown H, Bryan MC, Govaere O, Leslie J, et al. A Bioreactor Technology for Modeling Fibrosis in Human and Rodent Precision-Cut Liver Slices. Hepatology. 2019;70(4):1377–91.

159. Mazokopakis EE. Unusual causes of intrahepatic cholestatic liver disease. World J Gastroenterol. 2007;13(12):1879.

160. Primary Biliary Cirrhosis and Primary Sclerosing Cholangitis: a Review Featuring a Women's Health Perspective. J Clin Transl Hepatol [Internet]. 2014 Dec 15 [cited 2023 Sep 22];2(4). Available from: http://www.xiahepublishing.com/ArticleFullText.aspx?sid=2&jid=1&id=10.14218%2fJCTH.2014.00024

161. Mayo Clinic [Internet]. [cited 2023 Mar 1]. Chronic kidney disease - Symptoms and causes. Available from: https://www.mayoclinic.org/diseases-conditions/chronic-kidney-disease/symptoms-causes/syc-20354521

162. Bülow RD, Boor P. Extracellular Matrix in Kidney Fibrosis: More Than Just a Scaffold. J Histochem Cytochem. 2019 Sep;67(9):643–61.

163. Wei J, Xu Z, Yan X. The role of the macrophage-to-myofibroblast transition in renal fibrosis. Front Immunol. 2022 Aug 5;13:934377.

164. Kisseleva T, Cong M, Paik Y, Scholten D, Jiang C, Benner C, et al. Myofibroblasts revert to an inactive phenotype during regression of liver fibrosis. Proc Natl Acad Sci. 2012 Jun 12;109(24):9448–53.

165. Ye Q, Zhou Y, Zhao C, Xu L, Ping J. Salidroside Inhibits CCl4-Induced Liver Fibrosis in Mice by Reducing Activation and Migration of HSC Induced by Liver Sinusoidal Endothelial Cell-Derived Exosomal SphK1. Front Pharmacol. 2021 May 13;12:677810.

166. Wang R, Song F, Li S, Wu B, Gu Y, Yuan Y. Salvianolic acid A attenuates CCl_4-induced liver fibrosis by regulating the PI3K/AKT/mTOR, Bcl-2/Bax and caspase-3/cleaved caspase-3 signaling pathways. Drug Des Devel Ther. 2019 May;Volume 13:1889–900.

167. Sajja KC, Mohan DP, Rockey DC. Age and Ethnicity in Cirrhosis. J Investig Med. 2014 Oct;62(7):920–6.

168. Lee H, Kim J, Choi Y, Cho DW. Application of Gelatin Bioinks and Cell-Printing Technology to Enhance Cell Delivery Capability for 3D Liver Fibrosis-on-a-Chip Development. ACS Biomater Sci Eng. 2020 Apr 13;6(4):2469–77.

169. Vanaei S, Parizi MS, Vanaei S, Salemizadehparizi F, Vanaei HR. An Overview on Materials and Techniques in 3D Bioprinting Toward Biomedical Application. Eng Regen. 2021;2:1–18.

170. Tian F, Wang Z, He J, Zhang Z, Tan N. 4-Octyl itaconate protects against renal fibrosis via inhibiting TGF-β/Smad pathway, autophagy and reducing generation of reactive oxygen species. Eur J Pharmacol. 2020 Apr;873:172989.

171. Fu Y, Tang C, Cai J, Chen G, Zhang D, Dong Z. Rodent models of AKI-CKD transition. Am J Physiol-Ren Physiol. 2018 Oct 1;315(4):F1098–106.

172. Yan L. Folic acid-induced animal model of kidney disease. Anim Models Exp Med. 2021 Dec;4(4):329–42.

173. Azushima K, Gurley SB, Coffman TM. Modelling diabetic nephropathy in mice. Nat Rev Nephrol. 2018 Jan;14(1):48–56.

174. Takasato M, Er PX, Chiu HS, Maier B, Baillie GJ, Ferguson C, et al. Kidney organoids from human iPS cells contain multiple lineages and model human nephrogenesis. Nature. 2015 Oct 22;526(7574):564–8.

175. He M, Callanan A, Lagaras K, Steele JAM, Stevens MM. Optimization of SDS exposure on preservation of ECM characteristics in whole organ decellularization of rat kidneys: Optimisation of SDS decellularization. J Biomed Mater Res B Appl Biomater. 2017 Aug;105(6):1352–60.

176. Oakley F, Gee LM, Sheerin NS, Borthwick LA. Implementation of pre-clinical methodologies to study fibrosis and test anti-fibrotic therapy. Curr Opin Pharmacol. 2019 Dec;49:95–101.

177. van Leeuwen LL, Ruigrok MJR, Leuvenink HGD, Olinga P. Slice of Life: Porcine Kidney Slices for Testing Antifibrotic Drugs in a Transplant Setting. Transplantology. 2023 Apr 14;4(2):59–70.

178. Prins G, Luangmonkong T, Oosterhuis D, Mutsaers H, Dekker F, Olinga P. A Pathophysiological Model of Non-Alcoholic Fatty Liver Disease Using Precision-Cut Liver Slices. Nutrients. 2019 Feb 27;11(3):507.

179. Rønnow SR, Dabbagh RQ, Genovese F, Nanthakumar CB, Barrett VJ, Good RB, et al. Prolonged Scar-in-a-Jar: an in vitro screening tool for anti-fibrotic therapies using biomarkers of extracellular matrix synthesis. Respir Res. 2020 Dec;21(1):108.

180. Decaris ML, Schaub JR, Chen C, Cha J, Lee GG, Rexhepaj M, et al. Dual inhibition of αvβ6 and αvβ1 reduces fibrogenesis in lung tissue explants from patients with IPF. Respir Res. 2021 Dec;22(1):265.

181. Karmacharya MB, Hada B, Park SR, Kim KH, Choi BH. Granulocyte-macrophage colony-stimulating factor (GM-CSF) shows therapeutic effect on dimethylnitrosamine (DMN)-induced liver fibrosis in rats. Lin W, editor. PLOS ONE. 2022 Sep 2;17(9):e0274126.

182. Tan-Garcia A, Lai F, Yeong JPS, Irac SE, Ng PY, Msallam R, et al. Liver fibrosis and CD206+ macrophage accumulation are suppressed by anti-GM-CSF therapy. JHEP Rep. 2020 Feb;2(1):100062.

183. Xu L, Sharkey D, Cantley LG. Tubular GM-CSF Promotes Late MCP-1/CCR2-Mediated Fibrosis and Inflammation after Ischemia/Reperfusion Injury. J Am Soc Nephrol. 2019 Oct;30(10):1825–40.

184. Zhang J, Chu M. Differential roles of VEGF: Relevance to tissue fibrosis. J Cell Biochem. 2019 Jul;120(7):10945–51.

185. Mariotti V, Fiorotto R, Cadamuro M, Fabris L, Strazzabosco M. New insights on the role of vascular endothelial growth factor in biliary pathophysiology. JHEP Rep. 2021 Jun;3(3):100251.

186. Zadorozhna M, Di Gioia S, Conese M, Mangieri D. Neovascularization is a key feature of liver fibrosis progression: anti-angiogenesis as an innovative way of liver fibrosis treatment. Mol Biol Rep. 2020 Mar;47(3):2279–88.

187. Van Caam A, Vonk M, Van Den Hoogen F, Van Lent P, Van Der Kraan P. Unraveling SSc Pathophysiology; The Myofibroblast. Front Immunol. 2018 Nov 13;9:2452.

188. Li Y, Zhao J, Yin Y, Li K, Zhang C, Zheng Y. The Role of IL-6 in Fibrotic Diseases: Molecular and Cellular Mechanisms. Int J Biol Sci. 2022;18(14):5405–14.

189. Sadeghi M, Lahdou I, Oweira H, Daniel V, Terness P, Schmidt J, et al. Serum levels of chemokines CCL4 and CCL5 in cirrhotic patients indicate the presence of hepatocellular carcinoma. Br J Cancer. 2015 Sep;113(5):756–62.

190. Goos T, De Sadeleer LJ, Yserbyt J, Verleden GM, Vermant M, Verleden SE, et al. Progression in the Management of Non-Idiopathic Pulmonary Fibrosis Interstitial Lung Diseases, Where Are We Now and Where We Would Like to Be. J Clin Med. 2021 Mar 23;10(6):1330.

191. Tan W, Wang Y, Dai H, Deng J, Wu Z, Lin L, et al. Potential Therapeutic Strategies for Renal Fibrosis: Cordyceps and Related Products. Front Pharmacol. 2022 Jul 8;13:932172.

192. Tan Z, Sun H, Xue T, Gan C, Liu H, Xie Y, et al. Liver Fibrosis: Therapeutic Targets and Advances in Drug Therapy. Front Cell Dev Biol. 2021 Sep 21;9:730176.

193. Weiskirchen R, Friedman SL, editors. Hepatic stellate cells: methods and protocols. New York, NY: Humana Press; 2023.

194. Ruwanpura SM, Thomas BJ, Bardin PG. Pirfenidone: Molecular Mechanisms and Potential Clinical Applications in Lung Disease. Am J Respir Cell Mol Biol. 2020 Apr;62(4):413–22.

195. Bai X, Nie P, Lou Y, Zhu Y, Jiang S, Li B, et al. Pirfenidone is a renal protective drug: Mechanisms, signalling pathways, and preclinical evidence. Eur J Pharmacol. 2021 Nov;911:174503.

196. Togami K, Kanehira Y, Tada H. Possible Involvement of Pirfenidone Metabolites in the Antifibrotic Action of a Therapy for Idiopathic Pulmonary Fibrosis. Biol Pharm Bull. 2013;36(10):1525–7.

197. Sen R, Smale ST. Selectivity of the NF- B Response. Cold Spring Harb Perspect Biol. 2010 Apr 1;2(4):a000257–a000257.

198. Gerondakis S, Grumont R, Gugasyan R, Wong L, Isomura I, Ho W, et al. Unravelling the complexities of the NF-κB signalling pathway using mouse knockout and transgenic models. Oncogene. 2006 Oct 30;25(51):6781–99.

199. Kany S, Vollrath JT, Relja B. Cytokines in Inflammatory Disease. Int J Mol Sci. 2019 Nov 28;20(23):6008.

200. Jang D in, Lee AH, Shin HY, Song HR, Park JH, Kang TB, et al. The Role of Tumor Necrosis Factor Alpha (TNF-α) in Autoimmune Disease and Current TNF-α Inhibitors in Therapeutics. Int J Mol Sci. 2021 Mar 8;22(5):2719.

201. Rossol M, Heine H, Meusch U, Quandt D, Klein C, Sweet MJ, et al. LPS-induced Cytokine Production in Human Monocytes and Macrophages. Crit Rev Immunol. 2011;31(5):379–446.

202. Giraldez MD, Carneros D, Garbers C, Rose-John S, Bustos M. New insights into IL-6 family cytokines in metabolism, hepatology and gastroenterology. Nat Rev Gastroenterol Hepatol. 2021 Nov;18(11):787–803.

203. Liu Y, Wu P, Wang Y, Liu Y, Yang H, Zhou G, et al. Application of Precision-Cut Lung Slices as an In Vitro Model for Research of Inflammatory Respiratory Diseases. Bioengineering. 2022 Dec 4;9(12):767.

204. Kolbe U, Yi B, Poth T, Saunders A, Boutin S, Dalpke AH. Early Cytokine Induction Upon Pseudomonas aeruginosa Infection in Murine Precision Cut Lung Slices Depends on Sensing of Bacterial Viability. Front Immunol. 2020 Oct 30;11:598636.

205. Brooks D, Barr LC, Wiscombe S, McAuley DF, Simpson AJ, Rostron AJ. Human lipopolysaccharide models provide mechanistic and therapeutic insights into systemic and pulmonary inflammation. Eur Respir J. 2020 Jul;56(1):1901298.

206. Nonaka M, Pawankar R, Fukumoto A, Ogihara N, Sakanushi A, Yagi T. Induction of eotaxin production by interleukin-4, interleukin-13 and lipopolysaccharide by nasal fibroblasts. Clin Htmlent Glyphamp Asciiamp Exp Allergy. 2004 May;34(5):804–11.

207. Domscheit H, Hegeman MA, Carvalho N, Spieth PM. Molecular Dynamics of Lipopolysaccharide-Induced Lung Injury in Rodents. Front Physiol. 2020 Feb 5;11:36.

208. Huber AK, Giles DA, Segal BM, Irani DN. An emerging role for eotaxins in neurodegenerative disease. Clin Immunol. 2018 Apr;189:29–33.

209. Liu M, Guo S, Hibbert JM, Jain V, Singh N, Wilson NO, et al. CXCL10/IP-10 in infectious diseases pathogenesis and potential therapeutic implications. Cytokine Growth Factor Rev. 2011 Jul;S1359610111000293.

210. Davila ML, Xu M, Huang C, Gaddes ER, Winter L, Cantorna MT, et al. CCL27 is a crucial regulator of immune homeostasis of the skin and mucosal tissues. iScience. 2022 Jun;25(6):104426.

211. Beudeker BJB, Groothuismink ZMA, Van Der Eijk AA, Debes JD, Boonstra A. Circulating Cytokines Reflect the Etiology-Specific Immune Environment in Cirrhosis and HCC. Cancers. 2022 Oct 7;14(19):4900.

212. Winer H, Rodrigues GOL, Hixon JA, Aiello FB, Hsu TC, Wachter BT, et al. IL-7: Comprehensive review. Cytokine. 2022 Dec;160:156049.

213. Deshmane SL, Kremlev S, Amini S, Sawaya BE. Monocyte Chemoattractant Protein-1 (MCP-1): An Overview. J Interferon Cytokine Res. 2009 Jun;29(6):313–26.

214. Puntambekar SS, Davis DS, Hawel L, Crane J, Byus CV, Carson MJ. LPS-induced CCL2 expression and macrophage influx into the murine central nervous system is polyamine-dependent. Brain Behav Immun. 2011 May;25(4):629–39.

215. Yang N, Tan RP, Chan AHP, Lee BSL, Santos M, Hung J, et al. Immobilized Macrophage Colony-Stimulating Factor (M-CSF) Regulates the Foreign Body Response to Implanted Materials. ACS Biomater Sci Eng. 2020 Feb 10;6(2):995–1007.

216. Van Loo G, Bertrand MJM. Death by TNF: a road to inflammation. Nat Rev Immunol. 2023 May;23(5):289–303.

217. Lis K, Kuzawińska O, Bałkowiec-Iskra E. State of the art paper Tumor necrosis factor inhibitors – state of knowledge. Arch Med Sci. 2014;6:1175–85.

218. Bloom MJ, Saksena SD, Swain GP, Behar MS, Yankeelov TE, Sorace AG. The effects of IKK-beta inhibition on early NF-kappa-B activation and transcription of downstream genes. Cell Signal. 2019 Mar;55:17–25.

219. Jones BA, Beamer M, Ahmed S. Fractalkine/CX3CL1: A Potential New Target for Inflammatory Diseases. Mol Interv. 2010 Oct 1;10(5):263–70.

220. Indorf P, Patzak A, Lichtenberger F. Drug metabolism in animal models and humans: Translational aspects and chances for individual therapy. Acta Physiol [Internet]. 2021 Dec [cited 2023 Aug 2];233(4). Available from: https://onlinelibrary.wiley.com/doi/10.1111/apha.13734

221. Zhao M, Ma J, Li M, Zhang Y, Jiang B, Zhao X, et al. Cytochrome P450 Enzymes and Drug Metabolism in Humans. Int J Mol Sci. 2021 Nov 26;22(23):12808.

222. Xu SF, Hu AL, Xie L, Liu JJ, Wu Q, Liu J. Age-associated changes of cytochrome P450 and related phase-2 gene/proteins in livers of rats. PeerJ. 2019 Aug 2;7:e7429.

223. Duthaler U, Bachmann F, Suenderhauf C, Grandinetti T, Pfefferkorn F, Haschke M, et al. Liver Cirrhosis Affects the Pharmacokinetics of the Six Substrates of the Basel Phenotyping Cocktail Differently. Clin Pharmacokinet. 2022 Jul;61(7):1039–55.

224. Pinto B, Henriques AC, Silva PMA, Bousbaa H. Three-Dimensional Spheroids as In Vitro Preclinical Models for Cancer Research. Pharmaceutics. 2020 Dec 6;12(12):1186.

225. Cui Z, Wang H, Li S, Qin T, Shi H, Ma J, et al. Dihydroartemisinin enhances the inhibitory effect of sorafenib on HepG2 cells by inducing ferroptosis and inhibiting energy metabolism. J Pharmacol Sci. 2022 Jan;148(1):73–85.

226. Robinson NB, Krieger K, Khan FM, Huffman W, Chang M, Naik A, et al. The current state of animal models in research: A review. Int J Surg. 2019 Dec;72:9–13.

227. Agrawal S, Khazaeni B. Acetaminophen Toxicity. In: StatPearls [Internet]. Treasure Island (FL): StatPearls Publishing; 2023 [cited 2023 Jul 27]. Available from: http://www.ncbi.nlm.nih.gov/books/NBK441917/

228. Kitaeva KV, Rutland CS, Rizvanov AA, Solovyeva VV. Cell Culture Based in vitro Test Systems for Anticancer Drug Screening. Front Bioeng Biotechnol. 2020 Apr 9;8:322.

229. Ewart L, Apostolou A, Briggs SA, Carman CV, Chaff JT, Heng AR, et al. Performance assessment and economic analysis of a human Liver-Chip for predictive toxicology. Commun Med. 2022 Dec 6;2(1):154.

230. Heinz S, Freyberger A, Lawrenz B, Schladt L, Schmuck G, Ellinger-Ziegelbauer H. Mechanistic Investigations of the Mitochondrial Complex I Inhibitor Rotenone in the Context of Pharmacological and Safety Evaluation. Sci Rep. 2017 Apr 4;7(1):45465.

231. Rotundo L, Pyrsopoulos N. Liver injury induced by paracetamol and challenges associated with intentional and unintentional use. 2020;12(4):13.

232. McGill MR, Jaeschke H. Metabolism and Disposition of Acetaminophen: Recent Advances in Relation to Hepatotoxicity and Diagnosis. Pharm Res. 2013 Sep;30(9):2174–87.

233. Chen J, Jiang S, Wang J, Renukuntla J, Sirimulla S, Chen J. A comprehensive review of cytochrome P450 2E1 for xenobiotic metabolism. Drug Metab Rev. 2019 Apr 3;51(2):178–95.

234. Ramachandran A, Jaeschke H. A mitochondrial journey through acetaminophen hepatotoxicity. Food Chem Toxicol. 2020 Jun 1;140:111282.

235. Jaeschke H, Duan L, Nguyen NT, Ramachandran A. Mitochondrial damage and biogenesis in acetaminophen-induced liver injury. Liver Res. 2019;3(3):150–6.

236. Meechan AJ, Henderson C, Bates CD, Grant MH, Tettey JNA. Metabolism of troglitazone in hepatocytes isolated from experimentally induced diabetic rats. J Pharm Pharmacol. 2010 Feb 18;58(10):1359–65.

237. Tang C, Livingston MJ, Safirstein R, Dong Z. Cisplatin nephrotoxicity: new insights and therapeutic implications. Nat Rev Nephrol. 2023 Jan;19(1):53–72.

238. Ikeda K, Terashima M, Kawamura H, Takiyama I, Koeda K, Takagane A, et al. Pharmacokinetics of Cisplatin in Combined Cisplatin and 5-Fluorouracil Therapy: A Comparative Study of Three Different Schedules of Cisplatin Administration. Jpn J Clin Oncol. 1998 Mar 1;28(3):168–75.

239. Nayak Rao S. The role of heat shock proteins in kidney disease. J Transl Intern Med. 2016 Sep 1;4(3):114–7.

240. Zanger UM, Schwab M. Cytochrome P450 enzymes in drug metabolism: Regulation of gene expression, enzyme activities, and impact of genetic variation. Pharmacol Ther. 2013 Apr;138(1):103–41.

241. Wang X, Liu Q, Zhang B. Leveraging the complementary nature of RNA-Seq and shotgun proteomics data. PROTEOMICS. 2014 Dec;14(23–24):2676–87.

242. Gedeon T, Bokes P. Delayed Protein Synthesis Reduces the Correlation between mRNA and Protein Fluctuations. Biophys J. 2012 Aug;103(3):377–85.

243. Di Zeo-Sánchez DE, Segovia-Zafra A, Matilla-Cabello G, Pinazo-Bandera JM, Andrade RJ, Lucena MI, et al. Modeling drug-induced liver injury: current status and future prospects. Expert Opin Drug Metab Toxicol. 2022 Sep 2;18(9):555–73.

244. He Y, Li H, He Y, Lu C, Zhu P, Li M, et al. Troglitazone inhibits hepatic oval cell proliferation by inducing cell cycle arrest through Hippo/YAP pathway regulation. Dig Liver Dis. 2022 Jun;54(6):791–9.

245. Volarevic V, Djokovic B, Jankovic MG, Harrell CR, Fellabaum C, Djonov V, et al. Molecular mechanisms of cisplatin-induced nephrotoxicity: a balance on the knife edge between renoprotection and tumor toxicity. J Biomed Sci. 2019 Dec;26(1):25.

246. Meunier L, Larrey D. Drug-Induced Liver Injury: Biomarkers, Requirements, Candidates, and Validation. Front Pharmacol. 2019 Dec 11;10:1482.

247. Sharma R, Sinha R, Kaur R, Rani S. Drug-Induced Nephrotoxicity and Use of Biomarkers. In: Patel VB, Preedy VR, Rajendram R, editors. Biomarkers in Toxicology [Internet]. Cham: Springer International Publishing; 2023 [cited 2023 Sep 7]. p. 797–829. (Biomarkers in Disease: Methods, Discoveries and Applications). Available from: https://link.springer.com/10.1007/978-3-031-07392-2_50